A Techno-Economic Assessment of Solar Panel Integration onto a Wave Energy Converter

Macauley Versey

Engineering Doctorate

Industrial Centre for Offshore Renewable Energy

2023

For my Family,

Sophie, Archie & Harris

Abstract

A national grid based on renewable energy needs a diverse portfolio of technologies to reliably produce power for all variations in weather. Wave energy offers a new breed of renewable technology which is both predictable and energy dense. However, despite decades of funding and development, wave energy is yet to reach the commercialisation stages due to high testing costs and lack of convergence of design.

One way to achieve commercial success is to first target kilowatt-scale niche demands which are less concerned with the price of energy and instead desire consistent, year-round renewable power. Niche demands thus offer a stepping stone for wave energy converter developers to prove their technology, make revenue, and scale up to megawatt grid-tied devices. The main challenge to providing consistent power is that the available wave energy resource observes a seasonal variation peaking in the winter and lulling in the summer, especially in northern latitudes.

The smoothing of seasonal energy variations is critical for small-scale wave devices so that consumers do not have to rely on fossil fuel backups during summer months. The impact of seasonal variations can be reduced by oversizing the wave energy converter so that the minimum is satisfactory for the consumer. An alternative is to use large-capacity inter-seasonal energy storage. Whilst both solutions are plausible, they may not make economic sense. Instead, utilising the available deck area of a wave energy converter with solar panels will offer an alternate source of energy which is out of phase with the winter peaks observed in the wave energy resource.

This thesis explores the novel idea of combining wave and solar renewable technologies into one floating device, a Solar-Wave Energy Converter. It uses the Mocean Energy hinged raft BlueX wave energy converter as its example. A literature review shows that whilst this topic has been introduced before, the models to predict performance are basic and there are no published examples of experimentation at scale or at sea.

This work completes two sets of experiments to examine how the dynamic offshore environment of the BlueX wave energy converter influences the yield of solar panels on its deck area. In the first set of experiments flexible and rigid solar panels are compared before a storm damages the test kit after 16 days at sea. Despite the short

deployment period, the panels were covered in bird guano which could not be washed by the waves. This would have a significant impact on the yield and survivability of the panels. Methods to deter birds should be considered if the device is deployed in locations where birds are likely to reside.

The second experiment uses lessons from the first and applies flexible panels to the hull as they offer greater protection from the elements. The panels power a continuous hotel load of the wave energy converter, allowing the wave power produced to go directly to the consumer. The panels located on the front of the device were regularly washed by the waves and had deposits of marine growth on the surface. The panels located on top of the nacelle were in good condition as birds were not as prevalent at this deployment. Despite the marine growth, the panels powered the hotel demand for 96% of the 122 days of testing. It was found that the efficiency of the maximum power point tracking converter is sensitive to the motions of the wave energy converter, this is described by a linear relationship with significant wave height.

A numerical model is produced which takes into account the motions and heading of the wave energy converter as well as the curvature of the panels. This model is compared to the experimental results where a good agreement is found, with an average error over the 122 testing period of 1.1% and a worst-case error in March of 4.22%, increasing confidence in the results. The model is then used in sensitivity studies to obtain a performance ratio for various headings and hull diameters for deployments in the North Sea and the Caribbean Sea.

A six-kilowatt solar array is modelled to assess the benefits for deployments in the North Sea, Mediterranean and Canary Islands. The increase in the magnitude of the continuous available power, the amount of power which can be reliably provided to a consumer, is assessed for each location where increases between 13% and 35% are found, depending on the location. Additionally, the increase in annual energy production was found to be between 6% and 24%. The standard deviation of the monthly energy shows how variable the resource is. Assessing this before and after the addition of the solar array shows how it smooths the device output. It was found that the standard deviation can reduce by 43%. However, the addition of the solar array can also increase the standard deviation of the monthly energy when the wave and solar resources are not perfectly out of phase. This occurs for deployments near the Canary Islands, where the 6kW array increased the standard deviation of the monthly energy by 17%.

Finally, the costs of the experiments are used to obtain the cost of a full-scale array showing that the benefits reaped from hybridising the system far outweigh the costs. The cost metrics of the BlueX are confidential and thus, the levelised cost of energy scaling factor, the amount the original wave energy converter levelised cost of energy is scaled by, for varying wave device costs is found. For deployments in the north sea, the levelised cost of energy reduces up to 4.5% when the wave device costs more than 1.466 million GBP. For other locations, the reduction can be up to 17.5%.

This work shows that the addition of a solar array onto a wave energy converter can be beneficial by increasing the continuously available power, smoothing the monthly energy variations and reducing the levelised cost of energy. Further work suggests the exploration of deployable arrays to increase the capacity of the solar array beyond the available deck area, to improve the benefits further.

Lay Summary

To be able to power a country with renewable technologies, a range of types of renewables need to be included so that when the wind doesn't blow or the sun doesn't shine, an alternative type is available. There is a lot of energy in the waves and they are predictable. However, even though there have been decades of research and funding, wave energy converters are still not commonly available due to the high costs of development and the best design is still yet to be found.

One way to improve the development of wave energy is to supply power to marine users who do not have access to the grid and need round-the-clock power. These users are known as niche demands and are less worried about the price they pay for electricity, as long as they have the power they need, when they need it. The niche demands can act as the stepping stone for wave energy developers to prove their technology, make money and increase the size of their machines to be able to operate on the national grid. The main challenge is that there is a lot of wave energy in the winter but not a lot in the summer meaning the amount of power available changes throughout the year.

The smoothing of the power variation is important for smaller wave energy devices so that the niche demands do not have to rely on using fossil fuels to make up the difference in the summer. One way around this is to make the wave energy converter so large that the reduced power in the summer is still high enough for the consumers. Another way would be to include large battery storage with the wave energy converter so that the energy harvested in the winter can be used in the summer. Both of these solutions are possible but are costly, reducing the attractiveness of the wave energy converter solution. A final solution would be to fill the available area on the wave energy converter with solar panels as they have the most energy in the summer when it is needed.

This work explores the unique idea of combining wave and solar renewable technologies into one floating device. It uses the Mocean Energy hinged raft BlueX wave energy converter as its example. A review of existing work shows that this idea has been presented before but the calculations to estimate the energy are basic and no experiments have taken place.

This work completes two experiments to explore how the movement of the device affects the solar panels. In the first experiment, traditional panels are compared against flexible panels until a storm damaged the test rig after 16 days at sea. During the short testing period, the solar panels were covered in bird poo which could not be washed by the waves. This would reduce the amount of energy produced by the panels and also damage them. Ways to scare off the birds should be considered for future deployments.

The second experiment uses lessons from the first and applies flexible panels to the surface of the wave energy converter as they are less likely to be damaged than the traditional panels. The panels power a constant load of the wave energy converter, allowing the wave power produced to go directly to the customer. The panels located on the front of the device were regularly washed by the waves and had seaweed growth on the surface. Other panels, further from the water, were left in good condition as there were fewer birds at this site. The panels powered the constant load for 96% of the 122 days of testing. The efficiency of the converter which controls the panel output was found to decrease when there were large waves.

A mathematical model was made to account for the motion and direction of the wave energy converter and the curvature of the flexible panels. The outputs of this model are compared with the results from the experiments where they match within 1.1% suggesting the model is accurate. The model is then used to explore how different design decisions influence the performance of the array. A full-scale array is designed and then the model ran for deployments in the North Sea, Mediterranean and Canary Islands to explore if the addition of the solar array is beneficial to the device.

The amount of power which the solar wave energy converter can constantly supply to a niche demand is assessed for each location. Increases between 13% and 35% are found depending on the site. The increase in the total energy produced over a year is found to be between 6% and 24%. The variability of the monthly energy reduces for deployments in the North Sea and Sardinia but increases for the Canary Islands. This is because the wave energy and solar energy both peak at similar times.

Finally, the cost of the experiment is used to estimate the costs of a full-scale array. The variation in the price to produce one unit of energy by the addition of the solar array is assessed. This depends on the initial cost of the wave energy converter. As the value is not public knowledge, the variation of the cost to produce one unit of energy is found for varying wave energy converter costs. In the north sea, the cost per unit of energy can reduce by 4.5% when the device costs £3.5 million. In the other locations, this reduction can be as much as 17.5%.

This work shows that the addition of a solar array onto a wave energy converter can be beneficial by increasing the continuously available power, smoothing the monthly energy variations and reducing the cost per unit of energy. Further work suggests the exploration of deployable arrays to increase the capacity of the solar array beyond the available deck area.

Acknowledgements

The list of people who supported me throughout my pursuit of this doctorate was ever-growing. Hopefully, I haven't forgotten to include anyone that helped me during the long road it took me to get here.

Thank you to my Academic Supervisors, Zhiming Yuan, Lars Johanning and Aristides Kiprakis who gave me continual advice and guidance throughout the past three years.

Thank you to the IDCORE program, the ESPRC for funding and allowing IDCORE to continue to run. Thank you to David Ingram, Katrina Tait and Andrew Aveyard for the smooth running of IDCORE and continual support. Thank you to my fellow IDCORE cohort who have been on this journey with me from the start. I hope that we will all continue to be great friends and colleagues in the future.

Thank you to absolutely everyone at Mocean, you made me feel so welcome. Something especially hard to do when meeting you all for the first time over Teams during a pandemic. Big shout out to Alfred and Gabriel who helped me with all things numerical. Yan, Tom, Arhontia and Jon for support and manufacturing of experiments, they simply would not have gone ahead without your help. Andrea for his guidance in navigating an IDCORE EngD. Everyone in the Aberdeen office, Ian, Chris Z, Jay, Jamie and Chris W for countless hours of brainstorming and whiteboard discussions. Chris Retzler and Cam for founding and running Mocean in the first place, it is a great place to work and I am ecstatic to carry on my Mocean career. Extra special thanks to Chris R who was a constant support throughout my EngD and went well above and beyond his role as my industrial supervisor.

Thanks to Ian Gold at the University of Edinburgh and Tom Adcock at Blackfish Engineering for their support in developing the first at-sea experiment test rig.

I would like to thank my family, for their constant support throughout my entire life. For Mum and Dad for giving me the tools and ambition to even attempt this effort and for pushing me through to the end. For Connie, who has grown into a strong and confident young woman. For Emma and Steve, my parents partners, who have helped them grow into better people. We sadly lost Steve in the final months of this degree - I hope you are resting peacefully. Thank you for looking after mum and helping her onto her feet when she needed someone the most.

For my new Scottish family, Diane, Martin and Holly who have been consistent shoulders to lean on for all things EngD as well as day-to-day family life. You have really made my transition to life in Aberdeen incredible and I now call it my home.

Most importantly, for my own family, which seems to grow year after year. Deciding to have two children during an EngD perhaps is not the best idea to decrease stress and workload but you make it all worth it. The boys, Archie and Harris, are my reminders to keep going to be the best I can be. Sophie, I really could not have done this without you and this is your success as much as mine.

Declaration

I declare that this thesis was composed by myself, that the work contained herein is my own except where explicitly stated otherwise in the text, and that this work has not been submitted for any other degree or professional qualification except as specified.

Macauley Versey

Contents

Figures and Tables

Figures

Tables

Nomenclature

α_s	The altitude of the sun
ΔT	Temperature difference between the cell and the module back surface at Reference Irradiance. This temperature difference is typically 2 to 3 $^{\circ}C$ for flat-plate modules in an open-rack mount. For flat-plate modules with a thermally insulated back surface, this temperature difference can be assumed to be zero. For concentrator modules, this temperature difference is typically determined between the cell and the root of a finned heat exchanger (heat sink) on the back of the module.
η_{PV}	Efficiency of Solar Panel (At standard Test Conditons)
γ_s	The azimuth angle of the sun
$\overrightarrow{E}$	Unit Vector Facing East
$\overrightarrow{N}$	Unit Vector Facing North
$\overrightarrow{P_N}$	Solar Panel Normal Vector
$\overrightarrow{S}$	Solar Vector
$\overrightarrow{X}$	Solar Panel Axial Vector
$\overrightarrow{Y}$	Solar Panel Radial Vector
$\overrightarrow{Z}$	Unit Vector Facing Vertically Up
ρ	Density of seawater = 1035kg/m^3
θ_i	Panel Cell Angle
θ_T	Panel Tilt Angle
θ_Z	Panel Zenith Angle?
ε	Perez Diffuse Clearness Bin
a	Empirically-determined coefficient establishing the upper limit for module temperature at low wind speeds and high solar irradiance
A_{Array}	Area of Solar Array
A_{Panel}	Area of Solar Panel
b	Empirically-determined coefficient establishing the rate at which module temperature drops as wind speed increases
E	Solar Irradiance on Module Surface (W/m^2)
E_0	Reference Irradiance ($1000W/m^2$)
g	Acceleration due to gravity = 9.81m/s

H	WEC Heading Angle
H	Wave Height
Hs	Significant Wave Height
i	Cell Number
$I_{diff,isotropic}$	Isotropic Diffuse Irradiance
$I_{diff,Perez}$	Perez Diffuse Irradiance
I_{direct}	Direct Irradiance
I_{eff}	Effective Solar Irradiance
I_{mp}	Maximum Powerpoint Current (A)
$I_{reflect}$	Albedo Reflected Irradiance
I_{sc}	Short Circuit Current (A)
I_{Total}	Total Irradiance
L	Panel Length
P	WEC Pitch Angle
R	WEC Roll Angle
r	Hull Radius
T	Wave Period
T_a	Ambient Temperature ($^\circ C$)
T_c	Cell Temperature ($^\circ C$)
T_m	Module Temperature ($^\circ C$)
Te	Wave Energy Period
V_{mp}	Maximum Powerpoint Voltage (V)
V_{oc}	Open Circuit Voltage (V)
WS	Wind Speed measure at 10m (m/s)

Acronyms

AEP Annual Energy Production.

BNI Beam Normal Irradiation.

CAMS Copernicus Atmosphere Monitoring Service.
CAP Continuous Available Power.
CapEx Capital Expendature.
CF Capacity Factor.
CfD Contract for Difference.

DHI Diffuse Horizontal Irradiation.

EMEC European Marine Energy Centre.
EU European Union.

FF Fill Factor.

GHI Global Horizontal Irradiation.

HRES Hybrid Renewable Energy System.
HWPEH Hybrid Wave and Photon Energy Harvester.

LaRC Langley Research Center.
LCoE Levelised Cost of Energy.

ME Mocean Energy.
MPPT Maximum Power Point Tracking.

NASA National Aeronautics and Space Administration.
NREL National Renewable Energy Laboratory.

O&M Operations and Maintenance.
OpEx Operational Expendature.
OWC Oscillating Water Column.

POWER Prediction of Worldwide Energy Resources.
PR Performance Ratio.

PTO Power Take Off.

RSP Renewables for Subsea Power.

STC Standard Test Conditions.

SWEC Solar-Wave Energy Converter.

TOA Top of Atmosphere.

UK United Kingdom.

WEC Wave Energy Converter.

WES Wave Energy Scotland.


mocean
energy

PART I

Background

Chapter 1

Introduction

In order to achieve Net Zero by 2050 [1], the UK needs to develop a reliable and secure portfolio of renewable energy technologies to power the national grid. Whilst fossil fuels offer tried and tested methods of producing on-demand energy, the by-products of greenhouse gasses contribute to global warming. Additionally, Russia's invasion of Ukraine in 2022 and rising gas prices [2] have shown that international events can have impacts on consumers of energy and the national economy. The benefits and pressure to move towards an energy system powered by renewable technologies are obvious. However, at present, renewables can not solely satisfy the demands of the UK national grid as they are still plagued by a lack of installed capacity and intermittency [3].

The capacity of offshore wind is set to grow to 50GW by 2030 and onshore solar to 70GW [4]. However, when the wind does not blow or the sun doesn't shine, the UK still relies on fossil fuels and international transmission lines to power its infrastructure [5]. Large energy storage is plausible, however economic support mechanisms for this technology are immature. The UK government are supporting innovative solutions through the 32 million pounds Longer Duration Energy Storage Demonstration competition [6]. A potential solution is to invest in developing renewable technologies which derive energy from alternate sources to existing methods.

Ocean renewable technologies are still in early development, driven forward by the progression of offshore wind. The supply chain and expertise for this new branch of renewable technology is strengthening in the UK and can pivot into other technologies. The two emerging sources are tidal and wave energy. Tidal energy extracts energy from the flow of seawater. Early designs have similarities to wind turbine technology [7] [8] and thus benefit from years of industrial development. Wave energy is more unique from other renewables and still yet to mature, designs vary widely and convergence to the most efficient is still yet to happen.

1.1 A Brief History of Wave Energy

When the wind blows over the surface of the ocean, the shear force from the wind begins to produce waves. As the waves increase in amplitude, the wind now has a greater surface to act on and the waves grow further. The size of the resultant wave will depend on the length of time and the distance, known as fetch, the wind blew for. Additionally, the amount of wave breaking, viscosity and water depth will influence the size, shape and speed of the waves. The resultant ocean waves have an amplitude and speed and therefore, have both kinetic and gravitational potential energy. The amount of energy per meter length of regular wave can be calculated by $E = 1/8 * \rho * gH^2$ Where E is Energy per meter length, ρ is the water density, g is the gravitational constant and H is the wave height. The energy per m length is agnostic to water depth, however, the power is not. Power per meter length is given y $Ec_g = 1/8 * \rho * gH^2c_g$ Where c_g is the group velocity of the waves which depends on the water depth. Deep waves are classed as when the depth is more than half of the wavelength and shallow water is when the wavelength is more than 20 times the depth. Intermediate waves are found in between and classified by more complex equations. The effect of the sea bed creates a shear force on the waves, reducing their speed from the bottom up. The group velocity for deep waves is $gT/4\pi$ where T is the wave period and g is the gravitational acceleration constant. For shallow water, the group velocity is $\sqrt{(}gh)$ where g is the gravitational acceleration constant and h is the water depth.

The commercial and academic pursuit of wave energy converters began in 1976 with Stephen Salter and the Salter Duck [9]. Since then, several wave energy developers have attempted to design, optimise, commercialise, and operate a device that can reliably extract energy from ocean waves. Each developer has their respective design, with differing mechanisms and operations. Wave Energy Converter (WEC)s are categorised into one of several main groups, including but not limited to;

1. A point absorber, where the heave motion of waves is transferred into a buoy [10]
2. An oscillating wave surge converter, which is submerged under the wave surface [10]
3. An oscillating water column, a coastal device where waves rise and fall in a hollow chamber forcing air through a bi-directional turbine [10]
4. An attenuator or hinged raft, a multi-body device which floats on the water surface and extracts energy from the relative movement between hulls [10]

Several developers focusing on machines which could fall within one of these categories have made attempts at commercialising their technology. Two developers are most well known for their attempts, Pelamis and Aquamarine.

Aquamarine was an oscillating wave surge converter developer, building the Oyster. Oyster was a near-shore device, operating in waters up to 12 meters deep. The device was mounted to the sea bed and consisted of a buoyant flap which rotated in the wave action as seen in Figure 1.1. The reciprocating motion pumped seawater back to the shore into a traditional hydroelectric turbine. This method meant that all the electrical components were easy to access on shore. Aquamarine deployed its 315kW device in Orkney and connected to the national grid in November 2009. The second generation 800kW device was deployed in 2012. Unfortunately, despite an investment of more than £ 11 million in 2009, the company ceased trading in 2015 [11].

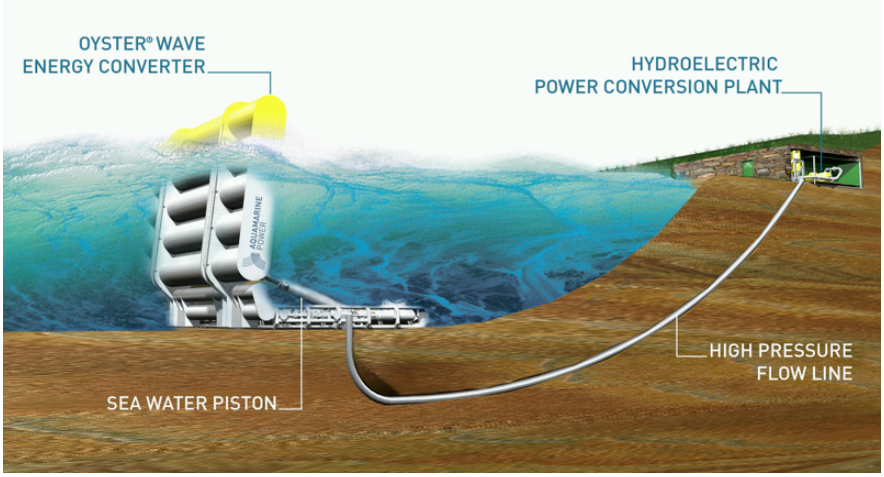

Figure 1.1: Oyster Operation [12]

Pelamis focused on the attenuator type of wave energy converter, deploying five Pelamis devices over its lifetime. The Pelamis device was designed to work in deeper water than the Oyster, in depths greater than 50m. In 2004, Pelamis became the first company to connect a wave energy converter to a national grid. The P2 was the final generation of the Pelamis device, it was 180m long and 4m in diameter. The device consisted of several tubular bodies connected with multi-degree of freedom hinges. The power was extracted at the hinge by multiple hydraulic cylinders, pumping high-pressure fluid to accumulators and hydraulic generators. Pelamis is the most well-known of the wave energy developers and was the most mature company before it went into administration in 2014 [13].

Figure 1.2: Pelamis Operation [13]

The pursuit of wave energy is tough, and thus unfortunately, no wave energy developer successfully crossed “The Valley of Death” - moving from being reliant on grants and investment to producing profit through sales. Fortunately, with newfound governmental support in Scotland and in the European Union (EU), a new age of wave energy developers has been pushing their respective designs. One such developer is Mocean Energy (ME), founded in 2015 at the University of Edinburgh. However, the same challenges which faced the early pioneers of wave energy still exist for the "Second Generation" of developers. The marine environment itself is tough, a salty and active environment lends itself well to corrosion-induced fatigue, increasing the engineering challenges. Additionally, the devices need to be able to survive the worst-case scenario storms, which may act once every one hundred years, bringing excessive wave heights and forces wanting to rip apart devices. The nature of wave energy is reciprocating and slow speed, a challenge for almost all existing electrical generation machines, requiring the need for new direct drive generators, hydraulics or the implementation of gearboxes. Finally, the cost and logistics of this R&D in tank testing and offshore lead to high costs, increasing the burden on grant funding to get as much out of it as possible. Mocean is striving to meet all of these challenges and has demonstrated success in doing so, and will continue to develop their novel and robust WEC for both on-grid and off-grid use cases at a range of power capacities.

1.2 Mocean Energy and BlueX

The Mocean wave energy converter design philosophy is an unsymmetric hinged raft with “Wave Channels”, a large scoop-like structure at the front and aft of the device as seen in Figure 1.3. The wave channels trap water to make the device resonate at frequencies close to the wave frequency, improving the response and efficiency of the device. Other machines, such as Pelamis, had to be very long to be able to resonate in the large wavelengths, adding cost. The Mocean technology allows the BlueX to "appear" approximately three times longer than it actually is.

This thesis uses BlueX, Mocean Energy’s first prototype, in experimentation and modelling. BlueX was completed in 2021 as part of the Wave Energy Scotland (WES) programme where it was one of two designs selected to be manufactured and tested. BlueX was first tested in European Marine Energy Centre (EMEC)s nursery wave test site in Scapa Flow in 2021 - discussed in Chapter 3. Since then, BlueX has been tested on the East Coast of Orkney as part of the Renewables for Subsea Power (RSP) programme - discussed further in Chapter 4. This thesis was fortunate enough to be able to use these two deployments as an opportunity for testing an onboard solar array.

Figure 1.3: BlueX on the Quayside [14] [15]

1.3 Motivation

Niche, kilo-watt scale, off-grid demands such as offshore oil and gas, island nations, or coastal security are less cost-sensitive than mega-watt utility-scale demands, driven by the levelised cost of energy [16]. Several niche demands are not suitable for existing offshore renewable technologies, due to large water depths or the visual impact of wind turbines. This offers a unique scenario for wave energy. By using niche demands as a stepping stone to earn revenue and mature designs, wave energy developers can scale up their machines to be more suitable for the utility-scale market, all whilst reducing costs and improving efficiency [17].

Wave power is very dense, especially in the winter when wave conditions are more energetic. However, in the summer, the available wave power can be 28% of the annual mean as seen in Figure 1.4, for the North Sea. Wave energy availability typically varies seasonally, with seasonal variation typically being greater in the northern hemispheres [18].

Seasonal variation is a common trait for all renewable energies. However, for niche demands, the availability of power all year round is critical. If wave energy converters are to target niche demands, the intermittency of supply needs to be solved. This could be done by sizing the device so that its minimum power in the summer months is high enough to satisfy the demand. However, this would lead to large over-engineering of the devices, increasing costs beyond economic feasibility.

Another solution would be to pair the machine with energy storage, but inter-seasonal battery capacities would be uneconomical. A more attractive solution is to pair the wave energy converter with an alternate source of energy, ideally, one that has an out-of-phase seasonal energy resource to wave power. Wind turbines are a tried and tested method to produce renewable power. However, wind and wave power have a slight correlation, as the wind can drive the waves and the blades of a small scale wind turbine may be too fragile to be deployed on a Wave Energy Converter. The summer lull points to the obvious choice of solar energy. This thesis explores the hybridisation of a wave energy converter with solar panels, to improve the year-round power supply of a standalone device to supply power to niche demands.

Solar panels are now the cheapest form of renewable energy technology [19] and research suggests that their efficiency will improve when deployed offshore due to cooler operating temperatures [20] and [21]. Additionally, their lack of moving components suggests a reduction in required maintenance, ideal for an offshore installation.

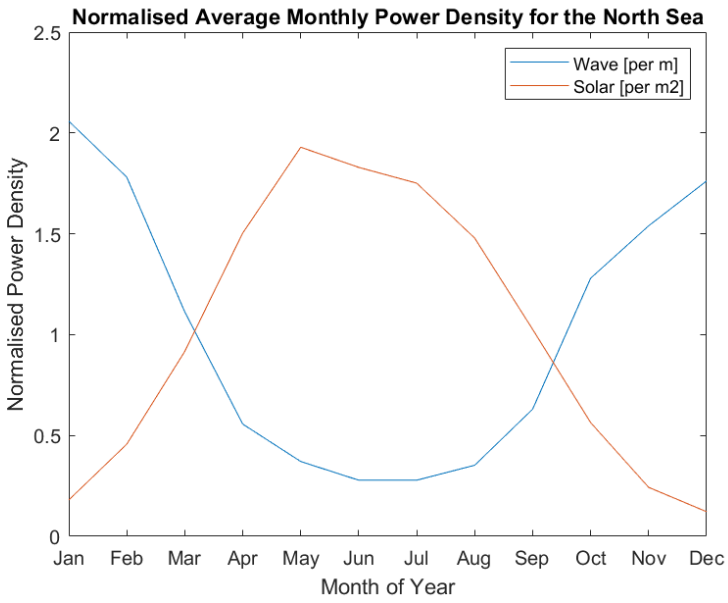

Figure 1.4: Power Density of Solar and Wave Resource in the North Sea. This figure was created by using the in-house Mocean Energy MOE Wave Analytics Tool to obtain the wave density and using Copernicus to obtain the solar energy density.

The combination of a solar array onto the WEC will be economically favourable, as the two systems can share electrical export components as well as moorings and floating structures. This would mean the solar panels onboard the WEC can have more attractive economic metrics than floating solar arrays, with comparable capacities and yields.

However, there are outstanding questions regarding the implementation of solar panels in such a harsh marine environment. The aim of this work is to analyse the cost/benefit of hybridising the wave energy converter with an on-board solar panel array by investigating the following points.

1. How likely are waves going to damage the panels?
2. Biofouling will cover the panels; can there be self-washing from the waves?
3. The panels will be moving with the wave energy converter and rarely orientated in the optimal position, how does this influence yield?
4. Which is the best way to mount the panels to address these concerns?
   (a) The panels could be curved and laid directly onto the hull, this will then have a penalty to yield
   (b) The panels could be rigidly mounted but would require additional steel structure, a penalty to cost

5. The panels, controllers and battery have a small cost compared to the remainder of the device but they may need frequent replacements. How economical is the system?

1.4 Aim and Objectives of the Thesis

AIM: To investigate the technical and economic impacts of implementing a solar array on-board a floating wave energy converter to examine whether a Solar-WEC will have a higher continuous available power than a WEC and thus be a more attractive solution for niche demands.

Objectives:

1. Deploy at-sea experiments of solar panels installed onboard a Wave Energy Converter and obtain yield and survivability data.
2. Develop a model to predict the energy yield from a solar array installed on a wave energy converter by combining established solar theory with WEC dynamics.
3. Use the yield data from the experiments, along with the WEC positional and power production data to verify the model.
4. Use the verified model to evaluate a full-scale hybrid Solar-WEC in locations around the world
5. Perform an economic assessment of the solar array and compare the cost/benefits of the addition of the solar panels to the wave energy converter system.

1.5 Contributions to the Knowledge, Conferences Attended, and Publications

One significant contribution to the knowledge of this work is a numerical model to predict the energy yield from a solar array on-board a dynamic wave energy converter, verified by real at-sea experimentation. The model considers the curvature of flexible solar panels, the position of the WEC, the temperature of the panel and PV array design.

The model is accompanied by an economic assessment where the benefit of the array is assessed on the ability to improve the seasonal fluctuation in device output power witnessed by the wave energy converter in the summer.

Another significant contribution to the knowledge is the publication of real-world data of testing solar panels onboard a wave energy converter, at sea. The data provides both panel and MPPT outputs as well as survivability data on the panel's conditions. This provides an opportunity for further researchers to compare and use in their studies.

During the experimentation and modelling phases, a number of other conclusions arose. A significant finding is that the efficiency of a Maximum Power Point Tracking converter is influenced by significant wave height. A second finding is that the use of flexible panels, directly adhered to a surface may be better protected offshore than rigid panels.

This work began during the first coronavirus lockdown in April 2020 and thus in person conferences were not taking place for a significant proportion of my EngD. However, I did attend the following conferences:

1. Supergen offshore renewables, Jan 2020
2. EUPVSC, Online, May 2021
3. IET RPG, Online, September 2022
4. Subsea Expo, Aberdeen, Jan 2022 & 2023
5. Decarbonising the North Sea, London, 2022

I submitted a paper to the Institute of Energy Technology Renewable Power Generation Conference 2022 held at Savoy Place in London. My paper, titled "EXPERIMENTAL RESULTS FROM THE HYBRIDISATION OF WAVE AND SOLAR ENERGY TO PROVIDE CONSISTENT POWER TO ISLANDED LOADS" was awarded the prize for the best student paper. The paper can be found in Appendix A.

1.6 Structure of Thesis

This Thesis is split into seven chapters. Firstly, this Chapter, the Introduction. Chapter 2 discusses published literature and industry examples relevant to progressing the thesis aims. Chapters 3 and 4 describe the two rounds of experimentation of a Solar-WEC. Chapter 5 describes the production and validation of the numerical model. Chapter 6 explores the full-scale design considerations and performance of the solar array. Finally, Chapter 7 concludes the findings of this thesis and suggests further work.

Chapter 2

Literature Review

This chapter describes a review of literature relevant to achieving the project aims as well as examples from the offshore renewables industry. As there is a limited number of available sources, the examples of hybrid wave and solar renewable energy systems are reviewed in detail in Section 2.1. A special focus on systems where the solar and wave energy conversion technologies are combined into one singular device is reviewed in Subsection 2.1.1.

In Section 2.2 special consideration is given to the emerging topic of combined wind and wave systems. Whilst section 2.3 reviews the commercially active topic of floating solar. This demonstrates the influence of being in the marine environment on the panels. Additionally, the influence of bird fouling on the performance of solar panels

2.1 Combined Solar and Wave Energy Systems

Two examples of a wave energy converter coupled with solar panels can be found in the industry; the AquaBuOY and the Sharp Eagle WEC.

The AquaBuOY 2.0 was a point absorber type WEC, built by Finavera and deployed off the coast of Oregon in 2007 [22]. It had a series of solar panels and small scale wind turbines installed on its floating section [23]. The capacity of the secondary solar and wind systems is unclear. However, between 4 and 6 panels are present on the device and 4 wind turbines. The WEC uses flat panels tilted at a high angle, orientated in every heading around the point absorber. The WEC was a test machine and thus never exported power. The solar and wind auxillary systems were intended to power onboard instrumentation and communications systems. The AquaBuOY unfortunately sank 7 weeks after the initial deployment.

The Sharp Eagle WEC was developed in 2015 by the Guangzhou Institute of Energy Conversion [24]. The Sharp Eagle is the main WEC platform operating on the oscillating water column principle. When modifications are made to the Sharp Eagle platform, they are given their own names such as; Pilot 1, Xiandao or Penghu all of which have 60kW of solar panels installed on the top deck of the platform [25] [26] [27] [28].

Very little information is publicly available regarding the performance of the solar panels on board these two commercial WECs. Whilst this Thesis may not introduce the idea of hybridising solar panels with wave energy, it does enter it into the public domain.

2.1.1 Wavevoltaics

The first analysis of “Wavevoltaics” is proposed in a 2018 techincal note by Kumar [29]. In this note, Kumar suggests filling the open sky area of wave devices with solar PV as shown in Figure 2.1 drawing inspiration from "floatovoltaics" and submerged PV. Kumar states "... the solar photovoltaic cell operation still remains the same even after it is integrated with the wave energy device" which would neglect the influence of WEC dynamics, the cooling effect on efficiency and soiling due to bio-fouling. The author follows this note up with a 2019 paper [30] and presents two equations; the first calculates the power of a wave energy converter based on the wave height H, period T, and group velocity.

$$WavePower = (g^2 * \rho * T * H^2)/(32 * \pi) \tag{2.1}$$

The second calculates the power output of a solar array using the array area A_{Array}, efficiency η_{PV} and effective radiation I_{eff} considering beam, diffuse Perez radiation, and albedo reflection. Kumar considers the cell temperature due to irradiance whilst noting that the temperature over water surfaces will be lower than that on land.

$$PVPower = A_{Array} * \eta_{PV} * I_{eff} \tag{2.2}$$

However, Kumar neglects to consider the effect of the movement of the WEC and assumes the panels are optimally orientated. This work does not offer any numerical results or discuss the seasonal relationship between the two energy sources. No input data is included so a comparison of energy generated is not presented.

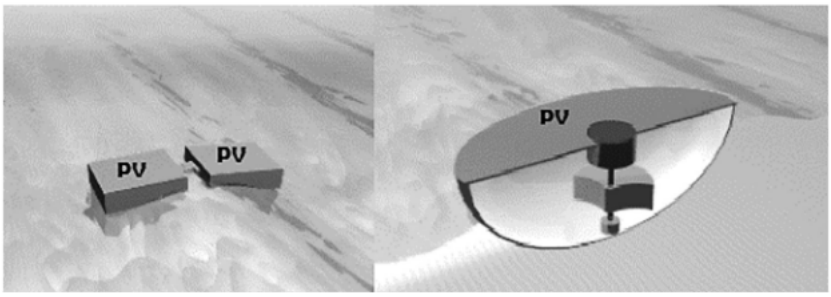

Figure 2.1: Wavevoltaic attenuator and wavevoltaic rotating mass devices taken from [29]

Kumar then goes on to co-author a review paper in [31] with Prasad et al.. In this review, over half of the content examines existing wave energy Power Take Off (PTO) configurations, from linear direct drive to overtopping devices. The Mocean Energy device is not included, perhaps because the most recent device examined was produced in 2019 and the paper was published in February 2022 whilst BlueX completed manufacture in 2021.

After the review of WEC PTOs, section 2.2 of [31] reviews wave energy HRES; discussing hybrid wind-wave before moving onto solar-wave where only the previously cited [29] and [30] are presented. No alternative literature discussing solar-wave is presented, suggesting that there is little published literature on this topic. A small section on hybrid wind-wave-solar is included where the authors present a three-in-one platform to harvest energy from waves, wind, or the sun, this is discussed further in Section 2.1.2. Section 3 of [31] introduces the conceptual design of a Hybrid Wave and Photon Energy Harvester (HWPEH) as seen in Figures 2.2 and 2.3.

The design consists of a floating buoy enclosed within a structure open at the bottom and top so that waves produce an oscillating water column. The buoy then heaves vertically so that a rack and pinion drives a gearbox and electrical generator. The structure then has a pitched roof upon which solar panels are mounted. Both systems feed into a battery energy storage system. The entire structure is then supported on two hulls which are moored to the sea floor. Power capacities of the WEC or solar array are not provided.

An Annual Energy Production (AEP) of 584kWhr is provided although it is not clear where this figure is derived from or where the system may be deployed to achieve this yield. It is claimed that 146kWhr is produced by the solar panels and 438kWhr from the wave energy converter. A cost of $1400USD is quoted which neglects the cost of

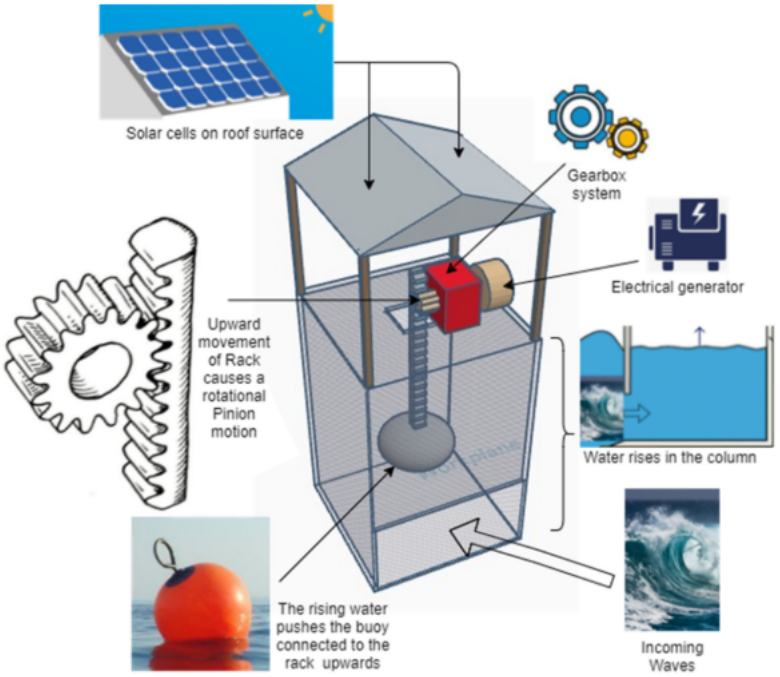

Figure 2.2: Conceptual design of the HWPE harvester taken from [31]

key components such as moorings and floats. The review does consider other solar cell technologies and concludes that monocrystalline silicon offers a good balance of efficiency and cost but only considers flat panels. The idea of using the HWPEH for island or coastal communities is presented, describing how these communities often rely on diesel to make electricity. This system does not appear to be designed to be deployable all year round and uses simple materials so that the communities can manufacture the devices locally. It is assumed that the capacity and robustness of this device are low and therefore not suitable to be a critical part of the energy infrastructure of an island.

The remainder of the review discusses challenges of the HWPEH but this focuses on the general challenges of WECs which are native to all devices and not the particular challenges of combining solar and wave devices or the challenges of installing solar panels in the marine environment. Sources further to the work of Kumar have not been found that describe a singular combined Solar-WEC, this highlights the gap in this area of research.

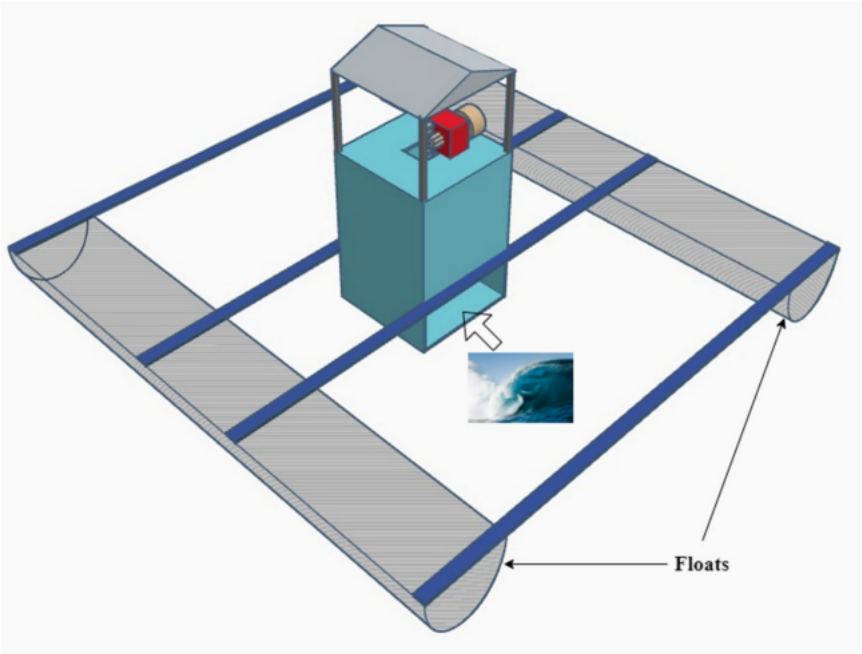

Figure 2.3: Conceptual design of the HWPE harvester with Floats taken from [31]

2.1.2 Hybrid Renewable Energy Systems

There are multiple examples of literature examining the benefits and cost implications of developing and modelling a Hybrid Renewable Energy System (HRES) [32]. Rosa-Santos et al. [33] Discusses major benefits of combining marine energy systems as improved energy yield, and smoothed power output as well as cost savings in common grid infrastructure, logistics, substructure and mooring. Additionally, a combined HRES can result in a lower Levelised Cost of Energy (LCoE). However, the examples of combined Solar and wave are sparse.

Wave-Solar Hybrid Renewable Energy Systems

Four examples of hybrid wave-solar systems have been found and are presented in [34] [35] [36] and [37]. In the first three of these sources, the authors consider a coastal grid-tied system where an Oscillating Water Column (OWC) WEC is deployed on the shoreline and a solar array is deployed close by on the land. The solar array therefore can not benefit from being offshore, as expanded in Section 2.3, but also would not face the same disadvantages of constantly movingThe power output of the

WEC is combined with the solar array on a common DC bus before being exported to an AC grid. This scenario is physically not the same as the one proposed in this thesis but they can still highlight the potential energy yield benefits of such a hybrid system as it is electrically similar.

Samrat et al. in [34] and Ahmad et al. in [35] are very similar papers. Samrat et al. considers a system comprising of a 2kW solar array, a 2.5kW OWC and a 14Ah battery deployed on the coast of Perhentian Island, North East Malaysia. The main aim of this work is to explore the ability of the system to maintain a consistent DC link voltage under a varying wave, solar and load conditions. Ahmad et al. has a smaller PV array capacity at 435W but maintains a 2.5kW OWC and the deployment location is not clear. The main conclusion from both papers is that the combination of the solar array and WEC performs well under steady-state power as well as transient solar, wave, and load power conditions. [34] says that in further work a stand-alone PV-WEC will be built in the University of Malay laboratory but evidence of this can not be found in the public domain. The benefit of this HRES to the small island community in Perhentian Island is noted and supports the aim of this thesis.

Levelised Cost of Energy of a Wave-Solar Hybrid Renewable Energy System

Saheli et al. presents a hybrid solar WEC system in [36] but focuses on the Levelised Cost of Energy (LCoE) of the system when deployed at three Iranian ports in the Persian Gulf and does use resource data to show the potential energy yield. The combined Solar-WEC in this case is still an Oscillating Water Column with a land-based solar array but has a higher capacity than in [34] and [35]. The hybrid system has a capacity of 15kW with a 3kW rated OWC and thus a 12kWp solar array. This system is heavily dependent on solar energy where 80% of the installed capacity is provided by the array. No energy storage is deployed in this system and the energy is fed directly to the Iranian grid.

The system is modeled using the single diode equation for PV cells and geometrical properties of the air chamber in the OWC, these equations are also used in [34] and [35]. The model uses monthly input data of irradiation, wind speed, wave height, and wave period, obtained from the Iranian Meteorological Organisation for each of the three sites.

The results of annual energy production for the three ports are shown in Figure 2.4. Each site produces more than 500kWh per year but the vast majority of this can be attributed to the production from the PV cells. This is due to the power capacity of the HRES being 80% solar. Additionally, the wave resource in the Persian Gulf is poor whilst the solar resource is abundant. The total contributions of solar and OWC to the total annual energy yield are only provided for one of the three locations, Chabahar, where of the 524kWh annual yield, 510kWh, 97%, comes from the solar array. Comparing this to Figure 2.4, Chabahar has the lowest contribution towards energy from WEC.

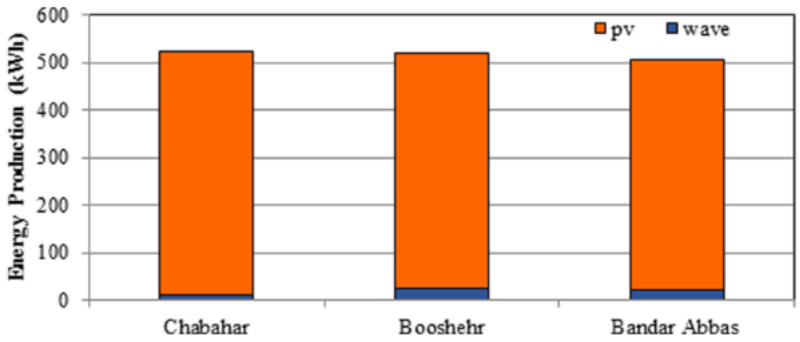

Figure 2.4: Annual energy production for the three locations from [36]

Saheli et al. then attributes a capital and annual Operations and Maintenance (O&M) cost to the HRES. The total capital cost is $58,531 where $47,387, 81%, is for the PV system.

By using a lifespan of 25 years and an interest rate of 12% and assuming that the annual yield is constant over the lifetime, a Levelised Cost of Energy is calculated for each port, presented below in Figure 2.5.

Location	Annual energy production (kWh/year)	LCOE ($/kWh)
Bandar Abbas	506	128
Bushehr	520	125
Chabahar	524	124

Figure 2.5: Levelised Cost of Energy for the three locations from [36]

Comparing the results of LCoE with the total AEP. Chabahar produces the most energy and thus has the lowest LCoE (As all locations have the same cost). However, this location also has the lowest contribution to AEP from the WEC and therefore relies on the PV array.

If the WEC had a larger capacity this may reduce the LCoE but would improve the energy diversity on the grid and thus reduce the dependence on solar energy. However, in locations such as Iran where the solar resource is consistent over the year, having a large reliance on solar energy with large energy storage is probably the best solution.

Oliveira-Pinto et al. [37] presents a good analysis of combining floating solar and wave renewable technologies to power offshore oil and gas platforms in locations where the seasonal resource fluctuates, namely the North Sea, Gulf of Mexico and Western Australia. In [37] the two technologies are physically separate systems and feed a common load, thus the area of the panel array is not confined to the open sky area of the WEC and the yield is not influenced by dynamics. Four types of WEC are considered; the Wavebob, Langlee, CETO and Pelamis. The power of each WEC is then scaled using Froude scaling so that they have equal power capacities. The available solar and wave resource at the three locations are assessed and a representative monthly oil and gas demand is assumed. Wave power is calculated using the power matrix of the respective WEC and the device which provides the best Annual Energy Production at that site is selected. The solar yield is based on the product of the total array cell area, the module efficiency, the performance ratio, the availability and the global horizontal irradiation and does not consider panel tilt or the motion induced by the waves.

The number of WECs or solar panels is increased so that the demand in the worst-performing month is met by 100% renewables. This means that the solar system has to meet demand in the winter and result in an oversized array in the summer whilst the same but opposite trend happens for the wave system, being oversized in the summer as shown in Figure 2.6.

The scenario with combined generation initially assumes a 50-50 installed capacity so that the solar capacity is equal to the wave capacity, this results in a large overcapacity but serves as the initial case. The balance of capacities is then varied in increments of 5% and the yield profile is assessed again. This is repeated until the optimal solution with the lowest over capacity is defined. The result for the Gulf of Mexico is found in Figure 2.7.

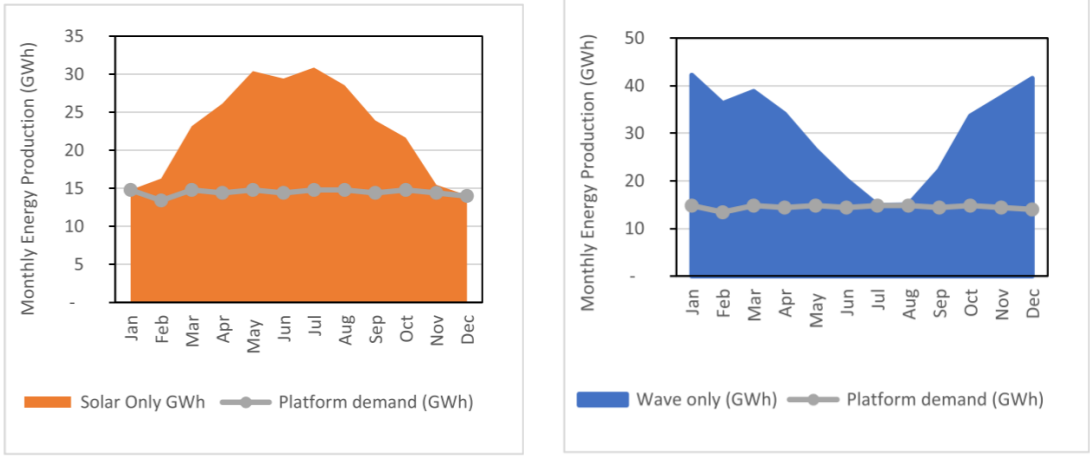

(a) Offshore Floating Solar System Only **(b)** Wave Energy Converter System Only

Figure 2.6: Yield Profile of Solar Only and Wave Only Renewable Energy Systems in the Gulf of Mexico [37]

The study finds that the optimal mix in the north sea is 60% wave energy and 40% solar whilst in the Gulf of Mexico and the West Coast of Australia it is 60% solar and 40% wave. The final results, comparing the Levelised Cost of Energy (LCoE) and Capacity Factor (CF) of stand-alone wave or solar systems and then the combined system for the three locations can be seen in Figure 2.8.

By combining the two systems, the capacity factor for all three locations improves by up to 18% and the LCoE is lower than for cases with individual systems in the Gulf of Mexico and the West Coast of Australia. Ultimately, this source is a great case study for the combination of the two energy sources of solar and wave energy in an offshore environment to meet an isolated load but treats the two sources of energy as physically separate. This means that the capacity of either source is not restricted and increases the costs of the total system through the duplication of moorings for the WEC and floating solar devices. It also neglects some potential reductions in the yield of the floating solar array.

The work presented in this thesis explores the scenario where the renewable energy resource is seasonal, and energy diversity is critical to an all-year-round demand. The solar and wave energy capturing technologies are combined into one device, saving on space, the number of electrical components and mooring requirements. However, by doing this the solar array is limited in deck space and its yield is influenced by the movement of the device.

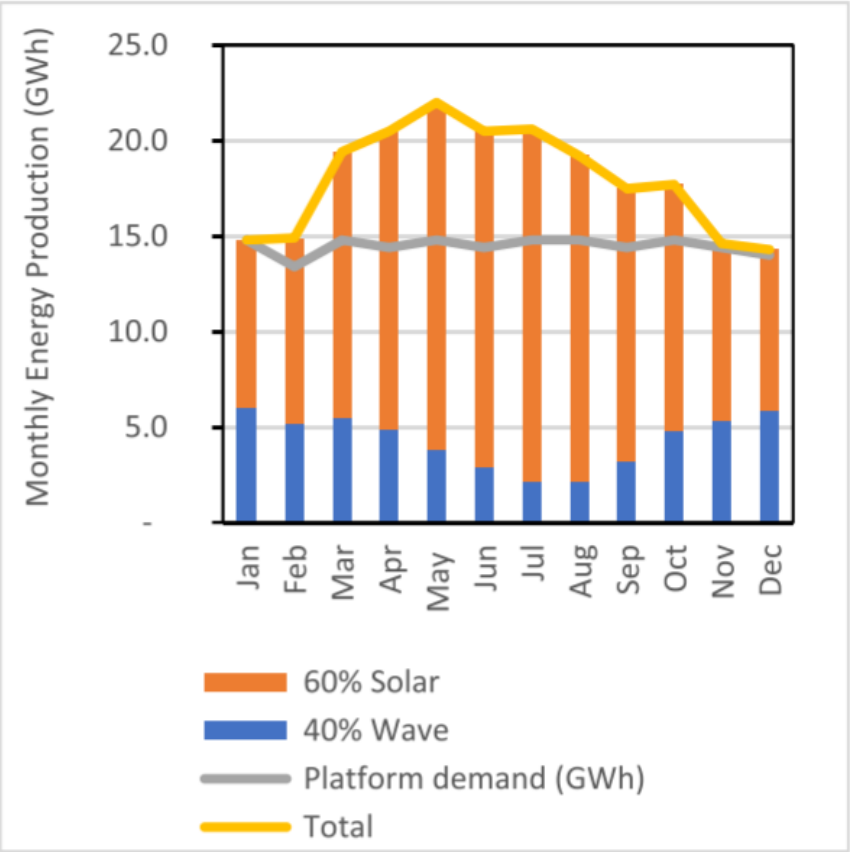

Figure 2.7: Combined Yield for Gulf of Mexico from [37]

Wind-Wave-Solar Hybrid Renewable Energy Systems

The next HRES reviewed, explores the effect on LCoE by combining different renewable energies; solar, wave, and wind coupled with battery energy storage. Additionally, Jahangir et al. in [38] uses the 750kW Pelamis WEC, an attenuator type machine, instead of an OWC. The solar array is assumed to be on land, as no considerations for being offshore have been discussed, and is made up of units of 250W panels. This paper has an additional renewable energy source than previously cited literature, from a 660kW wind turbine, also assumed to be onshore. The capacity of the solar array, battery storage, and the number of units of wind turbine and Pelamis converters are varied independently to explore the effect on LCoE at three locations in Iran. This includes investigating HRESs where only a WEC is combined with a solar array and battery energy storage and also the scenario where there is no contribution from wave energy.

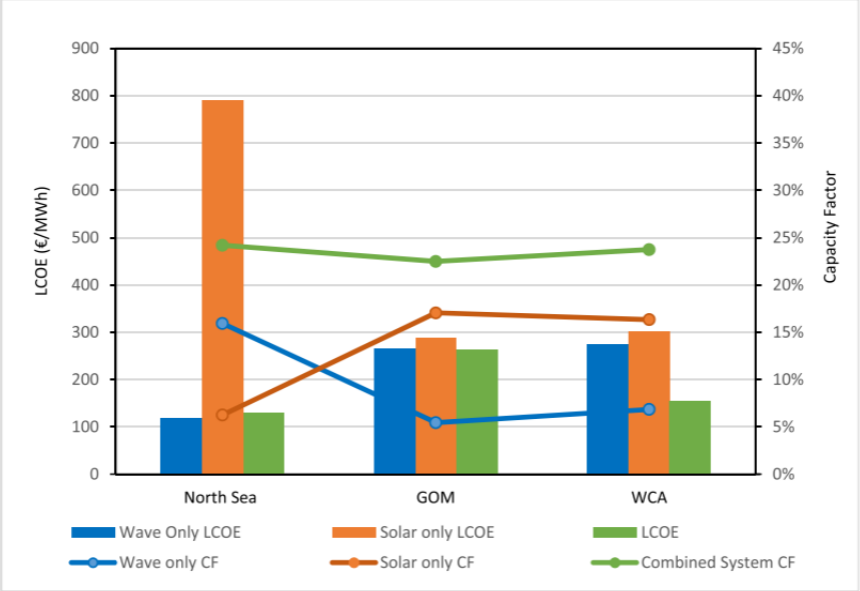

Figure 2.8: Results of the optimisation in all three locations from [37]

The three locations analysed in [38] are different from [36] but two are in similar locations to one another. The irradiance, wind speed, and wave height are available for all locations shown in Figure 2.9 where a clear seasonal fluctuation in solar power at all three locations can be seen as well as a prominent seasonal wave fluctuation for Anzali City and Genaveh City. The seasonal relationship between solar and wave is out of phase, where solar power peaks in June/July whilst wave peaks in December for Anzali and in May for Genaveh.

The power output of the Pelamis converter is assumed to be dependent on period and wave height and hits a power limit of 750kW at heights above 5m for wave periods less than 6.5 seconds. Wind turbine power output is based on the power curve provided by the turbine manufacturers with a cut-in speed of 4m/s and cut-out of 25m/s. Costs for the Pelamis converter, wind turbine, PV panels, battery, and power converters are included. For each location, HOMER Pro is used to find the optimal energy mix which provides the lowest LCoE. For all three locations, the optimal solution excludes the implementation of the WEC and has a mix of PV and wind with energy storage. When comparing the cases of PV-Wind-Bat with PV-Wind-Pelamis-Bat the LCoE increases by 11.8%, 11.2%, and 3.3% for Jask, Genaveh, and Anzali respectively. For HRES in Jask and Genaveh the second cheapest energy mix is a PV-Bat system however for Anzali, the second cheapest is the PV-Wind-Pelamis-Bat system. Anzali is therefore

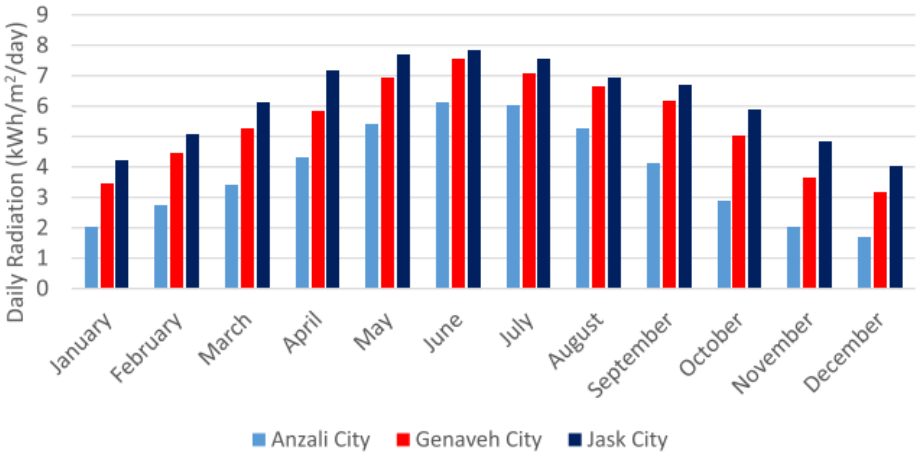

(a) Average Monthly GHI

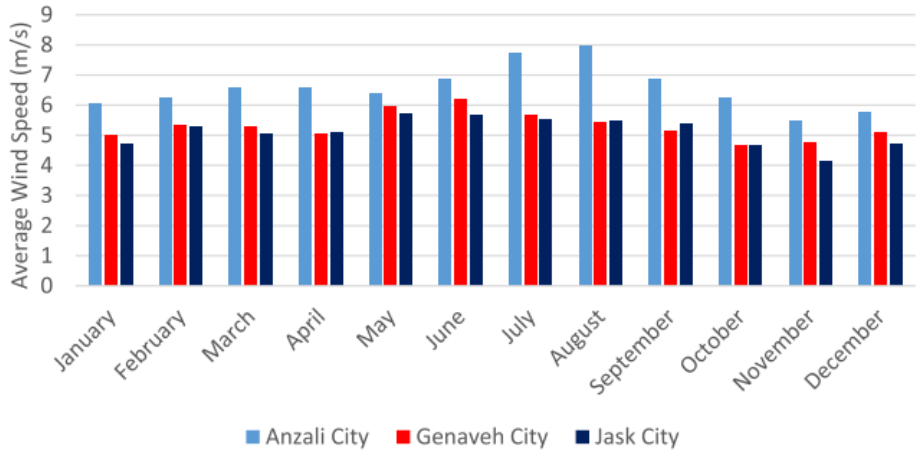

(b) Average Monthly Wind Speed

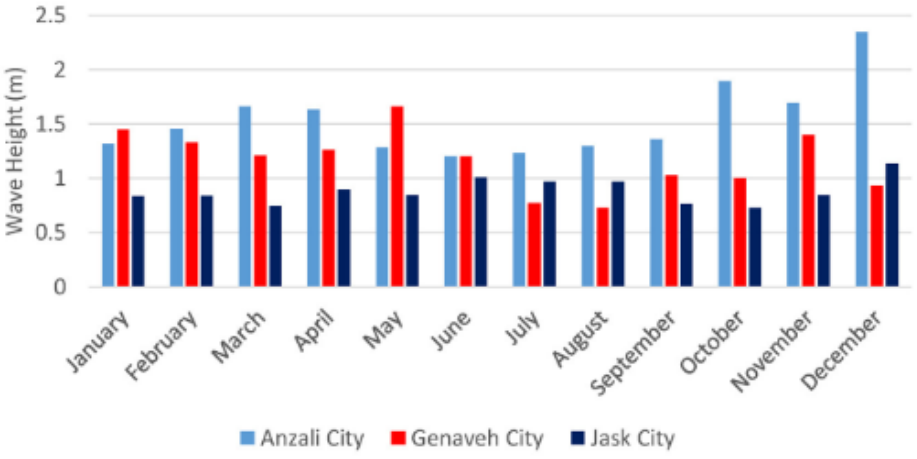

(c) Average Monthly Wave Height

Figure 2.9: Location Resource Data from [38]

clearly the best location for a triple system. Exploring the solutions which are only PV-Pelamis-Bat, Jask gives the lowest LCoE of 0.251$/kWh, for Anzali the PV-Pelamis-Bat system offers the worst LCoE of 0.383$/kWh probably as it has the lowest PV resource of the three locations.

Jahangir et al. Then completes a sensitivity analysis of the HRES in Anzali as this is the best candidate for the WEC. The sensitivity study reduces the cost of the Pelamis converter whilst keeping the average wave height the same at 1.53m and then completes a second analysis by increasing the average wave height to 2.03m and reducing cost.

As Figures 2.10 and 2.11 show, the Pelamis converter is not included in the optimum solution for a wave height of 1.53m until the cost is approximately 67% of the original modeled cost. Under this condition, the LCoE of the system reduces by 1.24% compared to the full cost scenario.

Average Wave Height	Pelamis Cost Multiplier	PV(kW)	WT (Unit)	Pelamis (Unit)	Bat(Unit)	Con(kW)	COE ($/kWh)	NPC($)	IC($)
1.53	1	7221	14	–	454	5878	0.242	48.8M	39.6M
	0.75	7221	14	–	454	5878	0.242	48.8M	39.6M
	0.5	6173	11	1	493	6135	0.239	48.8M	37.7M
2.03	1	5904	11	1	465	5744	0.241	48.8M	38.9M
	0.75	5734	12	1	439	5800	0.238	47.8M	38.3M
	0.5	6426	11	2	390	5095	0.235	46.8M	37.8M

Figure 2.10: Sensitivity analysis of the Optimum solution at Anzali from [38]

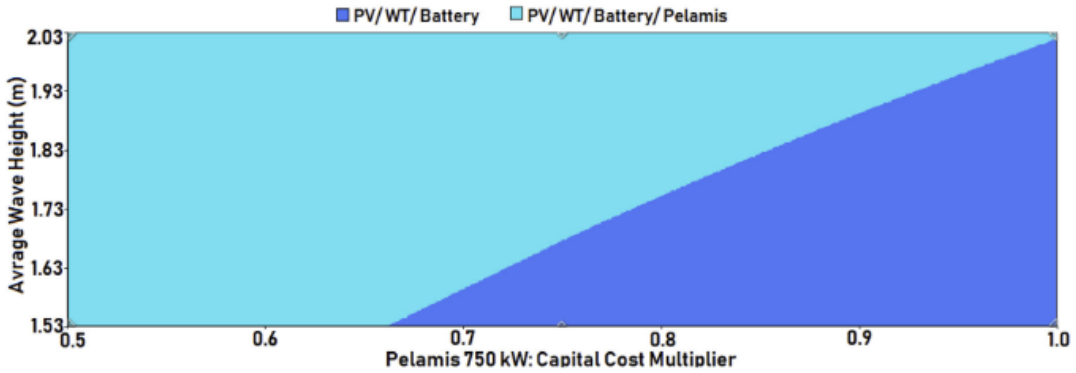

Figure 2.11: Graphical Results of the Sensitivity analysis of the Optimum solution at Anzali from [38]

The sensitivity analysis then also extends to explore other locations in the world such as Scotland, and NW Ireland where wave energy is more abundant but solar energy is more scarce. Other locations include NW Denmark, Spain, Portugal, Chile, and SW Australia. The resource available at each location is shown in Figure 2.12

Sample Area	Selected Region (Guanche et al., 2015)	Annual Average of Solar Radiation (kWh/m^2/d) (NASA, 2019)	Annual Average of Wind Speed (m/s) (NASA, 2019)	Significant Wave Height(m) ("Météo-France global wave model (MFWAM)," 2017)	Mean Wave Energy (kW/m) (Guanche et al., 2015)
1	Northwest of Denmark	2.9	6.4	2.5	12
2	West of Ireland	2.4	7.2	4	62
3	Chile	5.1	5.3	3.5	34
4	North of Spain	4.3	4.1	3	28
5	West-Portugal	4.4	5.6	3.5	29
6	South of Australia	4.7	5.9	4	62
7	West Scotland	2.7	7.6	3.5	50

Figure 2.12: Energy Resource at Each Location from [38]

The simulations were again run in HOMER. The LCoE of a sufficient PV-Wind-Bat system is calculated and then compared to the LCoE of a PV-Pelamis-Wind-Bat system. In all of the locations, the LCoE reduces when adding a Pelamis converter into the energy mix. This is the opposite finding the first section of the paper and is due to these location having access to a greater wave energy resource. The WEC now has a better contribution to annual energy production. This shows the importance of deployment location when analysing the contribution of any renewable energy into a HRES. Figure 2.13 highlights an additional benefit, by deploying multiple energy sources, the amount of battery power discharged is reduced as the energy mix is now more diversified.

Jahangir et al. then published in the same year in [39] where a number of other Wave Energy Converter (WEC) designs are considered in both an on-grid and off-grid connection using the same methods as in [38]. In the off-grid system, an additional diesel generator is connected to the system to provide backup when no renewable energy is available. This time, two different Iranian cities are analysed, Royan, on the Caspian Sea, and Shirinoo on the Persian Gulf. This study uses the same 250Wp solar panel as the Author's previous work but this time uses a 250W wind turbine. Jahangir et al. this time explores various WEC technologies, comparing each on their rated power and power produced at wave heights less than 4m, concluding that the Wave Star, OWC-SPA and OS-RM5 offer the best solution for the wave resource at the two locations.

WaveStar is a fixed bottom point absorber, where the motion of the floating buoy rotates an arm to drive a hydraulic PTO, rated to 600kW. OWC-SPA is a novel type of WEC combining principles of an OWC with a submerged point absorber, rated at 750kW. OS-RM5 is a concept design of a floating oscillating surge wave energy converter, produced by National Renewable Energy Laboratory (NREL), rated to 360kW. All analysis considers and compares all three WEC types.

Figure 2.13: Energy Profile with the Addition of a Wave Energy Converter from [38]

In the off-grid analysis, there are two scenarios: where diesel is used as a main component in the HRES and when the generator is only used when peak demand can not be met by battery or renewable energy. The former example is not described as it is not relevant to this literature review.

In Royan city, where the available wave energy resource is higher, the cheapest system is the PV-Wind-Diesel-WaveStar with an LCoE of 0.182$/kWh. The most expensive system is the PV-Wind-Diesel system with an LCoE of 0.242$/kWh but does use 35% of the amount of diesel used in the WaveStar system but has double the number of wind turbines and 2.8 times the amount of battery capacity. Figure 2.14 shows the power flow of the off-grid scenario in Royan city, with and without the WaveStar. It shows that the PV and Wind capacity increase when removing the WEC and the amount of diesel generation increases.

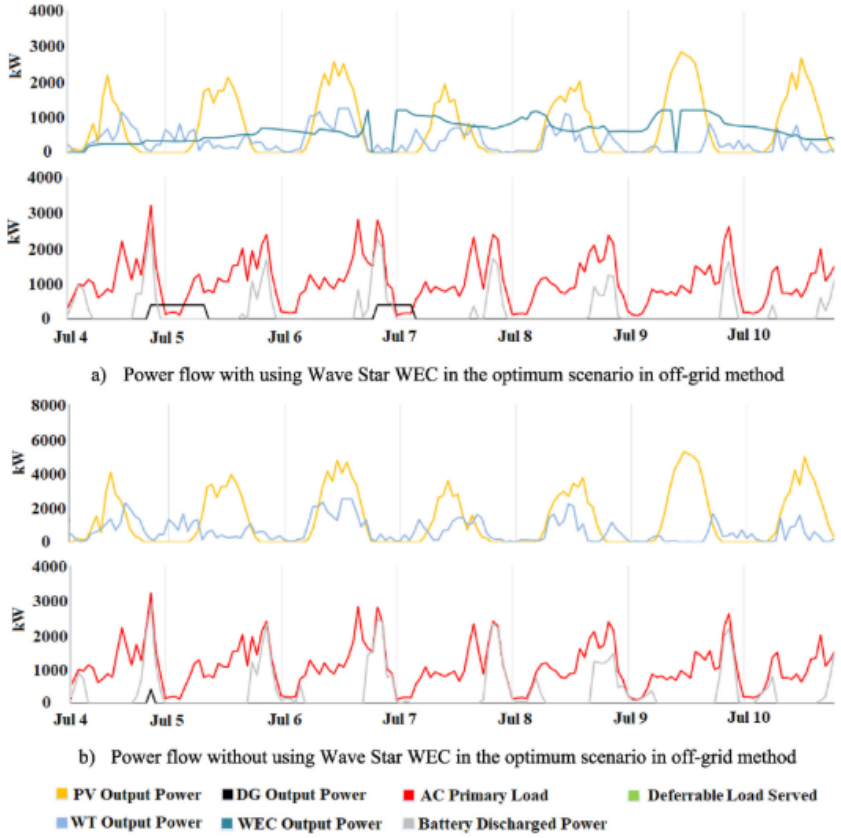

Figure 2.14: Energy Profile with the Addition of a Wave Energy Converter Edited from [39]

In Shirinoo City, where the wave resource is less abundant, the cheapest system is the PV-Wind-Diesel with a LCoE of 0.164$/kWh. The second cheapest system is the PV-Wind-Diesel-WaveStar with a slightly higher LCoE of 0.169$/kWh. There is 55% of the installed PV capacity and half the amount of wind turbines, the battery size and amount of diesel stay almost constant. This shows that for a small increase in cost, the system has been diversified with no negative effects. Strangely, the amount of diesel has only decreased by 0.5% despite the diversification of the supply. No comment on this is made within the source.

The remainder of the analysis is not relevant to this Thesis as it considers on-grid connection and diesel generation.

2.2 Combined Wind, Wave Platforms and Co-location

An emerging topic is that of combined wind and wave [40]. This takes two forms, co-deployment of wave energy converters and a floating wind turbine platform in one new device [41] [42] and co-location of wind turbines and WECs in-between the turbines [43] [44]. Both have the same aim, to increase the energy captured for a given area of sea bed, reduce the number of electrical and mooring structures, and to smooth power output. Wave Energy Scotland state that "Sharing infrastructure, services and supply chain between wind and wave energy projects can reduce the wind Levelised Cost of Energy (LCOE) by up to 7% and the wave LCOE can decrease by up to 40%. The combined LCOE of a shared project can be up to 12% lower than separate projects." [45] [46]

These are also key objectives of this thesis of combing wave and solar energy. However, the seasonal variation of wind and wave are more closely correlated than that of solar and wave. As [44] concludes "the combination of wave and offshore wind is more effective in reducing down- time and variability at sites where both resources are only weakly correlated". Even if the resources are strongly positively correlated, the combination of wind and wave resources will be valuable to a large scale grid, especially as national energy demand peaks in winter. However, they will not be as a significant benefit to continuously available power and seasonal resource smoothing as solar and wave combined resources. Whilst wind and floating offshore solar may be co-located, see Section 2.3, it may be difficult to co-deploy wind and solar on the same platform. Therefore, for niche off-grid demands, wave and solar are a logical combination.

2.3 Floating Solar

To better explore the impact of being offshore on the solar panels, the growing research topic of floating solar panels can provide insight into how the cooling effect influences yield and how the marine environment can increase O&M requirements of the solar panels onboard a WEC.

Renewable energy derived from solar photovoltaic panels is now the cheapest form of energy [19]. However, with conversion efficiencies in the region of 21.2 - 27.6% [47] (for crystalline silicon cells at standard test conditions), the land requirements are 0.5-0.7MWp/ha [48], using up scarce land resource. For example, The Bhadla Solar

Figure 2.15: Mocean BlueHorizon and Floating Wind Co-located farm

Park in India is the largest solar plant by area, over 56km^2 [49], and second largest by installed capacity, 2.25GWp [49] [50], costing $1.4billion [49]. This problem has become so prevalent that in 2015 the UK government removed the rights of farmers to "claim subsidies for fields filled with solar panels under new plans to ensure more agricultural land is dedicated to growing crops and food." [51].

Floating solar plants are a concept where solar panels are installed on floating platforms over water. The platforms comprise several plastic modular sections joined by hinges as in Figure 2.16, showing the installation of the UK's highest capacity floating solar array at the Queen Elizabeth II reservoir [52]. In this case, the reservoir is owned by the local water authority and the power produced offsets the energy expenses used to power nearby water treatment and pumping stations [52].

The majority of the installed floating solar capacity is installed on freshwater basins such as reservoirs or lakes. The significant benefit of floating solar is that it does not consume valuable land space, allowing for alternate uses such as housing or agriculture [53]. Additionally, the panels act as a cover that can reduce evaporation in reservoirs [53], and reduce algal blooms. This is especially important when combining floating solar with hydroelectric schemes where evaporation reduces the amount of energy stored [54] as in The Sirindhorn development in Thailand. Sirindhorn is the largest floating solar hydropower hybrid scheme in the world [55], owned by

Figure 2.16: Modular Pontoon used at the UK's largest floating solar plant [52]

the Electricity Generating Authority of Thailand, producing 45MW through 720,000 square metres of panels [56]. The Electricity Generating Authority of Thailand plan on installing more floating solar arrays in the country to reach a total capacity of 2.7GW [55]

Floating solar arrays also benefit from an 10-15% increase in efficiency arising from the cooling effect of the water [55]. However, the magnitude of this increase is disputed and is difficult to capture in numerical modelling [57] [53]. Some studies claim an increase up to 15.5% [58] but one example is as low as 2.3% [59]. One study compared floating solar to ground-mounted solar and found a 3.37 cents/kWh lower levelized cost of electricity, and 6.08% higher internal rate of return [20]. However, the marine environment can degrade the panels and motions between pontoons will fatigue the cables and joints.

The popularity of freshwater floating solar is increasing, with research suggesting that the worldwide installed capacity is likely to produce 710TWh/yr by 2030 [60] and the market size is estimated to be 30m USD and grow at a rate of 22.5% until 2030 [61].

China is a large proponent of floating solar arrays. In 2017, a 70MWp, 0.6km^2 floating array was commissioned near Huainan, when completed it was the largest floating solar farm in the world [62]. In the years since then, two larger arrays have been completed, both in China. The Three Gorges New Energy Floating Solar Farm is

also near Huainan but with a capacity of 150MWp [63]. The largest farm in the world is the Dezhou Dingzhuang Floating Solar Farm with a capacity of 320MWp, covering nearly 6km^2 [64] [65]. However, China will not hold this crown for long as the 600MWp Omkareshwar Reservoir floating solar park in India is due to go online in 2023 [66].

2.3.1 Floating Offshore Solar

Floating solar is still yet to make the leap to an offshore environment where the available area and capacity are many times that of the available freshwater basins [67]. Being offshore has similar benefits to being over fresh water, however, there are hurdles of the presence of waves, saltwater, sea life, bio-fouling, longer cable distances and deeper water to overcome. The initial target locations are close to shore where the wave action and length of transmission cables would be limited [67].

Whilst freshwater floating panels are exposed to wave action, the size of the waves is small due to the limited fetch distance. Despite this, freshwater arrays have been damaged by large winds, causing fires. For example, the destruction seen at the Yamakura Dam where wind speed exceeded 41m/s during a typhoon [68]. Deeper water combined with larger waves suggests that existing pontoon designs are not likely to survive an offshore environment [69]. Saltwater will accelerate the degradation of panels and electrical components [70] but can also be deposited on the face of the panel, shading it from sunlight [71]. It is therefore important that the panels selected to be used offshore have a suitable rating for saltwater as defined in the IEC 61701 salt spray test [72] and sufficient IP ratings to ensure protection from water. Larger sea life such as seals could potentially use large floating platforms to rest or hunt, potentially damaging the panels or floaters. Accompanying the sea life is increased bio-fouling from marine growth or sea birds, likely to cover the panels and shade the cells [69].

One paper [73] explores the modelling of an offshore floating pontoon in the North Sea and compares this to an onshore panel at Utrecht University. The model is comprehensive and includes the effect of wave action on the pontoon which in turn changes the tilt angles of the panels and thus the effective irradiance meeting the panel surface. Z.Golroodbari and van Sark state that the cooling system of a floating PV system is driven by wind speed and relative humidity and that the ambient temperatures tend to be lower at sea. In this case, the average ambient temperature is 5.05°C lower offshore, combined with wind speeds 3.76m/s higher and 8.1% higher humidity an apparent temperature is 9.36°C lower. The results show that the offshore

panels achieve a yield 3.49% higher than the onshore equivalent. However, the GHI is also 8.54% higher offshore, which would contribute to higher yields. A more like-for-like comparison is provided by comparing the performance ratio of the two systems. It was found that the offshore system had a performance ratio 3.15% greater than the onshore performance ratio of 81.66%. This suggests that given the same irradiance, the offshore system would still outperform the onshore system.

Floating Offshore Solar Panel Developers

Only a handful of companies exist which have installed floating offshore solar arrays, Oceans of Energy [74], Solar Duck [75], Ocean Sun [76] and Profloating [77]. They have different philosophies, with Oceans of Energy and Profloating using the tested method of pontoons. Whilst Solar Duck use experience from the oil and gas sector to develop a large floating tri-spar. Oceans of Energy will benefit further from the cooling effect due to the proximity to the water surface, but will however be more exposed to the wave loading. Solar Duck has the opposite approach whereby standing the panels off the water surface is less likely to be damaged but will not have the same cooling effect. The flexible membrane design used by Ocean Sun, is hoped to dampen the wave response to reduce structural stresses [78].

2.4 Biofouling

Biofouling is the fouling of structures due to the natural environment they are within, this is especially pertinent to marine structures where plants, algae and animals attach themselves to structures this can alter the performance of any structure in the sea [79]. For solar panels at sea, there are the added impacts on performance and yield.

Floating panel arrays in lakes and reservoirs are attractive to seabirds as they offer a large and sheltered platform from which to hunt and rest. Thus, it is unsurprising that floating solar panels tend to be covered in bird guano more so than rooftop panels [80]. The presence of the bird guano not only obscures the surface of the panel, reducing the power output by approximately 2% [81] [82], but this partial shading also can produce hotspots which would degrade the internal structure of the panel [83] [84]. Additionally, as guano is acidic, over time this can break down the materials of the panels [84], leaving an etching shadow on the surface reducing output even after the surface is cleaned [80].

It is clear than reducing the amount of biofouling on the surface of solar panels is critical to the yield and operation of the system. Panels can be cleaned once fouled, to differing levels of benefit, however, for large arrays, far from shore, this can be an expensive process, reducing the economic benefits of adding a solar array. Robotic cleaning is possible, albeit expensive, but the use of these machines offshore is limited. Therefore, preventing the amount of biofouling deposits is the best measure to improve up time.

2.4.1 Bird Guano Deposition Mitigation

To reduce the impact from bird deposits, birds can be deterred from the structure. This could be passive visual deterrents or more active deterrents like lasers [85] or loud speakers [86], both of which have been tested at sea on floating panels or oil rigs. Alternatively, the angle at which the panel is mounted may help reduce the impact of guano on production, offering a smaller “perchable” area by being steeper. However, at a certain point, the panel is mounted at a steep enough angle that birds may perch on the top edge and deposit guano down from there [84]. This results in the bathtub curve in Figure 2.17, where the average power loss is compared with the tilt angle for a flat plate panel. The impact on a curved panel is not documented.

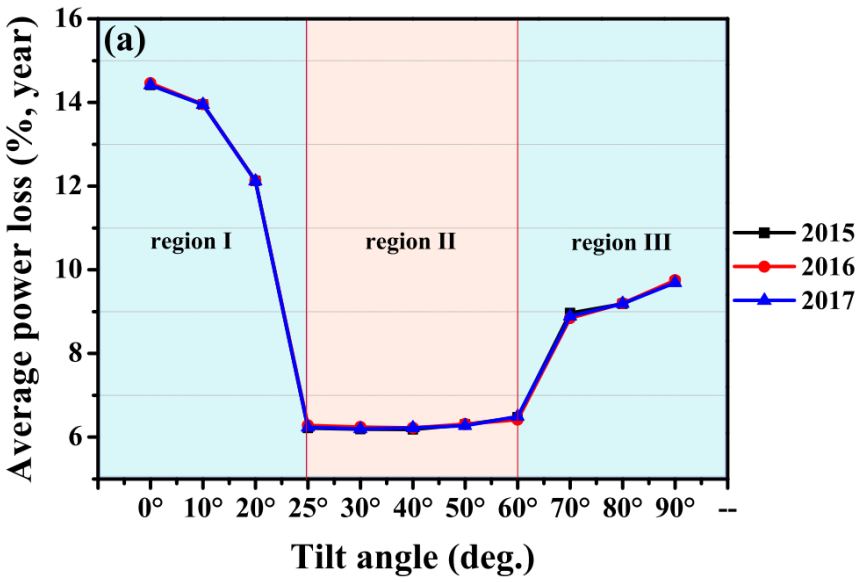

Figure 2.17: Guano Fouling Loss Due to Tilt Angle [84]

2.4.2 Marine Biofouling Mitigation

Historically, to reduce the effect of fouling due to marine life, paints containing toxic materials were applied to deter marine growth. However, this is now banned and would obscure the panels surface.

Recently, new methods in anti-soiling coatings which have minimal impacts on the optical absorption properties of the panels have been researched. These come in two main types; hydrophobic and hydrophilic coatings, both rely on water droplets to carry away contaminants [87]. Ideally the coating will have no impact on the yield of the panels and remove the need for entirely [88].

Coatings are made up of different chemcials but all see impacts on the PV yield and degrade over time, requiring re-coating. However, the results are positive and so is the trajectory of the research. Initial findings show reductions in soiling rates of 80% however, this can reduce to only 20% reductions after long term exposure [88]. Commercial coatings do exist such as the Nanoshield™ Liquid Glass [89] but these come with an application life of 12-18 months so will require regular reapplication. Furthermore, their effectiveness on marine biofouling is limited and appears to focus on airborne dirt or dust particles.

Generally, the focus of coatings for PV panels appears to be on land based, rigid glass panels repealing dirt or bird fouling rather than marine biofouling [90] [91] [92]. Research on marine biofouling mitigation tends to focus on structural components rather than the surface of solar panels [93] [94] [95] [96]. Therefore, the combination of the two, focusing on floating solar biofouling mitigations coatings appears to be novel and limited in scope.

2.5 Literature Review Summary and Identified Gaps of the Literature

This section concludes the findings of exploring literature focusing on combined solar and wave energy systems. The main findings are:

1. There is a lack of published literature focusing on a singular combined wave and solar device.
2. The idea of "wavevoltaics" has been introduced, where the open space of a WEC is utilised for solar energy

3. A combined wave and solar device has been conceptualised. However, this concept is basic and the influences of being offshore in a dynamic environment on yield, the full costs and a yield assessment are neglected.
4. Further literature describing the combination of the two energy systems but as separate physical installations have been identified, but this is still limited in quantity.
5. The majority of literature considers a land-based solar array combined with an oscillating water column wave energy converter. One example of land-based solar combined with the Pelamis converter was found. All of these examples were connected to a national grid, some had additional battery energy storage.
6. Combining wave and solar does offer more consistent energy production, reducing the need for large-capacity battery energy storage and maintaining a DC link voltage.
7. Combining energy sources can reduce the total levelised cost of energy if the capacities and available energy resources are appropriate.
8. Combining energy sources improves the capacity factor of a system.

Gaps discovered in the literature are:

1. A yield assessment of a combined WEC with on-board solar has not been published
2. Concept designs of a combined solar-WEC do not consider all the effects of being offshore or being mounted on a dynamic platform on the yield of solar array.
3. Curved panels on a solar-WEC have never been considered or assessed.
4. Experimental data, in a laboratory or in the real-world, of a combined Solar-WEC has never been published.
5. Effects of being offshore, in an energetic wave environment, on the survivability of panels have not been considered.
6. The possibility of bio-fouling and ways to overcome this have not been considered.
7. The effectiveness of a maximum power point tracker offshore, has not been considered


SPILL KIT

PART II

Experimentation

Chapter 3

Comparison of Panel Types Through At Sea Testing of Hybrid Solar Wave Energy Converter

Following a review of the state of the art, it was apparent that there is a lack of available data from real-world testing of a hybrid Solar-WEC. Results from Wave Energy Converter (WEC) testing alone are a closely guarded secret amongst the respective developers.

Fortunately, the timing of this project and the first deployment of BlueX allow for combined solar and wave testing. Although the timeline to develop and install the solar test kit was short and had to not interfere with the remainder of the deployment timeline.

This chapter presents the first experimentation of a Solar-WEC; detailing the approach, results, and discussions before drawing outcomes and commenting on the next steps.

3.1 Introduction

To explore how valuable the addition of solar panels may be, two solar “skids” were installed on the BlueX WEC during its deployment in the European Marine Energy Centre (EMEC) nursery wave test facility at Scapa Flow as part of the Wave Energy Scotland (WES) programme.

The experiment is designed to explore a number of questions.

1. What is the deliverable power of a solar panel array in dynamic offshore conditions?

2. What type of solar panel technology is most suitable for a WEC?
3. What is the expected lifetime of a solar array in the marine environment?
4. What are the impacts on the operations and performance of the WEC due to the addition of a solar panel array?

Question 1 is investigated by obtaining the yield data of panels deployed on the wave energy converter. Question 3 is answered by examining the panels over their deployment. Question 4 is answered by documenting all operations required to maintain the panels during the deployment and any impacts on the WEC.

Question number 2 is concerning the two broad solar panel technologies that exist: rigid panels and flexible panels. Rigid panels are the more traditional solar panel where silicon photocells are encapsulated between sheets of glass and a “backsheet”, held together by an aluminium frame. The backsheet is used to isolate the circuitry from the external environment, usually made of a polymer. Flexible panels do not have a metal surrounding frame or surface glass and instead are encapsulated in plastic; this allows the panels to bend up to 130 degrees to fit a surface.

Each technology has benefits and drawbacks. Rigid panels have a metal frame, so are easily mounted to the WEC with bolts, allowing easy maintenance and replacement. Flexible panels adhere directly to the surface using adhesive and thus are not be as easy to install and replace. However, they may last longer as they are made of plastic rather than glass and aluminium.

The operating temperature of the panels is critical to the efficiency of their output; a higher temperature reduces the efficiency to convert sunlight to electricity. Therefore, under the same irradiance, a cooler panel will produce more energy than a warmer one. Due to the different mounting methods, the two panels have different heat paths. The rigid panels have both sides exposed to the environment whilst the flexible panels only have their top surface exposed to the environment whilst the backside is in contact with the steel hull of the WEC. The conductive heat path could be more consistent and effective than convective air cooling as shown in Figure 3.1. Table 3.1 shows a comparison of the two technologies.

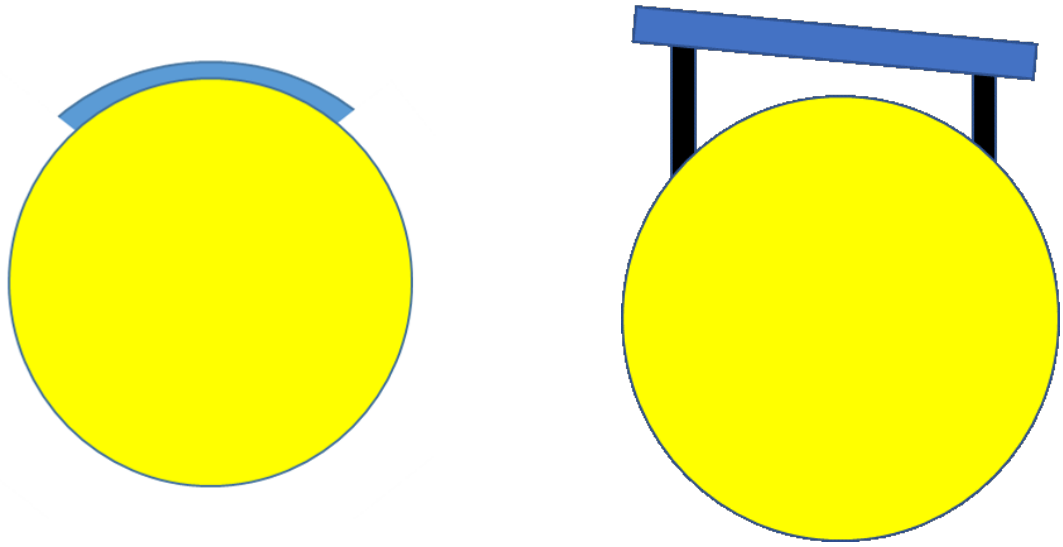

(a) Flexible Panel Mounting **(b)** Rigid Panel Mounting

Figure 3.1: Different Mounting Methods for the Two Solar Panel Types

Table 3.1: Benefits and Drawbacks of the Two Technologies

	Rigid	**Flexible**
Mounting Method	Bolted, easy to install and maintain	Adhesive, harder to remove if there is a fault
Materials	Glass, aluminium. Potentially brittle and easily corroded.	Plastic. Potentially more resilient to the environment.
Cost	More established tech, tend to be cheaper	More expensive
Mass	Heavy panels, heavier system when mounting frame included.	Lightweight panel and no mounting structure required.
Heat Path	Mainly convection driven, dependent on wind.	Conduction driven through back surface into WEC hull.
Efficiency	More established technology, tend to have higher efficiency	Lower efficiency at standard test conditions

3.2 Experimental Approach and Methods

3.2.1 Experimental Set Up

The first Mocean prototype, BlueX, was deployed in Orkney to evaluate the performance of the Wave Energy Converter. During this deployment, solar panels were installed on BlueX and the electrical output and panel temperature of them were monitored. Each set of panels is mounted to a “skid” with a self-contained data acquisition system which can then be bolted to the WEC via mounting brackets. One skid was mounted to the front section of the WEC and the second skid was mounted to the aft section of the WEC as in Figure 3.2.

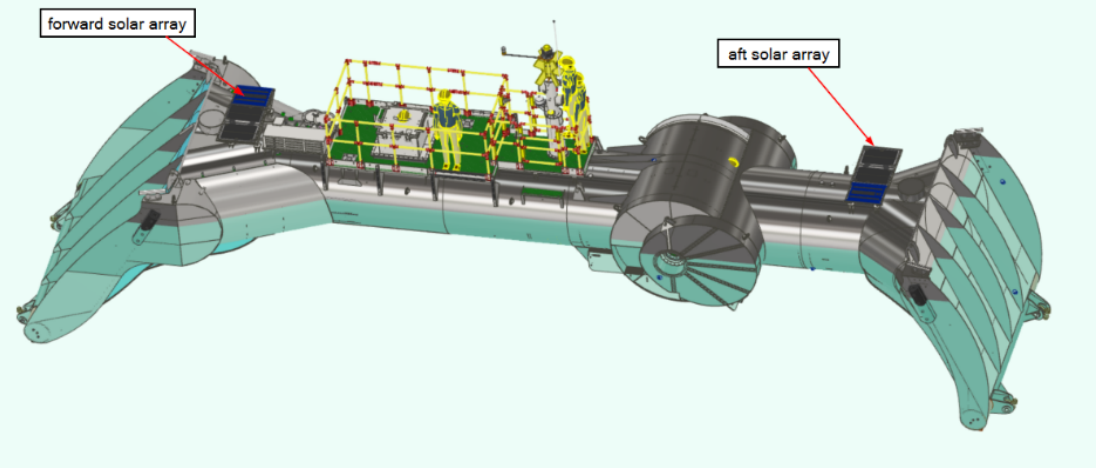

Figure 3.2: Location of Solar Arrays on BlueX Wave Energy Converter

Each skid consists of three 50W Renogy panels, one rigid panel and two flexible panels. One flexible panel was laid flat and the second was laid on a 3-meter radius curve. This allows the panel type to be compared, as well as the effect of curvature on the power production. A comparison between skids then measures how the front and more energetic aft section impacts yield. 3 meters was chosen as this is a future planned hull radius for large Wave Energy Converters.

The Panels

The panels were chosen due to their advertised use on boats suggesting robust manufacture and their size allowed three panels to fit side by side on the WEC. The panels have passed the necessary testing including IEC 61701:2020 [97] which details a salt spray test but doesn't necessarily cover submersion in salt water. To improve serviceability, the panels were further marinized by:

- Potting the junction box with epoxy to prevent shorts and water ingress. This would restrict the replacement of bypass diodes so may not be suitable for a full scale deployment.
- Additional silicone sealing against water ingress around the front and back edges of the rigid panels and outside edges of the flexible panels.

The panels, RNG-50D-SS and RNG-50DB-H, are shown in Figure 3.3.

The panels were electrically similar, thus allowing for common components to be used across both data acquisition systems, to reduce cost and complexity. Table 3.2 shows the properties of each panel.

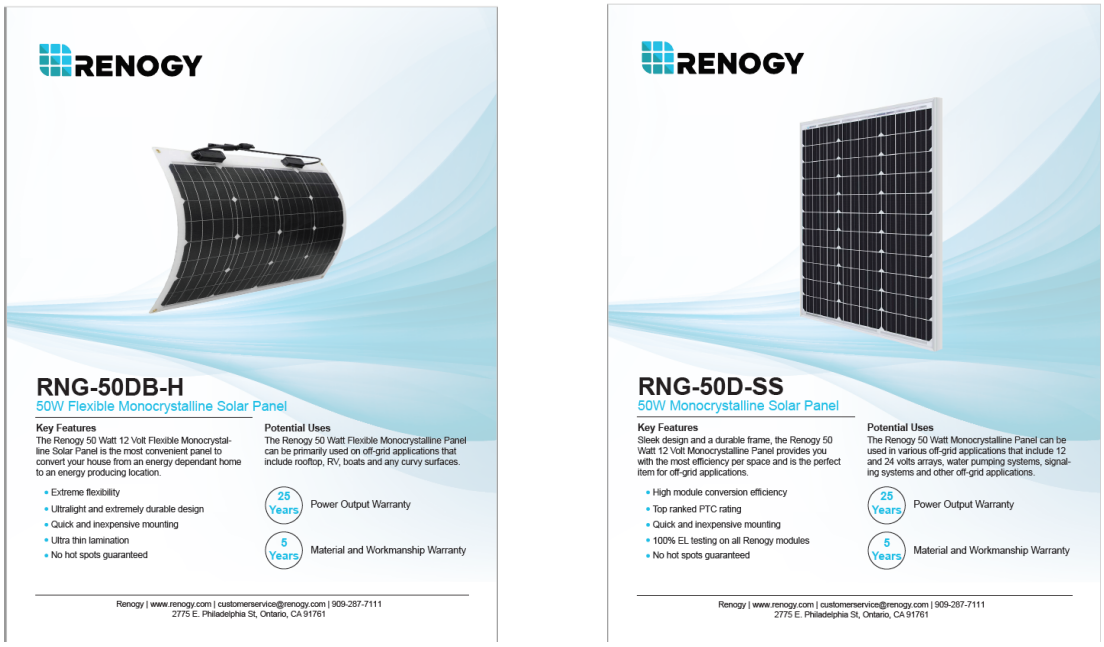

(a) Flexible Panel Datasheet **(b)** Rigid Panel Datasheet

Figure 3.3: Datasheets for the Two Solar Panel Types

Table 3.2: Electrical Parameters of the Two Technologies

	Rigid RNG-50D-SS	**Flexible RNG-50DB-H**
Power	50W	50W
Optimum Operating Voltage	18.3V	18.5V
Optimum Operating Current	2.9A	2.7A
Open Circuit Voltage	21.8V	22.6V
Short Circuit Current	3.1A	2.92A
Efficiency	21%	21%
Temp Coefficient of Pmax	-0.44%/C	-0.42%/C
Temp Coefficient of Open Circuit V	-0.30%/C	-0.31%/C
Nominal Operating Cell Temperature	47	45

3.2.2 Mechanical Work

To make sure the integration of the solar experiment was as smooth as possible, the mechanical design, fabrication and commissioning of the solar skids was completed by Blackfish Engineering [98]. The skid steelwork design can be seen in Figure 3.4a. The main components are the mounting feet, rigid panel mounting, and flexible panel mounting box. The structure below where the flexible panels sit was enclosed to simulate a full-scale development where the backside of the panel are protected by the WEC hull. There were cutouts for the temperature probes so that they can be mounted to the underside of the flexible panels.

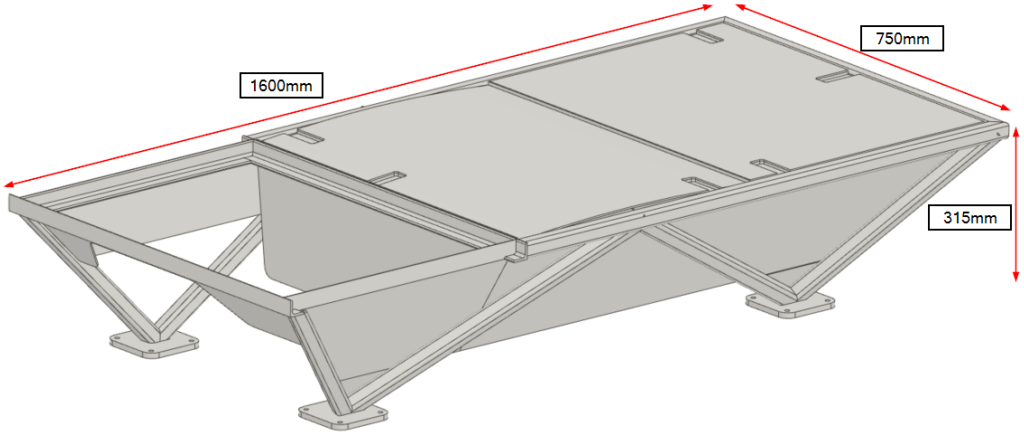

(a) Dimensions of Skid

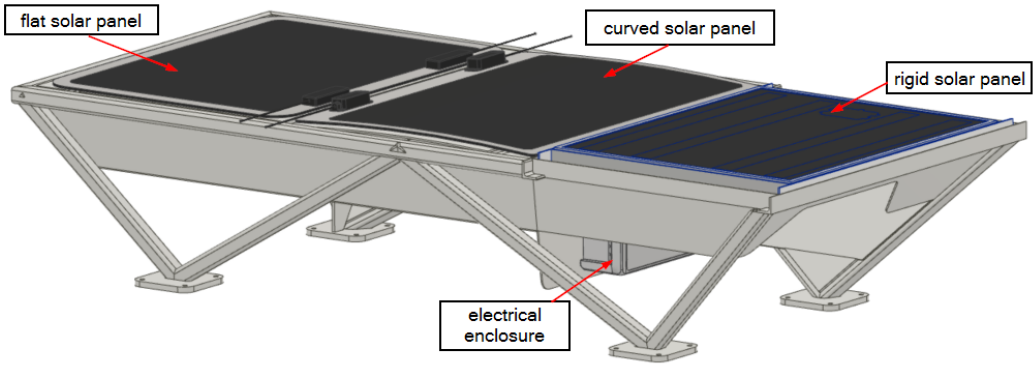

(b) Assembled Skid

Figure 3.4: Skid used in the Experiment

The skids were finite element simulated for wave loading and evaluated against relevant British standards. The rigid panel was spaced off the frame using rubber spacers to prohibit corrosion and then bolted to the skid. The flexible panels were stuck to the frame using marine-grade Sikaflex 291i adhesive and an additional marine tape was applied around the edges to prohibit peeling. The junction boxes of the panels were rated to IP68 and MC4 connector plugs were used for cable connections.

3.2.3 Data Acquisition System

The system was intended to be independent from the WEC to reduce the complexity of integration with the electrical system and to avoid bridging the hinge with a cable which could be prone to fatigue and failure.

The output of solar panels is dependent on their electrical load. If it was connected to a constant dump load then the voltage and current output would be restricted to those values which correspond to the chosen resistance and may not necessarily represent the maximum power output. This is what maximum power tracking techniques are for and is a focus of later research. Each system could be paired with a Maximum Power Point Tracking (MPPT), battery and load but this would increase the cost and complexity of the system. Instead, to get a good measure of the maximum potential power output, the open circuit voltage and short circuit current were measured and an estimated maximum power was calculated.

The system was controlled by an Arduino which uses a potential divider with a high resistance, more than a MΩ, to measure the voltage and an external chip – the ACS723 – to measure current. An external temperature-compensated oscillator real-time clock was used to keep an accurate time. The clock was powered via the Arduino but also has its own external power supply from a small coin battery cell which allows the Arduino to be put into sleep mode and awoken to account for hours of nighttime where no useful data could be harvested, this will extend the battery life of the system. To measure temperature, the DS18B20 Sensor was used as it is simple and waterproof.

The open circuit voltage and short circuit current cannot be measured simultaneously, so the data acquisition system uses a MOSFET to switch between an open circuit and a short circuit. The switch goes between each state every second and makes 10 measurements during its on-time. The 10 measurements are then averaged to obtain an average power for each 2-second cycle. The backsheet temperature of each panel was recorded every two seconds. The data was logged locally to a comma-separated file on a 32GB SD card allowing approximately 250,000 hours of data acquisition, plenty for this test.

The data acquisition system is powered by high-capacity D battery cells. Each cell has approximately 22,000mAh of capacity and operates at 1.5V. The pack consists of 12 cells, 6 parallel strings of two cells in series. A boost converter was then connected to the battery power output to increase the voltage from 3V to 5V. This pack can provide power for between 6 to 7 weeks before it needs replacing. Non-rechargeable primary cells are used for their lower cost and higher capacity.

The system was finalised and migrated to a PCB board, then tested for accuracy before being installed on the solar skid as seen in Figure 3.5.

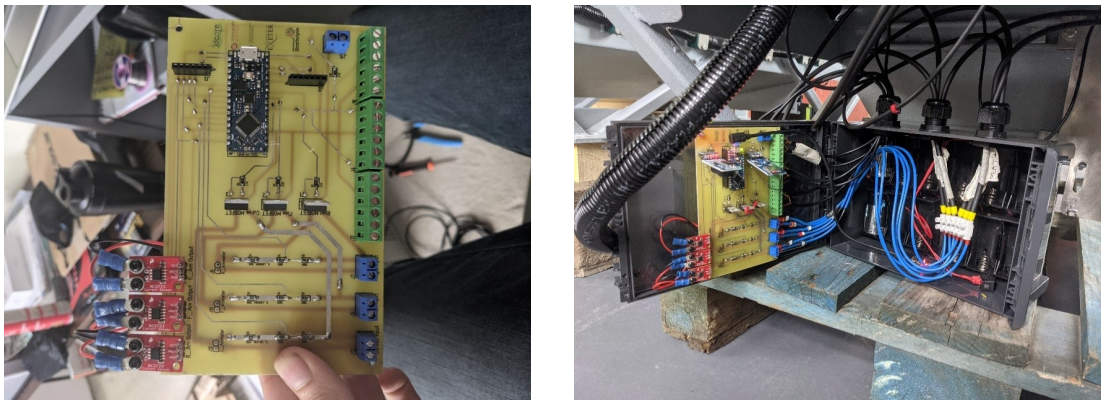

(a) Completed PCB **(b)** Completed Enclosure with Solar Inputs

Figure 3.5: Data Acquisition System

Accuracy of the Data Acquisition System

The completed PCBs were tested for voltage and current accuracy. This was done with an external power supply to give a known input and then compared against the Arduino output. The voltages were tested from 0V to 30V in steps of 2.5V. Similarly, the current was tested every 0.25A from 0.25A to 3.5A. Both tests extend over the expected range of the experiment. The results of this test for the aft board can be seen in Figure 3.6.The behaviour of the results was consistent between all three boards and the magnitude only slightly varied.

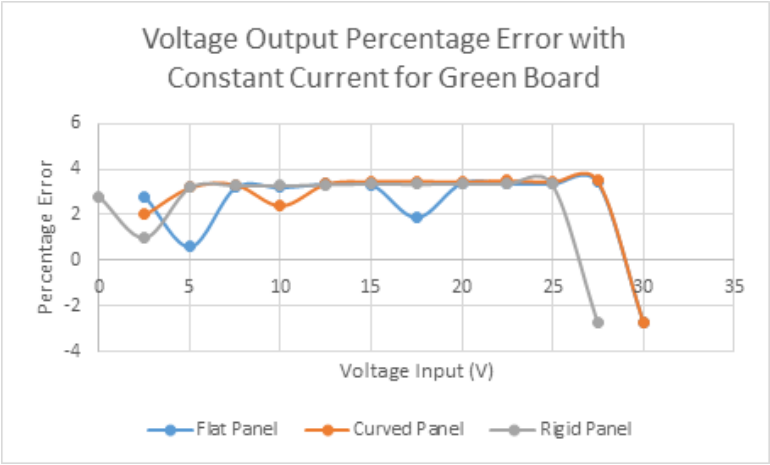

(a) Voltage Testing

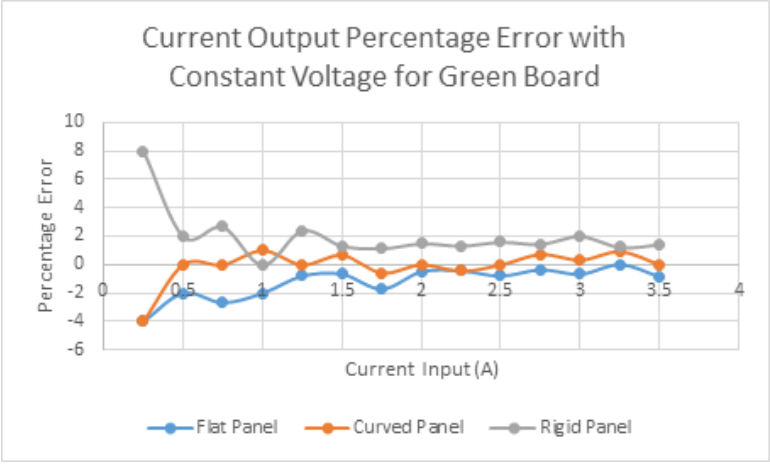

(b) Current Testing

Figure 3.6: Testing Results of the Data Acquisition System

Figure 3.6a shows that voltage has a consistent 3% over estimate at voltages between 0 and 25V. This can be down to the true values of the potential divider being slightly different to the value printed on the packed. The consistency over all three panels in all three boards can be explained by all resistors coming from the same “batch” and thus having the same error values. This error can be accounted for in post-processing and could have been negated by the addition of a variable resistor to get the resistance closer to that which was desired.

Another feature of these results is the sudden swing in error from consistent +3% to a negative value between 25 and 30V. This is down to the clipping of the voltage reading which occurs when the voltage input to the Arduino hits its maximum 5V. This is not an issue as standard test conditions state that open circuit voltage is 22V and the experiment is not likely to experience conditions above this.

As Figure 3.6b shows, the current output is not accurate at magnitudes below half an amp. This is because, at low readings, the magnitude of the noise in the ACS723 chip is significant when compared to the output current. Therefore, this error is random and should be accounted for in low-irradiance scenarios. The accuracy improves with higher readings as the noise becomes less significant.

3.2.4 Deployment Period, Location and Weather

The panels were installed onto BlueX on the 6th of September 2021 whilst it was deployed at the EMEC scale wave test site as shown in Figure 3.7, with approximate latitude and longitude of 58.9N 2.95W.

Figure 3.7: Scapa Flow Deployment Location [99]

The panels were powered on and left to gather data whilst the WEC was monitored. The wave conditions began calmly before a storm hit Scapa Flow on the 22nd and 23rd of September. This storm was severe with the largest hinge angles recorded in the solar testing period. A week after the storm, BlueX was brought off of its moorings and brought into dock for an inspection and modifications. Whilst the WEC was ashore, the solar skids and panels were inspected. Additionally, the data acquisition system batteries were to be replaced and data retrieved. As Figure 3.6 shows, the storm was so large that the rigid panel on the aft section was broken off its mounting on the skid, the power cables snapped and the panel was lost to the sea. As the remnants of the panel frame show, in Figure 3.8b the panel was bent up and away from the skid, suggesting a large upshot of water blasted the panel away from the WEC. This shows that even in the relatively calm and protected area of Scapa Flow, the panels can easily be damaged by waves. In a full-scale design, the panels will have to be suitably placed and protected to prevent waves from damaging the panels. Fortunately, the remaining 5 panels did not receive any significant damage. The panel was located on the sea floor using a remote-operated vehicle, shown in Figure 3.9, and later recovered using a fishing line and hook. This shows the relative shallowness of Scapa Flow and the ingenuity of the Mocean Operations Team.

(a) Aft Skid **(b)** Damaged Panel

Figure 3.8: Damaged Panel on Aft Section

Not only did the storm damage a panel, but both electrical enclosures housing the batteries, clock, memory card and control circuit also had severe water ingress. This damage destroyed the PCB board and batteries on both the front and aft section. All data on the front panels was lost. Fortunately, 16 full days and 2 partial days of data were retrieved from the aft panels giving over half a million data points to evaluate. The last data entry was on the 23rd of September at 05:08:22 which suggests the time when the experiment was destroyed.

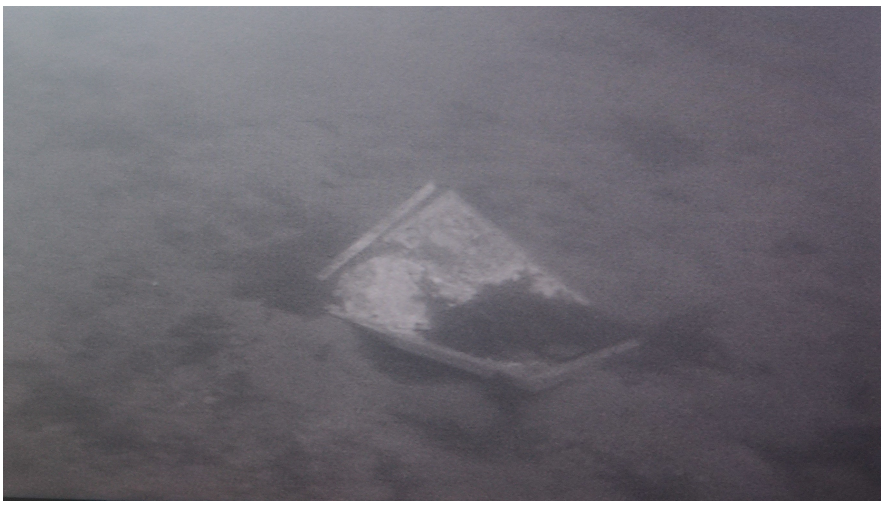

Figure 3.9: Removed Panel on the Sea Floor of Scapa Flow

Whilst the damage is disappointing, it shows how difficult it is to survive offshore and solidifies some initial concerns of the project that the panels may not be strong enough to survive the harsh environment. Further tests are carried out in which the electronics and panels are better protected in Chapter 4.

3.2.5 Bird Fouling

Birds, mostly terns, regularly rest and hunt from the WEC. The panels provided a flat and warm surface for the birds that consequently were heavily soiled as seen in Figure 3.10). As described in Section 2.4, this will reduce the yield and the lifetime of the panels.

Periodically, a team was deployed to the WEC to inspect its operation. Whilst there, the team inspected the conditions of the panels and documented the progress. Additionally, the team cleaned the panels as there was not significant enough wave loading to “self-wash” the panels as was initially hoped. This operation was only able to be carried out in calm sea conditions present on the 10th and 15th of September.

(a) Aft Skid on 10th September

(b) Aft Skid on 15th September

Figure 3.10: Bird Fouling of Aft Skid

3.2.6 Calculation of Panel Power Output

An estimate of the power output of the panels can be found by taking the product of the open circuit voltage, short circuit current and the panel Fill Factor (FF) at Standard Test Conditions (STC) as seen in Equation 3.1. The FF can be found by using Equation 3.2 and Table 3.3 which are values obtained from the panel datasheets.

$$Power = V_{OC} * I_{SC} * FF \tag{3.1}$$

$$Fill\ Factor = V_{MP} * I_{MP} / V_{OC} * I_{SC} \tag{3.2}$$

Table 3.3: Values used to calculate the Fill Factor

	Isc [A]	Imp [A]	Voc [V]	Vmp [V]	Fill Factor
Rigid Panel	3.10	2.90	21.80	18.30	0.7853
Flexible Panel	2.92	2.71	22.60	18.50	0.7597

Where “mp” is the maximum power point at STC, “oc” is the open circuit voltage and “sc” is the short circuit current. Initially, for ease and speed of calculation, the FF is considered to be constant throughout the testing period for each panel type. The FF can be analogous to efficiency and describes the ratio of the area described by the maximum power points of the I-V cure when compared to the area found by multiplying open circuit voltage and short circuit current as seen in Figure 3.11.

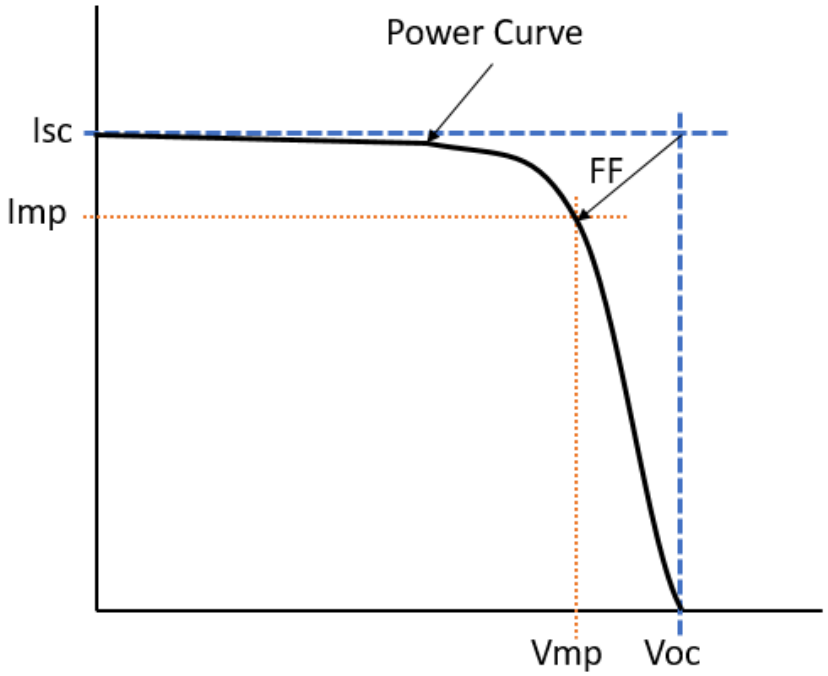

Figure 3.11: Typical I-V curve output of solar panel

3.2.7 Calculation of Daily Energy Output

A robust measure of performance is the energy produced by each panel on each day, found by integrating power over time, as shown in Equation 3.3, where the time step is the 2-second switching cycle. The result is energy in joules, which can be divided by 3600 to yield watt-hours.

$$Daily\ Energy = \sum_{i=n}^{i=m} Power(i) * (Time(i) - time(i-1)) = \sum_{i=n}^{i=m} (V_{OC} * I_{SC} * FF * 2) \quad (3.3)$$

Where “i” is the data point examined, “n” is the first point in the day and “m” is the final point in that day.

3.2.8 Temperature Compensated Fill Factor

In the calculation of panel power output, the FF is described as a constant characteristic of the panel, found in the datasheet. In reality, the FF is not constant and is heavily dependent on the cell temperature. Several sources in the literature [100] [101] [102] [103] describe the FF temperature coefficient for different panel types in different scenarios. By using the literature cited, an average of -0.00163/C is used to find an approximate FF compensation coefficient for the panels on the WEC. The true coefficient may vary from this value due to the difference in the panel used and the heat path which would affect how the cell temperature behaves.

To find the FF for the panel, the backsheet temperature is used in Equation 3.4. The power is then calculated in the same way as previously but the corresponding compensated FF is used instead of the constant value calculated form the STC. It should be noted that the temperature recorded is the backsheet temperature and not the cell temperature which would be higher than those recorded. To find the cell temperature, sensors would have to be inserted into the panel. Some thermal models can predict the cell temperature from the backsheet temperature but this depends on the makeup and thermal properties of the panel. Whilst the backsheet temperature is not perfect, it is a better representation than a constant fill factor.

$$Temperature\ Compensated\ Fill\ Factor = FF + (T_{Cell} - T_{STC}) * FF_{TempCoef} \quad (3.4)$$

3.3 Results

Over 540,000 data points were collected from 10:29:25 on the 6th of September to 05:08:22 on the 23rd of September. This set was trimmed to include only full days of data spanning 517,771 points from 04:00:00 on the 7th of September to 22:00:00 on the 22nd of September. The full number of points between these full days are not harvested as the skid system was set to sleep between 22:00 and 04:00 to save power whilst the sun was set. Therefore, it is assumed that irradiation and thus the short circuit current and open circuit voltage during the off period are both zero. This

is justified by multiple readings just before the off time and just after the on-time are 0. Showing that the on/off time selected was suitable and no useful data has been omitted from not monitoring during these times. When comparing these results to other data, the gaps overnight should be accounted for and time series synchronised.

Temperature occasionally presented erroneously as -127 Celsius this is thought to be due to a loose connection in the signal wire. For these scenarios, the reading is set to be equal to the last true data point.

3.3.1 Backsheet Temperature

Figure 3.12 shows the results from the backsheet temperature measurements through the testing period. There is a large flat spot on the 13th where there was a prolonged drop out of the temperature probes on all three panels and a smaller one on the afternoon of the 12th. All three temperatures seem similar but the rigid panel tends to peak higher than the others during the middle of the day. The panel temperatures spike way above ambient temperatures during periods of high irradiation, as the panel themselves produce heat as part of the photoelectric effect. The temperature on the 9th, 10th and 11th shows reduced peaks as well as on the 17th and 19th. This coincides with the measurements of current where the lowest short circuit current measurements are made on the same days. This makes sense as the current is the main driver of temperature through I2R losses. Similarly, the greatest peaks occur on the 7th, 15th and 16th which coincide with some of the largest current meausurements.

Table 3.4 shows the maximum, mean and standard deviation of the backsheet temperature for each panel for each day. It shows that the flat panel had the lowest mean daily temperature for 12 of the 16 days. The rigid had the highest mean temperature on 8 of the 16 days and the curved had the highest temperature for 5 days. The rigid panel recorded the highest peak temperature of 36.88C on the 7th of September whereas the maximum temp recorded by the curved and flat panels were, 35C and 35.63C respectively. The difference between mean temperatures of the two flexible panels is no more than 0.78 degrees during the testing.

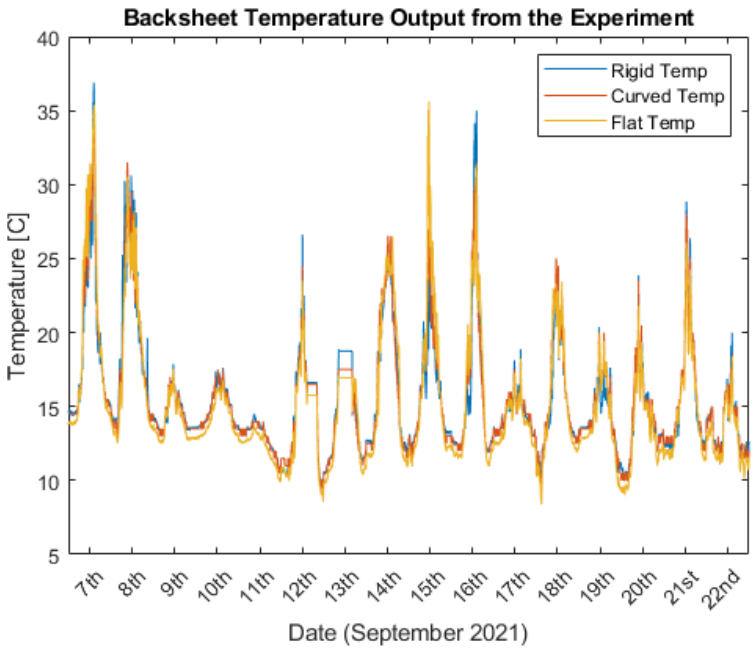

Figure 3.12: Backsheet temperature output from the panels on the Aft skid

3.3.2 Open Circuit Voltage

Figure 3.13 shows that the voltage value rises sharply from zero to a mean value which then oscillates for the remainder of the day. For most days, during the middle of each day, the voltage tends to be above 20V. The value at which the voltage appears to oscillate around varies from day to day. Measurements for voltage are lower on the 10th and 11th of September than on others. It can be observed that on all days, the open circuit voltage for the rigid panel is higher than the open circuit voltage for the curved and flat flexible panels. This is really evident on the 14th, however, this difference is less than 1 volt.

Table 3.5 shows the maximum, mean and standard deviation of the open circuit voltage for each panel for each day. It shows that the rigid panel has the greatest mean voltage of every day of the test period. The flat panel had the lowest mean voltage for 10 days and the curved panel for 6 days. The difference between the means of the two flexible panels is usually very small, less than 0.18V and an average absolute difference of 0.08V. The rigid panel is on average, 0.92V higher than the lowest flexible panel. The maximum voltage recorded was 22.85V on the 12th.

Table 3.4: Maximum, Mean and Standard Deviation of the Backsheet Temperature for each Panel for each day.

Backsheet Temperature [C]		Date (September 2021)															
		7	8	9	10	11	12	13	14	15	16	17	18	19	20	21	22
Rigid	Max	36.88	30.62	17.87	17.62	14.50	26.62	18.87	25.37	23.62	35.00	18.87	24.37	20.37	23.87	28.87	20.00
	Mean	19.55	19.76	14.45	14.19	13.00	10.62	8.66	17.14	15.91	16.24	14.52	15.34	14.28	13.94	15.50	13.72
	StdDv	5.74	5.35	1.14	3.58	0.94	6.93	6.15	4.60	3.05	5.85	1.19	3.71	1.78	2.67	4.41	1.65
Curved	Max	35.00	31.50	17.50	17.50	14.00	24.50	17.50	26.50	27.00	31.50	18.00	25.00	20.00	23.50	28.00	18.50
	Mean	19.89	19.47	14.44	14.12	12.94	10.55	8.50	17.22	16.25	16.28	14.49	15.63	14.53	14.03	15.67	13.53
	StdDv	5.87	5.25	1.13	3.57	0.99	6.70	6.00	4.90	3.72	5.35	1.14	3.98	2.20	2.77	4.31	1.64
Flat	Max	35.38	30.50	17.56	16.75	13.69	23.50	17.12	26.50	35.63	31.37	18.25	23.44	20.00	21.81	26.06	18.37
	Mean	20.18	18.91	13.97	13.54	12.28	10.10	8.42	17.27	16.78	16.24	13.97	15.25	13.98	13.25	14.95	12.94
	StdDv	6.69	5.16	1.29	3.42	0.96	6.48	6.09	5.35	5.52	5.44	1.30	4.19	2.46	2.77	4.01	1.71

Table 3.5: Maximum, Mean and Standard Deviation of the Open Circuit Voltage for each Panel for each day.

Open Circuit Voltage [V]		Date (September 2021)															
		7	8	9	10	11	12	13	14	15	16	17	18	19	20	21	22
Rigid	Max	22.43	22.34	21.94	21.37	21.34	22.86	22.85	22.20	22.66	22.71	22.77	22.66	22.17	22.61	22.62	22.44
	Mean	16.08	16.35	15.55	15.02	14.71	16.09	16.26	16.03	15.69	15.38	14.93	15.50	14.75	15.20	15.18	14.56
	StdDv	8.16	8.17	8.30	8.05	7.98	8.51	8.69	8.69	8.70	8.86	8.74	8.98	8.68	8.86	9.02	8.91
Curved	Max	22.33	22.03	21.69	21.11	20.91	22.54	22.46	21.89	22.26	22.40	22.46	22.34	21.89	22.20	22.26	22.14
	Mean	15.43	15.72	14.67	14.05	13.54	15.37	15.45	15.24	14.89	14.54	13.99	14.72	13.67	14.21	14.31	13.67
	StdDv	8.21	8.29	8.26	7.92	7.75	8.55	8.70	8.70	8.71	8.83	8.64	8.98	8.53	8.74	8.96	8.81
Flat	Max	22.23	22.00	21.61	21.04	20.86	22.43	22.31	21.86	22.20	22.31	22.43	22.23	21.89	22.09	22.32	22.09
	Mean	15.33	15.65	14.57	13.98	13.41	15.19	15.39	15.13	14.85	14.59	14.05	14.69	13.75	14.23	14.37	13.70
	StdDv	8.18	8.26	8.24	7.92	7.71	8.49	8.68	8.66	8.67	8.84	8.65	8.96	8.54	8.72	8.97	8.82

3.3.3 Short Circuit Current

The experiment short circuit current results are presented in Figure 3.14. As short circuit current is dependent on the value of irradiance, the magnitude of current varies day to day due to the daily changes in weather but also at a higher frequency due to the movement of BlueX. Any shading due to bird fouling should also be visible in reduced currents when compared to a clean panel. The currents spike towards the middle of each day as the sun gets higher in the sky, directly above the panel. There is a lot of noise in the graph. Some of this can be attributed to the noise in the current sensor but the more significant input is most likely down to the movement of the WEC.

The current rarely goes higher than 2 amps, as the experiment most likely never experienced high enough irradiances. It is hard to see how the three panels compare at this scale of the graph but it appears that the curved panel and flat panels have similar outputs with curved slightly higher and the rigid currents tend to be lower. Table 3.6 shows the mean, maximum and standard deviation of the panel currents per day. It shows that the curved panel had the highest mean current out of the three

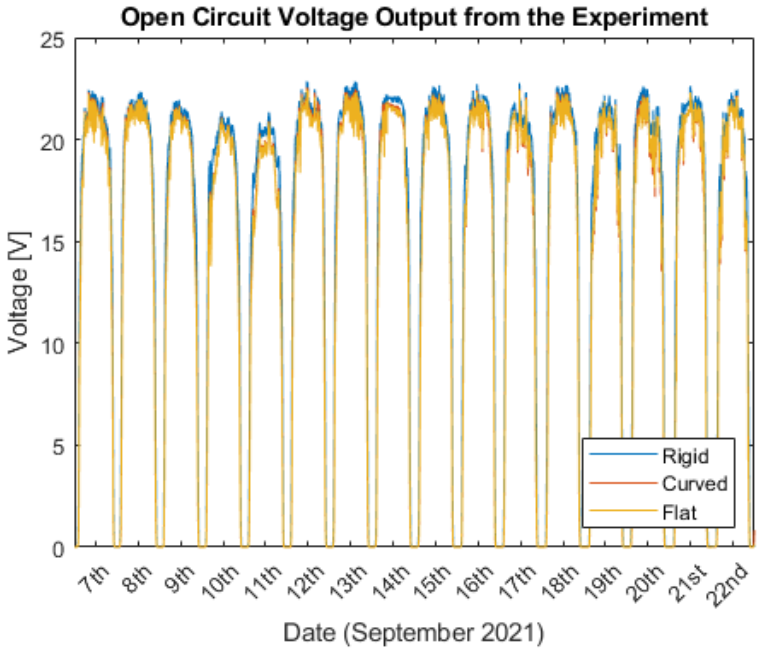

Figure 3.13: Open Circuit Voltage output from the panels on the Aft skid

panels on every single day during the testing period. The rigid panel had the lowest mean current on 13 days and the flat panel had the worst current on only 3 days. The highest currents recorded were 2.34A on the 12th for the rigid panel, 2.40A on the 7th for the curved panel and 2.16A on the 15th for the flat panel.

Table 3.6: Maximum, Mean and Standard Deviation of the Short Circuit Current for each Panel for each day.

Short Circuit Current [A]		Date (September 2021)															
		7	8	9	10	11	12	13	14	15	16	17	18	19	20	21	22
Rigid	Max	1.98	1.75	0.73	0.42	0.33	2.34	1.77	1.17	2.12	1.57	1.17	1.79	0.86	1.08	1.41	1.41
	Mean	0.42	0.40	0.18	0.10	0.06	0.33	0.45	0.39	0.34	0.32	0.13	0.29	0.14	0.17	0.25	0.20
	StdDv	0.50	0.41	0.19	0.11	0.07	0.35	0.53	0.40	0.41	0.39	0.15	0.34	0.17	0.21	0.29	0.25
Curved	Max	2.40	1.95	0.79	0.50	0.38	2.25	1.72	1.20	2.03	2.11	1.20	1.96	0.83	1.05	1.33	1.28
	Mean	0.54	0.51	0.23	0.15	0.11	0.36	0.47	0.45	0.39	0.41	0.19	0.41	0.19	0.20	0.27	0.23
	StdDv	0.60	0.46	0.19	0.11	0.08	0.34	0.49	0.40	0.40	0.45	0.17	0.42	0.16	0.20	0.27	0.23
Flat	Max	2.04	2.09	0.75	0.46	0.34	1.89	1.46	1.08	2.16	1.92	1.25	1.68	0.99	1.21	1.45	1.14
	Mean	0.44	0.48	0.20	0.12	0.08	0.29	0.41	0.40	0.37	0.40	0.16	0.34	0.17	0.19	0.26	0.19
	StdDv	0.50	0.48	0.19	0.11	0.07	0.29	0.43	0.38	0.42	0.45	0.16	0.38	0.18	0.22	0.29	0.22

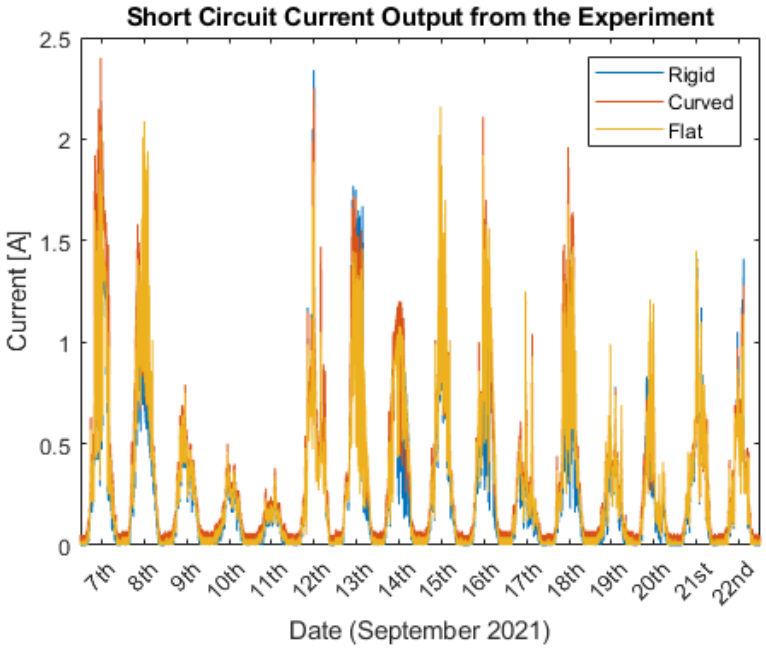

Figure 3.14: Short Circuit Current output from the panels on the Aft skid

3.3.4 Calculated Panel Power

Figure 3.15 shows the power output during the testing period of all three panels. The output looks very similar to Figure 3.14, in that the power closely follows the current due to the more uniform voltage output.

Table 3.7 along with Figure 3.15 show that on only two occasions is 40W exceeded from a panel. The curved producing 40.04W on the 7th and the rigid producing 41.80W on the 12th the maximum power produced by the flat panel was 36.10W on the 7th.

Table 3.7 shows that the curved panel produces the highest mean power on 12 of the 16 days with the rigid panel performing best on 3 days and the flat performs best only on one of the days. The rigid panel did perform the worst on average with the lowest recorded mean powers on 10 days. The greatest mean power is when the curved panel produced an average of 8.61W during the 7th of September. The lowest mean power recorded was on the 11th with 1.01W for the rigid panel.

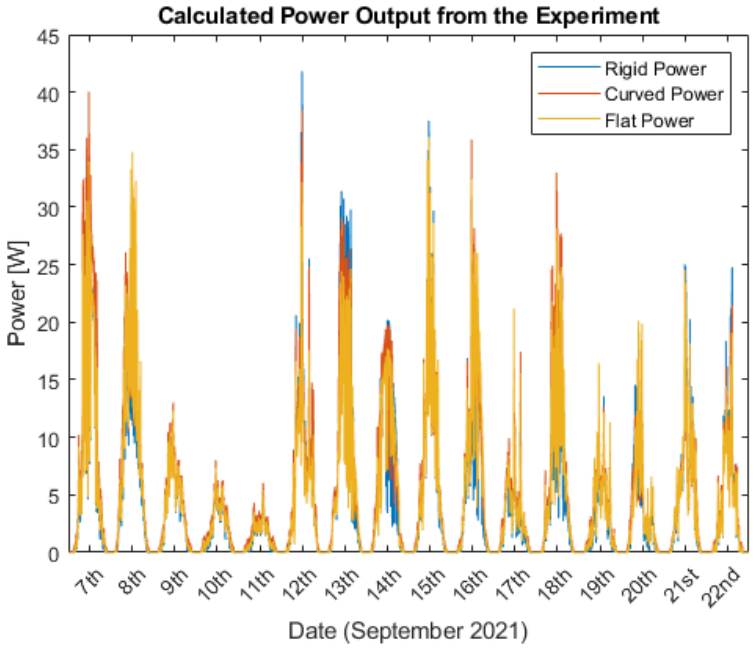

Figure 3.15: Calculated Power output from the panels on the Aft skid

3.3.5 Daily Energy

The daily energy is found from the methods described by Equation 3.3. Table 3.8 shows the results from this calculation. The best performing day for the rigid panel was the 13th where it produced 139Wh of energy and was the best-performing panel for that day. The best day for the curved panel was the 7th where it produced 155Wh of energy and the best day for the flat panel was the 8th where it produced 138Wh. The curved panel produced the most energy on 12 of the 16 days, the rigid on 3 days and the flat panel performed best on only one day. The day with the biggest difference between the best and worst performing panel was the 11th with a difference of 31% between the curved panel and the rigid panel. The 11th is also the day where all three panels gave their lowest yield. The day that the panels performed most similarly was on the 20th with a difference of 4%. The mean difference between all the best and worst performing panels over the testing period is 15%. The total energy for the rigid, curved and flat panels over the testing period is 1274Wh, 1422Wh and 1282Wh respectively.

Table 3.7: Maximum, Mean and Standard Deviation of the Calculated Power for each Panel for each day.

Calcultated Power [W]		Date (September 2021)															
		7	8	9	10	11	12	13	14	15	16	17	18	19	20	21	22
Rigid	Max	34.5	30.5	12.6	7.1	5.5	41.8	31.4	20.2	37.5	27.7	20.9	31.6	15.0	19.1	25.0	24.8
	Mean	7.1	6.7	3.0	1.6	1.0	5.6	7.7	6.6	5.9	5.5	2.2	5.0	2.3	2.8	4.3	3.4
	StdDv	8.6	6.9	3.2	1.8	1.2	6.1	9.4	6.9	7.2	6.7	2.5	6.0	2.9	3.6	5.1	4.4
Curved	Max	40.0	32.5	13.0	8.0	6.0	38.4	29.1	19.8	34.1	35.9	20.4	33.0	13.8	17.5	22.5	21.5
	Mean	8.6	8.0	3.5	2.1	1.5	5.6	7.5	7.1	6.2	6.4	2.8	6.5	2.7	3.0	4.2	3.4
	StdDv	9.9	7.8	3.3	2.0	1.3	5.7	8.5	6.8	6.8	7.5	2.9	7.2	2.9	3.4	4.5	3.9
Flat	Max	34.0	34.8	12.3	7.4	5.4	32.2	24.7	17.7	36.1	32.5	21.2	28.2	16.5	20.1	24.6	19.1
	Mean	7.0	7.7	3.1	1.8	1.1	4.6	6.7	6.3	6.0	6.5	2.5	5.5	2.5	3.0	4.1	3.0
	StdDv	8.2	7.9	3.1	1.8	1.2	4.9	7.2	6.2	7.1	7.4	2.7	6.3	2.9	3.7	4.7	3.6

Table 3.8: Daily Calculated Energy for each Panel.

Daily Energy [Wh]	Date (September 2021)															
	7	8	9	10	11	12	13	14	15	16	17	18	19	20	21	22
Rigid	127	121	54	29	18	101	139	119	105	100	40	90	42	51	78	62
Curved	155	144	63	37	27	101	135	127	111	116	51	116	49	53	76	61
Flat	126	138	56	31	20	83	120	114	107	116	44	99	46	53	74	54

3.4 Fill Factor Temperature Compensation

The process detailed Section 2.6 provides a FF which varies with backsheet temperature for each panel as seen in Figure 20. The horizontal lines show the constant FF used in previous calculations for the rigid and flexible panel types at 0.79 and 0.76 respectively. The temperature compensated FF is greater than the constant value for the majority of the period only reducing below during the peaks at midday on the 7th, 8th, 12th, 14th, 16th and 21st for the rigid panel whereas it is for the 7th, 8th, 14th, 15th,16th and 21st for both flexible panels. This is due to the backsheet temperature only increasing over the standard test condition of 25C at these times.

The daily energy was then calculated by using Equation 3 with a FF for each data point recorded. The energy with a constant FF and with a temperature compensation is then compared in Table 9. The comparisons between panels have not been affected by the use of a temperature compensated FF. The curved is still the best performing on 12 of the days, rigid for 3 days and flat for one day. However, the magnitude of energy harvested on each day over all three panels has increased on average by 1.3%. Individually, the rigid, curved and flat panels saw an average increase of 1.1%, 1.2% and 1.6% respectively. The only day in which the yield did not increase was the 7th of September where the rigid and flat panels saw no change but the curved panel

saw a decrease of 0.6%. The total extra energy collected by all three panels by using this method is 41Wh. The day with the most significant difference was on the 11th of September where the rigid saw an increase of 5.4% in its yield and the flat panel saw an increase of 4.9%, the curved panel saw no increase.

Table 3.9: Daily Calculated Energy with and without a Temperature Compensated Fill Factor.

Date (September 2021)	7	8	9	10	11	12	13	14	15	16	17	18	19	20	21	22
Rigid Panel																
Cnst FF	127	121	54	29	18	101	139	119	105	100	40	90	42	51	78	62
Temp FF	127	121	55	29	19	102	141	120	106	100	40	91	42	52	79	63
Difference [%]	0.0	0.0	1.8	0.0	5.4	1.0	1.4	0.8	0.9	0.0	0.0	1.1	0.0	1.9	1.3	1.6
Curved Panel																
Cnst FF [Wh]	155	144	63	37	27	101	135	127	111	116	51	116	49	53	76	61
Temp FF [Wh]	154	145	64	38	27	103	137	128	112	116	52	117	50	54	76	63
Difference [%]	-0.6	0.7	1.6	2.6	0.0	1.9	1.5	0.8	0.9	0.0	1.9	0.9	2.0	1.8	0.0	3.2
Flat Panel																
Cnst FF [Wh]	126	138	56	31	20	83	120	114	107	116	44	99	46	53	74	54
Temp FF [Wh]	126	139	57	32	21	84	122	115	107	117	45	101	46	54	75	56
Difference [%]	0.0	0.7	1.8	3.1	4.9	1.2	1.6	0.9	0.0	0.9	2.2	2.0	0.0	1.8	1.3	3.6

3.5 Discussion

The loss of the front panels and the land based panels no longer allows this experiment to determine a rigorous comparison between land and offshore solar panels, a main aim of the experiment. It also doesn't allow for a comparison between the front section and more energetic aft section to examine how WEC movement impacts the yield. It does however still allow for a comparison between the three panel configurations deployed onto the WEC.

Whilst the accuracy of the sensors and data acquisition system was investigated before the deployment began, and the results account for the error, they were not assessed again during or after the deployment. This was due to the damage incurred in the testing. However, the deployment did not last a significant amount of time and the data does not appear to change drastically over the time period. Therefore, the accuracy of the system and the results presented are expected to be accurate, or as accurate as the initial deployment.

3.5.1 Numerical Results

The flat panel saw the lowest temperatures on average but the curved panel saw the highest temperatures in the later period of testing from the 16th to the 22nd. However, the difference between the two panels is no more than 0.78 degrees during the testing. This is to be expected as they both share a connected thermal mass on which they are mounted. This temperature is directly correlated with the results for current. This is because if a panel has a higher current output, its temperature tends to be higher, for the same heat path.

All three panels experience similar noise in their voltage measurements but the behaviour of the noise changes day to day which suggests a systematic contribution, e.g. the movement of the WEC itself, as it turns towards and away from the sun. The rigid panel regularly has the greatest voltage. The voltages are more consistent day to day than the current but it does vary with ambient temperature, which is to be expected.

Current output is most dependent on the irradiance on the panel, which is a function of the orientation of its plane to the sun, which depends in turn on the time of day, WEC heading, roll and aft angle. There are additional factors which are less measurable or predictable such as the weather, water spray or bird fouling. The current measurements are very noisy, but all three currents of the panels seem to move together which is most likely to do with the WEC movements. The variability of the power output is dominated by the variability in the current, the voltage by comparison, being relatively stable. Meaning that the power has similar looking output to the current measurement. The highest peak power calculated was 41.8W on the 12th for the rigid panel. The panel with the best average performance, highlighted by the highest mean daily power is the curved panel on 12 out of 16 days. Unsurprisingly, the panel with the highest mean power on a day also had the highest daily energy.

The curved panel had the best energy yield compared to the other panels producing almost 150Wh more over the course of the testing period. This was not expected as it was initially thought that the losses would increase due to the difference in irradiance over the panel. This be due to the curve of the panel not being that pronounced and thus, the shadowing effect minimalised. The flat and curved panels should therefore behave more similarly than the results show. However, the flat panels underperforms, potentially due to manufacturing defects. The curved plate that the curved panel lays on was carefully produced to achieve the desired curvature. Whereas, the flat plate appears to have an element of warping which could be due to contraction during

welding. This may be the reason why the flat and curved panels do not behave in a similar fashion. The two panels may perform better than their rigid counterpart due to the reduced operating temperature, increasing the efficiency of the cells as initially hoped.

3.5.2 Fill Factor Temperature Compensation

Using a FF temperature compensation flattens out the power curves, reducing peaks and increasing the power at the start and end of the day. This calculation makes an attempt at capturing the fact that solar panel efficiency also varies with cell temperature. Using the FF temperature compensation only increases the energy yield by 41Wh or 1.3% over the course of testing. Additionally, as highlighted by the results on the 7th of September, using the FF compensation can result in lower energy yields which would be more likely on warm days. Therefore, over the course of a year, it is expected that the warm summers and cool winters would cancel each other out and the use of a FF temperature compensation would not be justifiable.

3.5.3 Operational Results

An operations team had to regularly visit the WEC to clean the solar panels from guano. This deployment was close to the coast, so cleaning the panels is a simple operation. However, as the distance to shore increases, this task becomes more significant and costly. The hope is that wave action would overtop the panels and give them an element of self-cleaning. This may work very rarely but if there is enough wave action to clean the panels, there will probably be enough wave energy to make the contribution from solar panel insignificant.

The damage sustained by the aft rigid panel in the nursery site shows how fragile the panels are in the marine environment. If a wave in a natural harbour can dislodge and destroy a panel, there is little chance in a more energetic site. The skids were designed with deflector plates on their front to protect from wave up jetting but the aft panel was left exposed from that angle due to the hull connection to the wave channel allowing a wave to ride up underneath the panel, almost from behind. In the future, more careful design steel work can be suitably placed to protect the panels from wave loading but will add to the mass and cost.

The flexible panels and the rigid on the front do not to have sustained any damage during testing or due to the marine environment. It is important to remember that the panels have only been deployed on the WEC for a short period of time, 16 days of numerical solar output data is available but the panels were actually out on the WEC for approximately 9 weeks.

Two additional conclusions have come to light during the decommissioning of the experiments, so are not described in the submitted paper. Firstly, the commonly used MC4 connectors are not suitable for use offshore, the connectors were investigated and severe corrosion was discovered despite the short deployment time. This would increase the losses in the system, reducing its effectiveness. This conclusion could also be relevant to offshore floating solar industry. Secondly, when the flexible panels were removed from the skid, despite taking extra care, it is possible that the panels experienced micro cracking. This reduces the effectiveness of the panels and makes them less likely to be re-used in scenarios where efficiency is critical.

3.6 Chapter Summary

This experiment set out to explore the hybridisation of solar panels deployed on a wave energy converter with the aim to answer four questions;

1. What is the estimated deliverable energy of a solar panel array in offshore dynamic conditions?
2. What type of solar panel technology is most suitable for a WEC?
3. What lifetime is to be expected of a solar array in the marine environment?
4. What are the impacts on the operations and performance of the WEC due to the addition of a solar panel array?

Unfortunately, circumstances prohibit some of these outcomes from being fully assessed as data was lost. However, the data from one set of panels for a period of 16 days was saved. Therefore an exploration into the impacts of installing one solar panel skid can still be carried out, answering questions 2 and 4 whilst partially answering 1 and 3.

1. The three 50W panels produced a total of 3.98kWh over the testing period. The curved panel produced the most out of the three panels, 1422Wh. The flat panel produced 1281Wh and lastly the rigid panel, 1276Wh.

2. The flexible panels produced more energy than the rigid panels over the same period, in the same location. The method of application is vastly different – bolts or adhesive – and would influence operations and maintenance strategies. The rigid panel was severely damaged during this short test, whilst the flexible panels were not.
3. This study did not last for a significant enough amount of time to determine the lifetime of a solar array. However, the rigid panel on the aft saw damage due to wave action.
4. Once the panels were installed, little operational work is required. Periodic cleaning may be required, if wave action cannot clean the panels. The panels are lightweight enough that they do not have a significant impact on the dynamic behaviour of the WEC.

It was found that the rigid panel regularly had the greatest open circuit voltage of the three whilst the curved panel tended to have the greatest mean short circuit current.

When initially calculating the power output of the panels, a simple approach was taken by multiplying the open circuit voltage and short circuit current by the FF determined by the standard test conditions. When carrying out this calculation, it was found that the curved panel had the highest mean power for 12 days of the 16 day test period. The rigid panel had the highest mean power for 3 days and the flat panel for 1 day. Unsurprisingly, this same pattern exists when examining the total daily energy where the curved panel produces the greatest energy on the same 12 days as its highest mean power. The same is true of the rigid and flat panels.

To examine if the use of a constant FF was inaccurate, a FF compensation method was carried out where the value of the FF depends on the panel temperature. It was found that by using this calculation the daily energy increased on average by 1.35% but on certain days was as high as 2.5% and on one day actually reduced the daily energy calculation by 0.5%.

Non-numerical results from the experiment suggest that the deposits of bird guano could be significant. This depends on the deployment location and time of year which would impact the yield of the panels and could require regular maintenance to clean them. This is something which could be costly for WECs far from shore. Another non-numerical result is that the rigid panels are susceptible to damage from waves up jetting from behind them and suitable steelwork design should be carried out to protect them.

A discussion was carried out considering the full-scale deployment of an array where it was found that a full 5kWp installed array may achieve an energy yield of 43.8kWp over the same time in the same conditions. Further to this, the design considerations for flexible and rigid panels discussed. I believe that whilst the curved panel did perform best in this experiment, and it may perform best in a full scale deployment, the maintenance and replacement of flexible panels adhered to the WEC surface is more complicated and less robust that the use of steelwork and bolting of the rigid panels. Ultimately making the decision down to the choice of design and maintenance policy against performance.

Chapter 4

Exploration of the Ability of a Complete Solar Array to Power the Onboard Loads of a Hybrid Solar Wave Energy Converter

After the first deployment of BlueX in Scapa Flow, the device was to redeploy as part of the Renewables for Subsea Power (RSP) program, in partnership with Verlume, Baker Hughes, and Transmark [104]. The aim of RSP was to demonstrate the ability of the BlueX to provide power to a subsea battery and load system, provided by the project partners.

The potential of the solar array was evident in the Scapa Flow testing in Chapter 3 as long as it was made more robust against the marine environment. This deployment period would cover the spring and summer months so would have a more favourable solar resource. After examining the available solar resource and using the outcomes of previous experimentation, two solar panel arrays were fixed to the hull of BlueX to supply the communications demand of the WEC. Renewables for Subsea Power was deployed on the 1st of March 2023 at Copinsay, approximately 3.5 nautical miles east of the Orkney Islands.

This Chapter presents the second round of experimentation; detailing the approach, results, and discussions before drawing outcomes and commenting on the next steps.

4.1 Introduction

The development of the solar experiments carried out in Scapa Flow, described in Chapter 3, showed promise for the ability of an onboard array to provide complimentary power. However, the experiment also showed the fragility of solar panels in a marine environment. Scapa Flow is considered a nursery site, where the energy from waves is limited. Despite this, the IP69-rated electronics boxes and one rigid panel were damaged beyond use. For deployment in more energetic sites, such as that in RSP, the solar panels and their electronics will have to be properly protected.

Additionally, an assumption of the results from Chapter 3 was that any controller connected to the system would be able to reliably track the maximum power point of the solar output despite the movement of the panels. It followed that by assessing the open circuit, short circuit and fill factor, it would give a reasonable estimate of the panel output power. Therefore, this assumption should be tested.

The second deployment of BlueX provided a good opportunity to obtain a longer dataset of at-sea experimentation. For this deployment, there was more time and budget to apply the panels and integrate the power output with the WEC, this is detailed in the following Section 4.2.

The objectives of this experiment were to:

1. Obtain extended yield data of solar panels on-board a WEC
2. Test the ability of an off-the-shelf maximum power point tracker under a fluctuating irradiance to reliably produce power
3. Explore the application of flexible panels directly to the hull to further prove their robustness
4. Supply power to an onboard load from solar panels
5. Obtain more accurate cost estimates by building a more complete system
6. Observe how biofouling is deposited and washed off from curved solar panels mounted in a splash zone

Objective one is satisfied by ensuring the testing continues for as long as possible by placing one array in a well-protected location on the nacelle. Objective 2 is achieved by installing a complete solar system on the WEC including an off-the-shelf MPPT converter. Objective three is achieved by testing survivability to the extreme by placing a second array in a location likely to be exhibited to wave action. Objective 4 is achieved by including a constant load in the solar system design. Objective 5 is

achieved by documenting all project costs throughout project management, design and budgeting. Objective 6 is completed by ensuring that panel inspections and documentation are included in the operations team's scope of work at regular intervals of testing.

4.2 Experimental Approach

4.2.1 Selection and Layout of Solar Panels

No footage exists of the panel destruction in Scapa Flow, but by examining the damage, we can assume that the panel was removed upwards due to a large upward jetting of a wave. To protect such a panel in the future, steelwork should be implemented behind the panels to protect from up-jetting. The impact of downwards-moving waves is not expected to be as severe. The implementation of this steelwork has two main consequences. Firstly, this is an added cost, complexity, and mass which is high up on the WEC which could impact dynamics. Secondly, enclosing the space behind the panel would restrict airflow and disrupt the ability to cool the panel, reducing efficiency.

The choice was made to use flexible panels, directly adhered to the hull of the WEC. This solution was simple in that it required no steelwork, saving cost and time whilst also providing a conductive heat path for the panels and protecting the backside of the panel from wave action. The junction box and the front of the panel are exposed to the marine environment, and placing them on the hull, where over-topping is frequent, could have both positive and negative impacts. The panels are now going to be slammed by the waves and spend some of their time underwater, which could impact the magnitude of irradiance reaching them. Alternatively, by now being washed by the waves, this could reduce the cell temperature of the panels whilst also clearing them of biofouling from sea birds. The main factors in selecting the flexible panels were the available deck area and the cost of the panels.

Front Panels

Scapa Flow testing used Renogy 50W panels, which were robust in the marine environment and produced reliable power. The original plan was to reuse these panels in this testing. However, whilst removing the panels from the skid, they were damaged. After testing the output of the panels after removal, it was clear that micro-cracks had formed in the cells as the output voltage was not as high as expected. This shows that whilst this method of adhesion is robust, it does not allow for panels to easily be replaced and reused and should be a consideration in full-scale long-term economic assessments.

Two 100W Renogy flexible panels [105], seen in Figure 4.1 were adhered to the front "Y-tubes" of the hull. This is in a similar location to the front skid during the Scapa Flow testing and is exposed to frequent wave loading. Due to the scarcity of available deck area, this location was only one of a handful available to place the panels. This location does offer an opportunity to test how wave loading influences the operation of the panels; will the waves wash biofouling from the surface, or introduce more from the sea? Will the waves damage the flexible panels in this location?

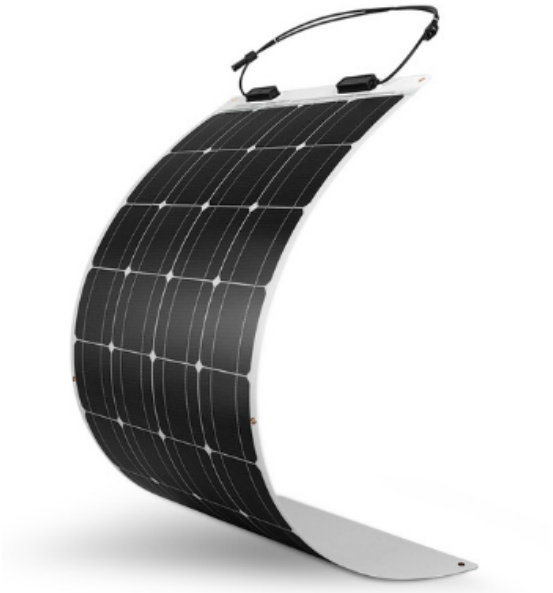

Figure 4.1: 100W Flexible Renogy Panels used in Deployment 2 [105]

The panels are fixed to the WEC as shown in Figure 4.2, the mounting pads from Scapa Flow testing were removed, and the surface was prepared by removing the old paint and replacing it with an epoxy-based paint to improve adhesion. The Y-tube on which each panel sits has a 25-degree offset from the WEC heading and is 0.9m in diameter.

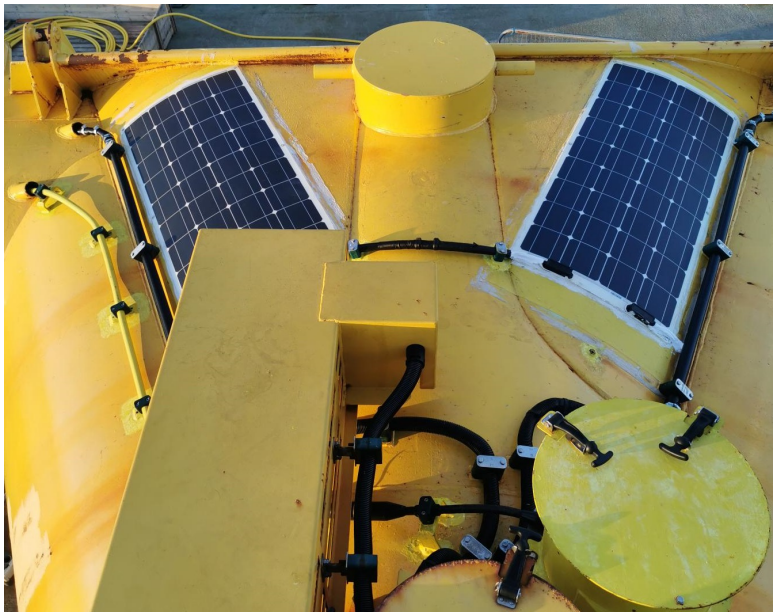

Figure 4.2: 200W Front Array of Renogy Panels

The panels are fixed in such a way that the cells on the innermost edge are horizontal to the ground when the WEC is stationary. The panels are laid so that the long edge of the panel runs axially to the centre of curvature of the y-tube. This means that each series string will receive the same irradiance (neglecting localised shading due to biofouling) and bypass diodes will be utilised. The panels adhered to the newly prepared surface with Sikaflex 291i, the same used in the Scapa Testing, with a thick layer on the back surface of the panel and a bead around the top edge after it has been laid. A bead of Sikaflex is also added around the edge of the junction boxes and cables are run through conduits on the WEC hull. Where cables must be exposed due to lack of conduit mountings, they are encased in Sikaflex. The cables pass along the top of the hull, to the front penetrator plate, and inside the hull as shown in Figure 4.5.

The panels are connected in series so that the voltage is above the requirement of the MPPT and battery. This results in a sub-optimal arrangement with a panel facing the port side of the WEC and the other facing the starboard side. This means that one panel is likely to be shaded compared to the other, creating an irradiance mismatch between the two panels, resulting in lower power output. A more optimal arrangement would be to have the port and starboard panels on separate controllers or in parallel with blocking diodes.

Nacelle Panels

The nacelle offers an open area with a small rate of curvature to adhere panels to. This allowed for the use of larger panels than on the forward section to increase the total installed capacity of solar panels. The Solbian SR186L, shown in Figure 4.3 [106], was selected due to its reported robustness (SR stands for super rugged) and high cell efficiency.

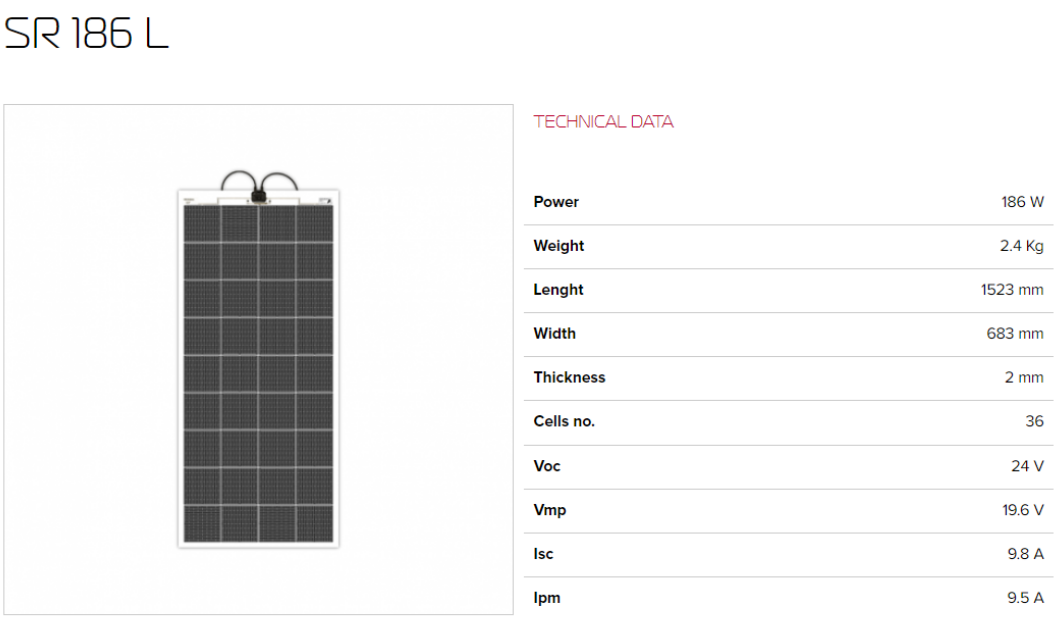

Figure 4.3: 186W Solbian Panels [106]

The main consideration for deploying panels on the nacelle is that during operation the hinge rotates and a section of the aft hull will pass over the nacelle and the panels will be shaded by the aft hull. This means that the panels need to be thin enough so that the aft section can pass over uninterrupted. To ensure no clashes, the panels are orientated so that the junction boxes are directed towards the front of the

WEC, away from the aft section, and beyond the maximum hinge angles. This has two consequences; the nacelle panels are now curved around a surface orthogonal to the main WEC hull and the series strings of the panels are now laid around the circumference of the hull. This results in a shading mismatch in the series string and bypass diodes are less likely to be triggered due to self-shading. Additionally, during southerly WEC headings, the nacelle panels are shaded by the WEC mast causing further losses. The panels mounted onto the nacelle of BlueX are shown in Figure 4.4 so that the midpoint of the panel is along the top of the nacelle tube.

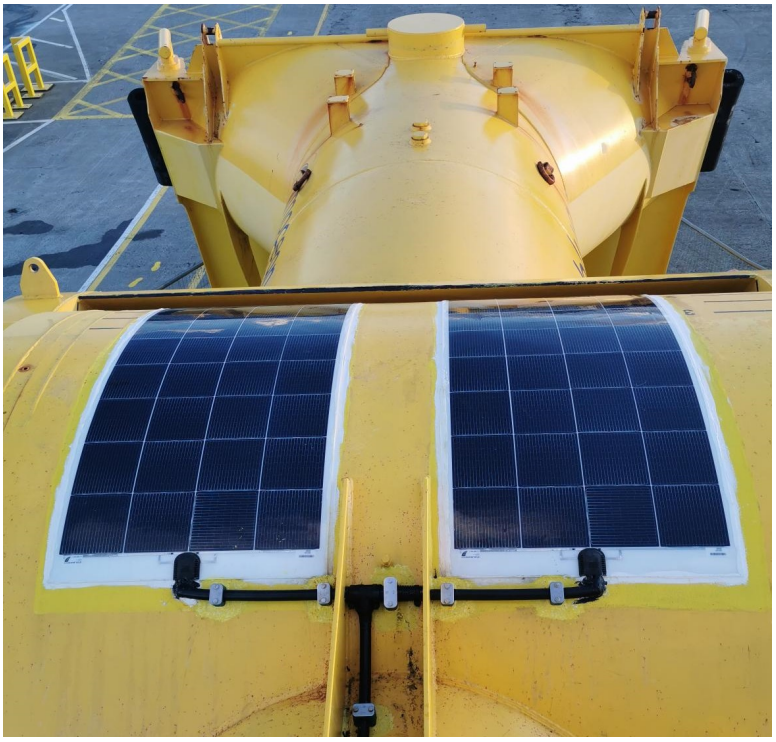

Figure 4.4: 360W Nacelle Array of Solbian Panels and Aft Section

The nacelle panels are also connected in series, to get the voltage above the requirements of the MPPT. The cables are inside conduits that pass through a web and along to the WEC mast penetrator plate inside the hull. The layout of the panels and the cabling routes can be seen in Figure 4.5. BlueX, just before deployment for RSP, complete with solar arrays can be seen in Figure 4.6.

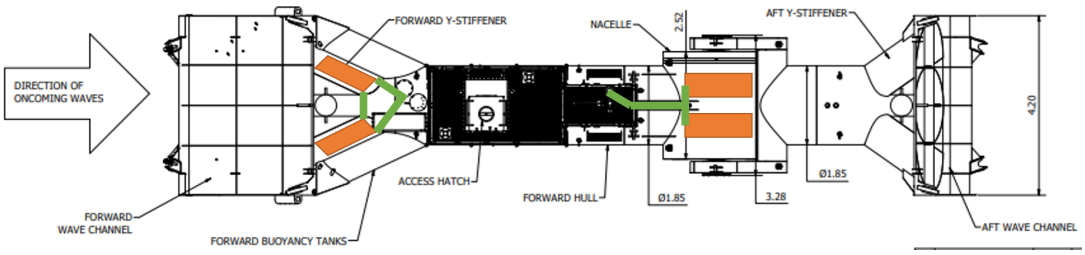

Figure 4.5: Drawing and Layout of Panels and Cable routing

Figure 4.6: BlueX being towed out to RSP deployment with solar panels [107]

4.2.2 The Electrical System

The cables from the two arrays pass into the hull of the WEC through penetrator plates and into the electrical system comprising of; a lithium-ion battery, Maximum Power Point Tracking controllers, a battery management system, and data acquisition system as well as feeding the communications load. All components are from a single supplier, Victron Energy.

Maximum Power Point Tracking

The MPPT is a DC to DC buck converter that applies a voltage to the output of the panel so that the maximum power is drawn from the solar cells. The controller used, shown Figure 4.7, the SmartSolar 75/15 [108] , where 75 is the voltage limit of the controller and 15 is the current limit. This controller was selected as it claims to have "ultra-fast Maximum Power Point Tracking, especially in case of a clouded sky, when light intensity is changing continuously, an ultra-fast MPPT controller will improve energy harvest by up to 30 % compared to PWM charge controllers and by up to 10 % compared to slower MPPT controllers". This is promising as the panels onboard the WEC will experience a constantly changing irradiance as the device moves in the waves. Therefore, an MPPT capable of dealing with fast fluctuations in irradiance is critical for efficient power output.

Figure 4.7: SmartSolar MPPT 75/15 [108]

Each array has one MPPT each as the voltage output needs to be at least 3V higher than the battery voltage, which a single panel could not achieve alone. As mentioned in Section 4.2.1 this results in a sub-optimal layout for the front panels as the output of the array is dependent on the lowest available irradiance.

An additional benefit is the ability to feed a DC load directly from the MPPT controller. The communications hotel load is therefore connected directly to the controller of the front panels, improving the efficiency of the system as it reduces conversion losses from the battery to load during times of solar power production.

Battery and Control System

The battery is the 25.6V, 50Ah lithium-ion "Superpack" [109] selected as lithium-ion has a more efficient round trip efficiency than cheaper alternatives. The Superpack has an integrated battery management system and safety switch to improve robustness. To monitor the battery, a "smartshunt" provides the battery state of charge, voltage, and battery current.

The system is controlled and monitored by the "CerboGx" [110] which logs the panel output, MPPT output, load current, battery voltage, and battery current and also allows a user to control relays inside the SmartSolar MPPTs to turn on loads. The CerboGx can log all data locally to an SD card or remotely via the internet. Data is logged once a minute to a cloud-based system which can then be downloaded as a csv file.

Loads

The energy stored in the Superpack needs to be dissipated so that the solar panels are not throttled by the system and are able to recharge the battery. Whilst this wouldn't necessarily be a problem in a full-scale deployment of the system, it would limit the data retrieved from the experiment and make verification more difficult. Instead of using a dump resistor to drain the battery, the system is instead used to power the communications load of the WEC. This load is continuous and provides a target for the daily yield of the solar arrays. This will highlight a benefit of the solar array system to be able to provide power to one of the hotel loads of the WEC so that the main Power Take Off (PTO) can solely power the consumer load. In times of low solar power, the larger WEC battery can top up the solar battery through a DC-DC converter to ensure that the communications demand is always met. This is an example of a hybrid renewable energy system and should ensure that the critical demand is always met, improving the communications uptime of the Wave Energy Converter and satisfying customer requirements.

4.2.3 Other Data Acquisition Systems

The BlueX has its own data acquisition system monitoring the WEC positional data as well as power output from the main PTO, this was covered in Section 3.2. The data points used in this analysis are values of heading, roll, and pitch. When the WEC is in hibernation mode, the data acquisition system is paused to conserve power and data gaps exist. During these data gaps, the pitch and roll angles are assumed to be very small values because if they were not small, the WEC would not be in hibernation mode. The heading is harder to predict as the WEC weathervanes according to the wave direction and the tidal current. For the purposes here, the missing Heading data is approximated using linear interpolation between the two present values on either side of the missing data field.

Two SOFAR spotter buoys [**?**] are deployed alongside BlueX, these buoys gathered data on significant wave height, wave period, wave direction, sea surface temperature, wind speed and wind direction. Each buoy monitors once a minute, but their sample points are offset by 30 seconds. Therefore, providing a reading every 30 seconds from alternate buoys. The proximity of the buoys to each other and BlueX allows for the data to be considered effective at the WEC.

4.2.4 Costs

The cost of implementing the two arrays is documented here so that when considering a full-scale system in Chapter 6 appropriate costs can be scaled up. Costs are presented in Table 4.1. Where by dividing the total cost by the installed capacity a pound per watt value is obtained.

4.3 Results and Discussion

The results from the testing are presented below, there are two sections, the numerical results detailing panel voltages, currents and yields and the operational results which show how the system coped with being deployed in the marine environment.

Values of the array voltage, current, and power are logged once a minute by the Cerbo monitoring system. RSP was deployed on 28th of February and the solar data acquisition ceased on June 30th. However, the assembly of the solar panel system onto BlueX was completed on the 26th of November 2022. This gave over three

Table 4.1: Costs of RSP Solar Testing

Component	Price	Comments
Solbian SR186L	£ 1,195.00	For two panels
Renogy 100	£ 299.98	For two panels
Lithium Battery	£ 820.27	for 50Ah 24V
Smartshunt	£ 81.76	
MPPT 1	£ 148.64	
MPPT 2	£ 98.65	
Adhesive	£ 179.80	
Cabling	£ 188.68	
Misc	£ 247.84	
Penetrator Plate	£ 1,103.46	Exclude?
Telehandler	£ 204.76	Exclude?
Man Hours	£ 4,000.00	50£ per hour 2 weeks at 8 hours per day
Total	£ 8,568.84	
Watts	572.00	
£/W	£ 14.98	

months of data, through the winter, when the WEC was stationary on the quayside in Kirkwall, Orkney. By comparing the stationary WEC results with the results during deployment and the available solar resource, an assessment of the influence on yield due to moving in the waves offshore can be made.

4.3.1 Stationary Wave Energy Converter Solar Yield

The period when the WEC was stationary can be divided into two testing phases. In phase one, the panels are all set up and connected to the battery system and communications load which is turned on and off periodically. During this time the WEC was on the quayside, undergoing preparations for the RSP deployment and was powered by a connection to the national grid. The panels still produced power, but the load was not continuous.

In phase two, which commenced on the 7th of February, the WEC was disconnected from the mains and lowered into the water, but moored to the quay. Whilst the WEC was able to pitch and roll, the moorings and harbour would make these movements small. During phase two, the solar system was now powering the communications load continuously and continued to do so up until the commencement of RSP testing.

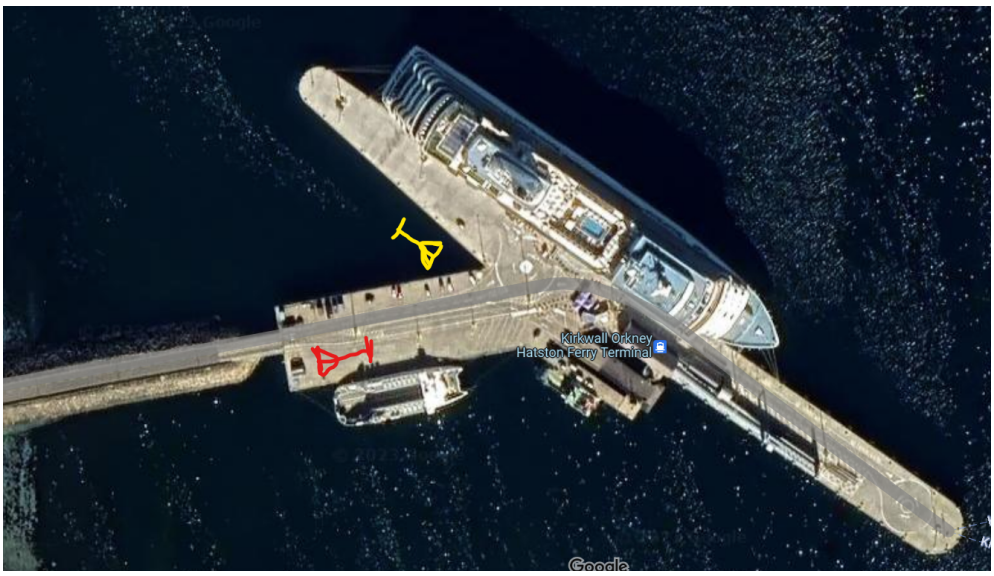

Figure 4.8: Approximate Locations of WEC on Hatston Pier, Red shows positions between 27th November to 7th Feb and Yellow between 8th Feb and 28th Feb

The stationary period provided 137,859 data points, between 00:00:27 26-11-2022 and 22:59:55 28-02-2023, representing 95 full days of data, which should be 138,240 data points. The occasional minute is missed due to a slight drift in the sample rate. If a sample is made at 00:59, then the sample drift moves the second sample to 03:01, skipping the sample at 02:00.

Array Output Voltage

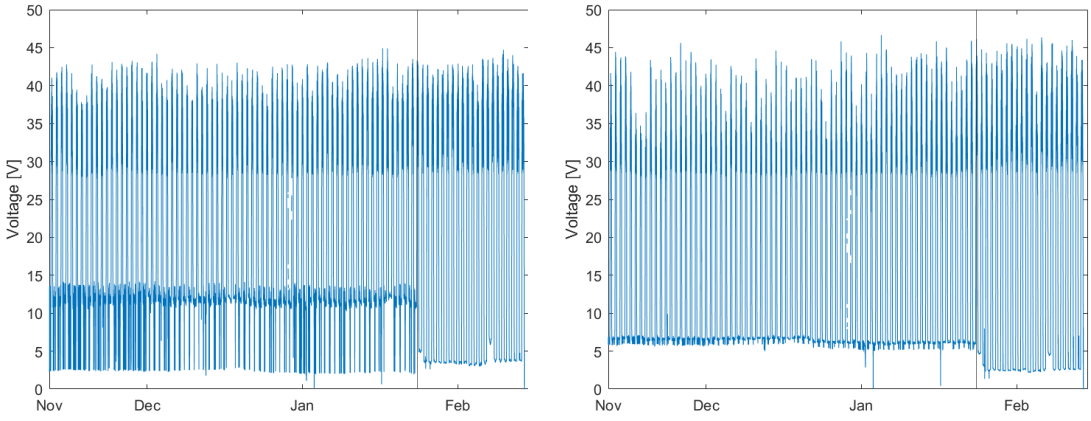

(a) Voltage of Front Array **(b)** Voltage of Nacelle Array

Figure 4.9: Output Voltage

The panel voltage rarely drops to zero as street lighting illuminated the port at night. The voltage does reduce after the WEC is placed in the water as it is no longer directly under the street lighting.

During the day, the voltage increases to be between 37.8 and 44.9V for the front array and 35.3 and 46.6V for the nacelle array. Additionally, as the starboard panel on the front is shaded, it will have a lower temperature and higher voltages. The nacelle is a large plate and will heat up quicker than the front Y-tubes.

Array Output Current

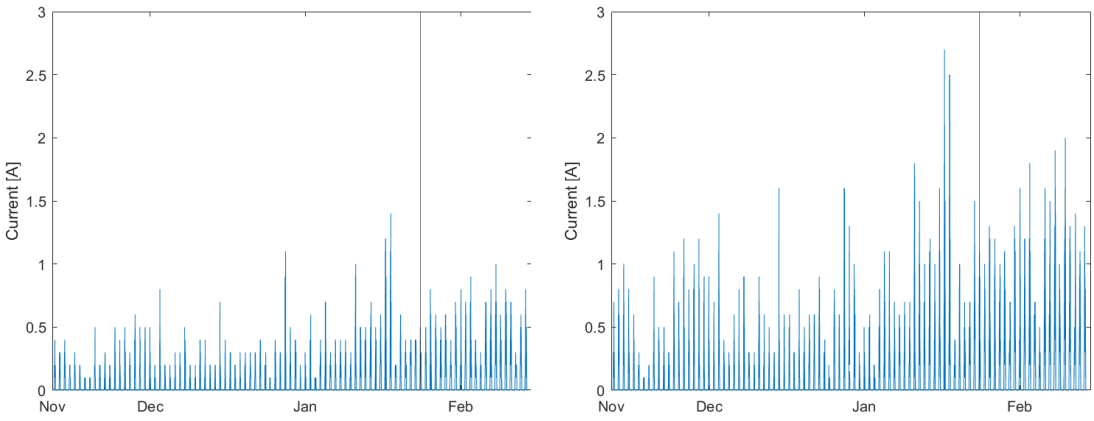

(a) Current of Front Array **(b)** Current of Nacelle Array

Figure 4.10: Output Current

The current is dependent on the irradiance on the cells of the panel and the panel short circuit current. The Solbian panels have a maximum power point current 79.6% higher than the Renogy panels.

Array Output Power

The power output curves are very similar in appearance to the current curves, as the voltage is more constant. The solbian panels produce powers much higher than the renogy panels but again this is because the rated power is 86% higher.

The raw panel data is noisy and hard to decipher at such a long time scale. A better measure is to analyse the energy produced by each array on a (near) monthly basis. The energy produced between the 27th of November to the 31st of December, the 1st Jan to the 7th Feb and the 7th Feb to 27th Feb are calculated and presented in Table 4.2 below.

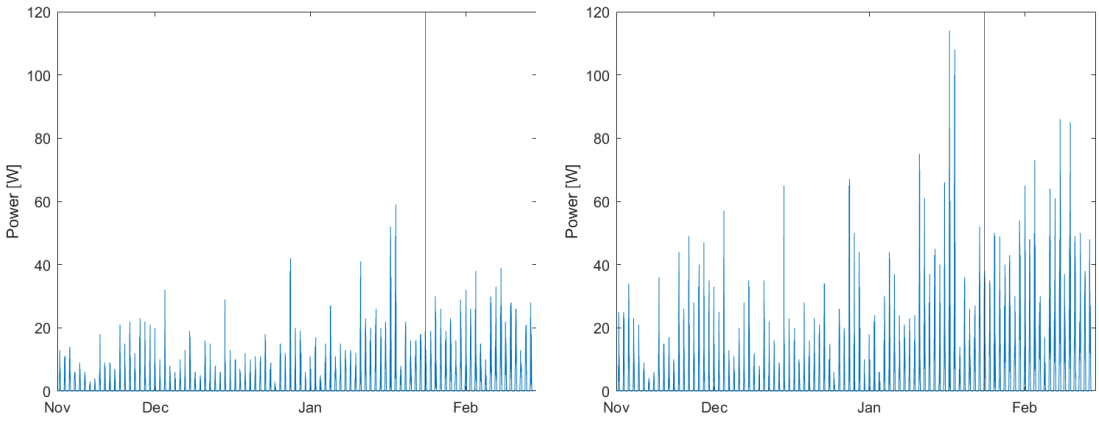

(a) Power of Front Array **(b)** Power of Nacelle Array

Figure 4.11: Output Power

Table 4.2: Energy Yield of Arrays during Static Test Period and the Daily Averages

	Forward		**Nacelle**	
Time Period	Monthly Total [Wh]	Daily Average [Wh]	Monthly Total [Wh]	Daily Average [Wh]
27-11 to 31-12	826	22.95	1529	42.47
01-01 to 07-02	1479	38.92	2731	71.87
08-02 to 28-02	1626	77.41	3180	151.42
Total Period	3931	41.38	7440	78.32

4.3.2 Dynamic Wave Energy Converter Solar Yield

On the 1st of March, the WEC was towed from the quay in Kirkwall, round to the RSP testing site, east of Orkney. The solar testing ended on the 30th of June after 122 days at sea. The RSP programme is planned to continue through to 2024, with the solar panels on board, still gathering data but the testing period ended to allow for the submission of this thesis.

For the entire testing period, the solar panel and battery system fed the communications load. The two PV arrays regularly produced enough power to meet the communications load of the WEC. However. the solar battery does have the ability to be charged from the main WEC battery if the state of charge becomes too low to maintain communications. This only occurred on 11 occasions during the testing period, all in March. The solar array maintained the demand for 83.5% of March, then it maintained 100% of the communications from the 1st of April until the end of the deployment.

The raw results from the experiment appear very noisy when examined over large time periods and little can be determined from them. Therefore, only the raw data from the first testing month of March is presented here whilst the remainder are in Appendix B. However, the daily mean values are presented for the entire testing period as they consist of fewer data points and therefore present clear results.

Firstly, the WEC positional roll, pitch and heading data is presented in Figures 4.12a - 4.12c.

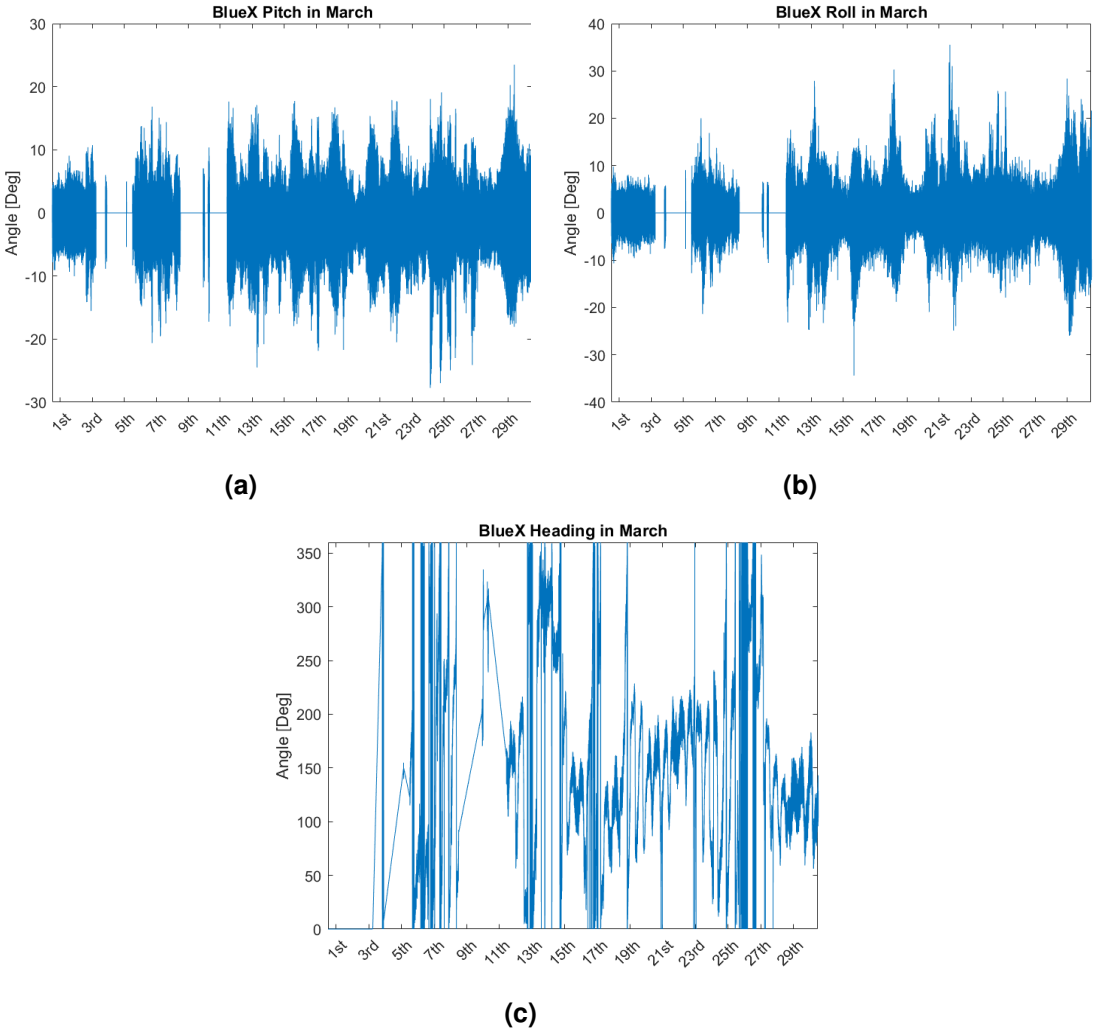

Figure 4.12: Raw BlueX Positional Data during March

The panel voltages and currents are provided in Appendix B whilst PV output power and MPPT output power are provided in Figures 4.13a - 4.13d. PV power is the power output from the panel terminals, whilst charger power is the output from the MPPT converter. The daily energy yields from the panel and the MPPT are calculated by

summing all the data points per day to give the yield in Watt minutes and then dividing by 60 to obtain watt hours. By dividing the charger output by the PV output, the daily efficiency of the MPPT converter can be calculated, this is shown, for the forward and nacelle arrays in Figure 4.14

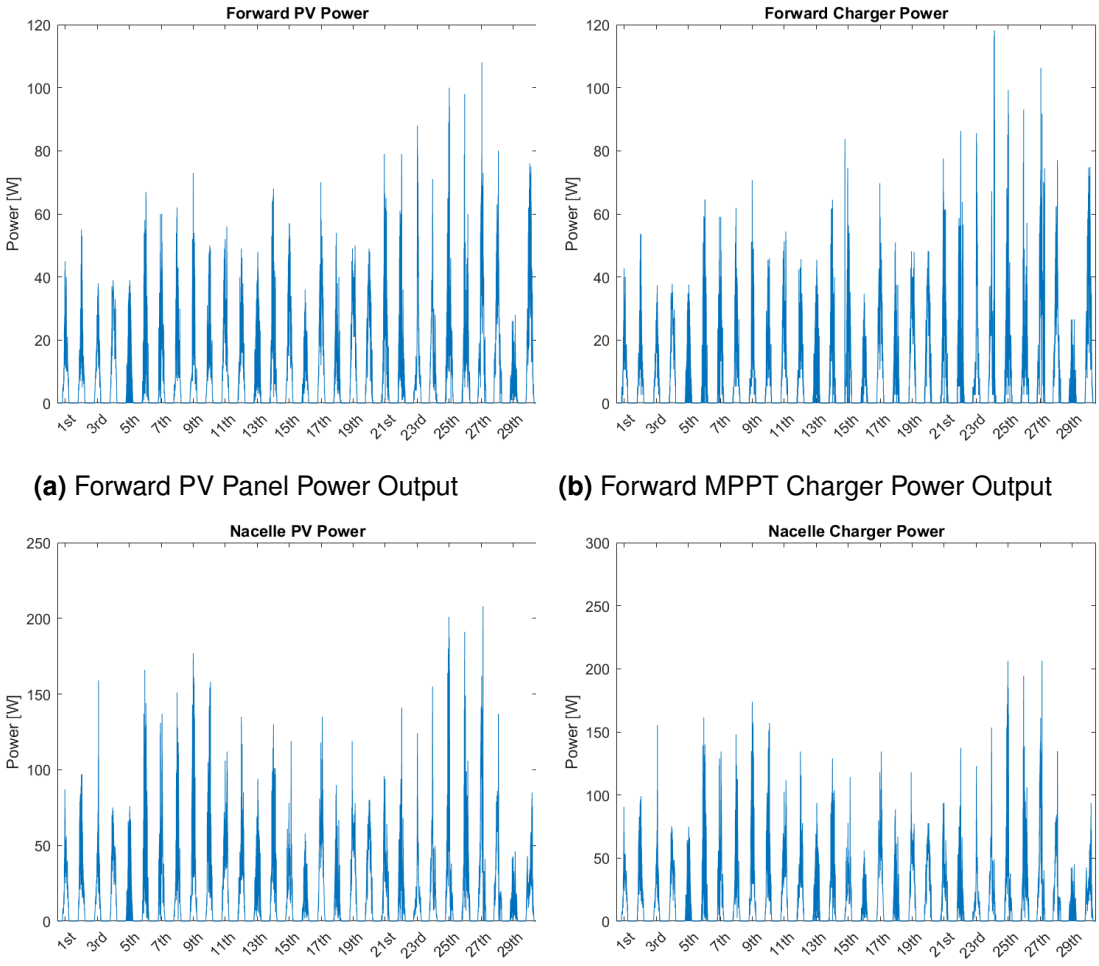

(a) Forward PV Panel Power Output

(b) Forward MPPT Charger Power Output

(c) Nacelle PV Panel Power Output

(d) Nacelle MPPT Charger Power Output

Figure 4.13: Raw Array and Charger Power During March

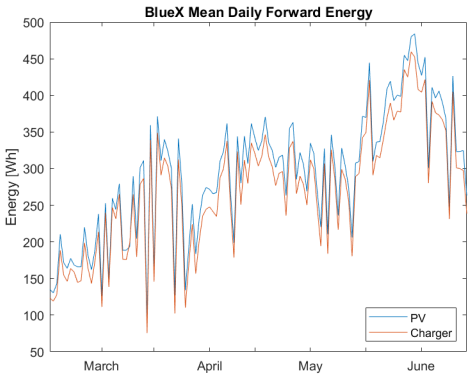

(a) Daily Energy of the Forward Array

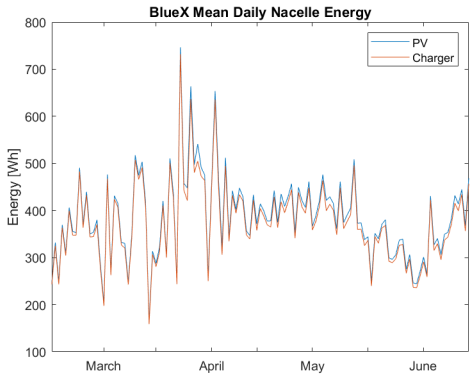

(b) Daily Energy of the Nacelle Array

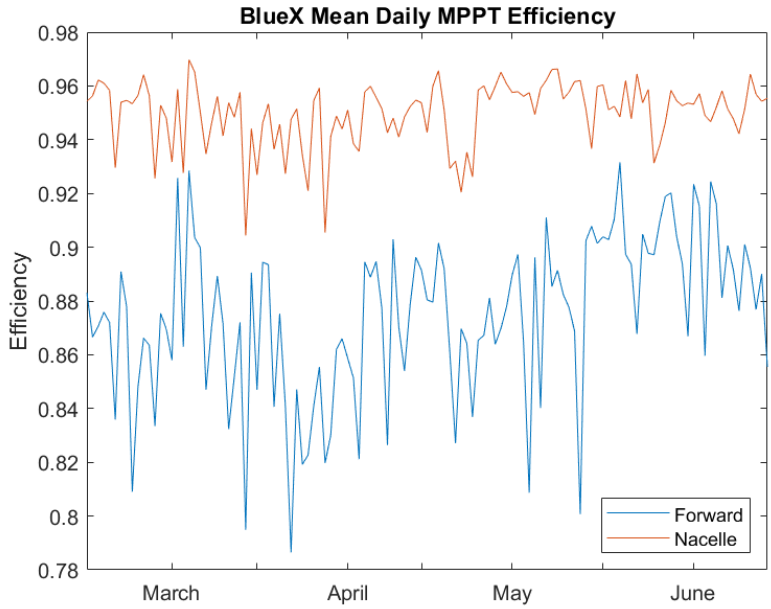

(c) Daily Efficiency

Figure 4.14: Daily Energy and Efficiency of the Forward and Nacelle Arrays during March

To offer more clarity, the daily mean heading, the daily standard deviation of pitch and roll, the mean significant wave height and the mean period are calculated and presented in Figures 4.15.

Finally, the monthly energy yields are summarised in Table 4.3, this time considering each calendar month in turn. Additionally, the percentage of the communications demand met by solar energy for each month is provided. It should be noted that the battery state of charge hit 100% charge almost every day beyond the 1st of April. This will result in a curtailment of energy as the controllers restrict the panel output.

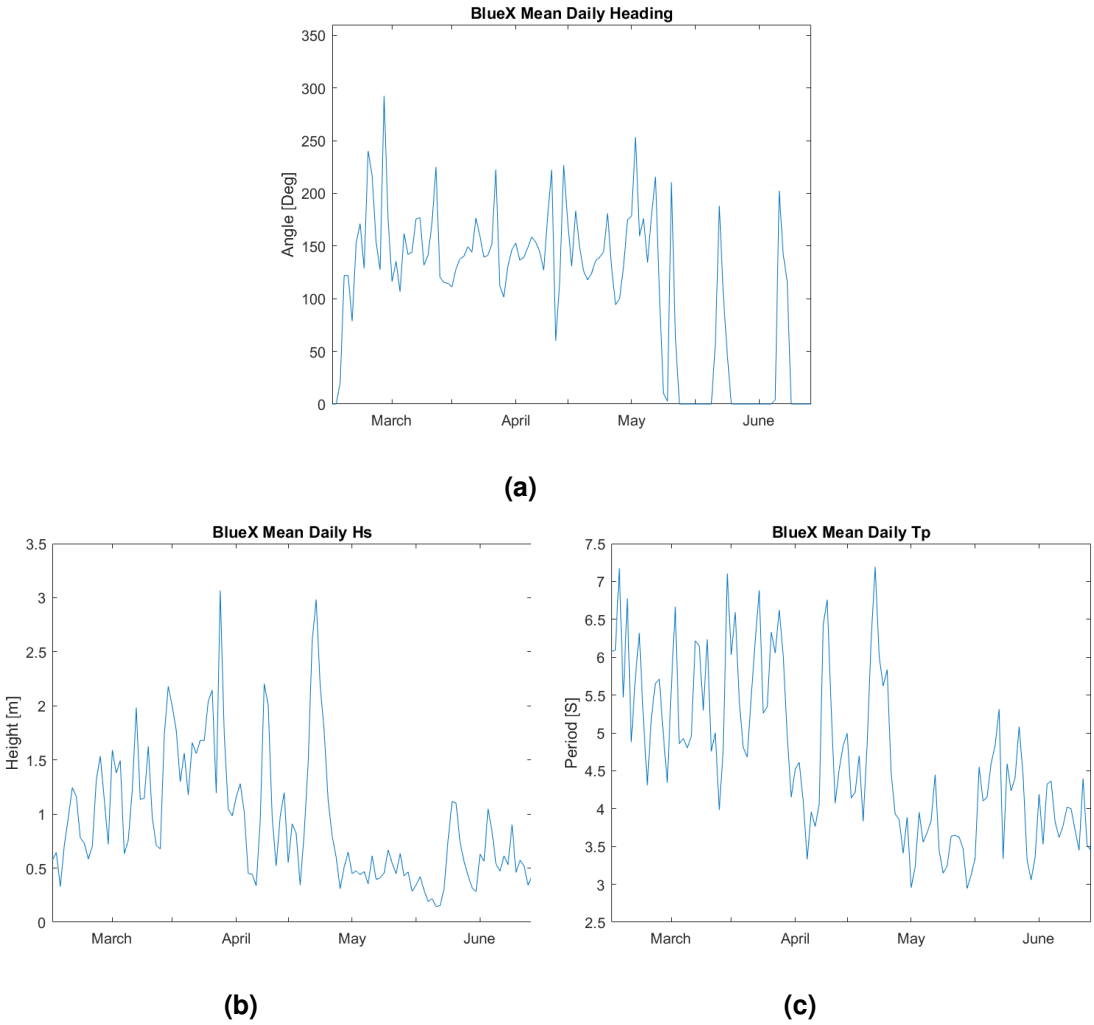

Figure 4.15: BlueX Daily Mean of Data

Table 4.3: Monthly Results from Solar Array Testing

	Total Energy [kWh]	Average Daily Energy [Wh]	Best Daily Energy [Wh]	Worst Daily Energy [Wh]	Maximum Power [W]	Communications Load Met
March	16.51	533	800	260	284.3	83.50%
April	20.56	685	1060	380	367.2	100%
May	20.36	657	800	570	371.0	100%
June	21.31	710	840	600	346.7	100%
Total Deployment	78.74	645.4	1060	260	371.00	95.88%

4.3.3 Panel Condition

The condition of the panels is monitored throughout the deployment to check for their robustness and any biofouling. The panels were inspected on the 20th of April and on the 5th of July. The visual results for the April inspection can be seen in Figure 4.16. The nacelle panels were surprisingly clean even after 51 days at sea, as seen in Figure 4.16a. This is in contrast to the results of the inspections of panels during the testing in Scapa Flow as described in Section 3.2.5 where after just 15 days the panels were covered in guano fouling from sea birds. This suggests that the time of year is a critical factor for biofouling as the first round of testing occurred in Autumn whilst this is in Spring and the quantity and type of birds may differ depending on the seasons. The two locations are close to one another, approximately 13km, so the marine life present at the two locations would not be vastly different. However, the natural harbour of Scapa Flow may attract certain birds as it offers a more protected location to hunt.

The panels on the front section were not as clean, as seen in Figures 4.16b to 4.16d. This location is the most exposed location tested and receives regular wave washing. It was theorised that this exposure would allow waves to wash away any bird guano from the panels. This location has not been subject to marine growth and is clean on the paintwork around the panel in Figure 4.16b. The surface of the Renogy panel is textured and rough so provides an attractive surface for growth whilst the smooth painted surface of the hull allows for run-off. The panels were cleaned with a soft bristle brush to improve yield.

The panels were again inspected on the 5th of July, after the data acquisition period. The results can be seen in Figure 4.17. Again, the nacelle panels were in good condition, despite being at sea for 127 days and installed on the WEC for 220 days. The front panels were in similar condition to that in April, with green marine growth on the front surface of the panels. This time, the biofouling was more prevalent on the hull surface. The panels were again cleaned with a soft bristle brush, but this was outside the data acquisition period so had no effect on the yield. This time, extra inspections of the junction boxes, Figure 4.17c and the panel edging, Figure 4.17d show that the biofouling covered the edges but no water ingress was found. The panels did not appear to be peeling around the edges and contact with the hull was still good.

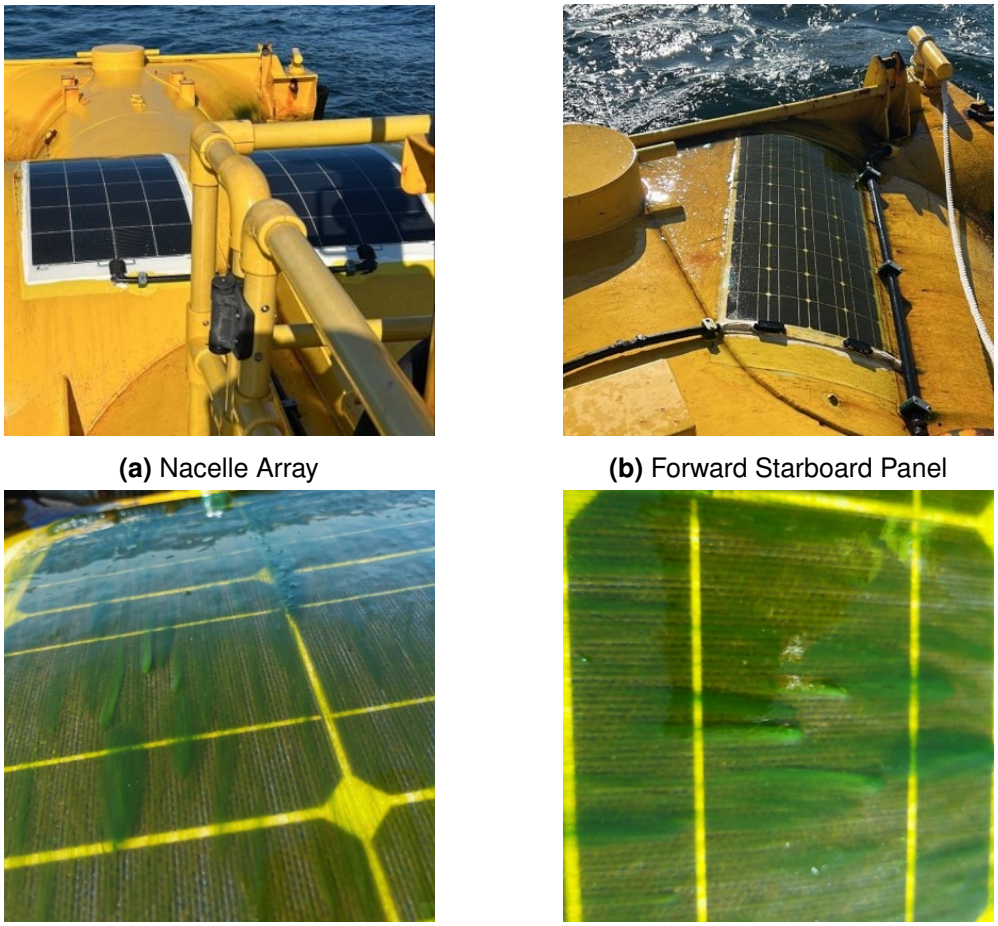

(a) Nacelle Array

(b) Forward Starboard Panel

(c) Close up of Biofouling on Forward Panel

(d) Close up of Biofouling on Forward Panel

Figure 4.16: Inspection of Panels on 20th of April 2023

For future deployments, panels should be located away from zones which are frequently washed. however, if there are birds, a small amount of washing would be beneficial. Biofouling and shading of the panels is a critical consideration of a full-scale array. Operations to regularly inspect and clean the panels would not be economically viable for deployments of arrays far from shore.

4.3.4 Maximum Power Point Tracking Converter Efficiency

When comparing the daily efficiency in Figure 4.14 with the daily mean significant wave in Figure 4.15b there is a clear negative correlation between the two. The correlation is examined by calculating the R and P values between the forward and nacelle efficiency with mean significant wave height. The results are in Table 4.4 below.

(a) Nacelle Array

(b) Forward Starboard Panel

(c) Close up of Biofouling on Junction Box

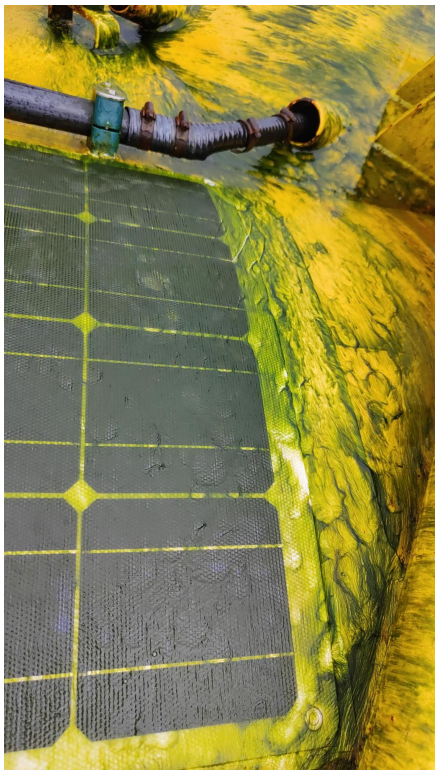

(d) Close up of Biofouling on Panel Edge

Figure 4.17: Inspection of Panels on 5th of July 2023

By finding the line of best fit using the MATLAB polyfit function, and obtaining the standard error using the polyval function, the relationship between MPPT converter efficiency and the significant wave height can be plotted below in Figure 4.18. This yields the linear realtionships for the forward converter efficiency in Equation 4.1 and the nacelle efficiency in Equation 4.2.

Table 4.4: Correlation Results of Converter Efficiency with Significant Wave Height and Windspeed

	Efficiency with Hs		**Efficiency with Ws**		**Hs with Ws**	
	P	R	P	R	P	R
Nacelle	4.64E-20	-0.71	6.56E-15	-0.63	4.93E-21	0.72
Forward	1.98E-08	-0.48	6.40E-08	-0.47	4.93E-21	0.72

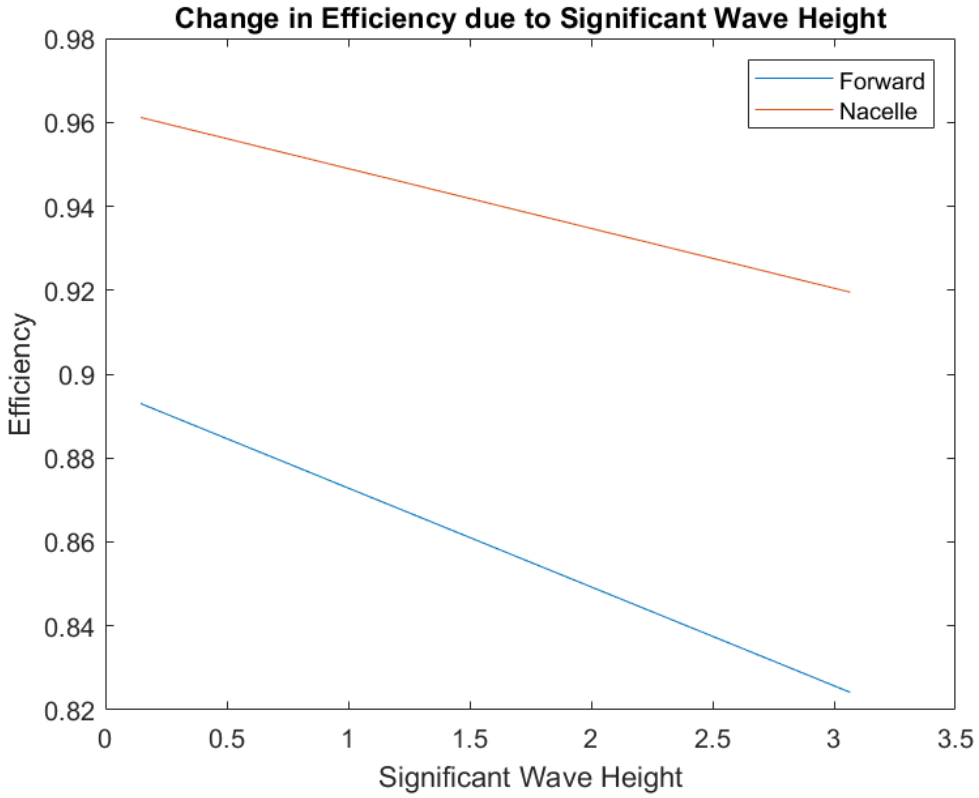

Figure 4.18: Efficiency of the MPPT converters varying with Significant Wave Height

$$Forward\ Converter\ Efficiency = 0.8964 - 0.0236 * WaveHeight \tag{4.1}$$

$$Nacelle\ Converter\ Efficiency = 0.9632 - 0.0143 * WaveHeight \tag{4.2}$$

4.4 Chapter Summary

This chapter has described the implementation and results of a solar array deployed at sea onboard BlueX, Mocean Energy's prototype wave energy converter. The array consists of two strings of flexible solar panels, directly adhered to seperate sections of the hull. The 200-watt forward array is mounted at the front of BlueX, in a splash zone where it is frequently covered by waves. A 372-watt array is mounted on the nacelle, further from the water surface and not regularly washed. Each string is connected to a 50Ah battery with a Maximum Power Point Tracking controller.

The status of the battery and output from both strings is monitored. The system feeds a continuous communications load of BlueX, ensuring that communications hotel load are no longer a burden on the main power output of the WEC.

The system produced a total of 82.9kWh over the deployment period from the 1st of March to the 30th of June. An additional 10.5kWh was produced during the period when the WEC was on the quayside during the winter months. This would have provided 17.7% of the communications demand over the 95 day period.

The solar array system successfully met the continuous load for 95.8% of the four-month deployment. Between the 1st of April and the 30th of June, the communications were powered 100% of the time by solar panels. The battery was regularly fully charged, suggesting that a larger load could have been met with this system or that a larger battery was required.

The condition of the two sets of panels was inspected on the 20th of April and on the 5th of July. It was found that the nacelle panels were "as good as new" whilst the panels in the splash zone were covered in marine growth. The panels were cleaned on the 20th of April and left until the end of the deployment.

This is very promising for the hybridisation of the two technologies and shows potential for a larger array to power more of the onboard hotel loads of the WEC or even send surplus power to the consumer alongside the main wave power. However, with the current power system design, bi-directional power electronics capable of stepping up from the 24V battery to the main WEC battery would be required. The main WEC PTO bus voltage is much higher than the 24V and is not disclosed for commercial reasons, however, finding a single power electronics device capable of such a large step-up is tricky.

When examining the converter efficiency, a strong correlation with significant wave height was discovered with P and R values, 4.64E-20 and -0.71 respectively. It is theorised that the larger waves induce a changing irradiance on the solar panel face which makes the MPPT system work harder than in lower wave heights. The forward and nacelle arrays have different relationships with converter efficiency due to their orientation on the WEC, and the quantity of biofouling reducing the amount of direct beam irradiation making it to the panel surface. This results in a slight drop in efficiency of 1.4% per m gain in wave height for the nacelle panels and 2.4% for the forward panels.

Although this experimentation was deemed a success, a longer period of data would be beneficial. In fact, the solar testing kit remains on the BlueX beyond the end of July 2023, when the results were compiled here. The RSP test programme is planned to continue until September 2023. Additionally, the capabilities of the solar battery system were upgraded so that the main WEC battery is able to be charged from the solar array output when the solar communications battery is full.

PART III

Modelling

Chapter 5

MATLAB Modelling of Hybrid Solar Wave Energy Converter

To better assess the cost-benefit of a hybrid Solar-Wave Energy Converter (SWEC), a numerical model was created to predict the energy generated from its solar array. The model was produced in MATLAB, using the PV Lib Toolbox as its foundation. PV Lib toolbox is a set of well-documented functions for simulating the performance of solar panel systems, available in MATLAB or Python [111]. The toolbox is produced and maintained by Sandia National Laboratories and offered as open-source software, used in several scientific publications [112] [113] [114] [115]. The functions inside the toolbox are well understood and documented. The total requirements of modelling the SWEC are beyond the capability provided in the PVLib toolbox. Thus additional code has been produced to model irradiance mismatch, curved panels, bypass diodes, and significant wave height dependant converter efficiency. Care must be taken when entering the geometric relationships between the solar panels and the WEC to ensure that the machine's dynamics and the orientation of the panels are correct.

This chapter describes the production of the model, the running of the model and comparisons of the outputs to experimental results described in Chapter 4. In Chapter 6 the model is modified to represent other size arrays, in different orientations and locations around the world.

The aim is to build a numerical modelling tool which could accurately predict the energy output of a solar array onboard a wave energy converter. The model can then be used in future wave energy devices.

5.1 Model Development

The modelling process is described in the flowchart in Figure 5.1. Data inputs are defined by black boxes whilst processes are defined by blue boxes.

The vectors describing the panel normal and solar direct beam are calculated and compared to obtain the view factor so that the direct irradiance can be calculated. In parallel, the diffuse irradiance is calculated using the Perez model and the reflected irradiance is calculated using a constant albedo factor. The total irradiance on each cell is then the sum of the diffuse, reflected and direct irradiance. This is repeated for each cell around the circumference of the curved panel to obtain the irradiance over each series string. Using the mean irradiance of each string, the cell temperature is estimated. The minimum irradiance is used as the "current producing irradiance". The voltage in subsequent strings is compared against the diode forward voltage of 0.6V to see if bypass diodes are engaged. The total number of connected strings is calculated and the total array power is obtained for each time step. This process is repeated for each timestep until the analysis is completed.

5.1.1 Data Sources

The model requires input data of the components of irradiance, wind speed, ambient temperature and the orientations of the Wave Energy Converter in addition to the panel properties and dimensions of WEC hull. All data is converted into a MATLAB timetable array so that the time series can be synchronised so that the timestep is consistent across all sources.

Wave Energy Converter Positional Data

The positional data of the WEC is required to be able to calculate the angle of the panel relative to the sun. During the experiments, the positional data of heading, pitch and roll are gathered by the onboard sensor data acquisition system of the BlueX. This data is sampled at a frequency of 25Hz and captures the position of the forward hull relative to the horizon and the heading clockwise from North. An abundance of other sensors gather data not necessary for this work. The degrees of freedom in heave, sway and surge are deemed to have an insignificant effect on the yield of the solar array as the distance travelled is likely to be small due to the containment of the WEC within it’s mooring circle.

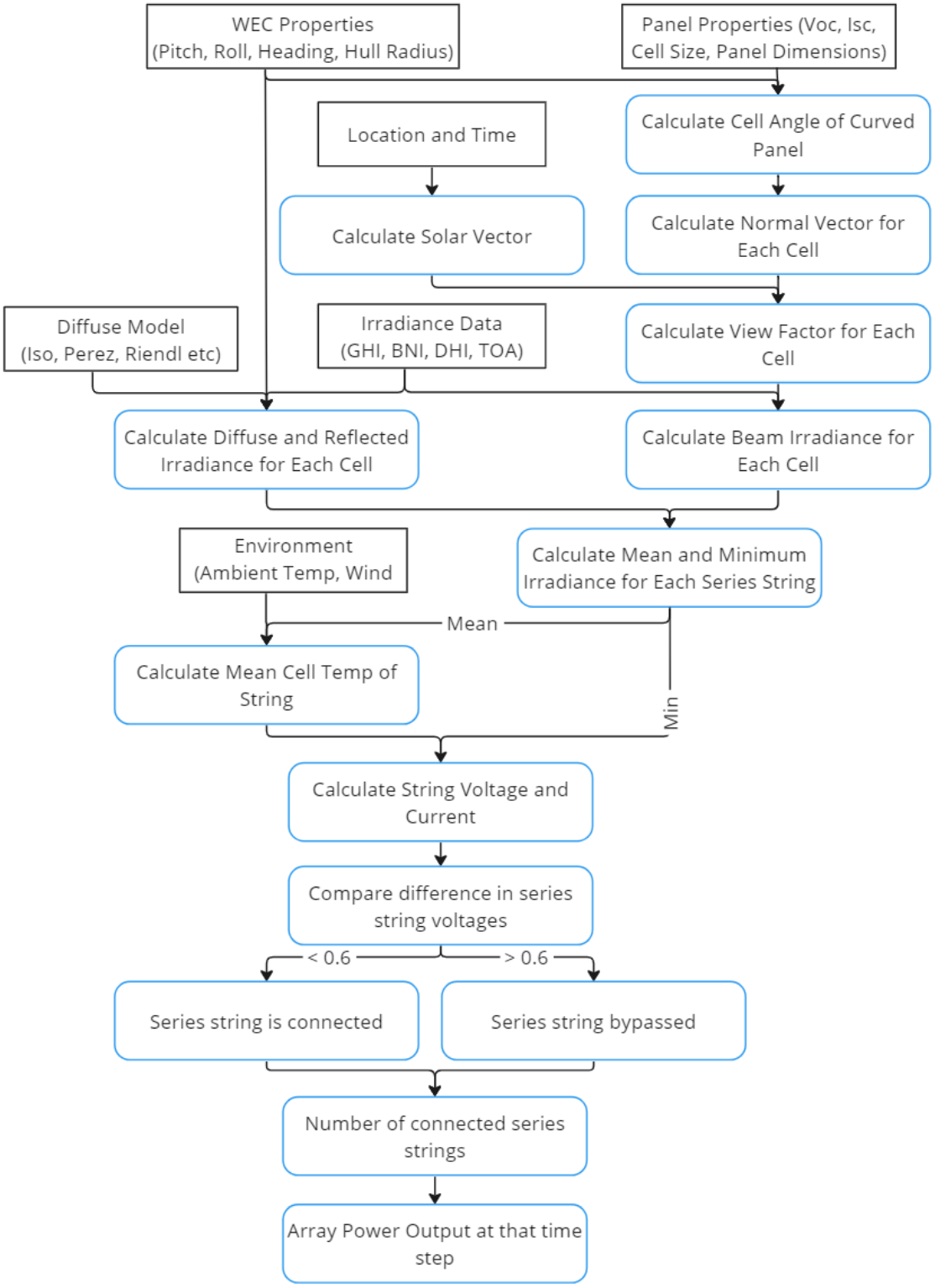

Figure 5.1: Modelling Flowchart

When estimating the yield of a hybrid solar wave energy converter in deployments outside of the experiments, the positions and power generated by the BlueX needs to be estimated. This is done by using Mocean Energy's in-house WAMIT-based, time-domain WEC simulation tool. This tool has been developed by the numerical modelling team at Mocean Energy and verified against scaled tank testing and full-scale deployments. The tool outputs are a secondly time series over a range of sea states. The sea states are then allocated to a real-life location by examining historic wave climates.

Irradiance Data

The output current of a solar panel is proportional to the irradiance that falls on the surface area of the solar cells. Irradiance is the power per square meter arriving on the earth's surface, irradiated from the sun. Whilst irradiation is the energy per square meter over a given time frame. To be able to calculate power, a solar model requires irradiance resource data in a given location and time.

The irradiance data is sourced from the Copernicus Atmosphere Monitoring Service (CAMS) [116] [117] [118]. CAMS provides historical irradiance data from 2004 to the present day in locations spanning Europe, Africa, the Atlantic Ocean, and the Middle East in temporal resolutions from minutely to monthly averages. Copernicus is the European Union's earth observation program, obtaining global information from satellites, as well as from ground, air and ocean-based measurements. All data is free to use and its aim is to improve people's quality of life.

Within the array of available data, Copernicus provides global solar irradiation values, provided in its main components of the Global Horizontal Irradiation (GHI), Beam Normal Irradiation (BNI), and Diffuse Horizontal Irradiation (DHI), both with and without weather effects. In addition, Top of Atmosphere (TOA), and tracked beam irradiation are also available. To obtain data, Copernicus requires the location coordinates, the temporal resolution desired, and the time scale over which to evaluate. Data is then downloaded as a comma-separated file.

Values of irradiation in Wh/m2, are provided for each time step, no matter the selected temporal resolution. To obtain irradiance we divide the irradiation values by the proportion of an hour of the temporal resolution. If the data is in a minutely time resolution, the irradiation is divided by 1/60 (multiply by 60) as a minute is one-sixtieth of an hour. If we had half-hourly time series we would divide by ½. If the resolution is in hourly time steps, the irradiation and irradiance are equivalent. To obtain a secondly time series irradiance the irradiation is multiplied by 3600.

Environment Data

The efficiency of a solar panel is dependent on the cell temperature, which in turn is dependent on the irradiance landing on the solar cell, the ambient temperature and wind speed. This data was obtained from the National Aeronautics and Space Administration (NASA) Langley Research Center (LaRC) Prediction of Worldwide Energy Resources (POWER) Project funded through the NASA Earth Science and Applied Science Program. POWER works in a similar way to CAMS where the location co-ordiantes and time scales are entered, the desired parameters and temporal resolution selected and a csv file downloaded. Data from POWER was used as Copernicus does not include all the environmental data required. The smallest resolution available is hourly data, a key assumption when increasing the resolution of this data is that the wind speed or ambient temperature varies linearly over the hour. This may be a fair assumption for ambient temperature but perhaps not for wind speed as gusts occur on a much smaller timescale than an hour and will not be included in any increase in temporal resolution.

POWER does provide irradiation data. However, this is not updated as frequently as the CAMS data and thus the CAMS data was used to obtain the solar data just after the deployments. Only CAMS is used in the model for continuity between the models which are verified against the experiments and full-scale modelling.

5.1.2 Vector Model To Calculate Irradiance on Arbitrarily Tilted Panel

The Solar Vector

The irradiance on the plane of a solar panel is influenced by the angle at which it meets the surface. The maximum irradiance occurs when the panel is perpendicular to the incoming direct beam. Therefore, to calculate the panel energy output, the angle of the direct sun beam relative to the panel surface needs to be found. Firstly, the vector representing the angle of the sun can be calculated using principal celestial equations as in [119]. This is summarised in Equation 5.1 below.

$$\overrightarrow{S} = [\cos(\alpha_s)\sin(\gamma_s)]\overrightarrow{E} + [\cos(\alpha_s)\cos(\gamma_s)]\overrightarrow{N} + \sin(\alpha_s)\overrightarrow{Z} \tag{5.1}$$

Where α_s is the altitude and γ_s is the azimuth angle of the sun. The unit vectors $\overrightarrow{E}$, $\overrightarrow{N}$, and $\overrightarrow{Z}$ describe the East, North and Vertical directions. α_s and γ_s are obtained by using the "pvl_ephemeris" function in PVLib. Ephemeris requires the location co-ordinates and the time over which to evaluate, the outputs then include; altitude, elevation, apparent elevation and the solar time.

Panel Normal Vector

Secondly, the vector which is normal to the surface of the panel is calculated. Usually, this can be done simply by using the panel tilt and azimuth angle. However, as the panel is installed on a WEC, the panels have 3 degrees of angular freedom which can change over time. It, therefore, makes sense to describe the angle of the panel by using the angles of the wave energy converter heading, pitch, and roll.

The heading is measured clockwise from North while roll and pitch are measured as zero degrees from the horizon. The vector normal to the panel surface can be found by calculating the cross product of the two orthogonal vectors describing the surface of the panel, shown in Equation 5.4. The vectors $\overrightarrow{X}$ and $\overrightarrow{Y}$ are calculated in Equation 5.2 and Equation 5.3 respectively. $\overrightarrow{X}$ is the vector tangential to the circumference of the hull and $\overrightarrow{Y}$ is axial to the hull circumference, a diagram showing the vectors and their relationship to the WEC can be seen in Figure 5.2.

$$\overrightarrow{X} = \cos(H+90)\cos(R)\overrightarrow{E} + \sin(H+90)\cos(R)\overrightarrow{N} + \sin(R)\overrightarrow{Z} \tag{5.2}$$

$$\overrightarrow{Y} = \cos(H)\cos(P)\overrightarrow{E} + \sin(H)\cos(P)\overrightarrow{N} + \sin(P)\overrightarrow{Z} \tag{5.3}$$

Where H is the WEC heading angle, P is the pitch angle and R is the roll angle. Care must be taken when examining the cross-product to obtain the normal vector. Cross multiplication is not commutative and will provide a normal vector pointing to the ground rather than the sky if the incorrect order is used. A check is performed to analyse the polarity of the $\overrightarrow{Z}$ component as this should only ever be negative for large pitch or roll angles. A negative $\overrightarrow{Z}$ for stationary WEC angles suggests that the cross multiplication has been performed in the wrong order.

$$\overrightarrow{P_N} = \overrightarrow{Y} \times \overrightarrow{X} \tag{5.4}$$

The dot product of the vectors $\overrightarrow{P_N}$ and $\overrightarrow{S}$ determines the view factor of the panel at that time step. If the view factor is equal to one, the panel is perpendicular to the incoming solar irradiance. A correction is included to set any negative view factors to zero as this represents when the panel is facing away from the sun due to large WEC angles or the timestep occurring at night.

Direct Irradiance

The direct irradiance on the panel plane is the product of the BNI and the view factor shown in Equation 5.5. This process should be repeated for each plane of panels. If multiple panels are mounted on the same section of the hull, orientated in the same way, it is assumed that they share the same normal vector and the difference in solar vector is negligible.

$$I_{direct} = BNI * (\overrightarrow{P_N} \cdot \overrightarrow{S}) \tag{5.5}$$

Diffuse Irradiance

The diffuse irradiance on the panel can be found using a number of diffuse sky models. PVLib provides functions to calculate the Isotropic, Reindl, Perez, Klucher, and Hay and Davies diffuse models. Initially, the isotropic model is used, shown in Equation 5.6 where R is the roll angle of the panel.

$$I_{diff,isotropic} = DHI * (1 + \cos(R)/2) \tag{5.6}$$

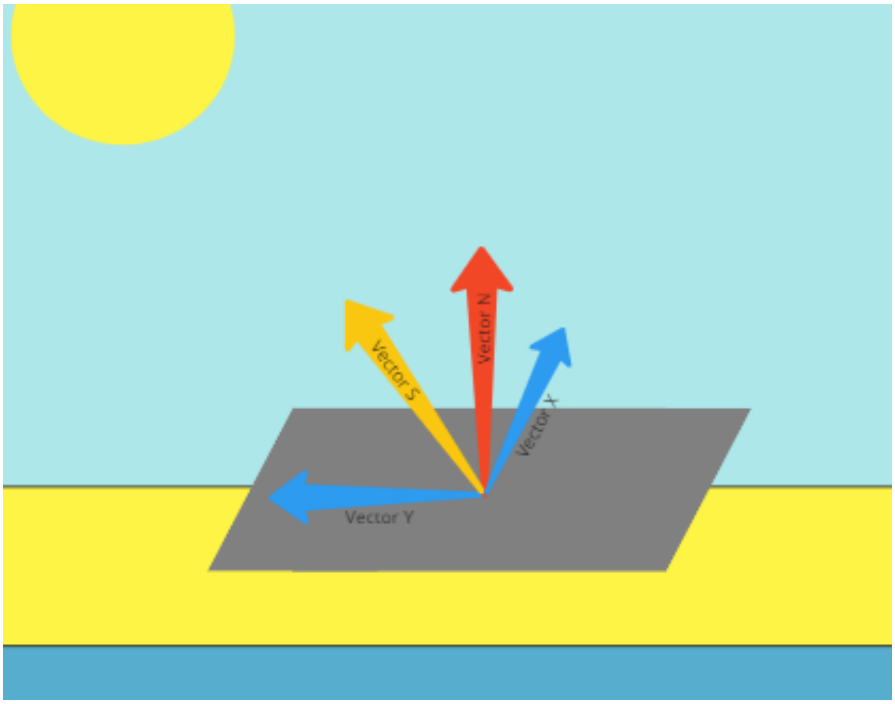

(a) Stationary WEC

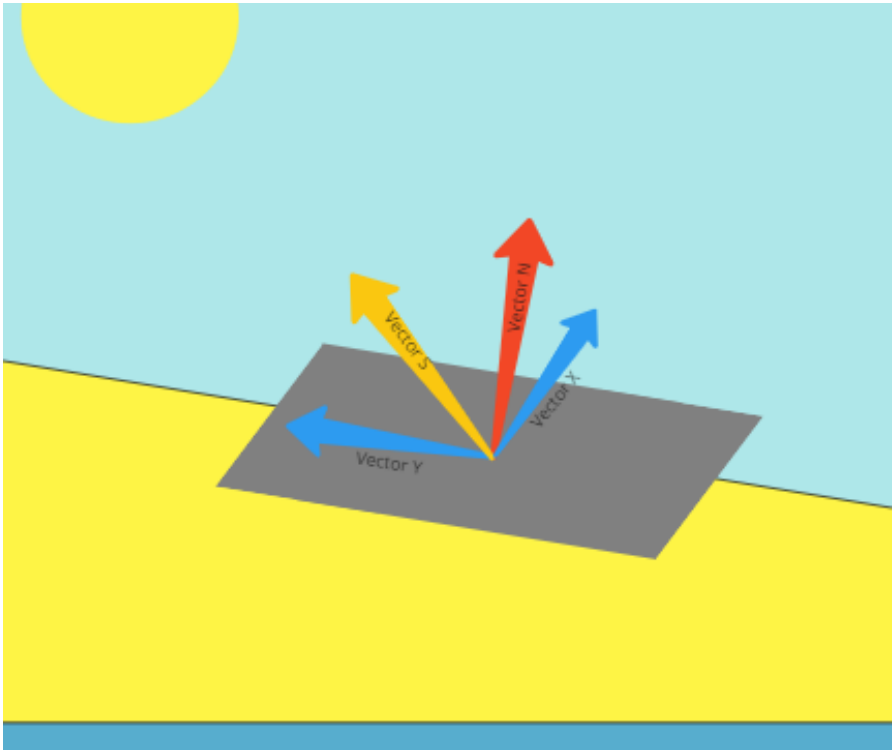

(b) Pitching WEC

Figure 5.2: Vector Diagram of a Flat Panel on a WEC

This model is the most basic of the diffuse models and assumes that the diffuse irradiance over the sky dome is uniform but provides a good approximation in diffuse environments. However, after examining and comparing results with experiments as described in Section 5.2.2, it was found that the Perez diffuse model provided the most accurate results. Therefore, it is the only one used in further analysis and modelling as shown in Equation 5.7 and Tables 5.2 and 5.1.

The Perez model is one of the most complex models as it treats contributions from isotropic, circumsolar and horizon brightening components separately by using a set of empirical coefficients based on the clearness index of the sky [120] [121] [122]. PVLib provides a function to model the Perez model, where the empirical coefficients are derived from [122] as these coefficients are suitable for worldwide analysis.

The Perez model first calculates the clearness, defined by $\varepsilon = ((DHI + DNI)/DHI + \kappa\theta_Z^3)/(1 + \kappa\theta_Z^3)$. Where κ is a constant equal to $5.535 * 10^-6$ if angles are in degrees and 1.041 for radians [123]. The value of ε then corresponds to an ε bin defined by the bounds described in Table 5.1. The ε bin then determines the constants f_{11} to f_{23} using Table 5.2. Finally, the values of f_{11} to f_{23} are used to calculate values F_1 and F_2 to be used in Equation 5.7.

Table 5.1: Perez Model Clearness Bins [122]

ε bin	Lower Bound	Upper Bound
1 Overcast	1	1.065
2	1.065	1.23
3	1.23	1.5
4	1.5	1.95
5	1.95	2.8
6	2.8	4.5
7	4.5	6.2
8 Clear	6.2	—

Table 5.2: Perez Model Coefficients [122]

ε bin	f11	f12	f13	f21	f22	f23
1	-0.008	0.588	-0.062	-0.06	0.072	-0.022
2	0.13	0.683	-0.151	-0.019	0.066	-0.029
3	0.33	0.487	-0.221	0.055	-0.064	-0.026
4	0.568	0.187	-0.295	0.109	-0.152	-0.014
5	0.873	-0.392	-0.362	0.226	-0.462	0.001
6	1.132	-1.237	-0.412	0.288	-0.823	0.056
7	1.06	-1.6	-0.359	0.264	-1.127	0.131
8	0.678	-0.327	-0.25	0.156	-1.377	0.251

$$I_{diff,Perez} = DHI * \left[(1-F_1)(1+\cos(\theta_T)/2) + F_1(a/b) + F_2\sin(\theta_T) \right] \tag{5.7}$$

Where:

a = $maximum(0, cos(AOI))$
b = $maximum(\cos(85°, \cos(\theta_Z))$
F_1 = $maximum(0, (f_{11} + f_{12}\Delta + \frac{\pi\theta_Z}{180°} f_{13}))$
F_2 = $f_{21} + f_{22}\Delta + \frac{\pi\theta_Z}{180°} f_{23}$
Δ = $DHI * AM_a / TOA$

Reflected Irradiance

The reflected irradiance is found by Equation 5.8 where $Albedo$ is the Albedo ratio of upward to downward radiation found to be 0.06 in [124] and [73], it is assumed to be constant for all sea states and sun elevation despite any white capping. One study [125] has shown using the effect of a dynamic albedo factor to account for angles and movements of the panels can marginally improve the yield by 1.03%. This difference is noted that the average difference may be sensitive to the time of year and location variances. Due to the small reported improvements which may or may not be accurate for our locations, and the increased modelling requirements, a constant albedo factor is used.

$$I_{reflect} = GHI * Albedo * ((1-\cos(R))/2) \tag{5.8}$$

Total Irradiance

The total irradiance on the panel is then the sum of the diffuse, reflected, and direct irradiances on the plane of the panel.

$$I_{Total} = I_{diff} + I_{direct} + I_{reflect} \tag{5.9}$$

When the WEC moves in the waves, the angle of the solar panels will move with it. Therefore, a view factor and I_{Total} will have to be calculated for each time step.

5.1.3 Modifiying the irradiance calculation for curved cells

Experimentation showed the benefits of better protecting the panels by adhering them to the hull resulting in the use of flexible solar panels. A curved panel will see a variance in the irradiance over each of its constitute cells. This section describes how the equations are modified to evaluate the irradiance falling onto the surface of a curved panel.

A solar panel is made up of several solar cells connected in series and parallel. To find the irradiance on the surface of the curved solar panel, the irradiance on each individual cell of the panel is calculated and compared as in [126], [127], and [128].

Each cell is treated as a flat plate mounted at a different angle around the circumference of the hull tube, as shown in Figure 5.3 and Figure 5.4. The cell angle is found by using Equation 5.10 where L is the distance between cells, r is the radius of the hull and i is the cell number measured from the vertical plane of the tube.

$$\theta_i = i * L/r \tag{5.10}$$

As long as the cell angle is measured from the top of the hull tube and the tube is axially in the direction of the WEC heading, the cell angle can then be added as an offset to the roll angle of the panel in the calculation of vector $\overrightarrow{X}$. This will give a vector $\overrightarrow{P_{Ni}}$ and thus view factor for each cell of the array at each time step. $\overrightarrow{Y}$ remains unchanged as the axial direction is not affected by the cell angle.

$$\overrightarrow{X_i} = \cos(H+90)\cos(R+\theta_i)\overrightarrow{E} + \sin(H+90)\cos(R+\theta_i)\overrightarrow{N} + \sin(R+\theta_i)\overrightarrow{Z} \tag{5.11}$$

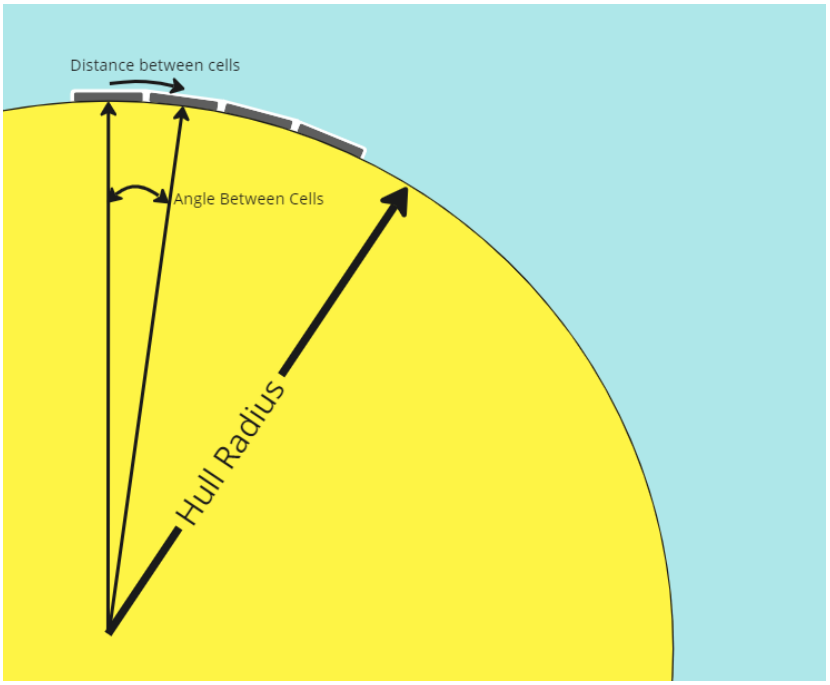

Figure 5.3: Cell angle for a curved panel

The direct irradiance per cell is then found by using the same method as for a flat plate but recalculated for each cell angle.

$$I_{direct,i} = BNI * (\overrightarrow{P_{Ni}} \cdot \overrightarrow{S}) \tag{5.12}$$

The diffuse irradiance is also influenced by the cell angle and found as

$$I_{diff,i} = DHI * (1 + \cos(R + \theta_i)/2) \tag{5.13}$$

Finally, the reflected albedo irradiance can be found as

$$I_{reflect,i} = GHI * Albedo * ((1 - \cos(R + \theta_i))/2) \tag{5.14}$$

The total irradiance on each cell is then the sum of the direct, diffuse and reflected irradiance for each angle offset, found by Equation 5.15.

$$I_{Total,i} = I_{diff,i} + I_{direct,i} + I_{reflect,i} \tag{5.15}$$

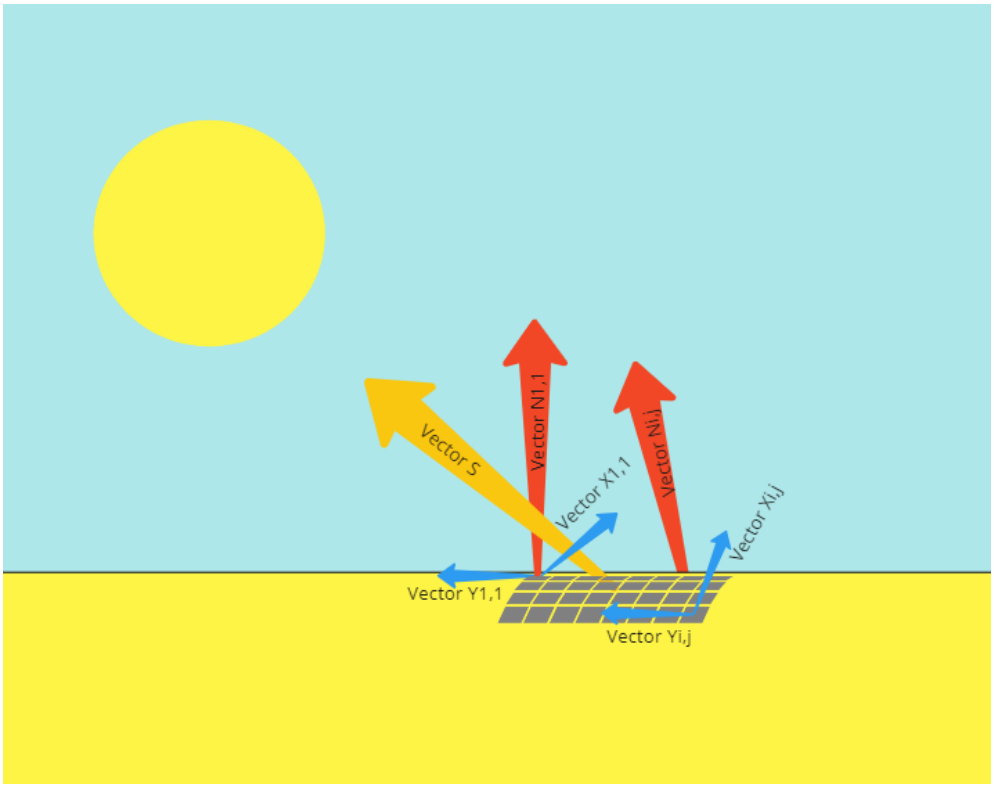

Figure 5.4: Curved Panel Cell View Angle Vectors

This results in an array of irradiances for each cell and each timestep as seen in Figure 5.5 corresponding to cells in Figure 5.4.

	SolarCell 1	SolarCell 2	SolarCell 3	SolarCell n
Time 1	Irr 1,1	Irr 1,2	Irr 1,3	Irr 1,n
Time 2	Irr 2,1	Irr 2,2	Irr 2,3	Irr 2,n
Time 3	Irr 3,1	Irr 3,2	Irr 3,3	Irr 3,n
Time t	Irr t,1	Irr t,2	Irr t,3	Irr t,n

Figure 5.5: Irradiance Matrix

5.1.4 Calculating Power Output

Given the irradiance on the cells of a panel and the panel's electrical characteristics the power output at the maximum power point can be calculated. However, in several instances a panel will see a variance in the irradiance over its cells due to shading from other objects on the WEC superstructure, bio-fouling from sea birds and marine life, or the self-shading due to the curvature of flexible panels. If the cells are connected in series, the output of the entire string is dependent on the output of the cell with the lowest output current.

The power output of the series string can be found by finding the minimum irradiance in each row of the irradiance matrix in Figure 5.5 shown in Equation 5.16, where m denotes the string number and n is the total number of cells belonging to string m.

$$Imin_{string,m} = min(I_{Total1,2...n}) \tag{5.16}$$

To reduce the impact from shading in larger panels, long strings are broken down into strings with bypass diodes as shown in Figure 5.6 which has 36 cells arranged into two series strings of 18 cells separated by bypass diodes. It should be noted that 9 of the cells of each 18-cell series string are arranged in one line of the panel and the subsequent 9 cells lie next to the first, when this panel is curved, half of the 28 cells will lie on one plane whilst the other half lies on another. In the event of partial shading of a panel, where one series string has a lower power output compared to the remainder of the strings, the mismatch in voltages allows for the shaded string to be bypassed by the bypass diode and the total power output improved.

To calculate if bypass diodes are engaged, the output characteristics of each series string must be defined. Each string is treated as a "panel" in the PVLib toolbox. This means a 36 cell panel with two strings of 18 cells connected with bypass diodes, as in Figure 5.6 will be treated as two "half panels". Therefore the voltage characteristics of the panels must be modified to represent two halves of the original panel by halving the voltage characteristics and maintaining the current characteristics.

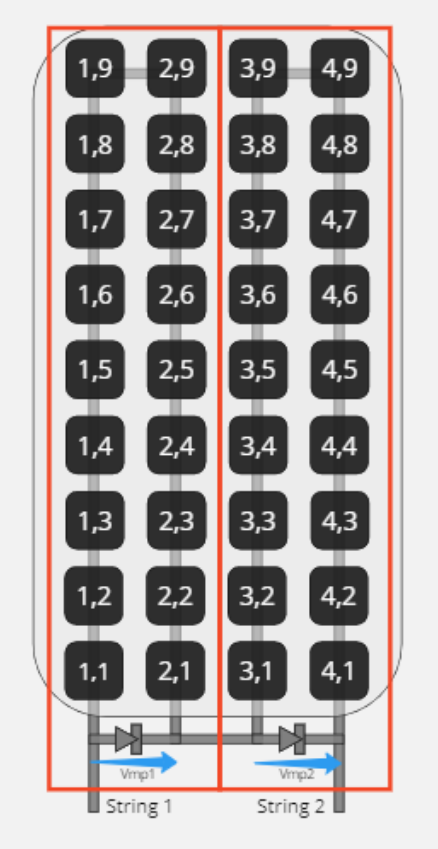

Figure 5.6: Diagram highlighting the series strings and bypass diodes

Cell Temperature

The first step is to calculate the cell temperature. This is done by using the PVLib toolbox "pvl_sapmcelltemp" function which describes Equations 5.17 and 5.18 derived from [129].

First, the module temperature is determined using Equation 5.17. This equation has been developed at Sandia and applied successfully for solar panels deployed in representative manners. This model was found to produce module operating temperatures with an accuracy of ±5℃ which would result in less than a 3% effect on the power output from the module.

The empirically determined coefficients are based on thousands of measurements performed by Sandia on traditional mounting methods and panels. The coefficients can be influenced by factors of the module construction and array arrangement and location. Therefore the factors used and the equation presented, may work well for panels mounted in their expected use cases but not necessarily for a curved flexible panel adhered directly to a steel hull. However, errors in temperature can only have a small expected error on the power produced.

$$T_m = E[e^{a+b*WS}] + T_a \tag{5.17}$$

Where:

T_m = Module Temperature ($^\circ C$)
T_a = Ambient Temperature ($^\circ C$)
E = Solar Irradiance on Module Surface (W/m^2)
WS = Wind Speed measure at 10m (m/s)
a = Empirically-determined coefficient establishing the upper limit for module temperature at low wind speeds and high solar irradiance
b = Empirically-determined coefficient establishing the rate at which module temperature drops as wind speed increases

After calculating the module temperature, the cell temperature can be calculated by Equation 5.18. This is based on a one-dimensional thermal heat conduction from the solar module to the solar cell. This is dependent on the panel materials and captured by ΔT.

$$T_c = T_m + (E/E_0)\Delta T \tag{5.18}$$

Where:

T_c = Cell Temperature
E_0 = Reference Irradiance ($1000W/m^2$)

ΔT = Temperature difference between the cell and the module back surface at Reference Irradiance. This temperature difference is typically 2 to 3 $^{\circ}C$ for flat-plate modules in an open-rack mount. For flat-plate modules with a thermally insulated back surface, this temperature difference can be assumed to be zero. For concentrator modules, this temperature difference is typically determined between the cell and the root of a finned heat exchanger (heat sink) on the back of the module.

"pvl_sapmcelltemp" requires inputs of irradiance, wind speed, ambient temperature and the module parameters. As the values of irradiance differ over the series string, the mean irradiance is used to estimate the mean cell temperature shown in Equation 5.19. Initially, values of a = -3.56 b = -0.075 deltaT = 3 are used which are shown to be equal to a Glass/Cell/Polymer sheet panel mounted with an open rack. This may not be an ideal approximation, however, without cell temperature data it is the best available.

$$Imean_{string,m} = mean(I_{Cell1,2...n}) \tag{5.19}$$

String Output

Now with a mean cell temperature the series string voltage, current and power can be calculated using the "pvl_sapm" PVLib Toolbox function. "pvl_sapm" requires inputs of module parameters, irradiance and cell temperature. This then produces a MATLAB structure with 7 results; Result.Isc, Result.Imp, Result.Ix, Result.Ixx, Result.Voc, Result.Vmp, and Result.Pmp.

The calculations within "pvl_sapm" are detailed in [130], specifically, equations 1 to 5 and equations 9 and 10. This is repeated for every series string in the array resulting in the matrix shown in Figure 5.7 where the cells can display string output power, voltage or current.

Array Output

The module is assumed to be operating at its maximum power point through the implication of suitable Maximum Power Point Tracking (MPPT) and thus the values of Imp, Vmp, and Pmp are used to assess the final output. The Vmp of each string is compared with the Vmp of the neighbouring string. If the difference between the strings is more than the diode drop voltage of 0.6V then the bypass diode is forward

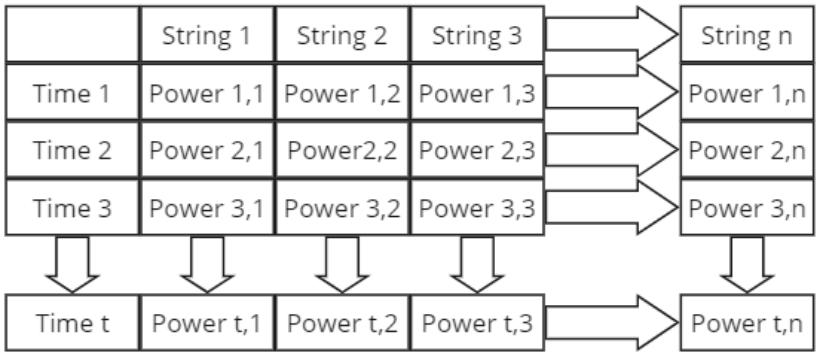

Figure 5.7: String Matrix

biased and the string with a lower voltage is bypassed. The total number of connected strings is counted and the total power of that array is then the number of connected strings multiplied by the minimum power output. The entire process is then repeated for the next timestep to achieve the matrix in Figure 5.8.

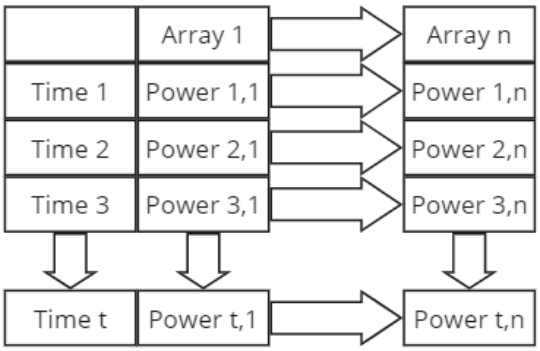

Figure 5.8: Array Matrix

System Output

The solar panel system is combined with a battery system to store excess energy. The system will also provide power to constant demands. This is modelled simply by evaluating the "energy balance" at each time step where power produced by the system are positive whilst loads are negative. A check is included to cap the energy balance at the battery capacity. When the battery is full, the output from the solar array will be curtailed so that the loads are met and the battery remains full. This is included in the model by simply only including the power required to meet the load from the solar arrays, any excess is set to zero.

The model inputs can now be sourced and the model ran over the desired timescale. The model is compared to the experimental results to determine its accuracy. The size of the timestep needs to be appropriate so that the model does not take excessively long to run but does not quantise the WEC positional data.

5.2 Comparing Model to Renewable Subsea Power Experiment

The model is compared to the results obtained from the experiment described in Chapter 4. The longer testing period and more complete solar test kit of the Renewables for Subsea Power program provides more data points than the Scapa Flow Testing. This allows for a more in-depth comparison between the Model and Experiment which is more statistically significant and therefore is better positioned to inform full-scale modelling.

First, the different temporal resolutions are analysed, and then the diffuse models are compared. Finally, the power at key points of the experiment is identified by comparing the daily energy results from the model and experiment.

5.2.1 Temporal Resolution

The different data inputs have varying temporal resolutions, varying from the 25Hz WEC positional data to the half-hourly buoy data. Additionally, the solar vector is calculated for every hour of the day and thus only changes a handful of times over the hours between sunrise and sunset. All the datasets need to be synchronised so that they are all using the same timestep. Using too large of a temporal resolution will quantise the WEC positional data and will reduce the peak angles. Using too small of a temporal resolution will lead to long run times and excess data. Figure 5.9 shows the WEC pitch angles during the 24th of April, chosen as it has a distinct peak and doesn't enter hibernation mode.

Figure 5.9a shows the original 25Hz sampling frequency where it peaks at 40.8 degrees. Figure 5.9b shows the same data on the same day, but averaged over a second. This means that 25 data points from the original dataset go into the calculation for the secondly data. The peak has reduced, but only marginally, to 36.8 degrees. This has been carried out for minutely and hourly means but the results show a near horizontal line when observed at the same scale as the original data.

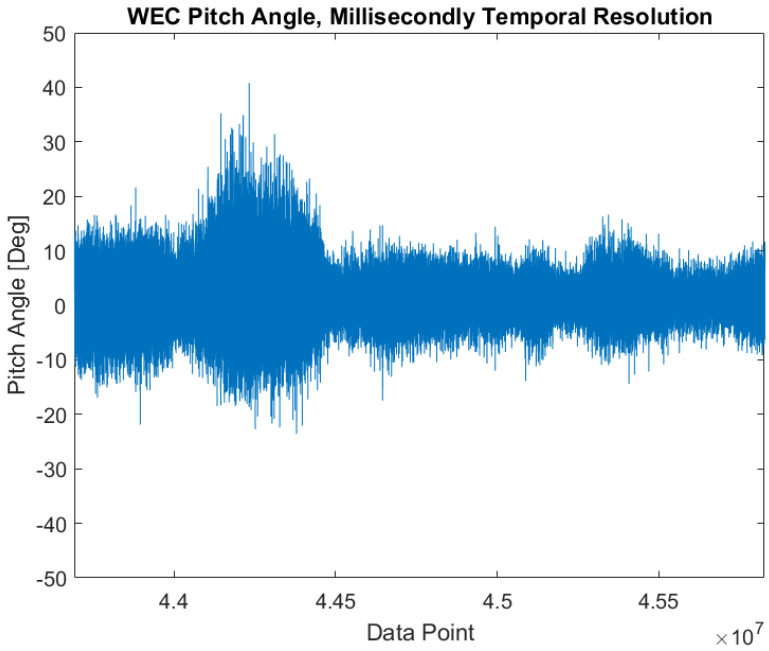

(a)

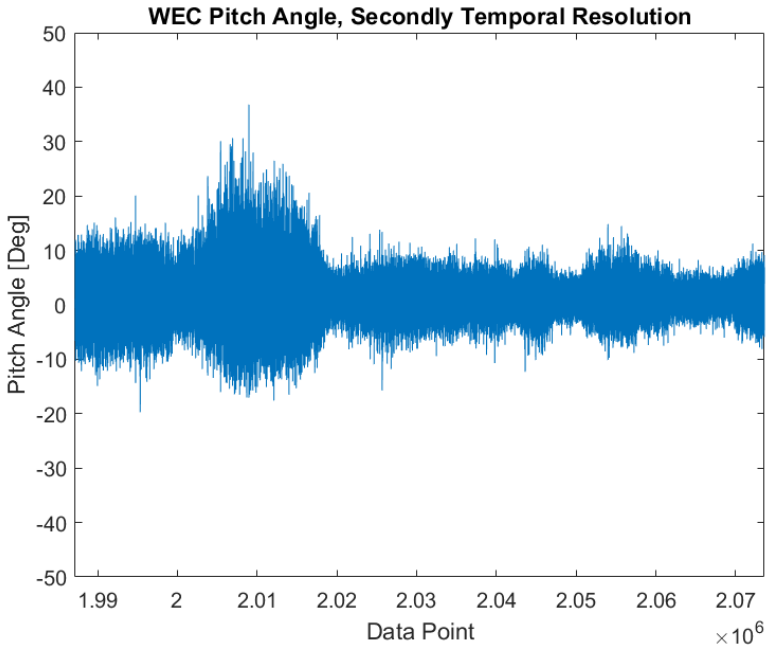

(b)

Figure 5.9: Temporal Resolution Comparison between Raw Data and Secondly Mean Data

The four temporal resolutions are compared in Table 5.3 where the percentage difference compared to the raw data is also presented. This shows that although the maximum has reduced by 9.8% and the standard deviation by 6.7% the number of points to be examined is now only 4% of the raw data. This considerable data

reduction will speed up the analysis with only a small impact on the angle data and is considered a worthwhile sacrifice. Using temporal resolutions larger than a second is deemed too inaccurate, therefore, a second time resolution is used for all further analysis.

Table 5.3: Variance in Pitch Angles with Reducing Temporal Resolution

	40 Millisecondly	**Secondly**		**Minutely**		**Hourly**	
Maximum	40.8	36.8	-9.8%	3.42	-91.6%	2.43	-94.0%
Standard Deviation	4.31	4.02	-6.7%	0.4	-90.7%	0.35	-91.9%
Number of Points	2130396	86400	-95.9%	1440	-99.9%	24	-100.0%

5.2.2 Diffuse Models

As discussed in Section 5.1.2, there are several different diffuse irradiance models, with varying levels of complexity. This section explores the influence on energy yield due to using different models and concludes on why the Perez model was selected.

The numerical model was run using five different diffuse irradiance models, namely, the Isotropic model, Riendl, Perez, Klucher and the Hay and Davies model. The results of energy are then compared to the experimental results for accuracy. This work was completed for the stationary period, covering dates from 27th November 2022 to the end of February 2023. Table 5.4 shows the energy modelled over each period for each diffuse model and is then compared with the experimental results shown in Table 4.2. As this period extends over winter months, diffuse days are more prevalent and thus the effect of the diffuse model is more significant. The energy is, therefore, more dependant on the selection of the diffuse model, highlighting the differences between the options.

By comparing the energy yields with the experiment, the error of each model can be identified. The calculation is split between the forward and nacelle arrays. The Hay and Davies model and the Riendl model produced similar errors when compared to the experimentation. The errors for these two models are the most significant and thus are discarded for further analysis. The best model for the forward array is surprisingly the isotropic model which assumes a uniform distribution of diffuse irradiance in the sky dome, giving a 0% error. However, the same model produces a 12% underestimate for the nacelle array. The Klucher model produces similar errors

Table 5.4: The Influence on Energy of Different Diffuse Models

Model	Time Period	Front [Wh/%diff]		Nacelle [Wh/%diff]	
Isotropic	27-11 to 31-12	790	-1%	1585	7%
	01-01 to 07-02	1310	-11%	3028	11%
	08-02 to 28-02	1550	13%	3081	15%
	Total	3649	0%	7695	12%
Riendl	27-11 to 31-12	2040	157%	459	-69%
	01-01 to 07-02	2220	50%	1695	-38%
	08-02 to 28-02	1352	-1%	2151	-20%
	Total	5613	54%	4304	-37%
Perez	27-11 to 31-12	884	11%	1324	-10%
	01-01 to 07-02	1351	-9%	2560	-6%
	08-02 to 28-02	1306	-5%	2570	-4%
	Total	3541	-3%	6454	-6%
Klucher	27-11 to 31-12	806	2%	1657	12%
	01-01 to 07-02	1321	-11%	3141	15%
	08-02 to 28-02	1559	14%	3198	20%
	Total	3685	1%	7995	16%
Hay & Davies	27-11 to 31-12	2041	157%	453	-69%
	01-01 to 07-02	2220	50%	1674	-39%
	08-02 to 28-02	1333	-3%	2121	-21%
	Total	5593	53%	4249	-38%

to the Isotropic model, yielding underestimates of 1% for the forward array and 16% for the nacelle array. The best model for the nacelle array is the Perez model, giving a 6% overestimate whilst the forward array has a 3% overestimate. Therefore the Perez model gives the lowest average error for the two arrays, over the time period.

5.2.3 Comparison of Energy

As described in Section 5.1.4, during the second series of experimentation, the panels fed the communications load of the BlueX Wave Energy Converter through a 50Ah li-po battery. The panel power output is curtailed when the battery is full, therefore, the model includes an energy balance calculation to account for this scenario. If this step was not included, the model would overpredict the energy produced by the system. At every time step, the energy produced by the panels is summed into the system, whilst loads are misused. The operation is capped by the total battery capacity. By ignoring the battery curtailment, the total potential energy gives an indication of the system if it were to power larger loads or had a larger capacity battery, this is shown in Appendix C.

The real system doesn't work as described here. The lithium-ion battery has different stages of charging; bulk, absorption and float. In bulk charging, the maximum current is absorbed until the battery voltage reaches the set limit where it enters absorption. In absorption, the current is limited so that the voltage is held constant, the amount of current reduces as the internal resistance increases. Absorption continues until either the current reduces to zero or a time threshold limit is reached. After absorption, the charge controller enters float mode where the voltage is held lower than the absorption voltage and current trickle charges in to balance loads of the system and keep the battery fully charged. Therefore, during these states, the magnitude of power is modified from the maximum available resource. This could be modelled using a more complex battery model, perhaps in Simulink. However, the time taken to model this basic battery model is already lengthy, and adding complexity is likely to extend it. The suitability of the simple battery model is examined here.

Method

BlueX positional data is downloaded from the WEC system whilst irradiance and temperature data are obtained from online sources. As described in Chapter 4, during periods of low wave action, the data acquisition systems of BlueX are put into standby mode to preserve power. This means that during these periods, there are no pitch, roll or heading data to be included in the model. Pitch and roll can be assumed to be small, as there is not sufficient motion to produce power. Therefore, they are set to zero for these times. The heading is harder to predict, and as will be shown in Section 6.1, it is important for power production. As shown in Chapter 4, the heading is cyclic and mostly follows the changing tides in the location with some variation due to wind and wave direction. The heading is modelled with a linear interpolation between the available data points on either side of the standby periods. The model is run using a temporal resolution of a second and thus all data inputs are synchronised to run at second timesteps.

Results

Whilst the power is modelled at each secondly timestep, examining this data is not useful as it is so dense. To better observe how the model performed compared to the experiment, the energy is calculated. Initially, this is done on a daily basis and then on a monthly basis. The daily energy of the forward, nacelle and combined arrays from the experiment and model is shown in Figure 5.10. Figure C.1 in Appendix C shows the modelling results with and without the battery curtailment model.

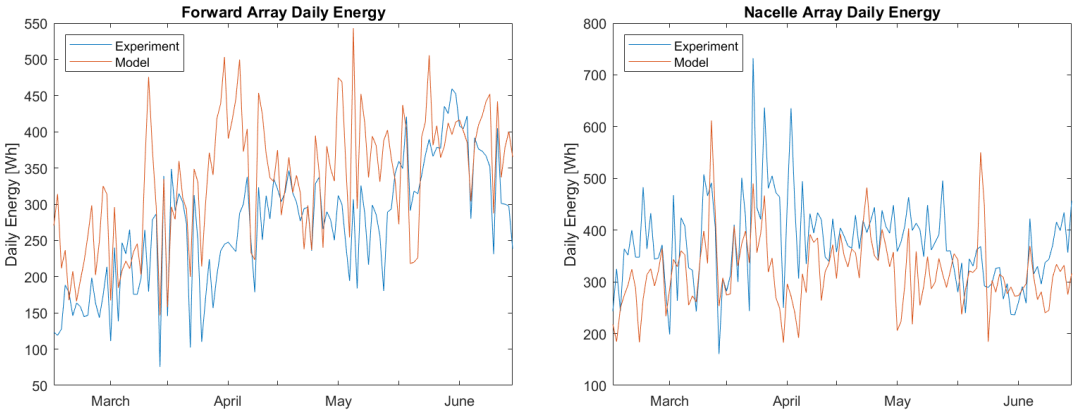

(a) Forward Array **(b)** Nacelle Array

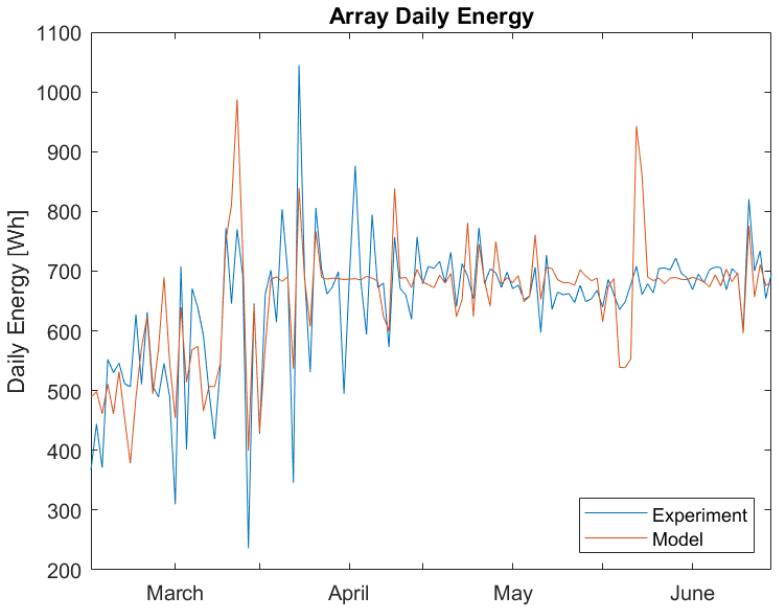

(c) Full Array

Figure 5.10: Daily Energy Comparison

The percentage error of the modelling of the daily energy is presented in Figure 5.11. Where the percentage error between experiment and model is calculated by $100 * (ModelledEnergy - ExperimentEnergy)/ExperimentEnergy$. This will help explore the conditions under which the model is most and least accurate.

Figure 5.11 shows that the forward array model regularly overestimates the produced energy. When the battery is full, the forward array powers the communications load and the nacelle array is curtailed. Thus, an overestimate of the forward array will lead to an underestimate of the nacelle array. One reason for the overestimation may be due to the biofouling obscuring the panels. The reduction in error at the end of April would then coincide with the cleaning of the panels on the 22nd of April. However, this wouldn't explain the improvement in accuracy at the end of May.

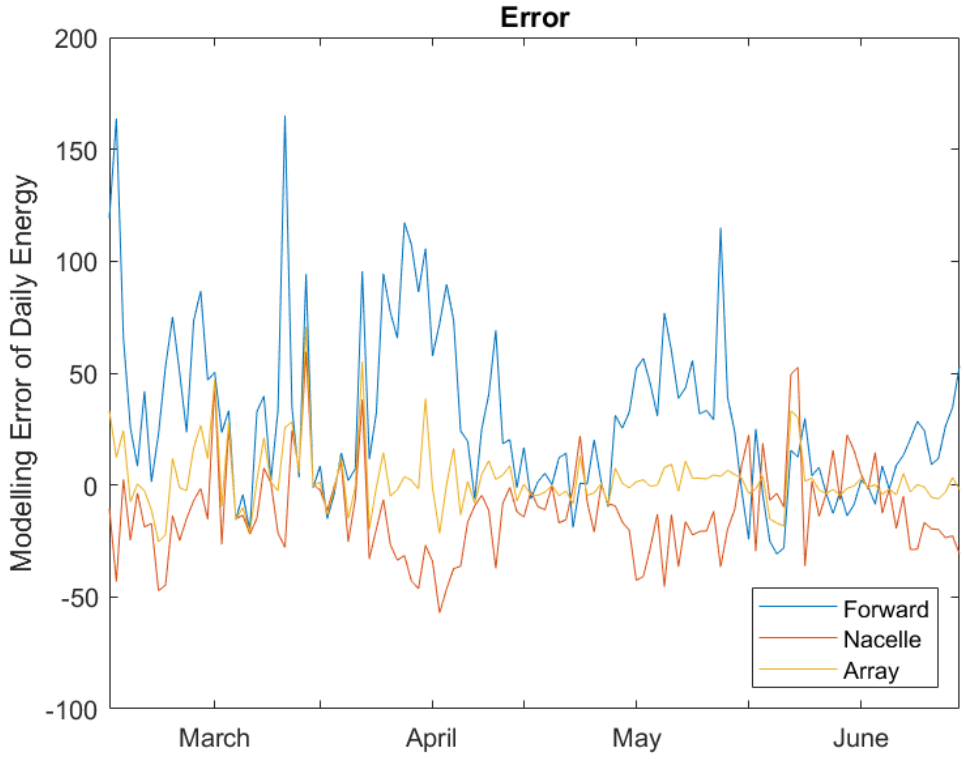

Figure 5.11: Modelling Percentage Error in the Daily Energy

The total energy produced per month of the testing period is shown in Table 5.5. This shows that agreement in the months of April to June has an error between -0.61% and 1.18%. In March, the error is larger, 4.22%. The percentage difference over the total deployment period is only 0.77%, suggesting that the model is an accurate representation of the energy produced. However, when looking at single

days, the errors in the array daily energy can be up to a 70% over prediction or a 25% under prediction whilst some days are accurate to 0.05%. When considering only the forward array, it reaches a peak error on the 26th of March of 165%. The nacelle array hits its peak error on the 29th of March at a 57% over-prediction, the highest under-prediction was also 57% on the 17th of April.

However, the larger error in March, where the battery system was rarely fully charged and thus power curtailed, suggests that the way in which the battery model is calculated is impacting the accuracy of the model. Essentially, if the daily energy produced by the panels is more than the daily demand of the communications, the energy is curtailed to meet the same magnitude. The error then comes down to any fluctuations in the load and mismatch between that modelled and that experienced in the experiment. This can happen as the load is modelled as a constant load but can actually fluctuate slightly. By examining the accuracy of the system in March only, the effect of the battery model on the accuracy of the model can be minimised as seen in Figure 5.12.

Table 5.5: Comparison of Monthly Energy From Experimental Results and Numerical Model

	Experiment [kWh]	Modelled [kWh]	% Difference
March	16.60	17.30	4.22%
April	20.70	20.50	-0.97%
May	20.36	20.60	1.18%
June	21.31	21.18	-0.61%
Total	78.97	79.58	0.77%

The error fluctuates on a day-to-day basis, to explore what may cause these fluctuations, the environmental data such as wave period, wave height and heading is examined. No significant correlation between error and these properties could be found. However, when examining the clearness index of the solar data, found by the ratio of Global Horizontal Irradiation to Top of Atmosphere Irradiation, a significant correlation between clearness index and error was found, as seen in Figure 5.13. P and R values of the error on the forward array and clearness were 0.0132 and 0.2239 whilst for the nacelle array error and clearness were 0.0000 and -0.3858. When examining the error of the array compared to the clearness, the P and R values are 0.1641 and -0.1268 which would be insignificant. This suggests that the clearness of the solar climate has a significant influence on the accuracy of the modelling of the forward and nacelle array where a clear environment will cause over-predictions of the forward array and under-predictions of the nacelle array. This is unfortunate, as

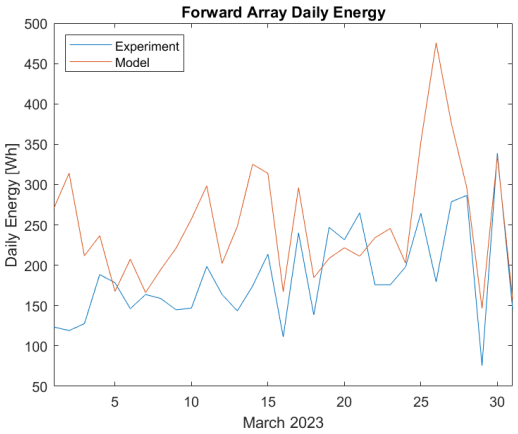

(a) Forward Array March

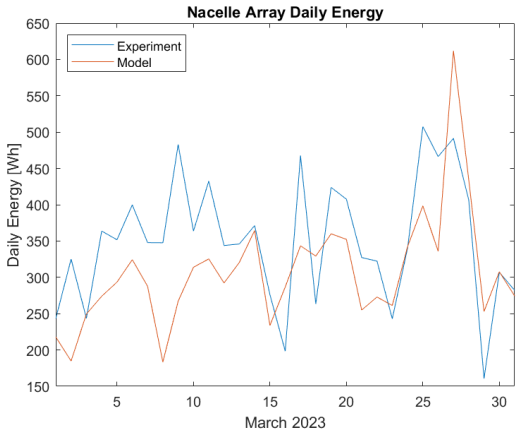

(b) Nacelle Array March

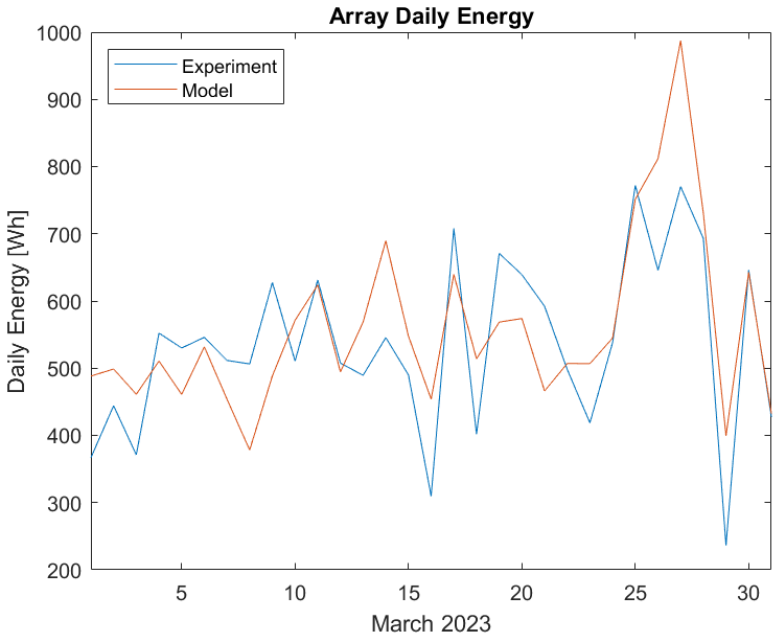

(c) Full Array March

Figure 5.12: Daily Energy Comparison for March

solar energy is most desired during the summer months when the clearness tends to be higher. Another factor may lie in the sub-optimal arrangement of the forward array, meaning the two panels in the array have opposite zenith angles. The influence of clearness appears to be negated when comparing the contributions from both arrays together. However, as the energy from both of these sources is not independent and limited by the load, this is perhaps not a good evaluation.

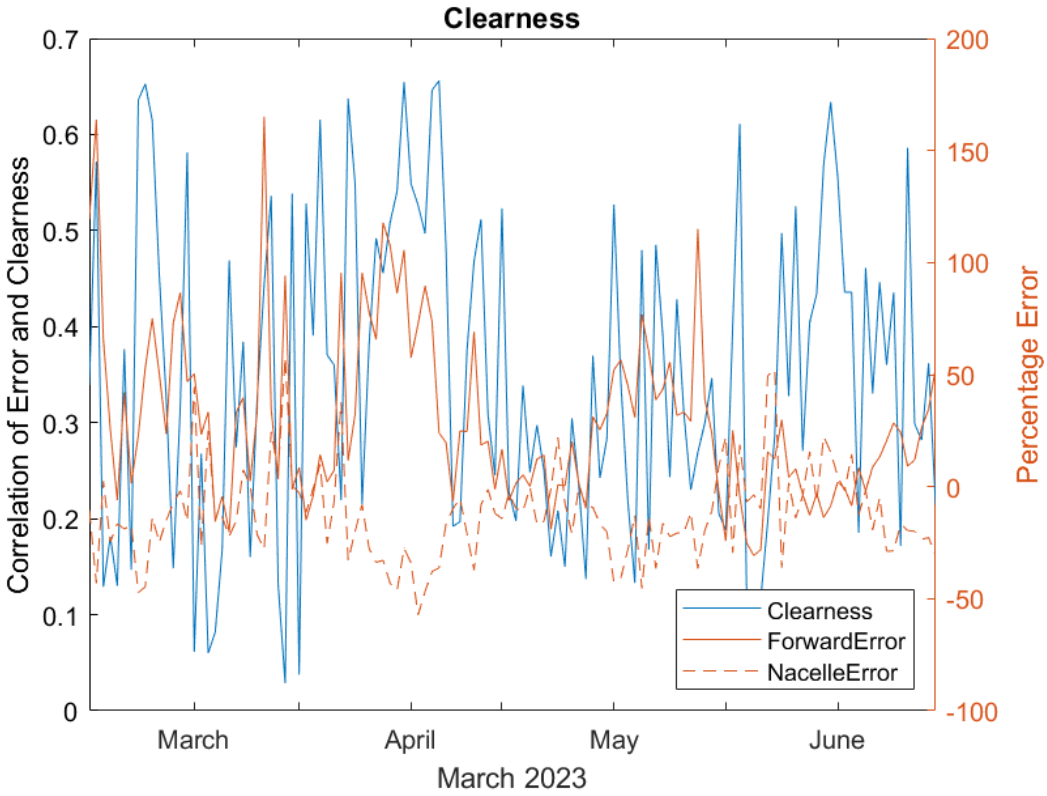

Figure 5.13: Modelling Percentage Error in the Daily Energy compared with the Clearness

By minimising the influence of the load on the correlation studies by just considering the data from March, shown in Figure 5.12 the array daily yield and experimental yield have an error of 4.22%. When examining the P and R values for the errors compared with the clearness, the P value for the forward array increases by a factor of ten to become insignificant. The array P value remains insignificant. However, the nacelle P value becomes 0.0015, so still significant and the R-value is -0.5394. This, therefore, suggests that the clearness has a significant influence on the energy modelled by the nacelle array where a clear environment leads to under-estimation of power.

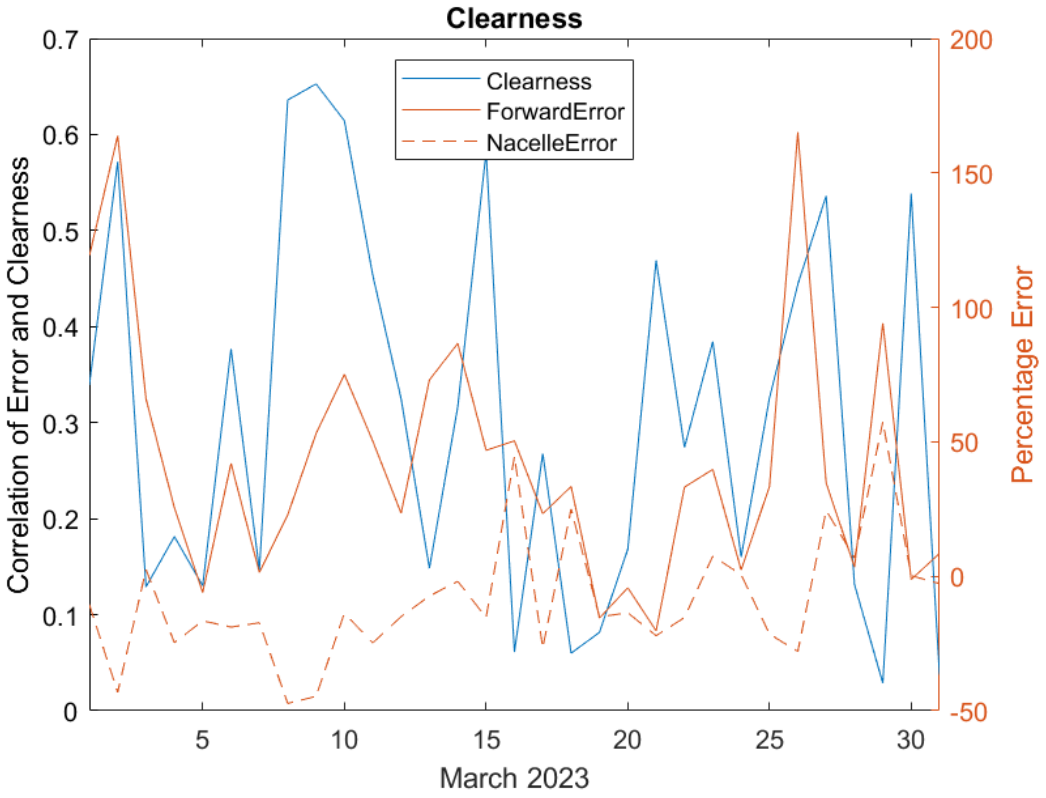

Figure 5.14: Modelling Percentage Error in the Daily Energy compared with the Clearness for March

5.3 Chapter Summary

To be able to predict the energy yield of a solar array onboard a wave energy converter, a numeric model has been produced. This model is based upon established solar modelling methods and has the ability to model flat or curved panels. The model is produced in MATLAB and uses and builds upon the Scandia Labs PV Lib Toolbox to incorporate curved panels and the WEC dynamics and headings.

After the model was produced, it was compared against the experimental results from the RSP testing period. Whilst the Scapa Flow experiments were useful, they only had 16 days of data and did not include a battery storage system or power electronics. Therefore, only the testing at RSP is compared against the model.

The temporal resolution was fixed at a second so that the dynamics of the WEC are captured whilst not requiring extensive modelling resources. By increasing the temporal resolution from 40 millisecondly to secondly, the maximum WEC pitch angle was reduced by 9.8% and the standard deviation of the pitch angle was reduced by 6.8% but the number of points to evaluate was reduced by a factor of 25.

Five diffuse models were compared for accuracy. The Perez model was found to present the lowest average error of 4% and was used in final assessments and future predictions, other models had errors up to 54% over the entire testing period.

To assess the accuracy of the model, the daily energy calculated in the model is compared against the actual experimental daily energy. It was found that the total system had an error of 0.77% suggesting a very good agreement between model and real life. However, when considering shorter timescales, the error increases. During the months between April and June, the battery was regularly at 100% state of charge and thus, as long as the daily energy demand was exceeded, the energy estimated by the model would be curtailed at that point. This would erroneously exaggerate the accuracy of the model, as the daily energy is limited by the daily demand. In March, the battery did not reach 100% state of charge as frequently. When examining this month, the error increases to 4.22% which is still low enough to provide a good estimate of energy produced by the solar array onboard the WEC. This is a good result, especially when considering the effects of quantisation on the WEC dynamics, the error in the diffuse model and the influence of biofouling and water splashing.

Following this examination, the model is deemed to provide a good approximation of the energy of the solar array onboard the BlueX. The model can now be used to explore the contributions of a full-scale array onboard the BlueX in different locations.

Chapter 6

Design Parameters, Yield and Economic Assessment of a Full Scale Solar Array

The model produced and validated in Chapter 5 is used to explore and compare the design parameters of a full-scale array. The contributions of a full-sized solar array onboard BlueX in locations where there is a strong seasonal variation are then explored where conclusions about the array performance and costs are drawn.

6.1 The Influence of Hull Diameter and Heading on Solar Yield

Chapters 3 and 4 suggest that adhering flexible panels to a WEC hull can provide more protection from wave damage than bolting rigid panels to a frame.

However, there are two problems with installing flexible panels directly on the hull of the WEC. As the hull is made from a round tube, the solar panels will not be flat. This creates a difference in the irradiance seen by the individual solar panel cells in the solar panel, resulting in partial shading, as discussed in Chapter 4 and 5. Secondly, as the WEC is free to weathervane into the principal wave direction, the curved panels are free to face any heading. This will continuously alter the relative angle of the cells to the sun, influencing the energy yield, especially at larger lattitudes. Instead of a curved array, a flat array could be installed by introducing a frame or platform, which would reduce the sensitivity of the array to the heading. However, this introduces cost and mass whilst also reducing the likelihood of wave washing of biofouling.

This section sets out to calculate and compare the energy yield of a curved solar array to a flat array on a Wave Energy Converter. Key parameters which would influence the yield are varied; WEC heading, array capacity, deployment location, and hull diameter to investigate the sensitivity of the results. The main conclusion is a determination of the estimated energy loss due to using curved panels rather than flat panels.

6.1.1 Methodology

The dimensions of the Solbian SR186L [106] panel are used in this analysis to provide continuity from the testing phase in Chapter 4 as seen in Table 6.1. The panel has four rows of nine cells connected in series. There are bypass diodes between rows but the effect of these are neglected in this study. Therefore, the results obtained are conservative and provide a worst-case scenario of curved power output.

Table 6.1: Solbian SR186L Reference Panel Properties

Parameter	Value
Panel Capacity	186W
Distance between Centre of Celle	0.17m
Panel Thickness	2mm
Open Circuit Voltage	24V
Short Circuit Current	9.8A

By laying this panel so that the longest length is along the axial direction of the machine, the four sets of series cells lie around the circumference of the hull. This means the irradiance on each row of nine cells is constant but is different from subsequent rows.

Three designs using the SR186L are investigated with different installed capacities and "coverage" of the circular hull. The designs initially are based on a 2m hull diameter but this is varied in Section 6.1.2. Diagrams of the designs are outlined in Figures 6.1 to 6.3

1. A single panel laid along the top of the hull, two cells on either side of the centreline.

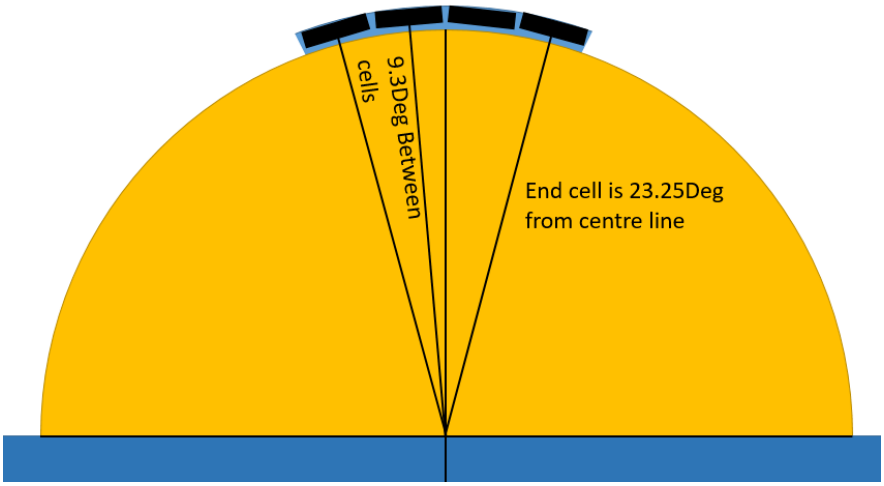

Figure 6.1: Cross Section of Design 1 Mounted on 2m Hull Diameter

2. Two panels laid with their common edge centred along the top of the hull.

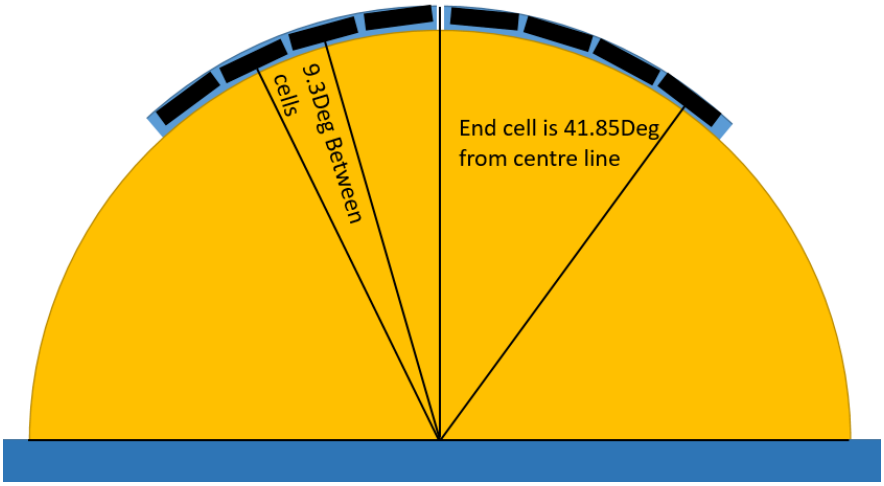

Figure 6.2: Cross Section of Design 2 Mounted on 2m Hull Diameter

3. Three panels with the central panel centred on the top of the hull and a panel on either side.

The model described in Chapter 5 is used to find the minimum irradiance on the panel. The Performance Ratio (PR) due to curvature is found using Equation 6.1 where the PR is the ratio of the irradiance on the curved panel to the flat panel.

$$PR = I_{panel,m}/I_{Total} \tag{6.1}$$

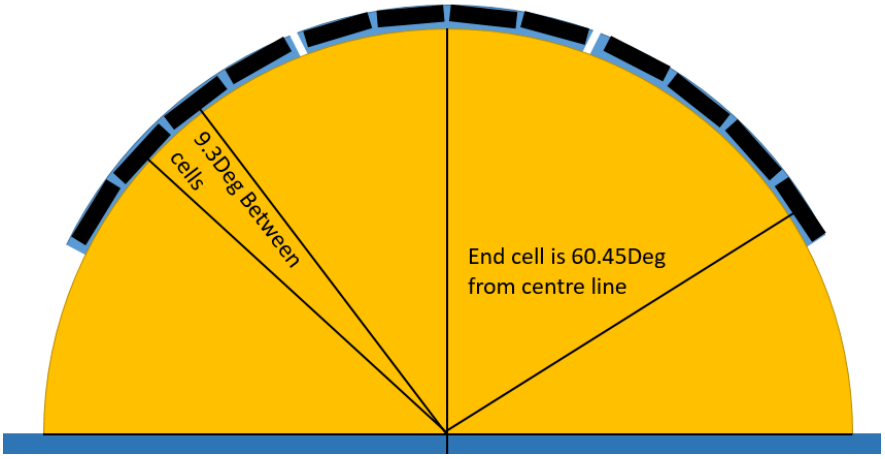

Figure 6.3: Cross Section of Design 3 Mounted on 2m Hull Diameter

By examining the PR instead of the absolute energy output, the results are independent of panel area, efficiency and temperature. Additionally, this means that the effect of seasons on absolute energy is removed. The results can then be used for alternative panel types, as long as the cell angles (Found in Equation 5.10) are comparable. To provide more comparison points, a number of cell angles are explored in this study by varying the hull radius and obtaining the PR for each combination of heading, hull radius, array design and location. The Performance Ratio can provide a quick way of evaluating the output of a curved panel by finding the corresponding PR for the location, month and heading and multiplying this by energy produced by a flat panel. This assumes that the flat panel and curved panel have similar operating temperatures.

The model is run for locations in the North Sea and Caribbean Sea to explore the influence of heading, curvature and location on the energy yield of a curved array.

6.1.2 Results and Discussion

Central North Sea – Influence of Capacity and Heading

Figure 6.4 through to Figure 6.6 show the PR of the three designs deployed in the North Sea for heading angles 0, 45, and 90 degrees. Results for headings beyond this are omitted as symmetry repeats the results.

Figure 6.4 shows that for a small array in the North Sea, the heading direction is critical for power production. This is especially true in the winter months where the PR can vary between approximately 0.74 and 0.99 for East-West Headings compared to North-South headings. For all angles, the curved panel produces less energy than the flat panel. Headings away from the North-South heading have lower PRs because when facing North, the panels are curved towards the east and west. While not optimal is a better option than having the panels curve towards the north (in the northern hemisphere).

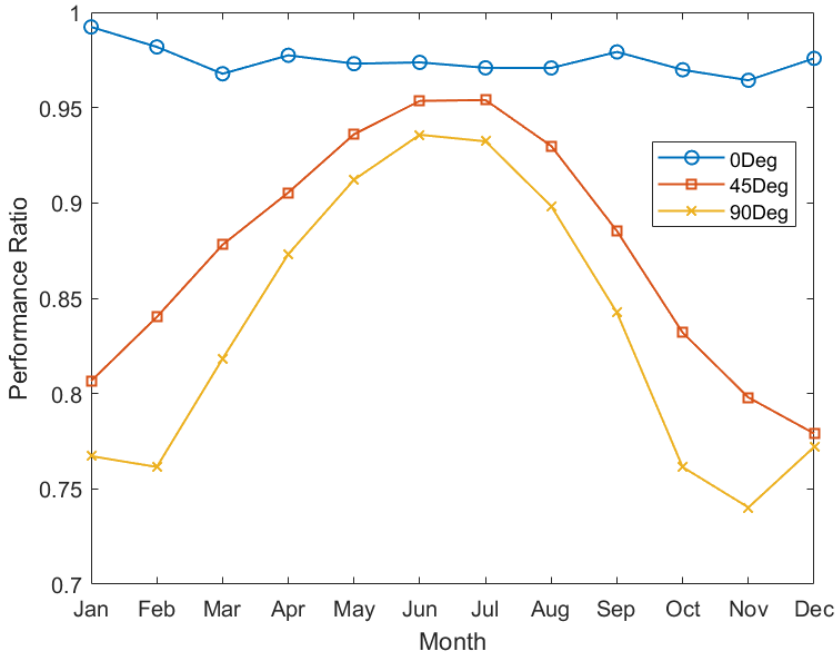

Figure 6.4: Performance Ratio of Design 1 in the Central North Sea at different Headings

At all headings in Figure 6.5 and Figure 6.6 the PR in the winter is higher than in the summer. This is because in the winter at high latitudes, the sun remains low in the sky and the curved panels have a tilt towards the direct beam whilst the flat array has a large incidence angle to the sun. Whereas in the summer, the sun is high and shines directly on a flat array. For Design 3, in Figure 6.6, this behaviour is so prevalent that for a heading of 90 degrees in December, the curved array can produce more energy than the flat array, indicated by a PR greater than 1.

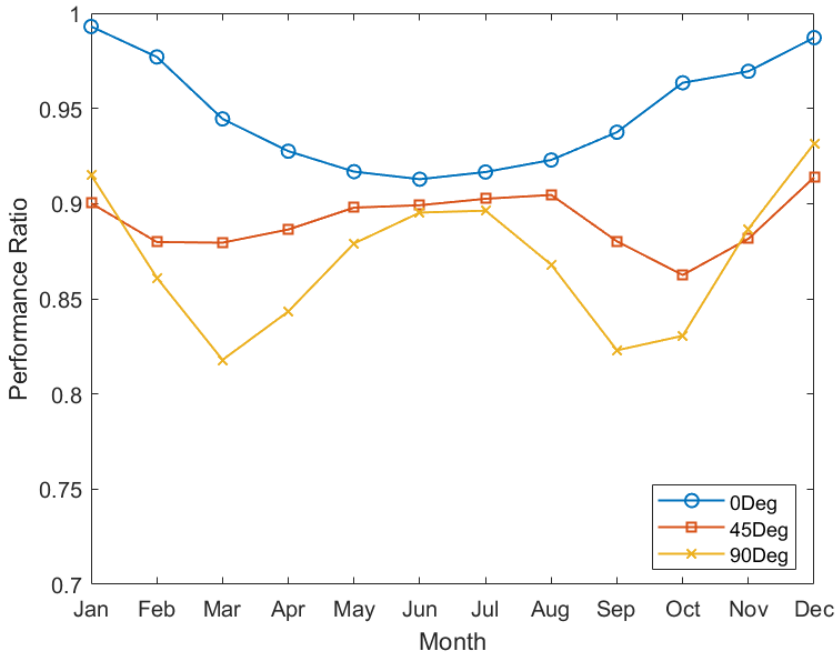

Figure 6.5: Performance Ratio of Design 2 in the Central North Sea at different Headings

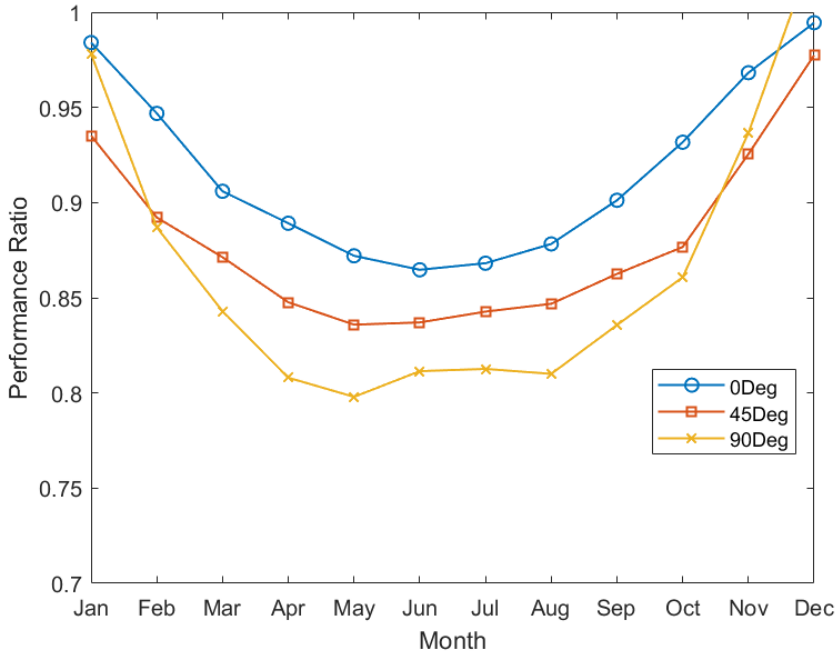

Figure 6.6: Performance Ratio of Design 3 in the Central North Sea at different Headings

Figure 6.7a compares the mean monthly Performance Ratios for the three designs. To do this, each monthly PR is averaged over all headings, this is modelling the WEC spending an equal amount of time at each heading. In reality, the WEC will weathervane into the prevailing direction which is likely to be seasonal or tidal. By averaging over the heading, we can focus on the impact of the design on the results rather than the heading. Figure 6.7b shows the standard deviation of the average monthly PR due to the variation in the heading angle and thus is the sensitivity of the energy yield to the heading, in that month, for that design.

Figure 6.7a shows that the higher capacity designs have lower PR in the summer than the smaller capacity designs. This shows the diminishing returns associated with installing further panels around the circumference of the hull. Design 3 has three times the capacity of Design 1 but will not produce three times the amount of energy. However, in the winter, the PR of higher capacity designs is greater. The benefit of this to the Solar-Wave Energy Converter may only be marginal as the wave resource in the winter will dominate the solar resource.

Figure 6.7b suggests that the influence of heading in the summer is reduced for deployments in the central North Sea. This is promising as this is when the contribution from solar panels is most valuable. By comparing design 1 and 2 the standard deviation does decrease with greater capacity, suggesting that the sensitivity to heading can be reduced by covering more of the hull with panels. However, design 3 is more consistent throughout the year and thus less sensitive to seasonal heading influence but is more sensitive than the other two designs in the summer. Interestingly, design 2 has the lowest sensitivity to heading out of the three. This shows that the arrangement of the panels may have a more significant effect than capacity on reducing the influence of heading as design 2 is the only design without a panel along the centreline of the WEC.

Caribbean Sea – Influence of Latitude

This section explores the influence of location on the behaviour of the same designs. Instead of presenting Figures of each design such as in Figure 6.4 to Figure 6.6 only the mean and standard deviation of the designs are shown in Figure 6.7a and Figure 6.7b but for the Caribbean Sea.

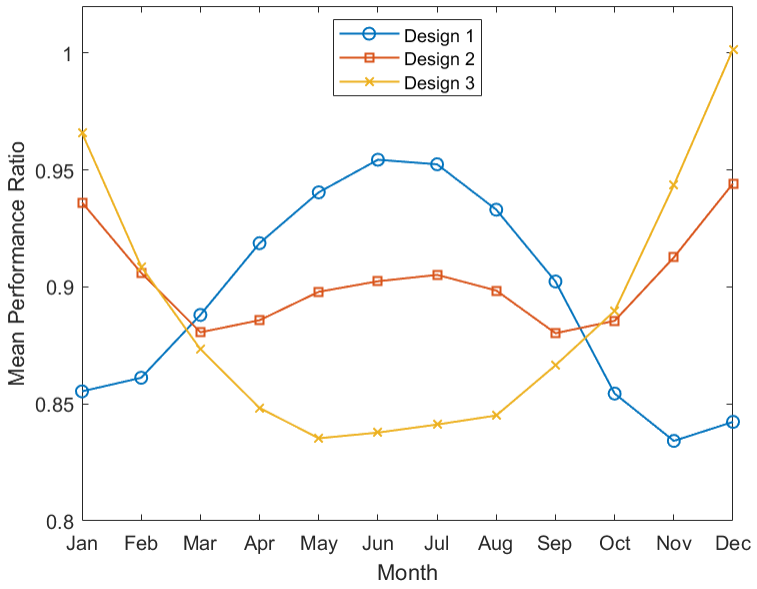

(a) Average Monthly Performance Ratio for all Three Designs in the Central North Sea over all Heading Angles

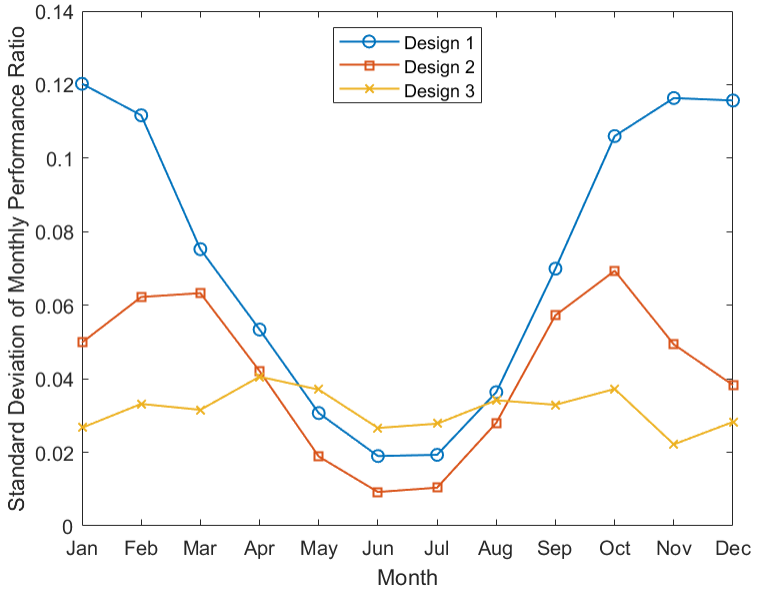

(b) Standard Deviation of the Performance Ratio due to Heading Variance for all Three Designs in the Central North Sea

Figure 6.7: Results for Central North Sea

Similarly to the deployment in the North Sea, Figure 6.9 shows the diminishing returns associated with adding capacity to the curved surface. This is more pronounced in the Caribbean Sea as there is no intersection point in autumn where higher capacity designs begin to work better in the winter. Similarly to the North Sea, the PR peaks

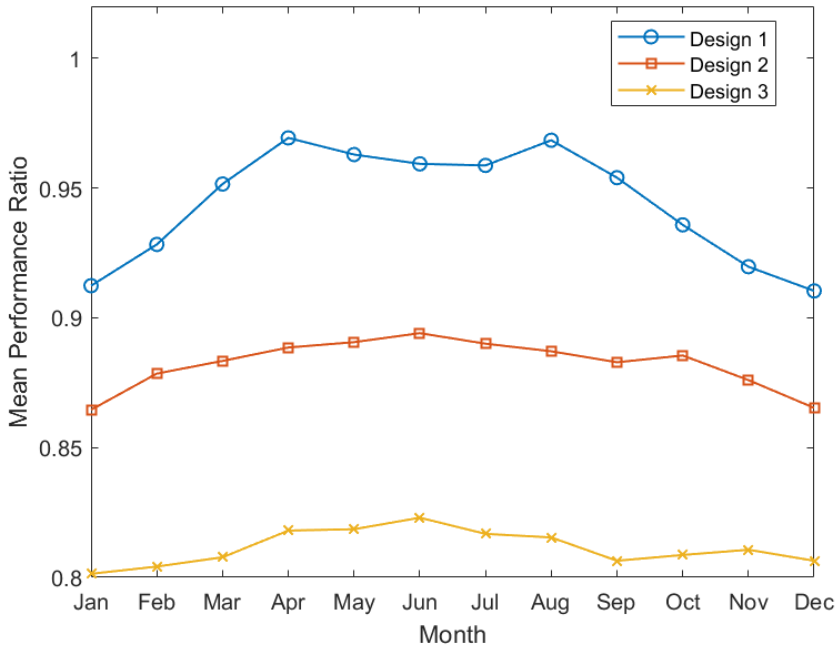

Figure 6.8: Average Monthly Performance Ratio for all Three Designs in the Caribbean Sea

in the summer (at close to the same peak values as in Figure 6.7a) but does not see the same dips in the winter. As this is the PR and not the absolute energy, this means that the same array in the Caribbean is less sensitive to the seasons compared to the North Sea.

When deploying in a location closer to the equator, the influence of the heading angle is diminished. This is highlighted in Figure 6.9 where the standard deviation is almost half of that in Figure 6.7b for all designs. The influence is again reduced in the summer versus the winter, which is beneficial for CAP.

Influence of Cell Angle

The next set of Figures explores the influence of tube radius, and thus the angle between cells on the PR of the array. To reduce the amount of data to be presented, only Design 3 is analysed for varying cell angle deployments in the North Sea and in the Caribbean Sea. The tube radius is varied from 0.5m to 2m thus changing the angle between cells, θ_i, as found in Equation 5.10 according to Table 6.2 where a radius of

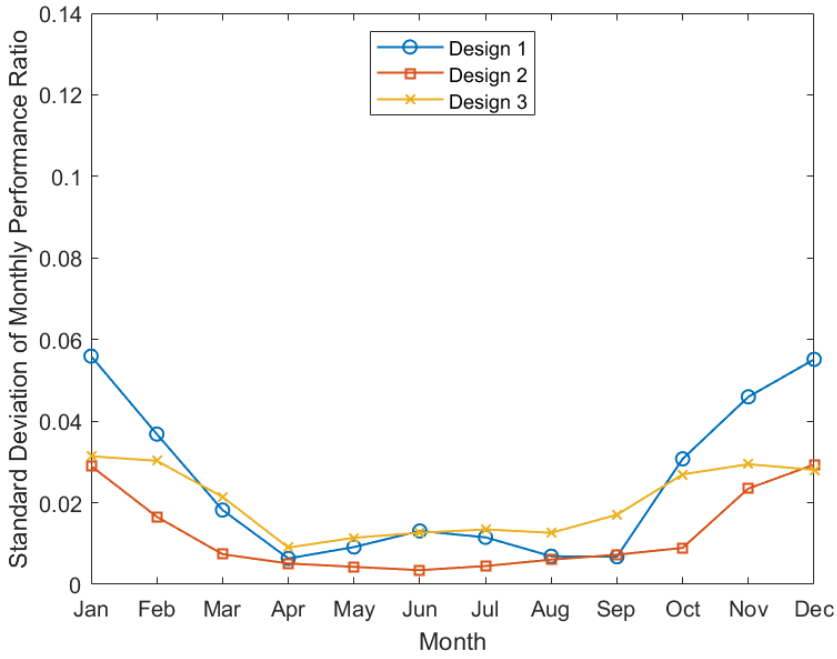

Figure 6.9: Standard Deviation of the Performance Ratio due to Heading Variance for all Three Designs in the Caribbean Sea

1m is has been used in the analysis thus far. Whilst the radius of the Mocean WEC hull is not expected to change so drastically from the nominal 1m, it is varied here to explore the effects of curvature on yield. The same effect could be explored by changing the panel dimension so that the distance between cells varies.

Table 6.2: Changing Cell Angle

Radius [m]	0.5	1.0	1.5	2.0
Cell Angle [deg]	19.6	9.8	6.5	4.9

Table 6.2 shows the inverse linear relationship between hull radius and cell angle, as the tube radius halves, the cell angle doubles. Figure 6.10 shows the PR of Design 3 deployed in the North Sea with varying cell angles. This shows that for very large cell angles in the summer, the panels will produce approximately 50% of the energy of a flat panel. Unsurprisingly, the smaller the angle, the closer the PR is to unity as the "flatter" the panel becomes. However, even for small angles less than 5 degrees, the summer energy will be approximately 5% less than that of the flat panel. As the cell angle increases, the summer PR reduces whilst keeping the winter values similar.

This is true until the angles become so large that all the energy yield is affected all year round. Cell angles smaller than 6.5 degrees have a consistent annual mean PR, meaning that they can be described by a constant PR whereas other cell angles may need to be described by a seasonal PR.

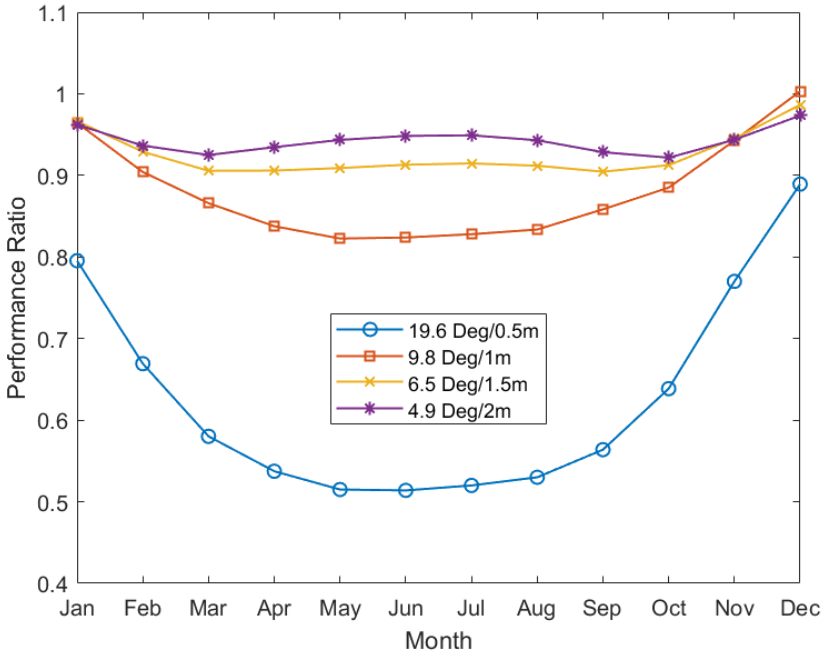

Figure 6.10: Average Monthly Performance Ratio for Different Cell Angles for Design 3 in the North Sea

Figure 6.11 shows that for angles less than 9.8 degrees, the sensitivity of PR due to heading has a similar profile as to those previously explored. A reduced sensitivity in the summer is met by an increase in the winter. When examining the standard deviation in the summer, there is very little difference between the results for the 2m radius and 1.5m radius hulls. In the winter the difference between the two reduces to zero, showing that the cell angle has a small effect on the winter yield for all headings.

Figure 6.12 and Figure 6.13 are the mean PRs and standard deviations due to heading for the same cell angles in Table 6.2 but deployed in the Caribbean Sea.

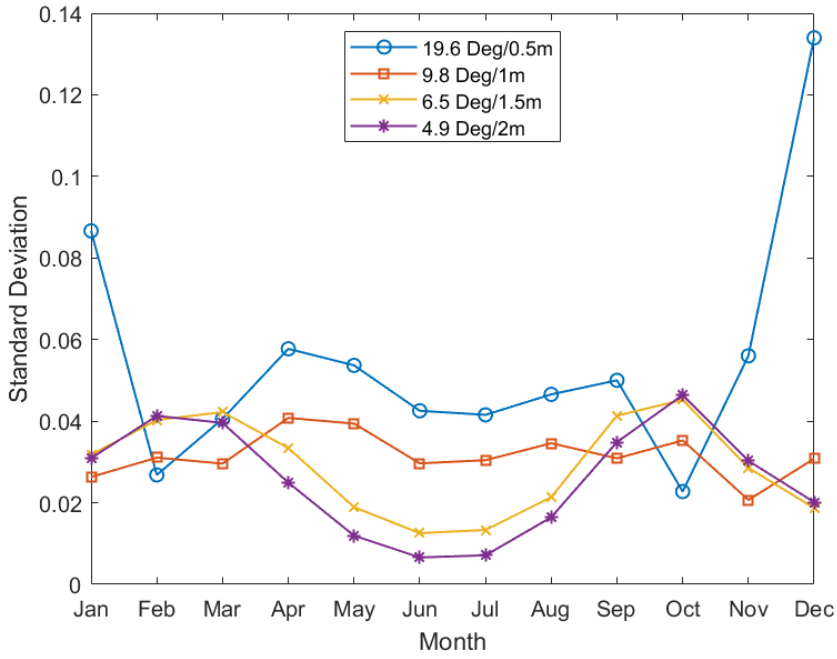

Figure 6.11: Standard Deviation of the Performance Ratio due to Heading Variance for Different Cell Angle for Design 3 in the North Sea

Figure 6.12 is similar to Figure 6.10, showing that for increasing cell angle, the panels return less energy when compared to a flat plate. The seasonal variation is much lower in the Caribbean Sea than in the North Sea, most likely due to a lower latitude and thus more annually consistent solar elevation angles. The smaller angle designs can lose approximately 8% of their energy when compared to a flat plate but the larger angles can lose 52%.

The sensitivity to heading in the Caribbean Sea is lower than in the North Sea, despite a changing cell angle. Unlike in the North Sea, the larger cell angles have a larger standard deviation in all of the months and are typically more than double that of smaller angles as the sun is higher in the sky.

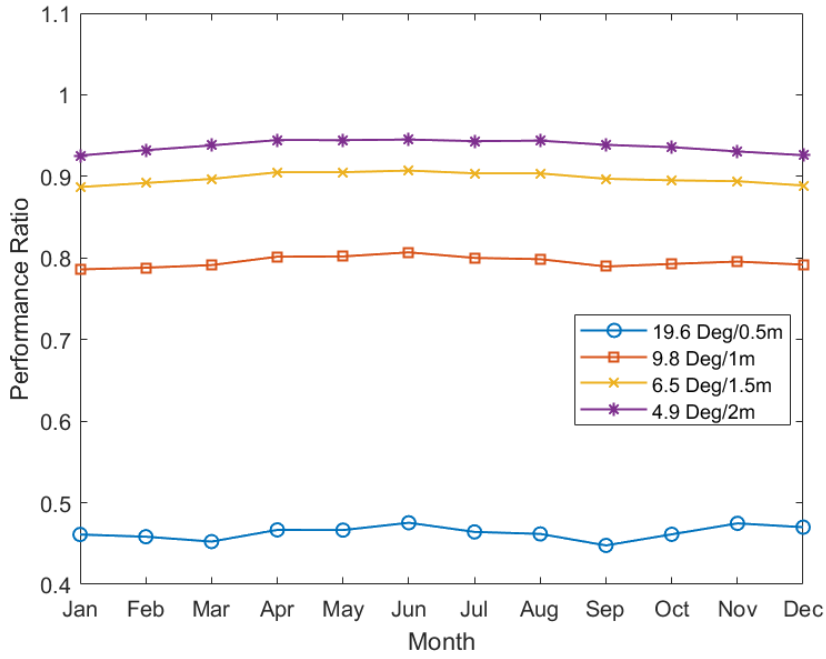

Figure 6.12: Average Monthly Performance Ratio (PR) for Different Cell Angles for Design 3 in the Caribbean Sea

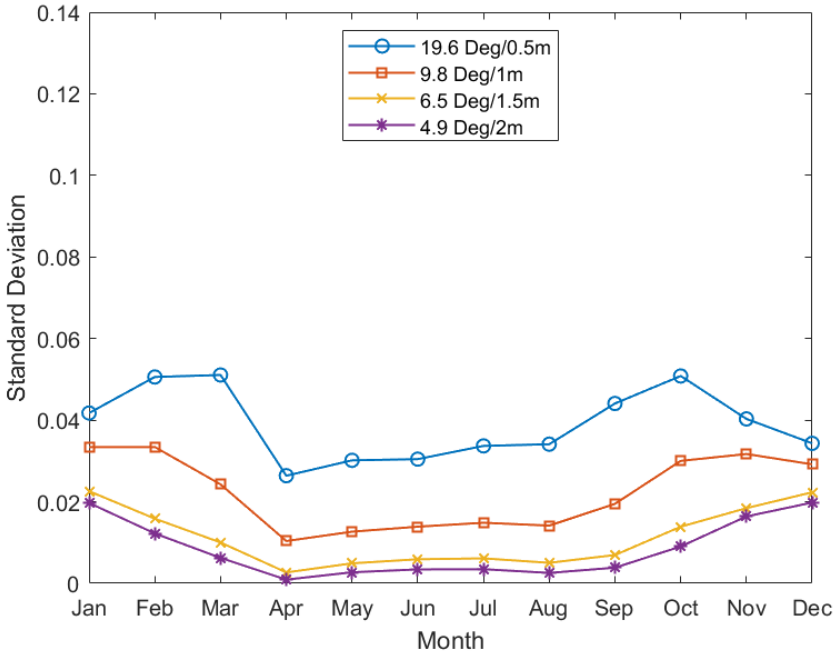

Figure 6.13: Standard Deviation of the Performance Ratio (PR) due to Heading Variance for Different Cell Angle for Design 3 in the Caribbean Sea

6.1.3 Section Summary

This study has used a numerical model to investigate the influence of layout, heading, curvature and location of a solar array on board a wave energy converter.

The first key result is that as expected, curved panels achieve a lower yield than flat panels, owing to reduced projected area normal to the sun's rays and partial shading. The energy can reduce by up to 18% in the North Sea during summer and by 21% in the Caribbean Sea. The variation of yield throughout the year is highly dependent on the WEC heading but this impact is reduced in the summer when the solar resource is most abundant. The heading has a greater influence on yield in the North Sea, where the solar angles are lower. At certain combinations of times of year and heading, the curved array can outperform a flat array due to cells being tilted towards the incoming irradiation. Whereas in the Caribbean Sea, the yield is significantly less sensitive to heading all year round, no matter the array capacity or hull radius and never outperforms the flat array.

Increasing the area of a curved array by extending it further down the sides of the WEC hull tube brings diminishing returns - but does reduce the sensitivity of the array to heading. Varying the tube radius and thus the angle at which each cell of the panel is mounted, shows that a high cell angle will produce a lower yield for both locations.

6.2 Full Scale Modelling

The overall aim of this thesis is to evaluate the potential of a solar array to improve the continuous available power output of a wave energy converter. Two at-sea experiments have taken place and a model was produced to compare against the experimental data. Now that validation has taken place, the model can be used to scale up the array to cover the available deck area of the BlueX to explore just how significant the installation would be.

In modelling up to this point, the values of the WEC pitch, roll and heading are data inputs, sampled from real-world testing. This limits the modelling to locations and times where BlueX has already been deployed. To estimate the dynamic behaviour and wave energy yield of BlueX, Mocean Energy has developed a WAMIT-based, time-domain WEC simulation tool. This tool has been developed by the numerical modelling team at Mocean Energy and verified against scaled tank testing and full-scale deployments in Scapa Flow. The main focus of the tool is to estimate energy

yields but an additional output of BlueX roll and pitch angles can be used in this work. The in-house tool produces a 3D matrix comprising of a range of H_s and T_e values on the X and Y axis whilst the Z axis contains a half-hour-long time series of pitch angles at a 0.1-second resolution resulting in 18,000 data points for each combination of H_s and T_e. A second 3D matrix is provided for Roll angles of BlueX for the same range of H_s and T_e.

When a location is selected, the wave climate is assessed using the other Mocean in-house tool, the wave resource assessment tool. Examining the previous fifteen years of data provides monthly mean significant wave heights and monthly mean energy periods for any location, worldwide. The monthly mean H_s and T_e can then provide a half-hour time series to represent the mean WEC response. The inputs of irradiance, wind speed and ambient temperature are collected from Copernicus and NASA Power as in Chapter 5. Now the model can be run using simulated BlueX positional data and the other required inputs.

The array is the same as that in Design 3 in Section 6.1 and Figure 6.3 with 3 Solbain 180L panels on the surface of a 1m radius hull. If the gantry walkway is removed, this is what is expected to be possible on the BlueX. The hull lengths of BlueX allow for 7 panels to be laid end to end along the main hull tube of the forward hull and 4 on the aft, resulting in a total of 33 180Wp panels for just under 6kWp. In addition to the curved array, a design comprising of a flat panel tilted at 45 degrees, a horizontal panel and a third panel pitched at -45 degrees as seen in Figure 6.14 are modelled to be compared.

6.2.1 Methods

Using the same methods described in Section **??**, the in-house Mocean Energy tools are used to produce a time series of pitch and roll for the BlueX device depending on the monthly H_s and T_e. The monthly average H_s and T_e are obtained for all locations.

To get the energy yield for a month, the results from the in-hours tool are multiplied by the number of half hours in the month. So for a 31-day month, the result is multiplied by 1488. This assumes that the WEC response is consistent over the month and is simply a repetition of the half-hour response, as the monthly mean H_s and T_e are sued to produce the time series, this is a fair method. .

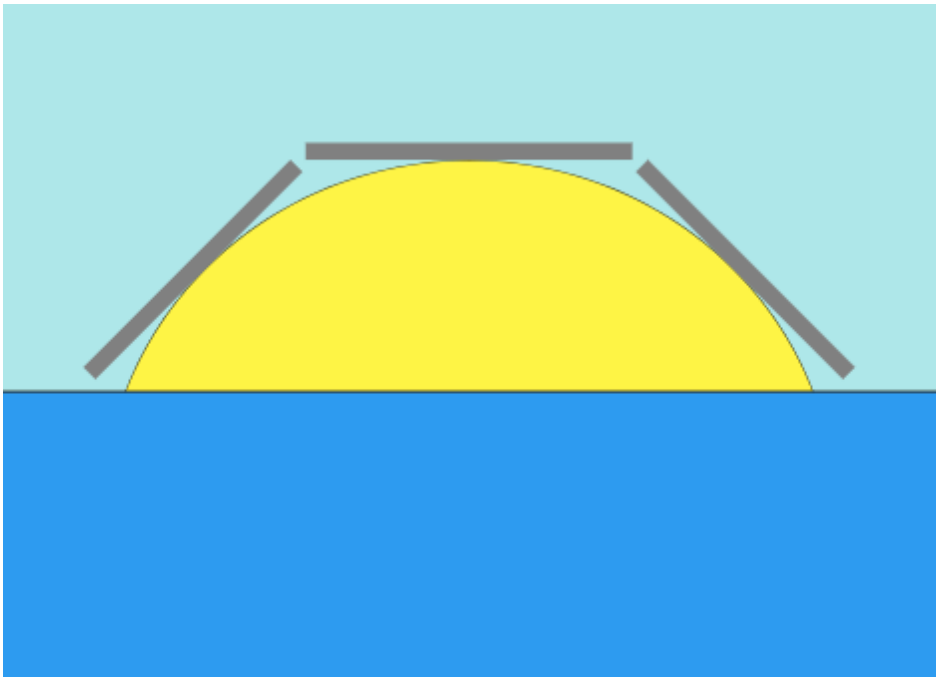

Figure 6.14: Cross section of tilted array design

Calculating the monthly solar contribution is more complex. In calculating the wave energy, a response of pitch and roll angles is obtained. However, this is only over half an hour. Finding the solar array yield over half an hour and scaling up would omit the influences due to the time of day and the length of the day in the summer compared to the winter. Therefore, a single 24-hour period is analysed for the 16th day of each month using the same half-hour pitch and roll angle time series repeating 48 times. The mean monthly heading is obtained from the Mocean Energy Wave Analytics tool. Additionally, the significant wave height sensitive converter efficiency can be calculated using the Equation found in Chapter 4. The solar energy calculated over the 24-hour period for the midpoint of each month is then multiplied by the number of days in the month to obtain a monthly energy yield.

6.2.2 Location Analysis

Additional locations are selected for their strong seasonal variation in wave power described by the standard deviation in monthly energy. From this, several island locations are determined where Wave Energy Converter technology may be best implemented as island nations desire to move away from fossil fuels or large umbilical cables and do not desire large wind turbines.

There is an additional restriction to stay within the +-66deg longitudes due to Copernicus irradiance data only being available between these limits. The location of the RSP deployment is analysed to give a base of comparison, as well as locations in the Sardinian Sea and the Canary Islands. This gives a mixture of a location with low solar resources (Northern Scotland) and two locations with good resources but different wave resources. By showing that the solar array benefits the WEC in a low solar resource environment like Scotland, the benefits should be higher in locations with even more resources.

6.2.3 Results and Discussion

Deployment at the RSP site

The monthly energy of the wave power alone and combined wave and solar are compared in Figure 6.15, where the curved array is shown in Figure 6.15a and the tilted array in 6.15b.

In April, the WEC generates the least amount of wave energy, 1272kWh. By dividing this by the total hours in April, this corresponds to a Continuous Available Power (CAP) of 1.76kW. This assumes that all the energy harnessed in April is used in April and thus a sufficiently large battery is installed. By installing the 6kWP solar arrays, the monthly energy increases to 1439kWh and 1502kWh for the curved and tilted arrays respectively. This corresponds to a CAP of 1.93kW and 2.02kW, increasing by 13% and 18% from the wave power. The implementation of this array has improved the commercial prospects of the device by increasing the CAP. This benefit is hard to express economically as this improvement will present new opportunities previously outside of the capabilities of BlueX and could therefore increase sales of the first-generation device.

Installing a solar array on BlueX will raise the energy produced in the summer and reduce the variance in the monthly energy production. This is examined by calculating the standard deviation of the monthly energy. The standard deviation of the wave monthly energy is 0.582MWh. With a 6kW curved array, the standard deviation reduces to 0.506MWh and to 0.481MWh for the tilted array. A consistent monthly energy production means that the components of the device are well utilised, presenting good value for money.

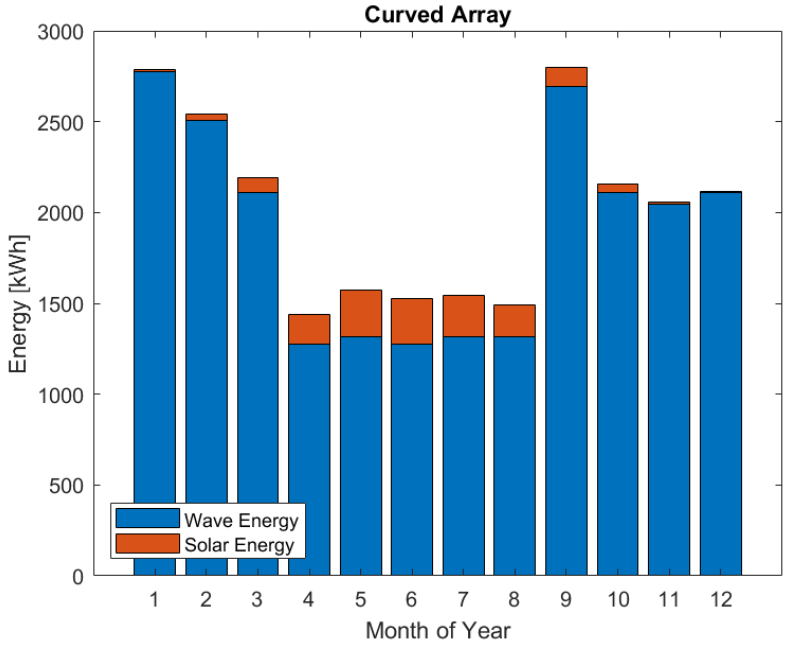

(a) Monthly Energy of Curved Array

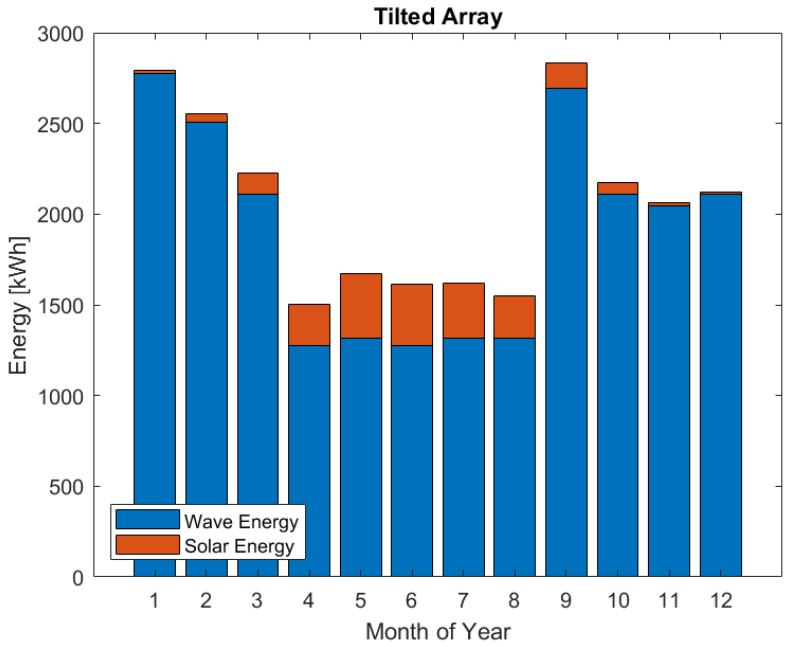

(b) Monthly Energy of Tilted Array

Figure 6.15: Monthly Energy for combined wave and solar resource in the North Sea

It should be noted that the RSP site has been selected for analysis here as a means of continuity from previous experimentation and modelling chapters. It is a sub-optimal deployment site so the average powers produced by the wave device are lower than expected in fully commercial sites. This is ratified in later analysis where the location is more optimal.

Larger Scale Arrays

To explore how increasing the capacity of the solar array impacts the CAP of the device, the output of the solar array is increased linearly. This assumes that both the cost and the yield of the array increase with the installed capacity and thus the panels are arranged onto the same plane as the original 6kW array. The standard deviation of the monthly energy is then examined for each combination of wave and solar capacity. This is presented in Figure 6.16.

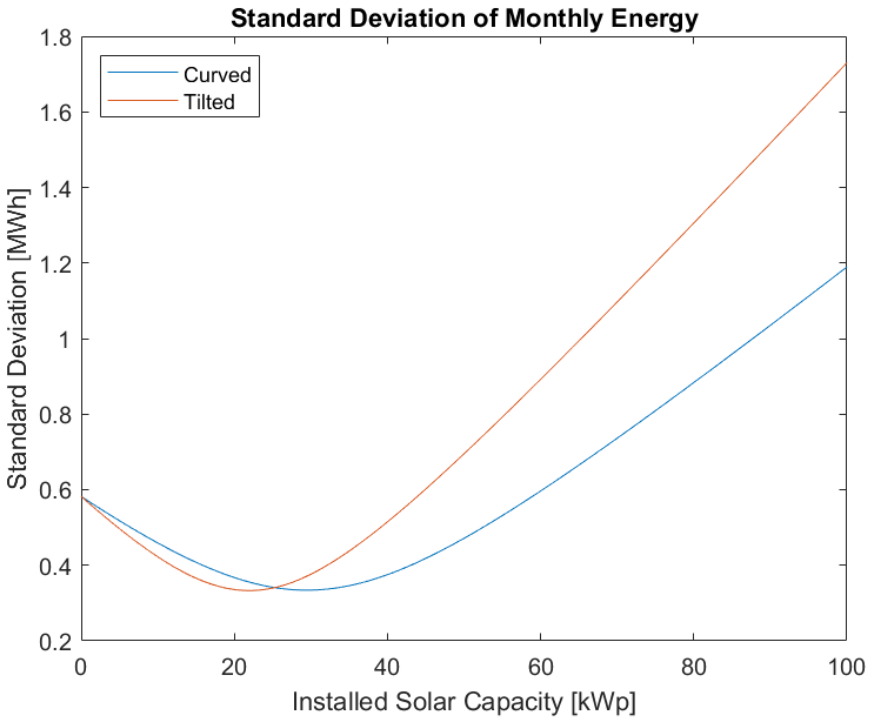

Figure 6.16: Standard Deviation of Monthly Energy of Increasing Capacity Arrays in the Northern North Sea

A minimum standard deviation is clearly observed for the curved array and the tilted array. The curved array minimum occurs at a solar capacity of 29.5kWp and the tilted at 22.0kWp, 75% of the curved array capacity. The monthly energies of the wave-only device, with 6kWp of curved solar and then the capacity with the lowest standard deviation, can be seen in Figure 6.17. Beyond this capacity, the standard deviation increases as the hybrid machine observes a summer peak and a winter lull.

By finding the month with the lowest energy and dividing it by the number of hours in that month, a continuously available power can be found. This is done for increasing solar capacity and provides Figure 6.18a.

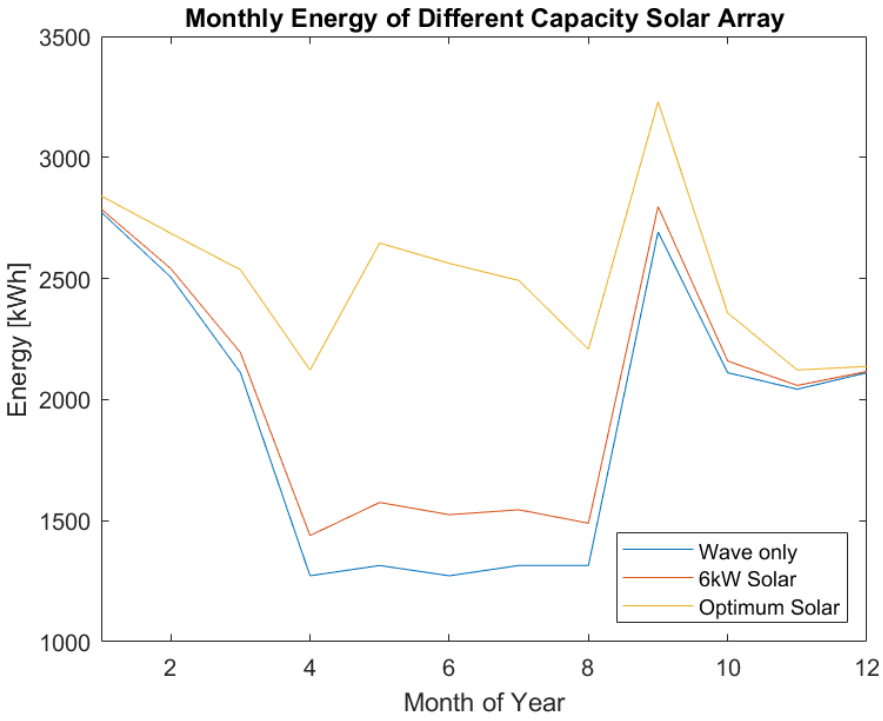

Figure 6.17: Monthly Energy of the wave only device and then with differing capacities of solar array

The CAP shows an obvious knee point. This occurs at the same capacity as the lowest standard deviation. This is because at this point, the month with the lowest energy moves from the summer months (in this case, April) to the winter months (in this case November and December) as seen in Figure 6.18b. As the worst performing month moves to the winter, where solar has reduced resource, the benefits to CAP from increasing solar capacity have diminishing returns.

This can, therefore, be used as a sizing tool; by examining the minimum standard deviation for a given deployment zone, the maximum capacity of the accompanying solar array that will provide the most benefit per cost can be determined. Alternatively, if a certain CAP is desired, Figure 6.18a can show what capacity solar array is required to achieve that goal.

The caveat here is that fitting over 20kWp of solar panels would require more deck area than what is available on the BlueX. Deployable arrays may be required to achieve this capacity and are the subject of further work in Chapter 7.1

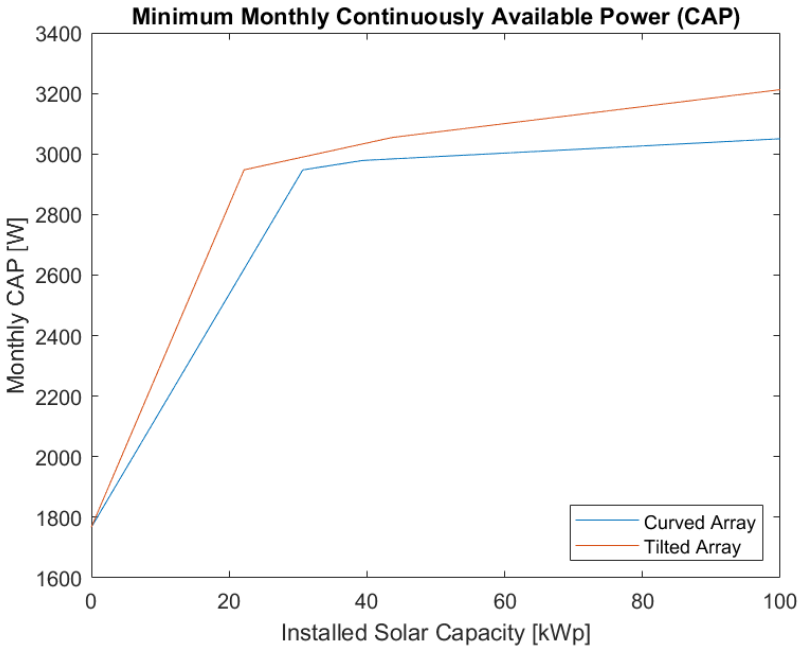

(a)

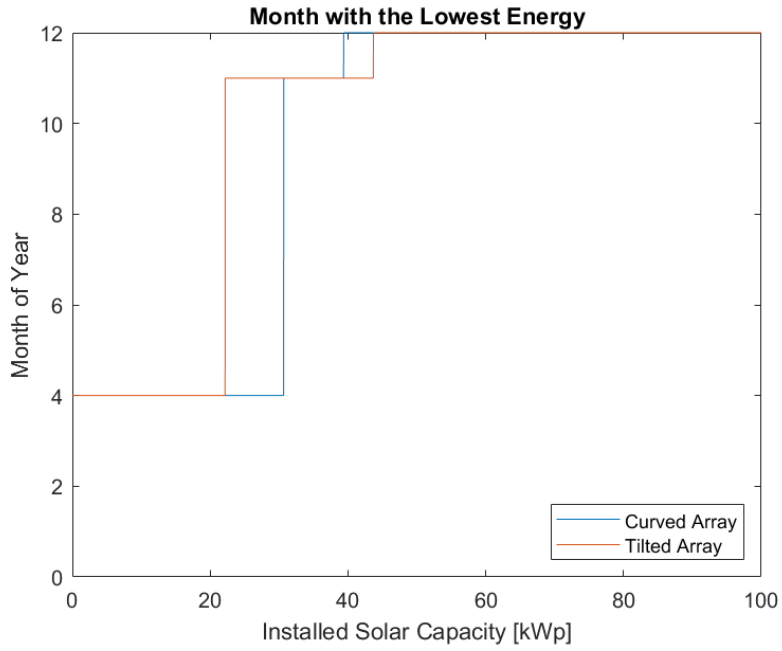

(b)

Figure 6.18: Variations due to Increasing Capacity Arrays in the Northern North Sea

6.2.4 Costs

By using the costs described in Section 4.2.4, a unit cost of 15 GBP per Watt of solar panels is determined. This value includes all costs incurred in fixing the 572Wp panels to BlueX for the RSP deployment. By using this value, the estimated cost of the 6kWp array is expected to be £90,000. The optimum arrays of 22.0kWp and 29.5kWp are £330,000 and £442,500 respectively. The costs of the tilted array are estimated to be similar to that of the curved array as the panels will be cheaper but there are additional costs associated with mounting the panels.

The increase in CAP can be presented as a scaling factor. This compares the CAP of the Solar-WEC directly with the stand-alone WEC. Similarly, the cost of the solar array can be compared with the cost of the WEC to find the increase in Capital Expendature (CapEx) of the device. The actual cost incurred in the manufacturing of the BlueX is confidential and would not be a good representation of a fully commercial device which benefits from economies of scale. Therefore, a range of potential BlueX CapExs are used to present Figure 6.19.

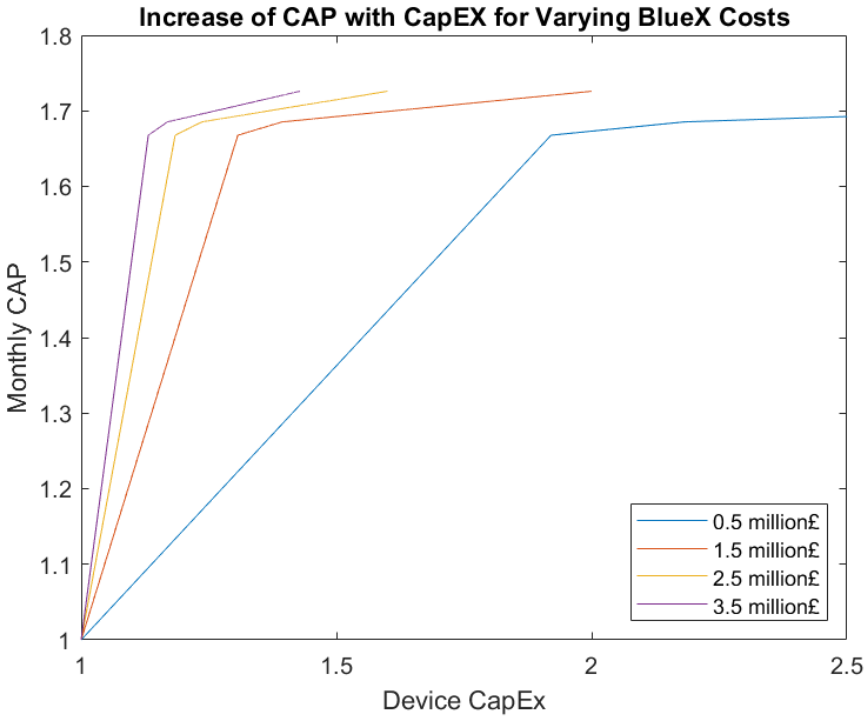

Figure 6.19: CapEx costs for increasing CAP

Figure 6.19 shows that for WEC costs above £1.5 million, the increase in CAP is greater than the increase in CapEx. This means that for every 1% extra you spend on the device you get more than 1% additional CAP. As previously stated, the value of additional CAP is hard to quantify but this figure allows for a comparison between the project costs and desired CAP.

Levelised Cost of Energy

The Levelised Cost of Energy (LCoE) is the total lifetime costs of the device divided by the lifetime energy produced as shown in Equation 6.2. LCoE is considered a critical metric for grid-tied renewable energy and is used as a method of bidding for Contract for Difference (CfD) by showing the minimum price an asset needs to sell energy for to make a profit. A large proportion of the total cost will be embedded in the capital expenditure of the device and thus the LCoE can be approximated by examining the CapEx divided by the total energy produced. Total energy produced can be found by multiplying the Annual Energy Production (AEP) by the lifetime of the device.

$$LCoE = \frac{Total\ Cost}{Total\ Energy} \approx \frac{CapEx}{Lifetime * AEP} \tag{6.2}$$

To examine how the addition of a solar array influences the LCoE of a combined device, a calculation is performed using Equation 6.3. To show how the original LCoE is modified, the additional CapEx is divided by the additional energy to obtain an LCoE scaling factor. As the actual cost of BlueX is confidential, as with the LCoE, this is the best way to show how the solar array influences the cost metrics of the device. This calculation assumes that the solar AEP and CapEX increase linearly with solar capacity.

$$LCoEScalingFactor = \frac{1 + \frac{CapEx_{Solar}}{CapEx_{Wave}}}{1 + \frac{AEP_{Solar}}{AEPWave}} \tag{6.3}$$

Implementing the 6kWp array on the BlueX deployed at the RSP site in the North Sea yields Figure 6.20. Due to the higher energy yields of the tilted array, it has a lower LCoE scaling factor than the curved array. The influence on LCoE is sensitive to the cost of BlueX. At costs below £1.01 million the tilted array has a negative impact on

the LCoE whereas this point is at £1.55 million for the curved array. The LCoE scaling factor levels off with increasing WEC costs showing a maximum benefit achievable with 6kWp of 4.5% with the tilted array and 2.9% with the curved array, for costs below £3.5 million.

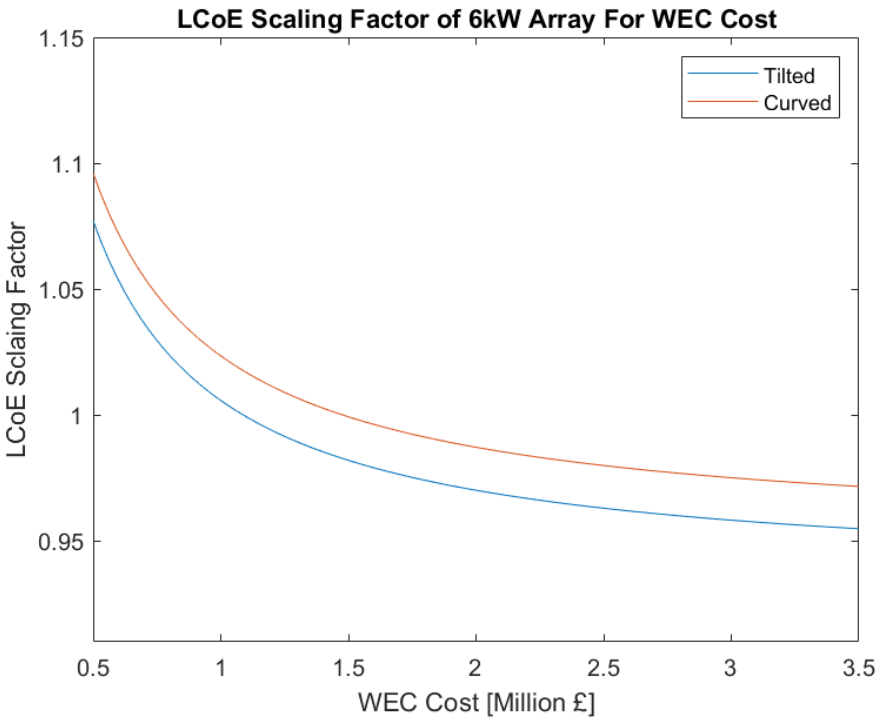

Figure 6.20: LCoE reduction for a 6kWp array

Figure 6.21 shows the influence on LCoE scaling factor with increasing solar array capacity for different WEC costs. At a WEC cost of half a million pounds, the LCoE increases with any solar capacity. At a cost of £1.5million, the LCoE slightly reduces down to 84% of the original with a solar capacity of 100kWp. At costs greater than £1.5million the LCoE reduces to a minimum of 67% and 60% for costs of £2.5million and £3.5million respectively. Therefore, the addition of a solar array can have significant impacts on the LCoE of the WEC.

This suggests that there is a WEC cost where the addition of a solar array has no impact on the LCoE of the device, no matter the capacity. This will occur when the LCoE of the solar array is equal to the LCoE of the wave device, shown in Equation 6.4. When the solar LCoE is lower than the WEC LCoE, the combined device LCoE reduces with the addition of a solar array.

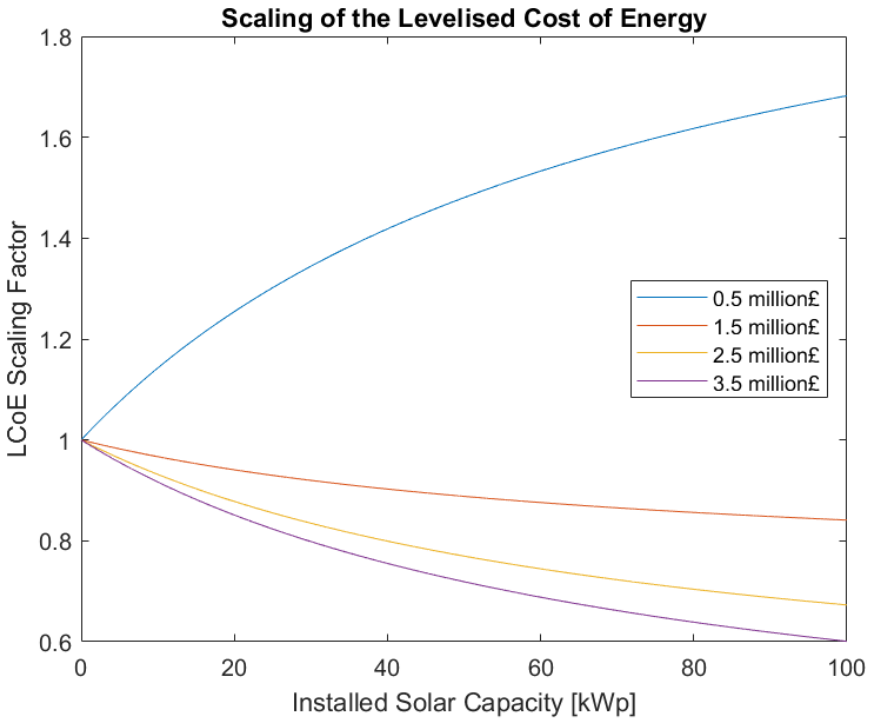

Figure 6.21: LCoE reduction for increasing array capacity

The wave energy converter "cross over cost" is the WEC CapEx where the two LCoEs are equal. Using the AEP and solar cost values obtained from the RSP model and Experimentation, the cross-over cost at the RSP deployment site occurs when the WEC costs £ 1.48 million.

$$LCoE\ is\ insensitive\ to\ Solar\ Array\ Capacity\ when: \frac{CapEx_{Solar}}{AEP_{Solar}} = \frac{CapEx_{Wave}}{AEP_{Wave}} \quad (6.4)$$

For a given design of combined solar-WEC where the costs are known, locations suitable for the combined system can be found by exploring the ratio of the costs and the ratio of the AEPs. For example, if the CapEx of the solar array is 15% of the CapEx of the WEC, the solar array needs to produce at least 15% of the wave energy for the addition of the solar array to reduce the LCoE. This can be used to determine suitable locations for the combined Solar-WEC.

As the methodology presented in this work is transferable to large scale WECs, Figure 6.21 shows that the solar array not only helps kilowatt scale Wave Energy Converters to power niche demands through raising the CAP, but it also has the potential to improve the attractiveness of large-scale WECs to grid demands through reducing the LCoE. This is a significant problem which WEC technology faces. The results from this analysis are summarised in Table 6.3

Table 6.3: Results from implementing a Solar array of BlueX in the North Sea

RSP Deployment Site	WEC	Curved	Tilted
AEP [MWh]	22.84	24.23	24.72
AEP Increase	-	6%	8%
CAP [kW]	1.767	2	2.09
CAP Increase	-	13%	18%
Std [MWh]	0.582	0.506	0.481
Minimum Std [MWh]	-	0.334	0.333
Minimum Std Capacity [kW]	-	29.5	22

6.2.5 Other Locations

To explore how the 6kW array performs in other locations, the analysis has also been carried out for a deployment in the Canary Islands and Isle of Sardinia. The monthly energy of the curved design array is presented in Figure 6.22 for both locations. The full results are in Appendix D whilst a summary of the results is presented in Table 6.4.

The monthly solar energy in the Canary Islands is more consistent than in the North Sea, with a standard deviation of 88.33kWh compared to 97.08kWh. Unusually, the wave monthly energy peaks in the summer, rather than the winter, meaning the solar and wave resources are alligned. The Sardinian solar climate is the most variable with a standard deviation of 145.57kWh.

The CAP can be improved by up to 27% in the Canary Islands by implementing a 6kW tilted array. The same array integrated into BlueX in the Sardinian deployment boosts CAP by up to 35%. These are significant improvements and could make the deployment of small-scale WECs possible in locations where wave energy alone can not satisfy customer demand. A tilted array can also improve the annual energy production by 21% in the Canary Islands and 24% in Sardinia.

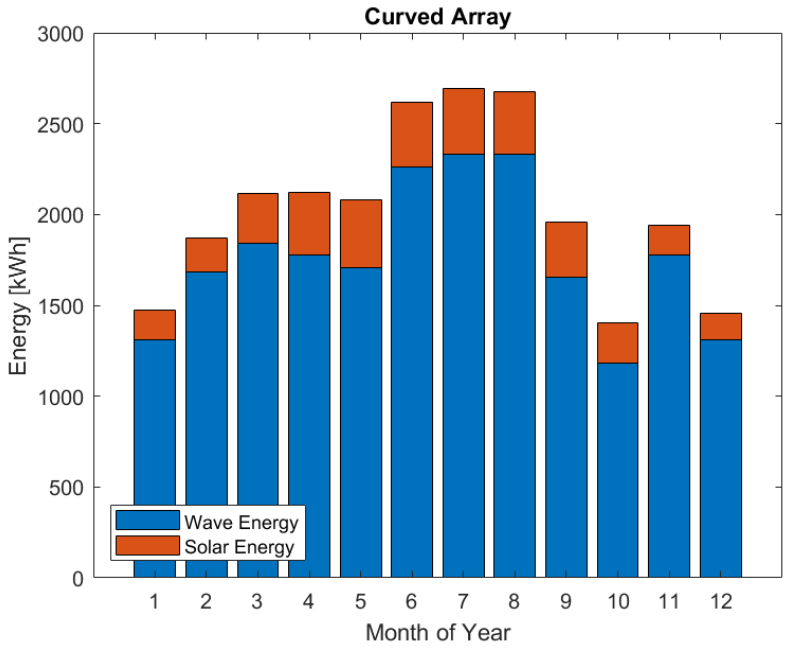

(a) Canaries

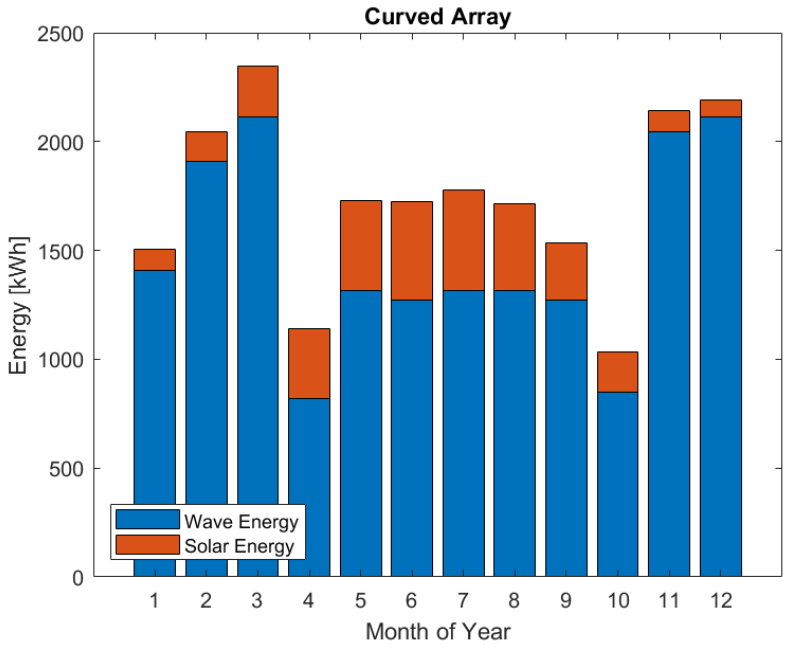

(b) Sardinia

Figure 6.22: Monthly Energy of Curved Arrays

The standard deviation in the canary islands always increases with increasing solar capacity, meaning the standalone WEC has the lowest standard deviation. This is due to the in-phase energy profiles of the wave resource and solar resource. In the deployment near Sardinia, the standard deviation reduces with capacities up to 7.4kW and 9.6kW for a tilted or curved array.

Table 6.4: Results from implementing a Solar array on BlueX in Different Locations

	Canary			Sardinia		
	WEC	**Curved**	**Tilted**	**WEC**	**Curved**	**Tilted**
AEP [MWh]	21.18	24.4	25.67	17.74	20.88	22.07
AEP Increase	-	15%	21%	-	18%	24%
CAP [kW]	1.64	1.95	2.08	1.14	1.43	1.54
CAP Increase	-	19%	27%	-	25%	35%
Std [MWh]	0.39	0.457	0.479	0.457	0.403	0.398
Minimum Std [MWh]	-	0.390	0.390	-	0.393	0.395
Minimum Std Capacity [kW]	-	0	0	-	9.6	7.4

The LCoE scaling factor for both array is both locations for varying WEC costs are presented in Figure 6.23. Due to the higher solar resource in the Canary Islands than in the North Sea, the LCoE only increases when installing a curved array on WECs cheaper than £0.59 million. The LCoE for the tilted array is always beneficial for costs greater than £0.5 million. At a cost of £3.5 million the LCoE would improve by 11.0% for a curved array and by 15.4% for a tilted array. Figure 6.23b shows that the LCoE in Sardinia always improves for both panel types and for all costs greater than £0.5 million. At a WEC cost of £3.5 million the LCoE improves by 12.9% for the curved array and by 17.5% for the tilted array. With increased solar array capacity, these numbers will improve and the benefits to the WEC with it.

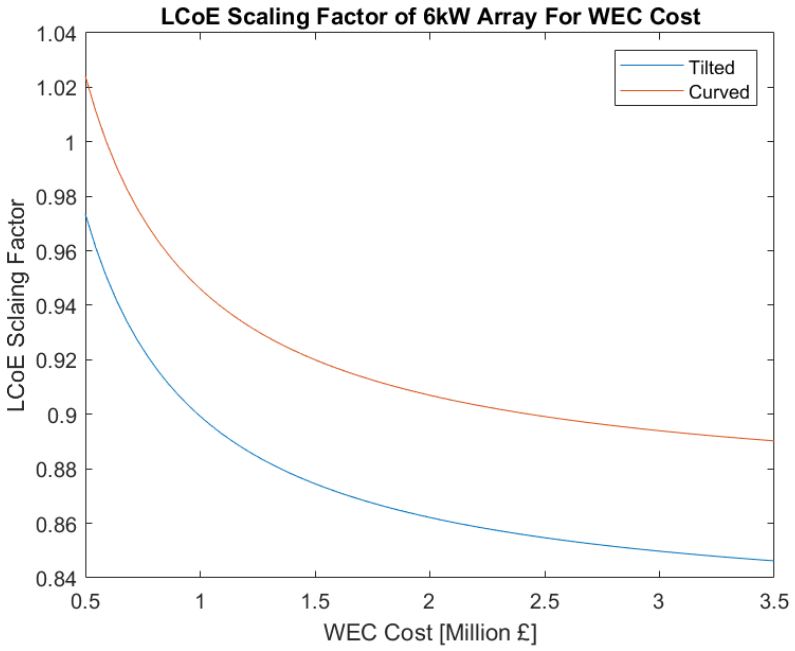

(a) Canary's

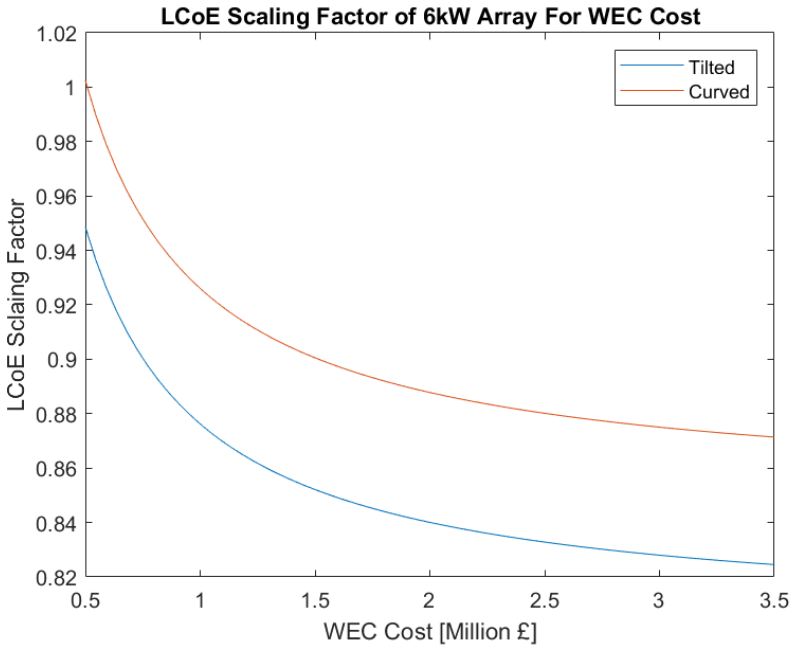

(b) Sardinia

Figure 6.23: LCoE of 6kW array in Canary Islands and Sardinia

6.3 Chapter Summary

This chapter has applied the model developed in Chapter 5 to a number of design parameter studies to explore how certain design choices influence the yield of the solar-WEC. The influence of array positioning, WEC heading, deployment location and hull diameter have all been explored by assessing the performance ratio of yield from a curved array against that from a horizontal flat plate.

It was found that the positioning of the panels can influence the PR. A panel placed along the top edge of the tube will perform closest to the flat plate and have a higher performance ratio.

It has been found that the heading of the WEC can have a significant impact on yield which varies depending on the month of the year and deployment location. This has been characterised by examining the If the energy yield from a flat plate is known, the energy of a curved array can be estimated by using the performance ratio corresponding to the WECs heading.

The performance ratio due to variance in the radius of the hull is then obtained to explore how the rate of curvature influences yield.

The full-scale modelling is then carried out for a 6-kilowatt array, determined to be the maximum-sized array that can fit onboard the available deck area. First, a curved array is analysed and then an array of flat plate panels is analysed where the middle panel is horizontal whilst the outer panels are tilted at 45 degrees. It was found that the tilted panel array outperformed the curved panel by an average of 25%.

The effect of installing a 6kWp array in the North Sea raised the amount of continuous available power by 13% for the curved array and by 18% for the tilted array. The annual energy production increased by 6% and 8% by installing a curved or tilted array. By examining the standard deviation of the monthly energy before and after the implementation of the array, the influence of the solar array on the seasonal smoothing of the device can be explored. The standard deviation of the monthly energy in the North Sea was reduced by 13% and 17% for the curved and tilted arrays respectively.

By scaling up the capacity of the array, the minimum standard deviation of the monthly energy can be determined. That shows the point where the seasonal variation in energy is minimised and thus provides the most consistent power throughout the year and in turn a high utilisation of power electronics. The capacity which provides a minimum standard deviation is 29.5kWp for a curved array and 22kWp for a tilted array.

By examining the continuous available power with increasing capacity it can be observed that for the north sea, this relationship is not linear and provides a knee point. Beyond this knee, the worst-performing month now becomes the winter, where increasing the solar array capacity has a negligible impact. The capacity at which the knee point occurs is also the capacity with a minimum standard deviation.

This process was carried out for other locations in the Sardinian Sea and the Canary Islands. Here it was found that the positive results experienced in the North sea are exaggerated by the higher available solar resource. Increases in the continuously available power are up to 27% in the Canary Islands and 35% for Sardinia. Annual energy production increases by up to 21% and 24% for a 6kWp array in the Canary Islands and Sardinia respectively. The minimum monthly standard deviation is 9.6kWp of curved array or 7.4kWp of tilted array in Sardinia, close to the design of 6kWp. However, in the Canary Islands, the standard deviation of the monthly energy increases with solar array capacity. This is due to the in-phase solar and wave resource. Therefore, the continuously available power in the Canary Islands is linear with installed capacity.

Chapter 7

Conclusions and Further Work

The aim of this thesis is to investigate the technical and economic impacts of implementing a solar array on board a floating wave energy converter to prove that a Solar-WEC will have a higher continuous available power than a WEC and thus be a more attractive solution for niche demands.

It has achieved this by completing the following objectives:

1. Deploy at-sea experiments of solar panels installed onboard a Wave Energy Converter in order to obtain yield and assess the survivability of different panel types and mounting methods.
2. Develop a model to predict the energy yield from a solar array installed on a wave energy converter by improving on established solar theory.
3. Use the yield data from the experiments, along with the WEC positional and power production data to validate the model.
4. Use the validated model to evaluate a full-scale hybrid Solar-WEC in locations around the world
5. Perform an economic assessment of the solar array and compare the cost/benefits of the system by using all available results.

The topic of combined wave and solar is still emerging. The published literature does introduce the idea of "wavepholtaics" where the deck of floating wave energy converters is used to mount solar panels. However, this literature is limited in scope and does not include in-depth models or experimentation. This thesis significantly expands on this topic by showing and comparing experimental results and an in-depth model for the first time. To our knowledge, no results from similar experiments have been published. Therefore, this thesis offers an opportunity for other researchers to compare their work.

Two experiments took place in Orkney using the Mocean Energy BlueX wave energy converter. The first experiment compared the suitability and yield of flexible and rigid panels offshore. It showed that despite wave action, solar panels will become soiled by biofouling. This experiment was cut short after 16 days due to wave damage to the panels and testing kit, this shows that the panels need to be sufficiently robust to protect against the wave action. Especially as this deployment site was considered a "nursery site" and thus not exposed to the full potential wave climate.

The second experiment used only flexible panels adhered directly to the hull of the WEC to protect against the marine environment. Two sets of panels were deployed, one in a splash zone on the front of BlueX and the second on the nacelle away from the water. The front panels experienced consistent wave washing which left deposits of marine growth on their surface. This is in contradiction to the initial thought process, where the wave action would wash the panels from biofouling due to bird guano. Biofouling obscuring the panel surface reduces panel output and could potentially lead to a reduction in the lifetime of the panels.

The panels on the nacelle fared much better and looked "good as new" even after 122 days at sea. The panels fed a continuous communications hotel demand of the wave energy converter, allowing the main wave power take off to supply power to the battery and load. The panels powered 84% of the communications demand in March and 100% from April onwards. The panels produced 82.9kWh of energy over the total deployment period but this is curtailed from the maximum value due to reaching a 100% state of charge on most days. The efficiency of the maximum power point controller was found to vary depending on the significant wave height. The converters were less efficient during periods of high wave action due to the larger movement of the wave energy converter increasing the rate of change of irradiance. The efficiency of the front panels was different to the nacelle panels, described by the linear relationships.

A numerical model was produced in MATLAB which uses open-source irradiance and environmental data to predict the energy output of a curved array onboard a wave energy converter. The dynamics of the wave energy converter are included by using the in-house Mocean Energy dynamics tool which predicts the motion of BlueX for different combinations of significant wave height and energy period, this model has

been validated against tank testing and at-sea testing. The model uses PV-Lib, a toolbox built by Scandia Laboratories for use in MATLAB. The model incorporates established solar theory to model the irradiance on the cells of a curved panel on a dynamic wave energy converter.

The results from the experimentation are compared against the model outputs where the inputs are based on the experiment location. The results are first used to assess the temporal resolution to find a timestep of one second which offers good accuracy but not long-running computational times. The results are also used to explore different diffuse irradiance models to find which gives the most accurate results. The Perez model was found to present an average error of 4% and was used in final assessments and future predictions. It was found that the total energy between the 1st of March and the 30th of June matched within 0.77% and therefore presents a good match of the two sources. However, when considering the energy over a month-by-month basis the error found in March was 4.22%. However, when looking at single days, the errors in the array daily energy can be up to 70% over prediction or a 25% under prediction whilst some days are accurate to 0.05%.

The validated model was then used to assess the design considerations of a full-scale array. Curved and flat plate panels are compared for a wave energy converter in the north sea where the heading is assessed over 360 degrees and diameter of the hull is fixed at 2m. It was found that the curved array has up to 50% lower energy than the flat plate. The heading is important to the energy yield, headings facing North-South have an energy yield 25% higher than those facing East-West. The hull diameter plays an important role in the energy yield of a curved array. Larger diameters make the panel appear "flatter" with lower angles between the cells of a panel. A flatter panel can achieve an energy yield similar to that of a flat panel but even cell angles of 4.9 degrees yield 5% less energy compared to a flat panel.

A full scale 6kWp array is then theorised for the BlueX device. The combined wave and solar resource is then assessed for locations in the North Sea, Sardinian Sea and near the Canary Islands. It was found that by implementing the 6kW array, the continuous available power can improve by 18% in the North Sea, by 35% in the Sardinian Sea and by 27% near the Canary Islands. The annual energy production can improve by 8%, 24% and 21% in the same locations respectively.

By using the costs incurred in the experimentation, an approximate cost of the 6kWp array can be estimated at £90,000. The costs of the BlueX are confidential so can not be published. However, by taking WEC cost estimates between £0.5 million and £3.5 million the percentage change to the original wave energy converter levelised cost of energy can be made. This scaling factor of LCOE is sensitive to location. In the North Sea, the LCoE can decrease by 4.5% for WEC costs of £3.5 million but can increase by 7% for costs of £0.5 million. In the Sardinian Sea, the LCoE can reduce by a maximum of 17% for costs up to £3.5 million. Near the Canary Islands, the reduction can be as much as 15%.

7.0.1 Influence on the Industrial Sector

This work has had an impact on the wave energy converter industry as Mocean Energy is planning on installing solar arrays onboard all future wave energy converters. However, the installed capacity of the arrays is still uncertain. I will be continuing to work on this with Mocean beyond the conclusion of my EngD.

Floating offshore solar is becoming more prevalent and will begin to move further offshore. The conclusion that the MPPT controller efficiency can depend on the significant wave height is also relevant to this industry.

7.0.2 Key Conclusions and Original Findings

This work has shown for the first time:

1. Real-world testing of a hybrid solar wave energy converter deployed in the Orkney Islands.
2. Solar panels powered onboard critical demands of a wave energy converter.
3. Compared the suitability, economics and yield of flexible and rigid panels offshore.
4. Showed that despite wave action, solar panels will become soiled by biofouling.
5. Discovered that there is a sensitivity of maximum power point tracking efficiency to significant wave height.
6. Produced a numerical model which is compared to experimental results.
7. Numerical model shows that the yield of a array is sensitive to WEC heading and hull dimensions.
8. Numerical model predicts the output of a SWEC in island communities where the solar and wave resource is in antiphase.

9. Showed that the implementation of a solar array on a WEC will improve the continuous available power of the device by up to 18% in the North Sea.
10. Whilst costs of the BlueX device are confidential, the solar array will cost approximately £90,000 which is estimated to be a fraction of the total machine cost. This coupled with the increase in annual energy production can reduce the LCoE by 4.5% in the North sea and up to 35% in the Mediterranean.

7.1 Further Work

The research in this thesis has expanded on the idea of combined wave and solar energy converters. It has led to conclusions which could lead to the following further work.

7.1.1 Electrical System Design, Integration and Analsyis

In a full scale Solar-WEC, where the solar output is to be integrated with the main WEC power, take off and potentially with the power export, the electrical system will have to be properly integrated. Questions arise with the bi-directionality of the power flows from 24V to the higher bus voltage and the potential addition of new fault levels.

7.1.2 Continued testing of solar panels at sea

The testing of solar panels in this thesis was bound to the timelines of deployments of the BlueX. Only 5 months of data were gathered with 4 months of this in one location and 16 days in another. Further testing to provide data on the long-term performance and survivability of solar panels in such a rough environment would be beneficial. Investigating how light-induced degradation reduces performance in the offshore environment and how biofouling degrades the panels structure.

Fortunately, the panels will continue to remain on BlueX throughout the remainder of the RSP testing programme and potentially beyond. Gathering survivability data in the winter, where the wave action is most pronounced will provide a worst-case scenario for the survivability of the panels.

Analysis of how the panels can be removed and replaced would be beneficial to analyse the operations and maintenance costs and procedures that affect the long-term costs of the additional solar array. This could highlight problems with the method of adhesion and perhaps a secondary hull should be implemented so that the entire array does not rest directly on the WEC steel hull. This could influence the thermal path of the panels and should be considered.

7.1.3 Solar Panel Development

As solar panel research continues, more efficient cells will be developed. Additionally, the costs of solar panels will reduce. This combination of factors will compound and reduce the LCoE of solar arrays drastically making their addition to the WEC more beneficial.

Additionally, other types of panels such as bifacial panels could unlock further energy. By having bifacial panels placed over water surfaces they might have the opportunity to absorb energy twice. Alternatively, mounting the bifacial cells vertically, like a sail, may provide an alternative method of boosting yield but they would be exposed to environmental loading.

7.1.4 Resource Assessment Model Integration

The model produced and validated as part of Chapter 5 yields accurate results for the performance of a solar panel array on a dynamic wave energy converter. However, the run time for these models is long, taking approximately 16 hours to analyse the results for a one-month period. The MOE Analytics Mocean tool is used to perform resource assessments of different Mocean wave energy converters in any global location and only takes minutes.

The hope is that the MOE Analytics Tool will also include a solar array to show the full potential of a combined system. To do this, the model produced in this thesis will first have to be reproduced in Python. Secondly, the computational demand will have to be reduced so that the model can be run very quickly to provide monthly and annual solar resources in a matter of seconds so that several locations and array configurations can be analysed. Perhaps this can be done by using the performance ratios for a flat plate array to provide an approximate estimate, suitable for quick feasibility studies. A high-fidelity model can then be run when a deployment site is more concrete.

Additionally, as the Mocean WEC designs mature and scale up, the need for the layout of the arrays will need to be modelled in a representative way. Panels may be located on different planes and not necessarily lie on the main hull tube.

7.1.5 Deployable solar arrays

This work has shown that the benefits of adding a solar array to a wave energy converter can increase with added capacity. However, a limited deck area restricts the maximum capacity of the onboard array.

The harsh offshore environment means that having panels overhanging the hull of the WEC or mounted with an exposed back surface may lead to damage from waves. Therefore, a way to increase the installed solar capacity without risking the integrity of the panels would be to use deployable arrays. A deployable array would be sheltered during periods of dynamic wave action and can be deployed when the WEC senses low waves. Fixed panels such as those discussed in this thesis can be used to sense how good the solar environment is to confirm if the array deployment will result in a net gain of energy.

Designs could draw inspiration from satellites, with huge unravelling arrays. However, this may be too fragile for the environment. Alternate designs could be based on umbrellas, large rolling drums or "briefcases". I have drafted a couple of designs for a deployable array. A CAD of a "briefcase design", can be seen below in Figure 7.1. If the deployable array can articulate, it also opens the opportunity for tracking solar array which can improve the yield and benefits further.

A sketch of a roller deployable array can be seen in Figure 7.2. A large drum rolls out a flexible solar array with a float at the end to support its mass. The panels could also be bifacial to absorb energy from both sides, however flexible bifacial panels are still in early development. The slot through which the panels pass through could also have a wiper to remove water or biofouling. I hope to explore this topic further with my time at Mocean beyond my EngD.

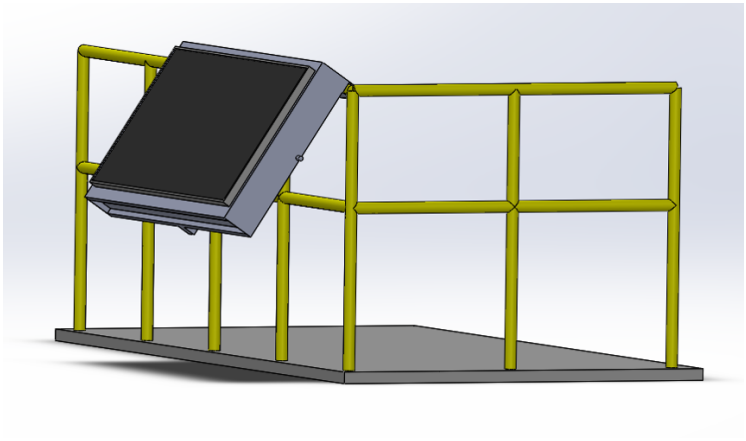

(a) Retracted

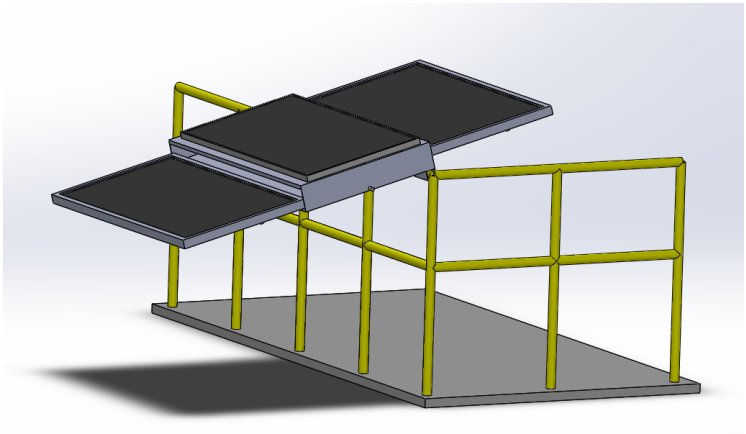

(b) Deployed

Figure 7.1: CAD of Deployable Array mounted onto the Gantry Railing

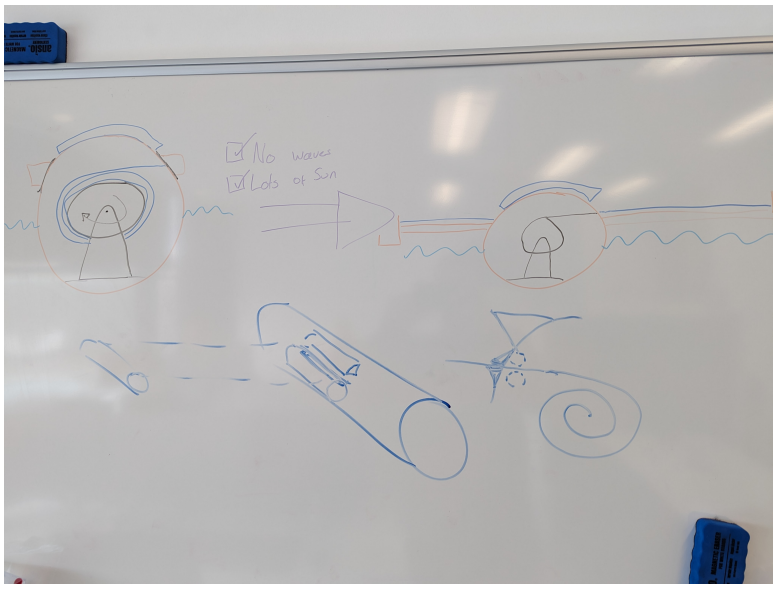

Figure 7.2: Sketch of a roller solar array

Appendix A

IET RPG Conference Paper

EXPERIMENTAL RESULTS FROM THE HYBRIDISATION OF WAVE AND SOLAR ENERGY TO PROVIDE CONSISTENT POWER TO ISLANDED LOADS

Macauley J Versey[1,3], Aristides Kiprakis[2], Chris Retzler[3]

[1]IDCORE, University of Strathclyde, Glasgow, United Kingdom
[2]School of Engineering, University of Edinburgh, Edinburgh, United Kingdom
[3]Mocean Energy, 10 Max Born Crescent, Edinburgh, United Kingdom
Corresponding email:

Keywords: WAVE ENERGY, SOLAR ENERGY, HYBRIDISATION, TEMPERATURE COMPENSATION.

Abstract

The power output of a wave energy converter could be smoothed by the addition of a solar panel array as wave and solar energies are complimentary. To explore this theory, an experiment was devised where six solar panels were mounted to the Mocean Energy BlueX wave energy converter deployed in the Orkney Islands. The aims of the experiment was to explore how much power could be expected, what type of panel is best suited, what lifetime is to be expected and what impacts are there on the operations of the WEC. Conclusions from the experiment are: the panels can produce 4kWh over a 16 day period, the flexible panels produced more energy than rigid panels, the rigid panels are susceptible to damage, the panels did not have an influence on the performance of the WEC but do introduce a new operation to the deployment to clean the panels from bird deposits. By using outputs from the experiment, a 5kWp array is suggested which could produce an average daily yield of 2.7kWh.

1 Introduction

A wave energy converter [WEC] is a device which produces electricity from ocean waves. The WEC electrical power take off system is supported with battery energy storage to take the slack when there is a lack of wave energy. However, in some summer months calm conditions can persist for prolonged periods of time where the batteries discharge to a low level resulting in a loss of load.

An attractive solution is to equip the WEC with solar panels to supplement power output in the sunnier, calmer summer months, smoothing the output of the machine. Additionally, solar panels have become the cheapest source of energy [1] making this addition potentially negligible compared to the cost of the WEC.

No examples of literature about the specific topic of combining solar and wave energy into one device exists. However, there is literature that can be relevant in areas of offshore floating PV [3][4][5], cooling effects [6] bird guano [7] and the benefits of hybridisation of independent solar and wave plants [8].

To explore how valuable the addition of solar panels may be, an experiment was performed where two identical solar "skids" were installed on the Mocean Energy [9] BlueX WEC during its deployment in the European Marine Energy Centre [EMEC] wave test facility at Scapa Flow. This paper details the experimental set up, results and some outcomes for the future of full scale solar array hybridisation before concluding with some further work to be completed.

The experiment attempts to solve four questions:

1. What is the estimated deliverable power of a solar panel array in offshore dynamic conditions?
2. What type of solar panel technology is most suitable for a WEC?
3. What lifetime is to be expected of a solar array in the marine environment?
4. What are the impacts on the operations and performance of the WEC due to the addition of a solar panel array?

2 Methodology

2.1 Experimental Set up

Each set of panels is mounted to a "skid" with a data acquisition system to measure panel outputs and temperature. One skid was mounted to the front section of the WEC and the second mounted to the aft. A third control skid was mounted nearby on shore. All three skids are identical, measuring open circuit and short circuit parameters of each panel, with the addition of an anemometer to the land based skid to measure wind speed. Open and short circuit is measured to decouple the load from power production.

Each skid consists of three 50W Renogy panels, one rigid panel and two flexible panels. One of the flexible panels was laid flat and the second was laid on a 3 meter radius curve. This allows the panel type to be compared, as well as the effect of curvature on the power production. Switching between states is controlled via MOSFET and has a period of

two seconds where ten measurements are made and an average calculated to reduce the influence of sensor noise.

The panels were electrically similar, allowing for common components to be used across both data acquisition systems, to reduce cost and complexity. Table 1 shows the relevant properties of each panel.

Table 1 – Relevant Properties from Solar Panel Datasheets

	Rigid RNG-50D-SS	Flexible RNG-50DB-H
Power	50W	50W
Voltage Max Power	18.3V	18.5V
Current Max Power	2.9A	2.7A
Voltage Open Circuit	21.8V	22.6V
Short Circuit Current	3.1A	2.92A
Efficiency	21%	21%

2.2 Accuracy of Sensors

The data acquisition system was tested for accuracy with an external power supply to give a known voltage and current input compared against the output. The voltages and currents were tested over ranges extending over that expected to be seen during the course of the experiment. Results show; a consistent 3% overestimate of voltage, ±8% error with currents less than 0.5A where noise makes up a significant amount of the signal magnitude, which reduces down to ±1% at currents greater than 1Amp.

2.3 Calculation of Power

The power output of the panels can be estimated by taking the product of the open circuit voltage, short circuit current and the panel fill factor [FF]. The FF can be calculated from the panel datasheets with properties described at standard test conditions [STC] as seen in Equations 1 and 2.

$$\frac{Vmp_{STC} * Imp_{STC}}{Voc_{STC} * Isc_{STC}} = Fill\ Factor \quad (1)$$

$$V_{oc} * I_{sc} * FF = Power \quad (2)$$

Where "mp" is the maximum power point, "oc" is the open circuit voltage and "sc" is the short circuit current.

In reality, the FF is not constant and is dependent on the cell temperature. Several sources in literature [9][10][11][12] describe the FF temperature coefficient for different panel types. By using the literature cited, an average FF compensation coefficient of -0.00163/C is used to calculate power output in Equation 3. It should be noted that the temperature recorded is the backsheet temperature and not the cell temperature which would be higher.

$$FF + (T_{Cell} - T_{STC}) * FF_{TempCoef} = Temp\ Compensated\ Fill\ Factor\ [TCFF] \quad (3)$$

2.4 Calculation of Energy

A robust measure of performance is the energy produced by each panel on each day, found by integrating power over time, as shown in Equation 3, where the time step is the 2-second switching cycle. The result is power in joules, which can be divided by 3600 to yield watt-hours.

$$Daily\ Energy = \sum_{i=n}^{i=m} (V_{oc}(i) * I_{sc}(i) * FF * 2) \quad (4)$$

Where "i" is the data point examined, "n" is the first point in the day and "m" is the final point in that day.

3 Results

3.1 Deployment Period, Location and Weather

The panels were installed onto BlueX on the 6th of September 2021, moored at the EMEC scale wave test site in Scapa Flow as shown in Figure 1

Fig.1 Deployment Location and EMEC Facilities [13]

The wave conditions began calm before rough weather hit Scapa Flow on the 22nd and 23rd of September. The next section presents 16 days of data taken during the deployment period, the original experimental campaign was planned to be longer but for reasons later discussed, only 16 days were obtained.

3.2 Backsheet Temperature

Figure 2 shows the backsheet temperature from the three panels, the horizontal sections on the 12th and 13th are periods of faulty readings where the data resorts to the last measured point. All three temperatures are similar but the rigid panel peaks higher than the others during the middle of the day, obtaining the highest recorded temperature of 36.88C on the 7th.

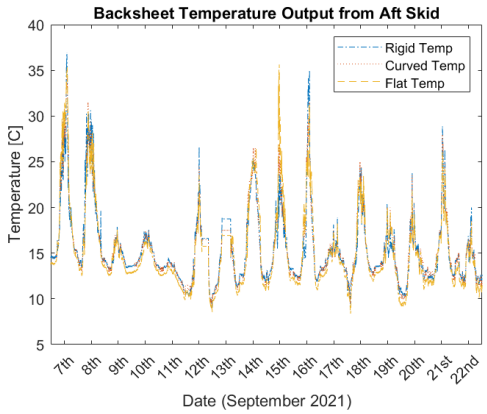

Fig.2 Backsheet Temperature Results

3.3 Solar Panel Power Outputs

Figure 3 shows the open circuit voltage from the three panels. The mean amplitude of the voltage does vary on a daily basis and follows the recorded backsheet temperature, lower voltages and temperatures on the 10th and 11th. This is to be expected as open circuit voltage is correlated to temperature. The rigid panel produces the highest voltage on the 12th of 22.86V and has the greatest mean voltage on every day of testing.

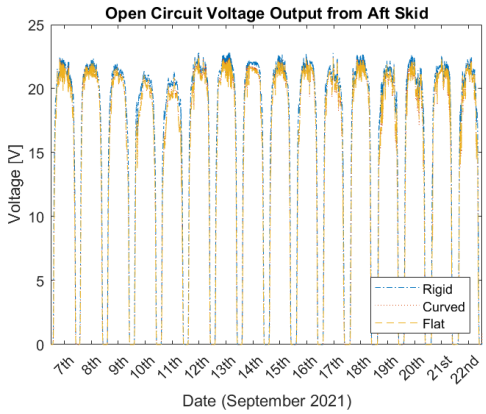

Fig.3 Open Circuit Voltage Results

As short circuit current is dependent on the value of irradiance, the value of current varies greatly not only day to day due to the daily weather but also at a much smaller time scale due to the movement of BlueX. As seen in Figure 4, the current rarely goes higher than 2 amps, as the experiment never experienced high enough irradiances. The curved panel had the highest mean current output of the three panels on every single day during the testing period with the highest peak current of 2.40A on the 7th.

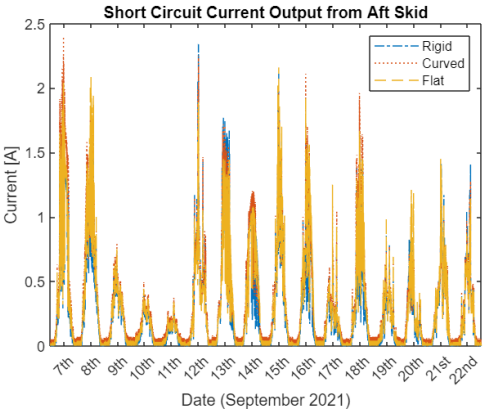

Fig.4 Short Circuit Current Results

Figure 5 shows the variation of FF when using a temperature compensation factor. For the majority of the time, the TCFF is greater than the constant FF for a given panel. The TCFF is less than the FF on only 6 periods when panel temperature is greater than 25C. This figure has a mirrored image to figure 2 with different offsets for each panel type.

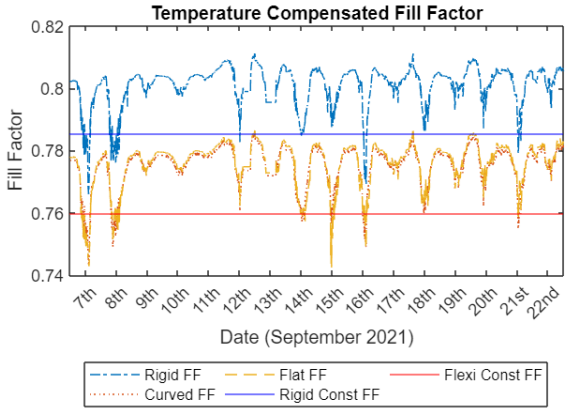

Fig.5 Value of TCFF for each panel and their constant values

Figure 6 shows the power calculated by using Equations 1, 2&3. By comparison with Fig. 5, power closely follows the current due to the more uniform voltage output. The curved panel produces the highest mean power on 12 of the 16 days with the rigid panel performing best on 3 days and the flat performs best only on one of the days.

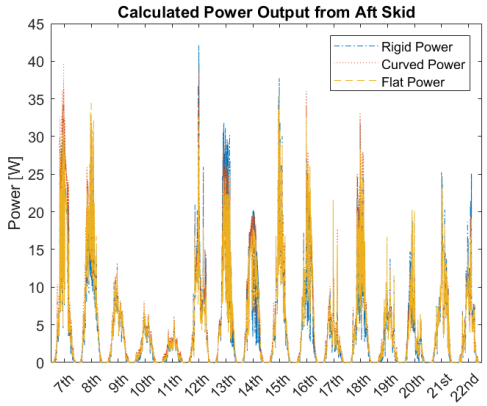

Fig.6 Calculated Power Results with TCFF

3.4 Panel Daily Energy

The daily energy is calculated using Eq. 4 and results presented in Table 2 below. It shows the total energy produced per panel over the testing period and the differences between using a constant FF and the TCFF. The influence of using a TCFF on the array of panels over the course of the testing period is small, increasing the calculated yield on average of 1.02%.

Table 2 – Total Energy of Each Panel Calculated using a Temperature Compensated Fill Factor and Constant Fill Factor

	Rigid	Curved	Flat	Array
TCFF Total [Wh]	1287	1436	1297	4020
FF Total [Wh]	1276	1422	1281	3979
% Diff	0.85	0.97	1.23	1.02

4 Discussion

The results presented allow for a comparison between the three panel configurations deployed onto the WEC, assisting in future decisions for further deployments.

The rigid panel saw the highest voltages during testing but some of the lower currents and highest temperatures. This along with its higher FF mean the rigid panel produced the least energy out of the three panels. The influence of the TCFF had the least impact on rigid energy yield.

The flat panel saw the lowest average temperatures and the lowest voltages resulting in producing the second highest yield but only marginally, 5Wh more than the rigid panel. The influence of the TCFF had the greatest impact on the flat panel, improving yield by 1.23%.

The curved panel had the greatest average current during testing, this resulted in the highest energy yield during the experiment, 146Wh more than the rigid panel. This is puzzling as the influence of curvature tends to reduce output due to reduce output as it creates a difference in irradiation over the panel surface. However, in this experiment, the curvature is slight and uniform. This coupled with the movement of the WEC may reduce the influence of curvature.

Using a FF temperature compensation makes an attempt at capturing the fact that solar panel efficiency also varies with cell temperature. Using the FF temperature compensation increases the energy yield by 41Wh or 1.02% over the course of testing. Over the course of a year, it is expected that the warm summers and cool winters would cancel each other out and the use of a FF temperature compensation would not be justifiable.

4.1 Operational Results

The rigid panel on the aft section was broken off during the storm on the 23rd and the panel lost to sea before being later retrieved. Fortunately, the remaining 5 panels did not receive any significant damage. Additionally, the enclosure housing the electronics suffered severe water ingress, despite being rated to IP69. This damage destroyed the PCB board and batteries on both the front and aft skids. All data from the front panels was lost. Fortunately, 16 full days and 2 partial days of data were retrieved from the aft panels giving over half a million data points to evaluate. Additionally, it appears that the land based panels experienced some sort of unknown failure. In the future, more careful design steel work can be suitably placed to protect the panels from wave loading but will add to the mass and cost.

Periodically, a team was deployed to the WEC to inspect its operation. Whilst there, the team found that the panels were heavily soiled from bird guano, as seen in Figure 7, impacting their power yield and introducing hotspots on the panels. The team cleaned the panels as there was not significant enough wave action to “self-wash” the panels from bird droppings as was initially hoped.

Fig.7 Soiled Panels during the deployment

However, as the WEC moves further offshore or to more energetic sites, sending a crew out once a week to manually clean the panels may not be economically viable. The hope is that wave action would overtop the panels provide an element of self-cleaning which may be possible if the panels were closer to the hull and not on a skid.

4.2 Full Scale Considerations

The choice of panel will have a significant impact on how the physical integration of the panels to the WEC occurs and how the maintenance of the panels is carried out.

A rigid panel would be bolted onto the WEC. Replacement of a faulty panel could be as simple as disconnecting the cables, unbolting the panel before replacing the new panel in the same way.

If flexible panels are used, they are fixed to the WEC using adhesive. This option does have a benefit of the panels being in direct contact with the hull of the WEC providing a strong conductive path to the sea which would lower the temperature of the panels, increasing efficiency. Replacement of a faulty panel may need to be scraped off of the hull before the surface repaired/cleaned and the new panel adhered to the surface – it is not obvious if this could be done at sea.

In future WECs, there will be more available deck area allowing for a much larger array. An investigation into available panels for use offshore has provided an “average flexible marinised panel” yielding an average watt peak per square meter, and efficiency been found to be 175Wp/m2 and 22.65%. 29 of these average panels are required to achieve a target of 5kWp installed capacity. If these panels behave similarly to the curved panel found in this experiment, they would produce 43.8kWh over the same testing period in the same conditions giving an average daily yield of 2.7kWh. This is a rather crude calculation but gives a general sense of the contribution of solar energy in a relatively calm wave environment during autumn in the Orkney Islands.

5 Conclusions

This experiment set out to explore the hybridisation of solar panels deployed on a wave energy converter with the aim to answer four questions posed in the introduction section. The data from one set of panels for a period of 16 days was obtained and exploration into the impacts of installing one solar panel skid carried out, answering questions 2 and 4 whilst partially answering 1 and 3.

1. The three 50W panels produced a total of 4.02kWh over the testing period. The curved panel produced the most out of the three panels, 1436Wh. The flat panel produced 1297Wh and lastly the rigid panel, 1287Wh.

2. The flexible panels produced more energy than the rigid panels in the same environment. The method of application is vastly different – bolts or adhesive – and would influence operations and maintenance strategies.

3. This study did not last for a significant enough amount of time to determine the lifetime of a solar array. However, the rigid panel on the aft saw damage due to wave action and suitable steelwork design should be carried out to protect them or they may need to be regularly replaced.

4. The panels are lightweight enough that they do not have a significant impact on the dynamic behaviour of the WEC. However, the deposits of bird guano could be significant requiring regular maintenance to clean them.

An additional outcome was the assessment of the use of a temperature compensated fill factor where it was found that by using this calculation the calculation of daily energy increased on average by 1.02%

A discussion was carried out considering the full scale deployment of an array where it was found that a 5kWp installed array may achieve an energy yield of 43.8kWp. Further to this, the design considerations for flexible and rigid panels discussed.

5.1 Further Work

The re-running of the experiment to be able to correct some of the flaws of this one. Ensuring that the land based skid operates so as to have a solid comparison between those offshore and on land would be greatly beneficial as well as being able to compare the two sections of the WEC. Add in to this test the exploration of maximum power point tracking techniques to explore if they respond rapidly enough to capture solar energy even when the WEC is moving. This could help determine the cut-off point at which the WEC is moving too rapidly to be able to effectively harvest solar energy.

Additional further work that is to produce a model which can use freely available irradiance data to predict the power output of a WEC deployed at any given location. This model can be verified against data produced from this and subsequent experiments to check its accuracy. This work is already in progress and should be completed very soon.

6 Acknowledgements

This research is funded by the EPSRC and NERC for the Industrial CDT in Offshore Renewable Energy (EP/S023933/1) and sponsored by Mocean Energy. For the purpose of open access, the author has applied a Creative Commons Attribution (CC BY) licence to any Author Accepted Manuscript version arising from this submission.

7 References

[1] – IEA, World Energy Outlook 2020, IEA, Paris, pp238 https://www.iea.org/reports/world-energy-outlook-2020
[2] –'Mocean Energy', https://www.mocean.energy/, accessed 10 May 2021
[3] - Golroodbari, S., van Sark, W.: 'Simulation of performance differences between offshore and land-based photovoltaic systems', Progress in Photovoltaics: Research and Applications., 2020, 28, (9), pp 873-876
[4] - Mignone, A., Inghirami, G., Rubini, F et al.: 'Numerical simulations of wind-loaded floating solar panels', Solar Energy, 2021, 219, pp 42-49
[5] - Dörenkämper, M., Wahed, A., Kumar, A et al.: , The cooling effect of floating PV in two different climate zones: A comparison of field test data from the Netherlands and Singapore', Solar Energy, 2021, 219, pp 15-23
[6] - Dubey, S., Sarvaiya, J., Seshadri, B et al.: 'Temperature dependent photovoltaic (PV) efficiency and its effect on PV production in the world - A review', Energy Procedia, 2013, 33, pp 311-321
[7] - Sisodia, A., Mathur, R.: 'Impact of bird dropping deposition on solar photovoltaic module performance: a systematic study in Western Rajasthan', Environmental Science and Pollution Research, 2019, 26, (30), pp 31119-31132
[8] - Oliveira-Pinto, S., Rosa-Santos, P., Taveira-Pinto, F.: 'Assessment of the potential of combining wave and solar energy resources to power supply worldwide offshore oil and gas platforms', Energy Conversion and Management, 2020, 223
[9] – Min, K., Min, K, Kim, T et al. 'An Analysis of Fill Factor Loss Depending on the Temperature for the Industrial Silicon Solar Cells', Energies, 2020, 13, (11), pp 1-10
[10] - Chander, S., Purohit, A., Sharma, A et al., 'A study on photovoltaic parameters of mono-crystalline silicon solar cell with cell temperature', Energy Reports, 2015, pp 104-109
[11]- Chander, S., Purohit, A., Sharma, A. 'Impact of temperature on performance of series and parallel connected mono-crystalline silicon solar cells', Energy Reports, 2015, pp 175-180
[12] - Qu, H., Li, X., 'Temperature dependency of the fill factor in PV modules between 6 and 40 °C, Journal of Mechanical Science and Technology, 2019, 33, (4), pp 1981-1986
[13] – 'EMEC Facillities', https://www.emec.org.uk/facilities/, accessed 10 May 2021

Appendix B

Renewable for Subsea Power Experimental Results

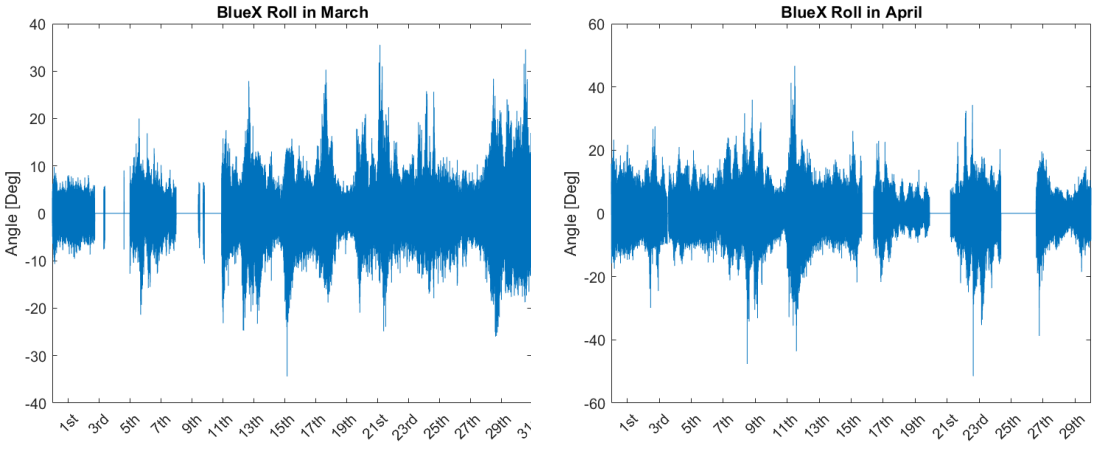

(a) March **(b)** April

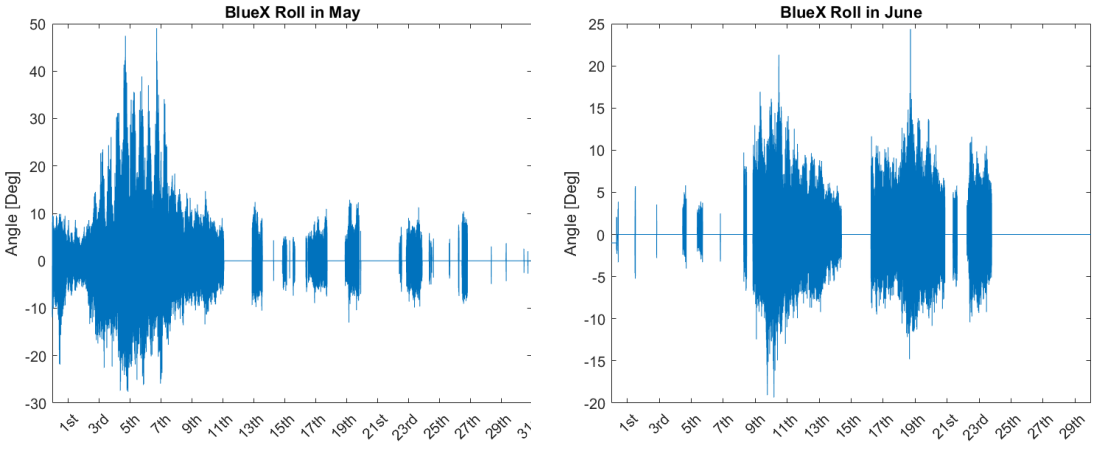

(c) May **(d)** June

Figure B.1: Roll Angles of BlueX

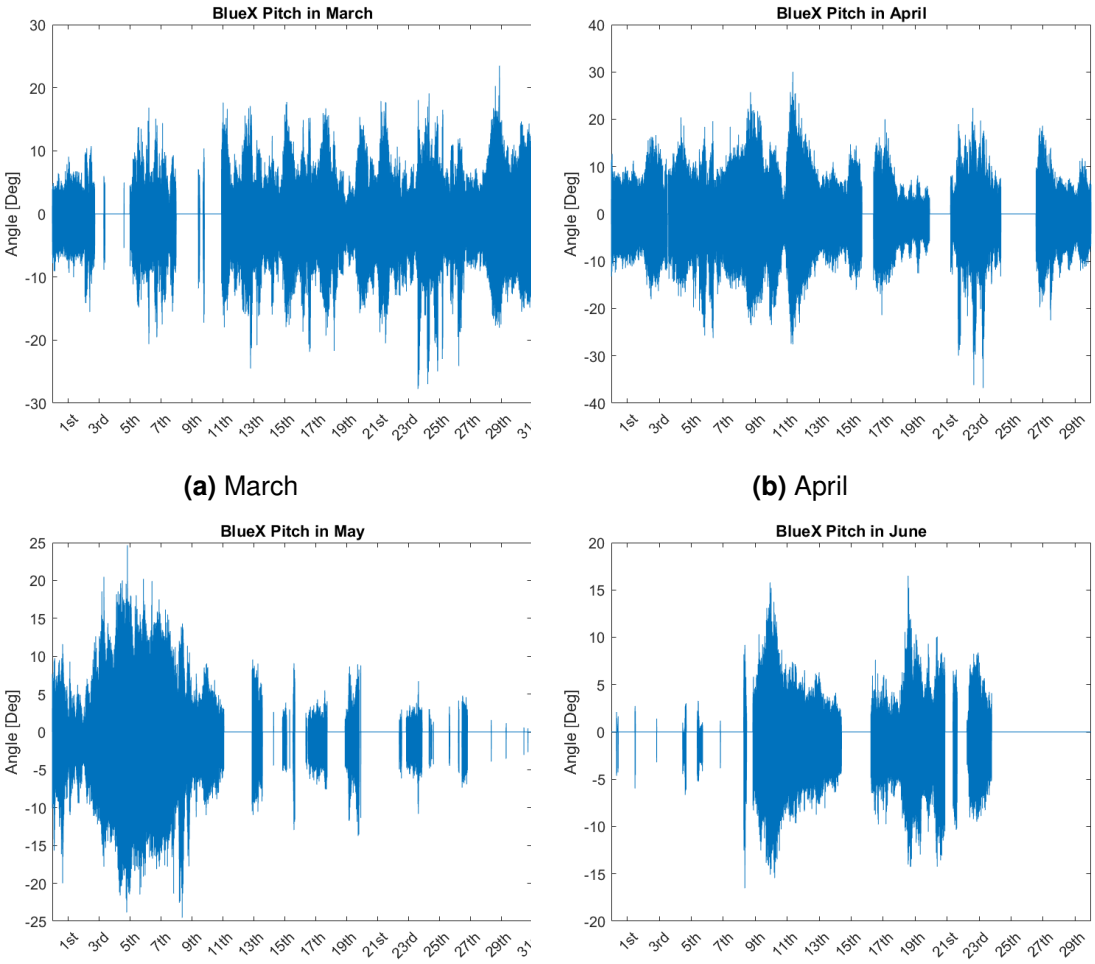

(a) March **(b)** April

(c) May **(d)** June

Figure B.2: Pitch Angles of BlueX

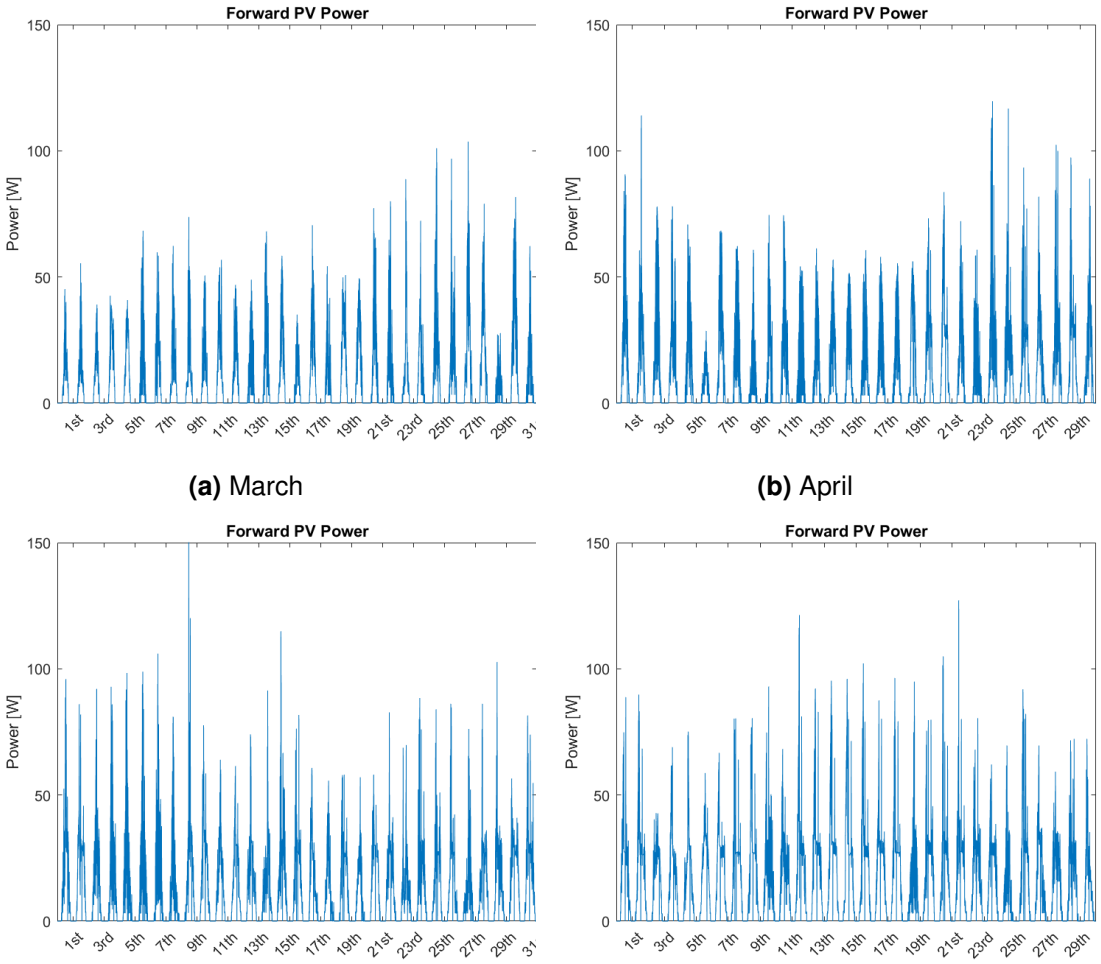

(a) March

(b) April

(c) May

(d) June

Figure B.3: Power Produced from Forward PV Array

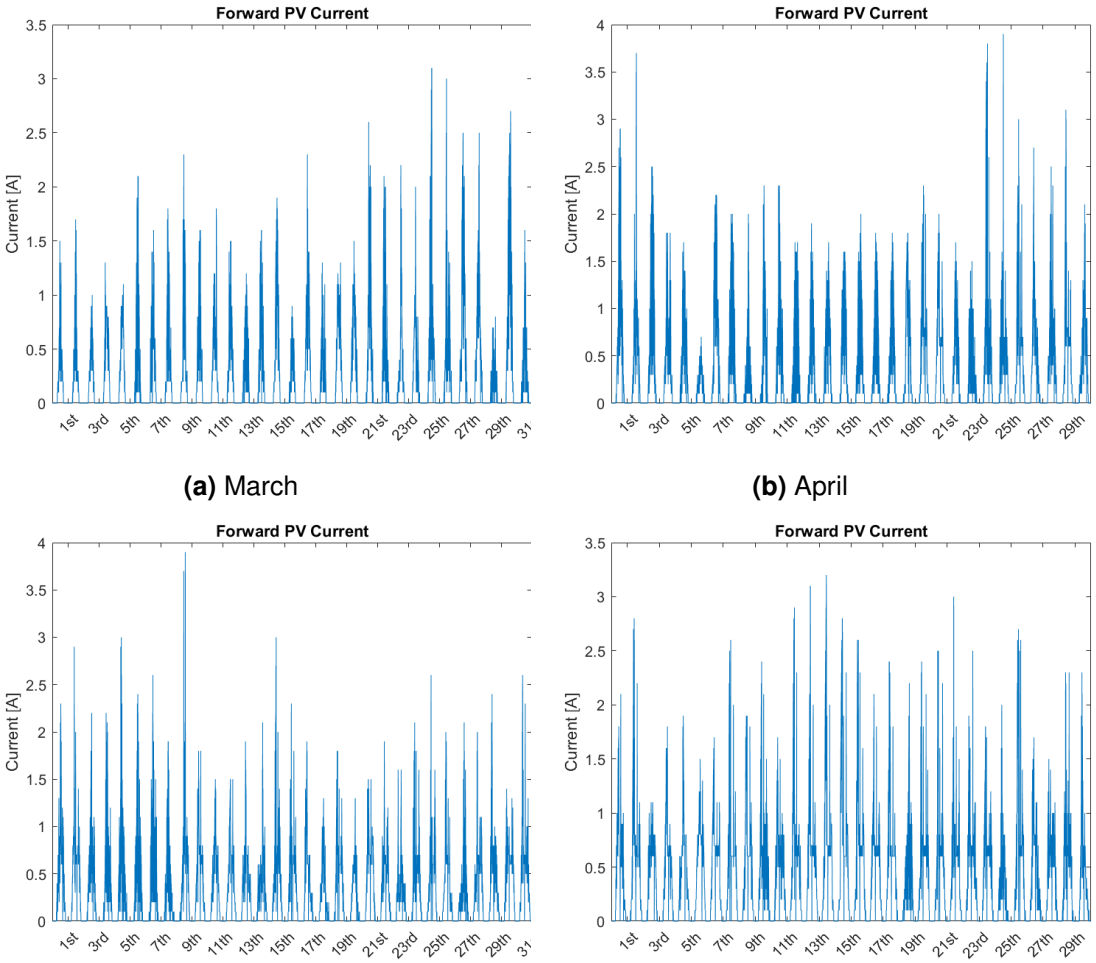

(a) March **(b)** April

(c) May **(d)** June

Figure B.4: Current Produced from Forward Array

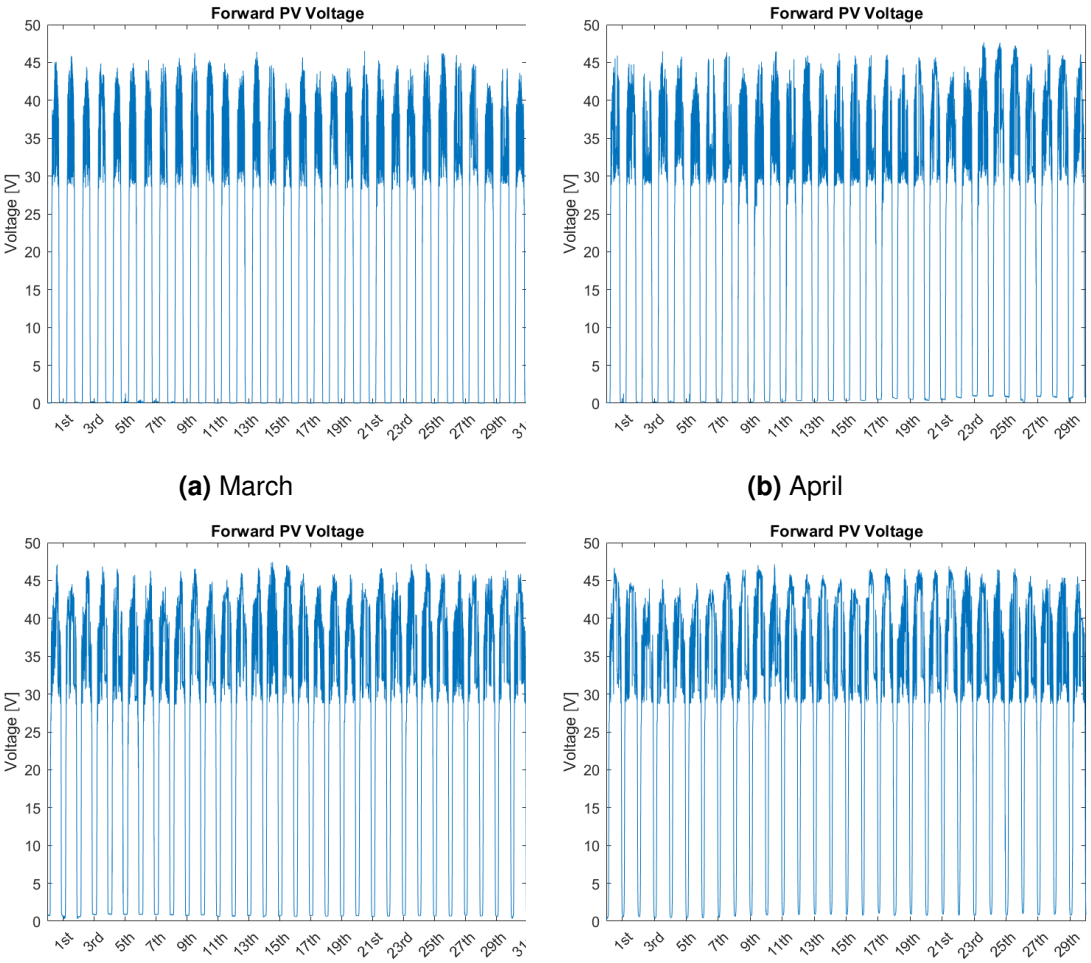

(a) March

(b) April

(c) May

(d) June

Figure B.5: Voltage Produced from Forward Array

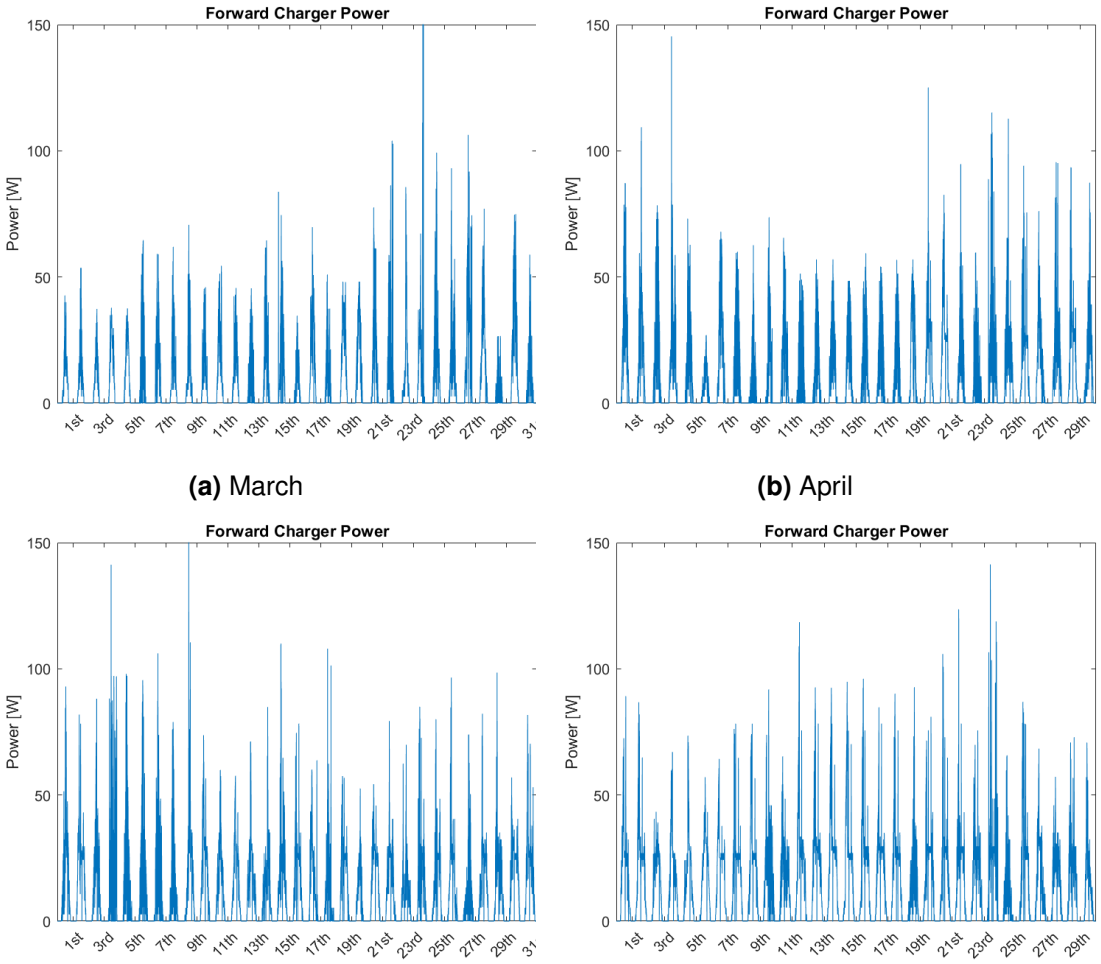

(a) March **(b)** April

(c) May **(d)** June

Figure B.6: Power Produced from Forward MPPT Charger

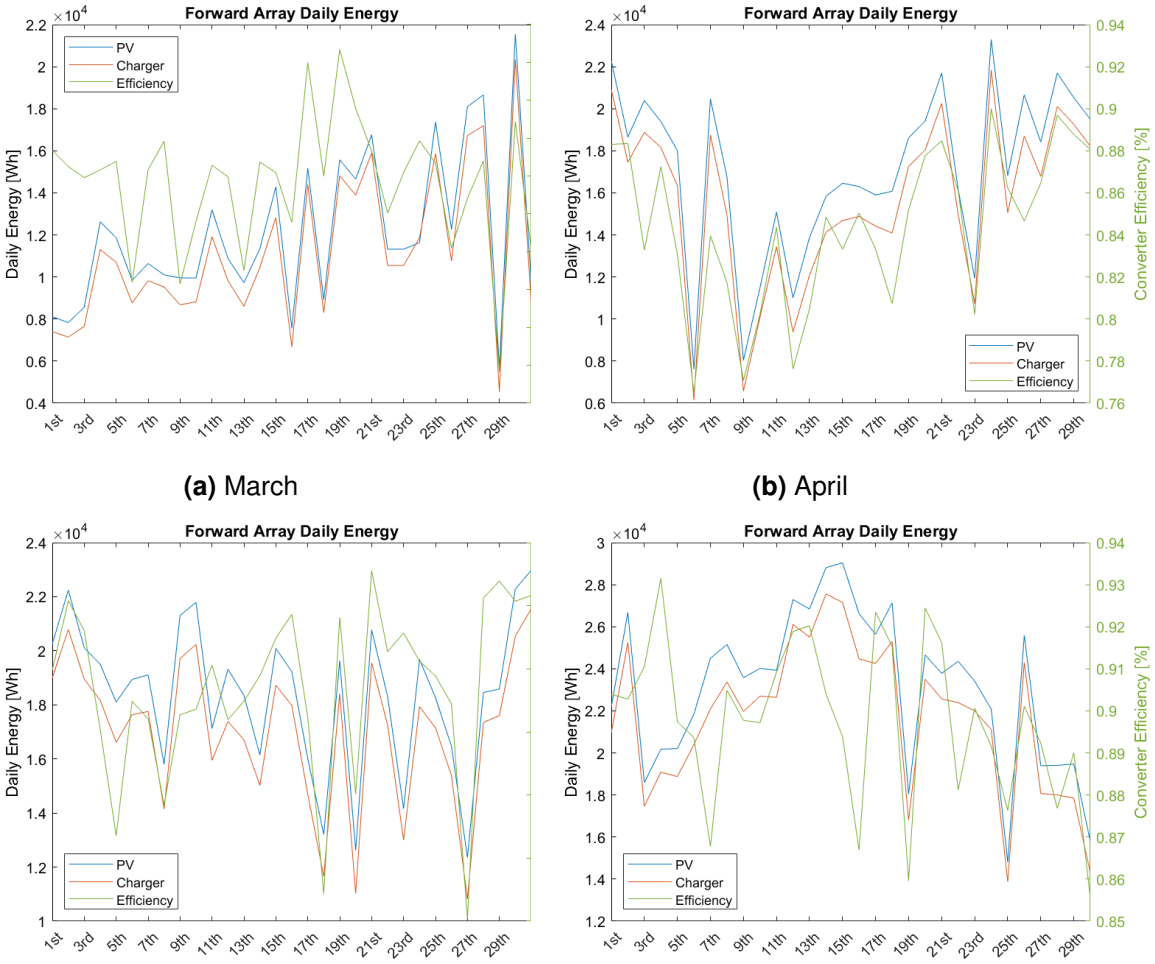

(a) March **(b)** April

(c) May **(d)** June

Figure B.7: Energy and Efficiency from Forward Array

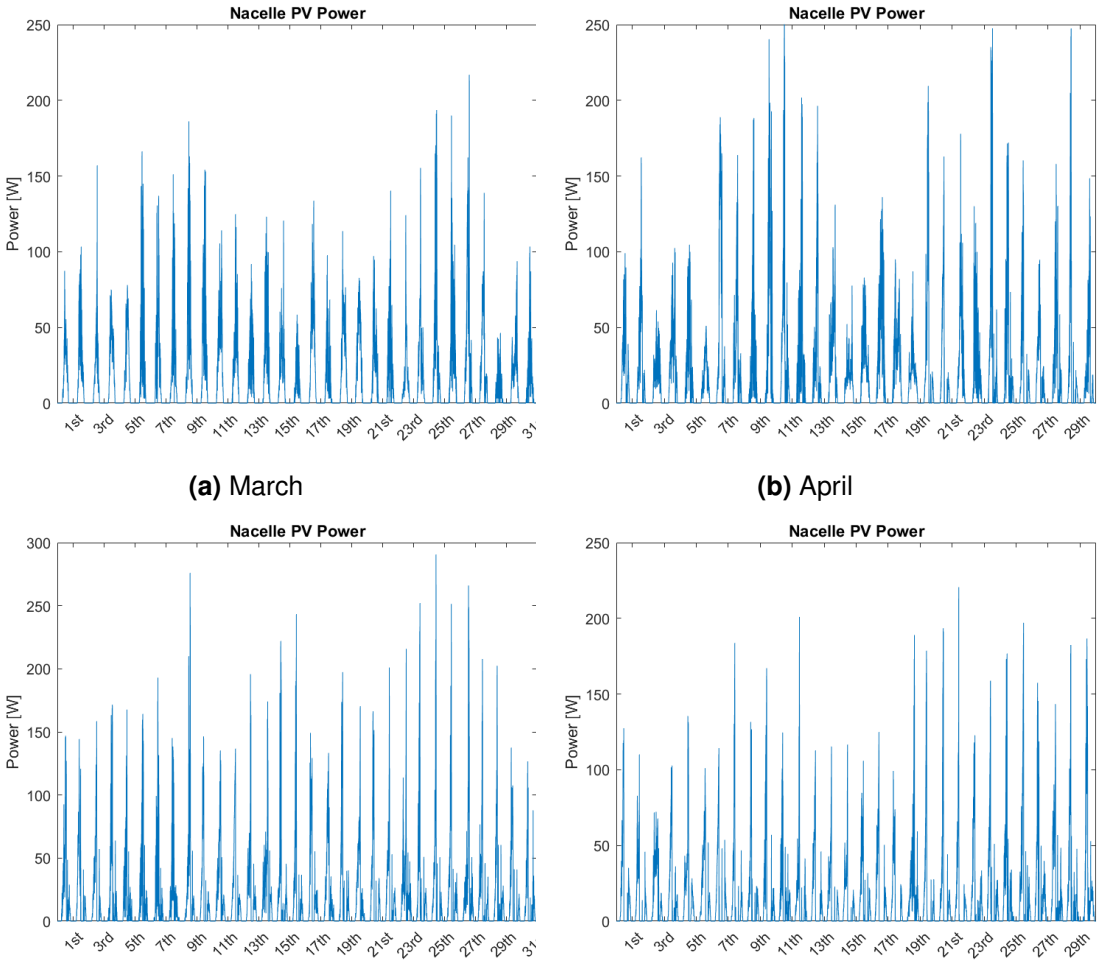

(a) March **(b)** April

(c) May **(d)** June

Figure B.8: Power Produced from Nacelle PV Array

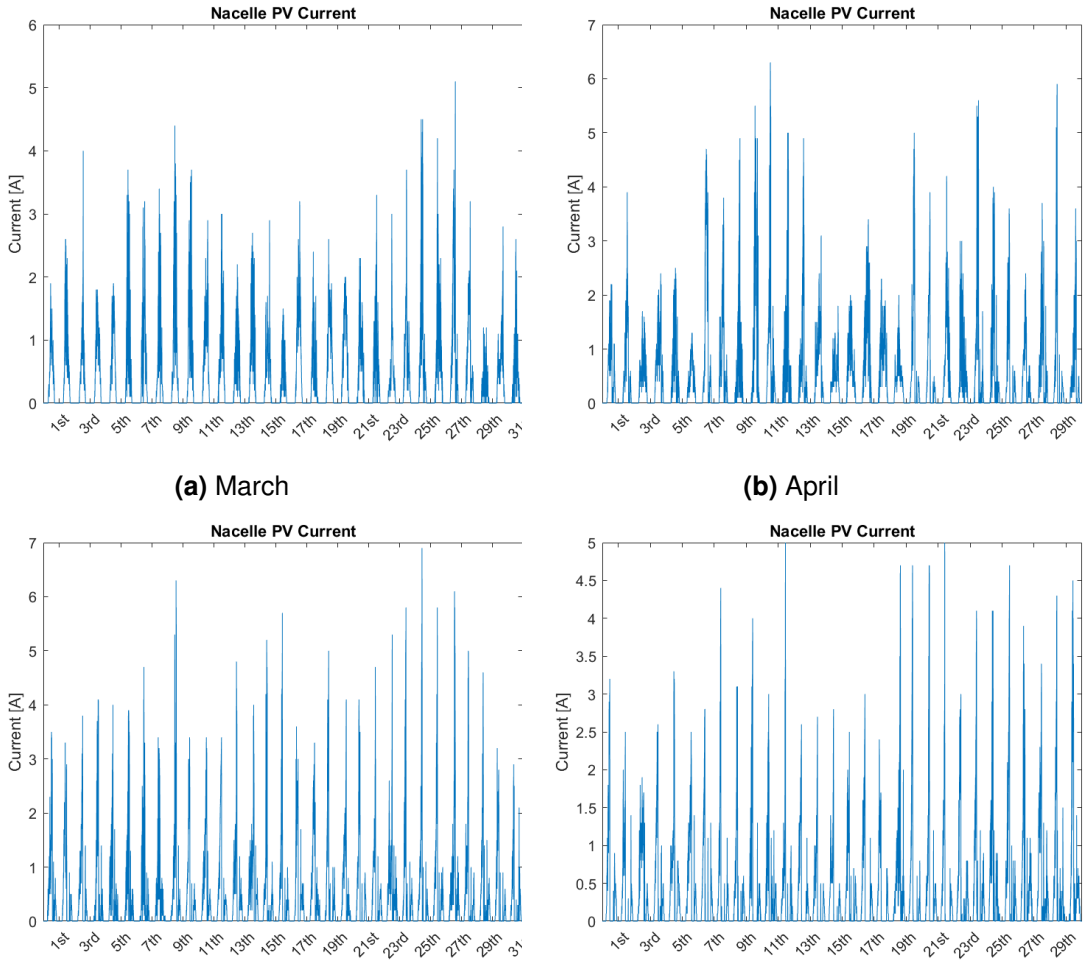

(a) March **(b)** April

(c) May **(d)** June

Figure B.9: Current Produced from Nacelle Array

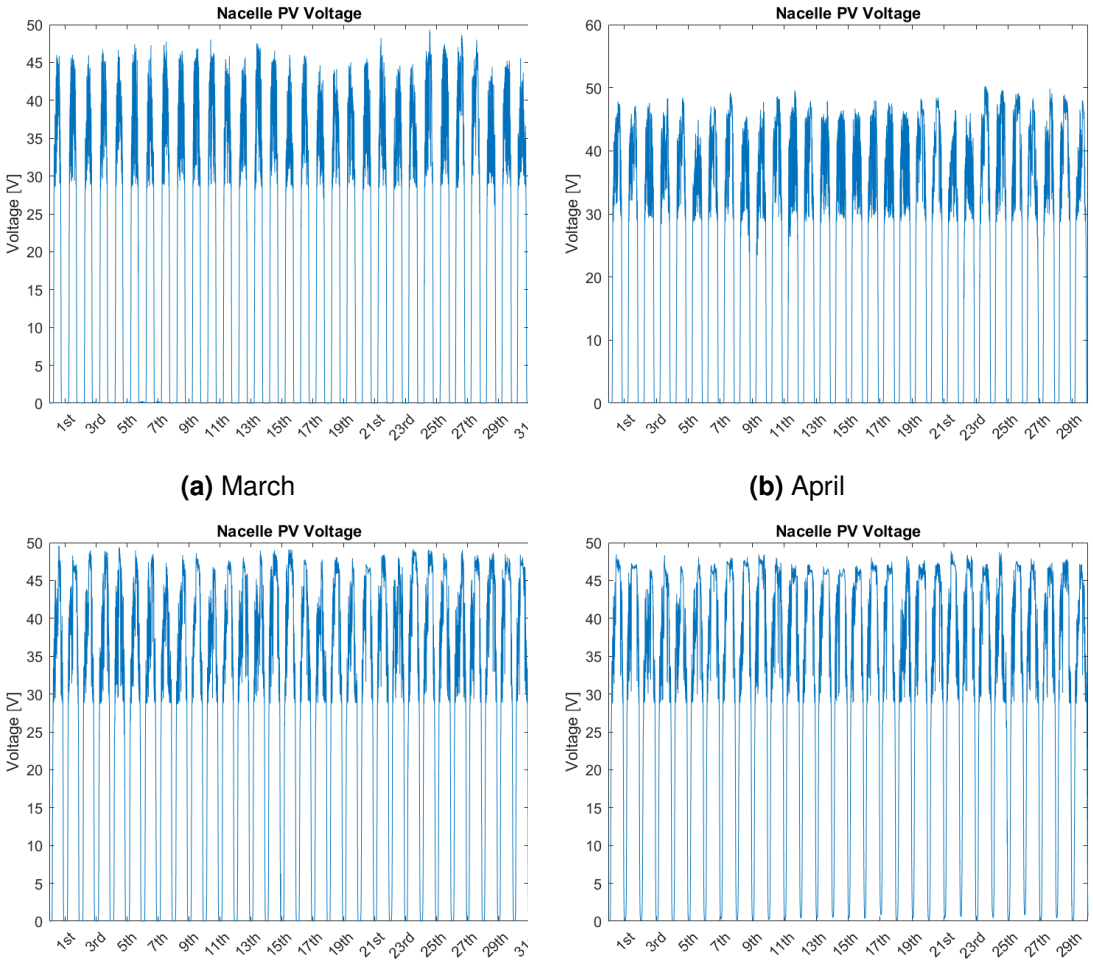

(a) March **(b)** April

(c) May **(d)** June

Figure B.10: Voltage Produced from Nacelle Array

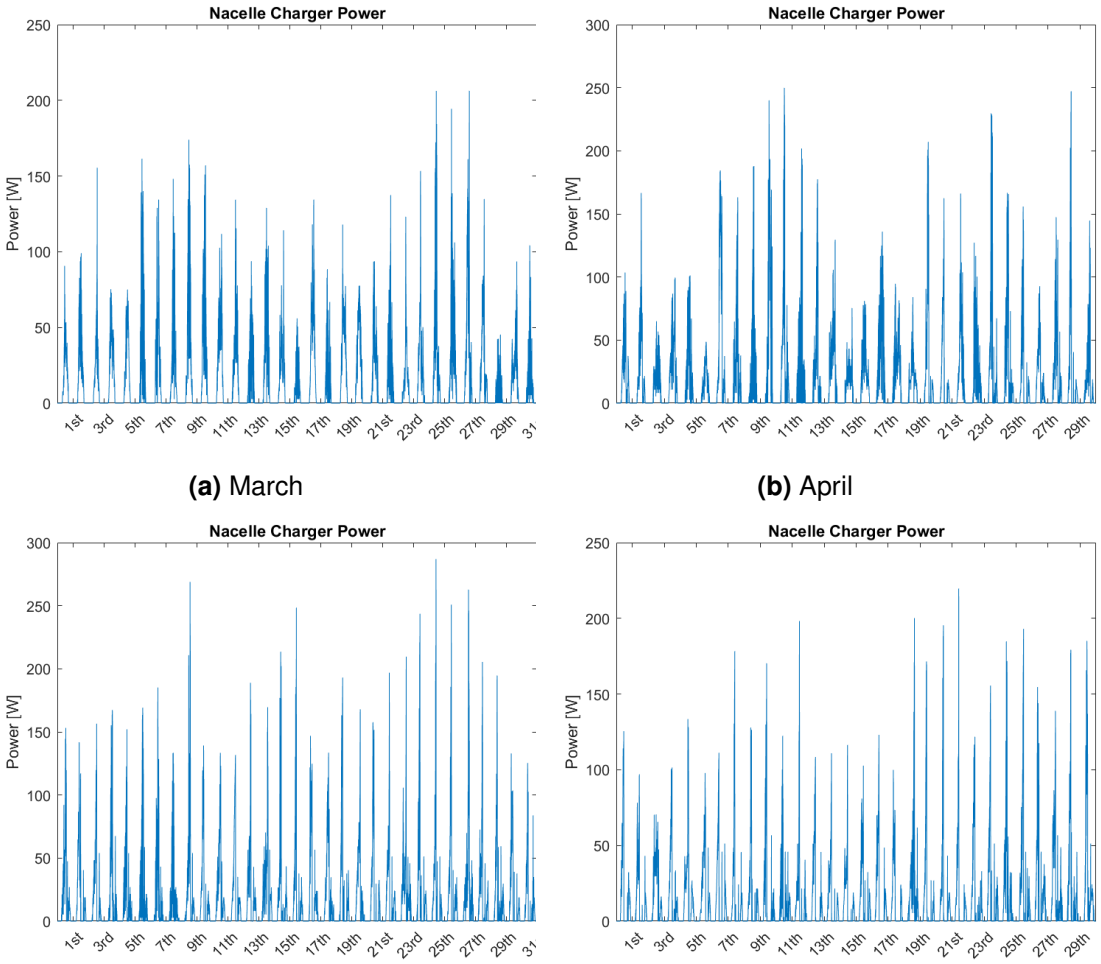

(a) March **(b)** April

(c) May **(d)** June

Figure B.11: Power Produced from Nacelle MPPT Charger

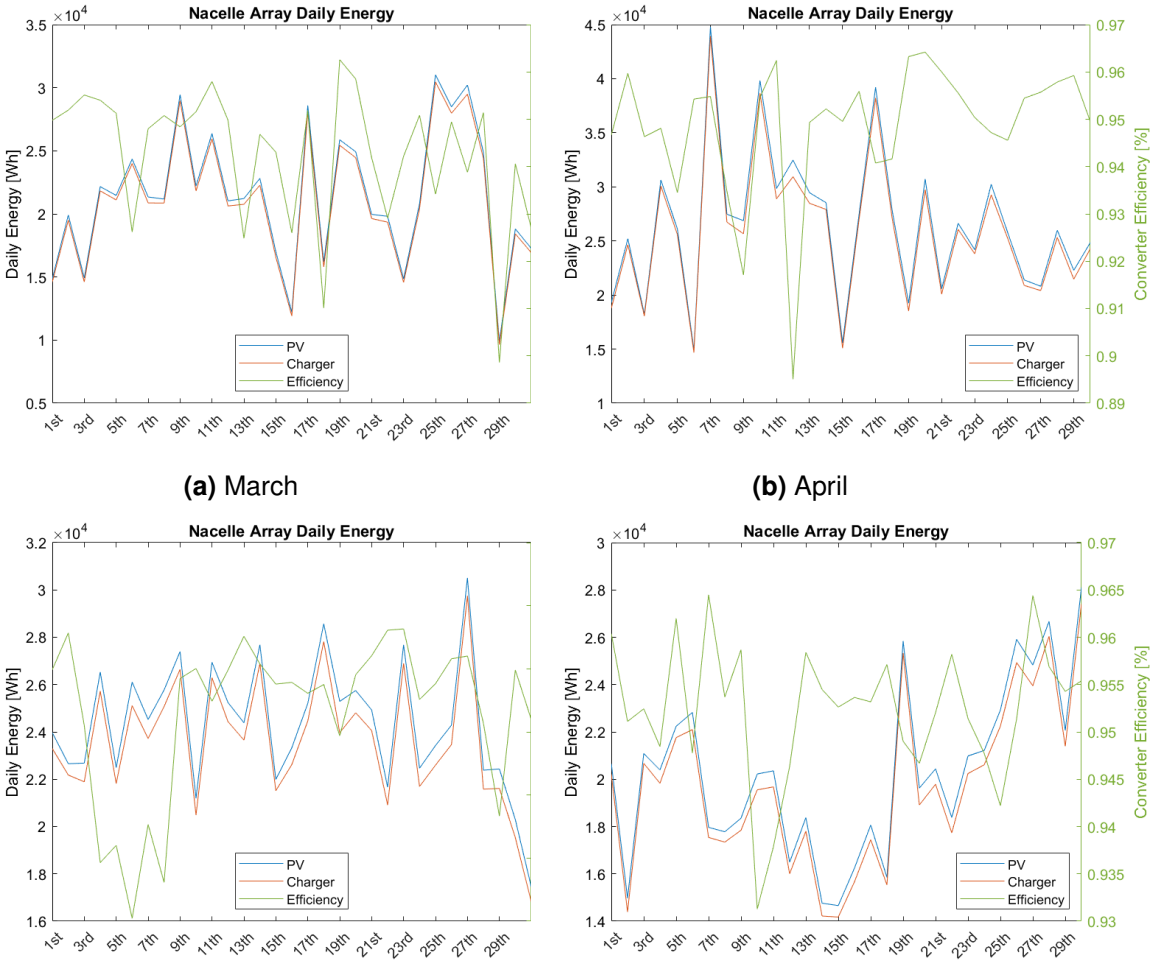

(a) March

(b) April

(c) May

(d) June

Figure B.12: Energy and Efficiency from Nacelle Array

(a) March **(b)** April

(c) May **(d)** June

Figure B.13: Daily Efficiency of the MPPT controller

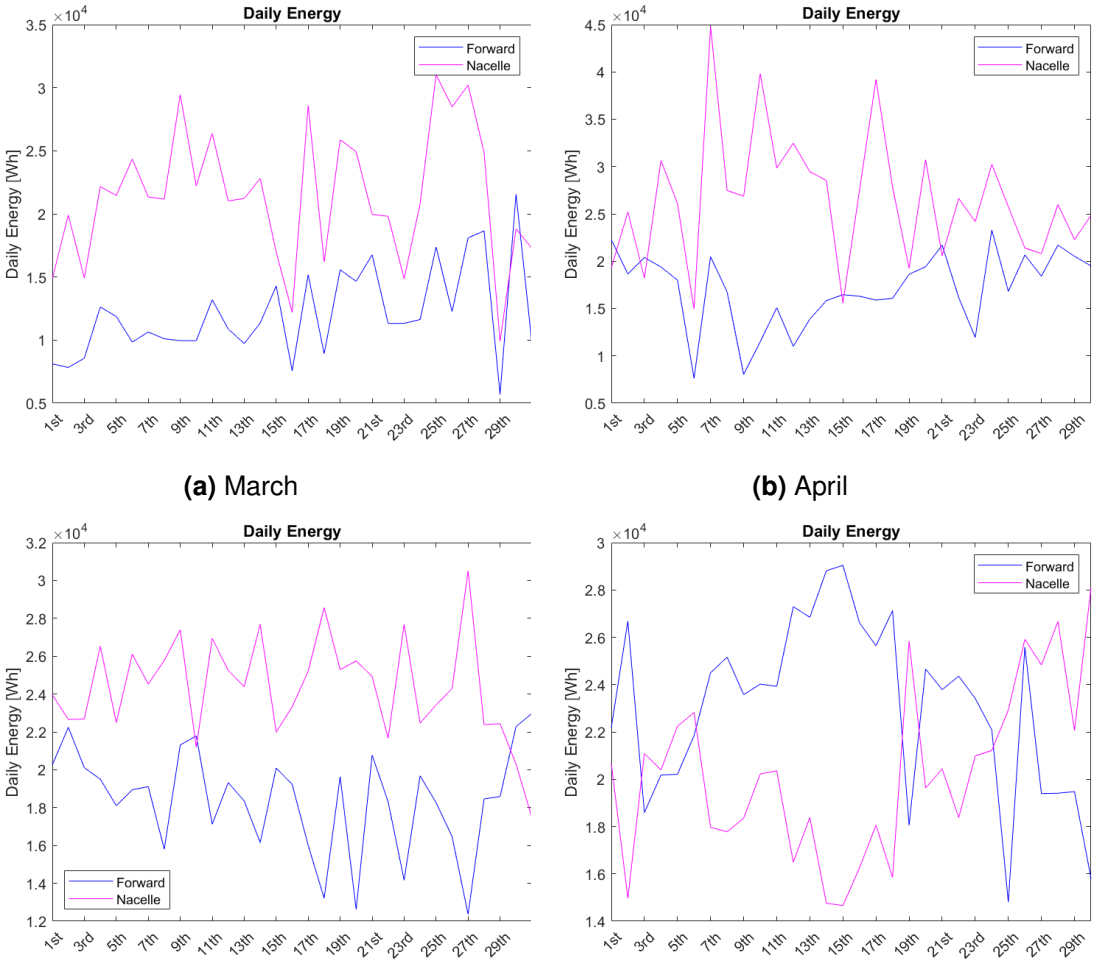

(a) March **(b)** April

(c) May **(d)** June

Figure B.14: Daily Energy Produced by the System

Appendix C

Comparison Modelling Results for Renewable for Subsea Power

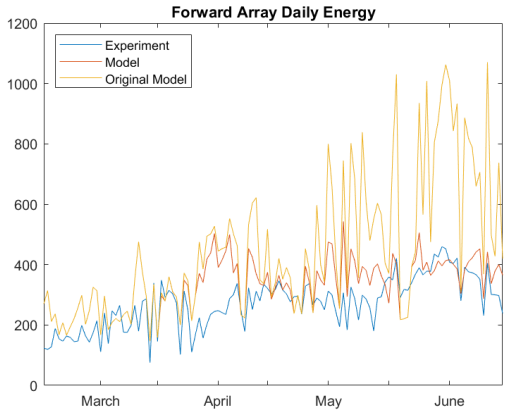

(a) Forward Array

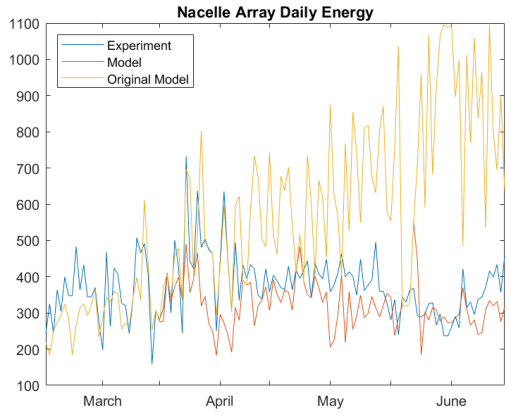

(b) Nacelle Array

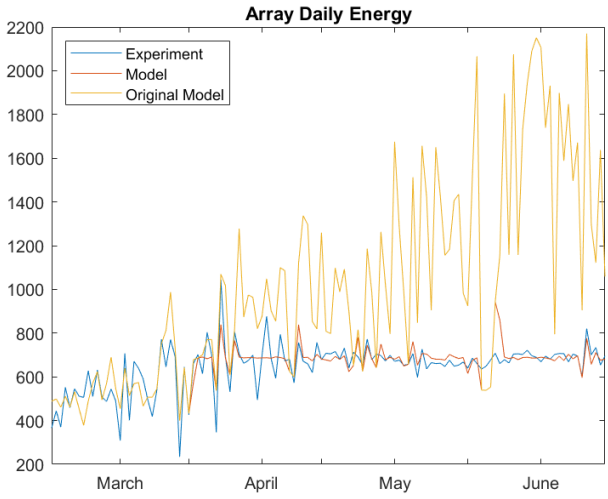

(c) Full Array

Figure C.1: Daily Energy Comparison with Full Yield Potential

Appendix D

Full Scale Modelling Results for Deployments in The Canary Islands and Sardinia

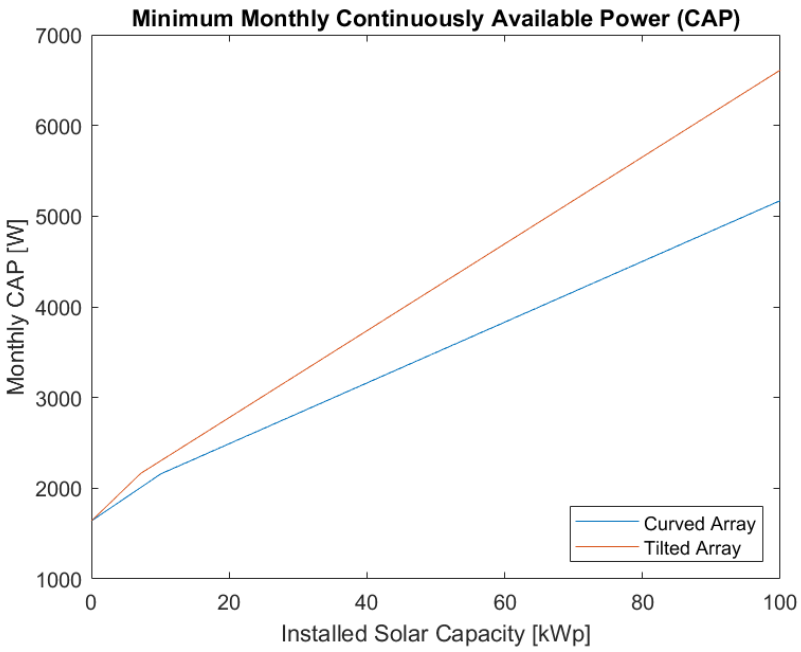

(a) Canary's

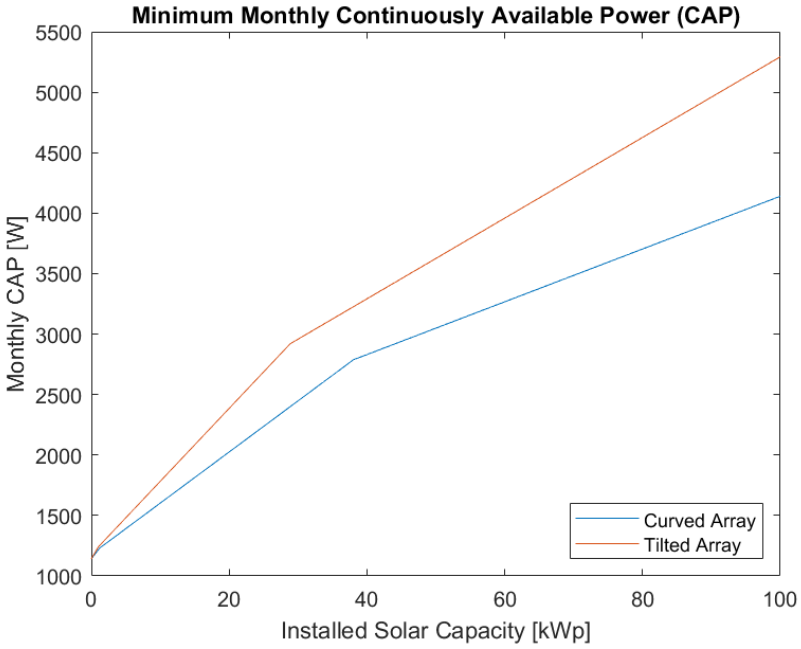

(b) Sardinia

Figure D.1: Continuous Available Power

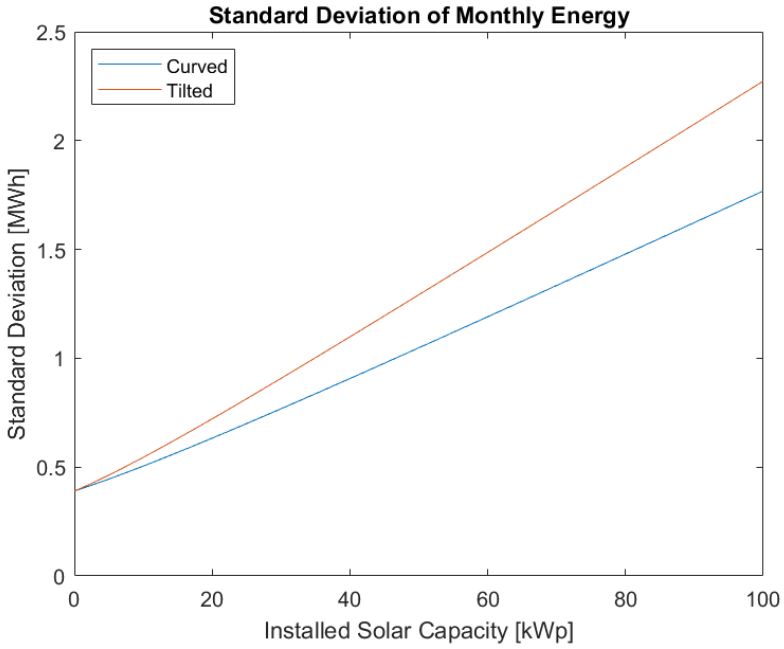

(a) Canary's

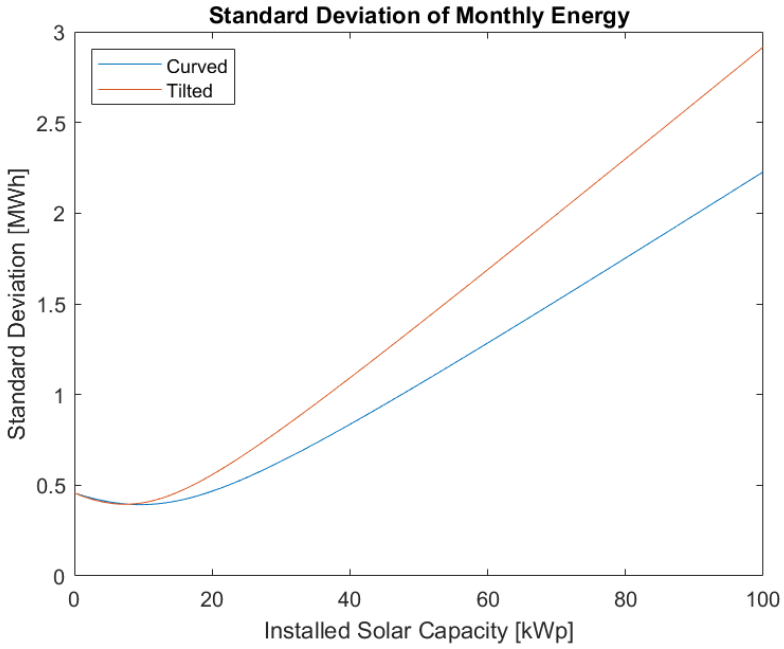

(b) Sardinia

Figure D.2: Standard Deviation of Monthly Energy

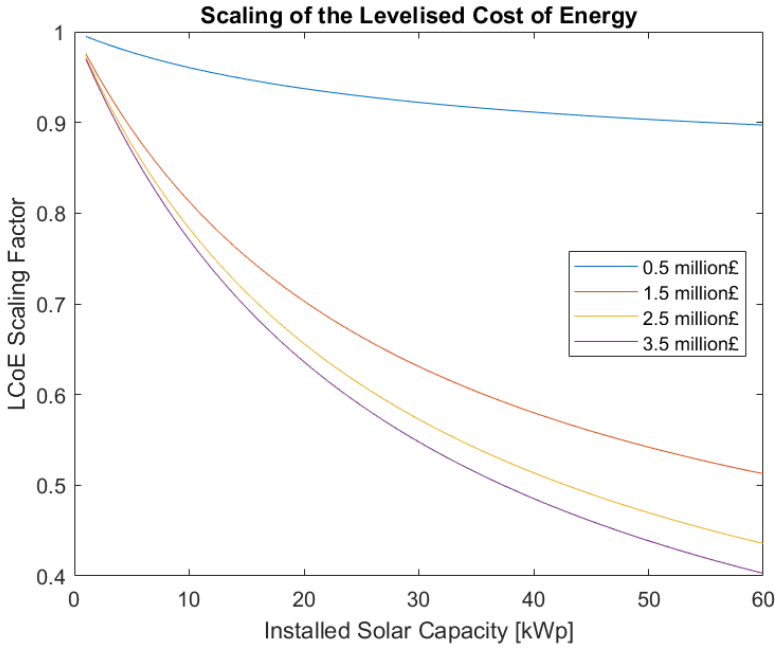

(a) Canary's

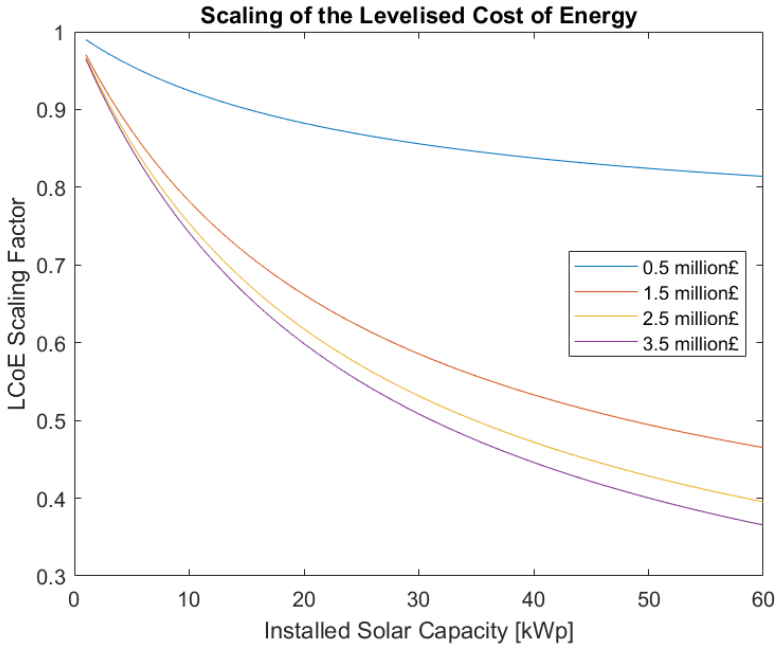

(b) Sardinia

Figure D.3: LCOE of Increasing Solar Capacity

Bibliography

[1] HM Government. Net zero strategy: Build back greener, 2021.

[2] P. Bolton and I. Stewart. Domestic energy prices - commons library research briefing, 2023.

[3] Committee on Climate Change. Technical annex: Integrating variable renewables into the uk electricity system 2.

[4] National Grid. How much of the uk's energy is renewable?, 2023. URL https://www.nationalgrid.com/stories/energy-explained/how-much-uks-energy-renewable.

[5] POSTnote 464 May 2014. Intermittent electricity generation. URL www.parliament.uk/post.

[6] Energy Industrial Strategy Department for Business. Longer duration energy storage demonstration (lodes) competition (closed to applications), 2023. URL https://www.gov.uk/government/collections/longer-duration-energy-storage-demonstration-lodes-competition.

[7] Orbital Marine Power. Orbital marine power homepage, 2023. URL https://www.orbitalmarine.com/.

[8] Nova Innovation. Nova innovation homepage, 2023. URL https://www.novainnovation.com/.

[9] SH Salter, DC Jeffrey, and JRM Taylor. The architecture of nodding duck wave power generators. 1976.

[10] EMEC. Wave devices, 2020. URL https://www.emec.org.uk/marine-energy/wave-devices/.

[11] BBC News. Jobs lost as wave energy firm aquamarine power folds, 2015. URL https://www.bbc.co.uk/news/uk-scotland-scotland-business-34901133.

[12] HydroInternational. Oyster wave power wins innovator of the year, 2009. URL https://www.hydro-international.com/content/news/oyster-wave-power-wins-innovator-of-the-year.

[13] BBC News. Wave power firm pelamis calls in administrators, 2014. URL https://www.bbc.co.uk/news/uk-scotland-scotland-business-30151276.

[14] A. Garanovic Offshore Energy. Mocean energy unveils blue x wave power prototype, 2021. URL https://www.offshore-energy.biz/mocean-energy-unveils-blue-x-wave-power-prototype/.

[15] Mocean Energy. Mocean energy homepage, 2023. URL https://www.mocean.energy/.

[16] E. Renzi, S. Michele, S. Zheng, S. Jin, and D. Greaves. Niche applications and flexible devices for wave energy conversion: A review, 10 2021. ISSN 19961073.

[17] S. Jin and D. Greaves. Wave energy in the uk: Status review and future perspectives. *Renewable and Sustainable Energy Reviews*, 143:110932, 6 2021. ISSN 1364-0321. doi: 10.1016/J.RSER.2021.110932.

[18] O. Edenhofer, R. P. Madruga, Y. Sokona, United Nations Environment Programme., World Meteorological Organization., Intergovernmental Panel on Climate Change. Working Group III., and Potsdam-Institut fur Klimafolgenforschung. *Renewable energy sources and climate change mitigation : special report of the Intergovernmental Panel on Climate Change*. Cambridge University Press, 2012. ISBN 9781107607101.

[19] IEA. World energy outlook 2020, 2020. URL https://www.iea.org/reports/world-energy-outlook-2020.

[20] A.P Sukarso and K.N Kim. Cooling effect on the floating solar pv: Performance and economic analysis on the case of west java province in indonesia. *Energies*, 13, 5 2020. ISSN 19961073. doi: 10.3390/en13092126.

[21] M. Dörenkämper, A. Wahed, A. Kumar, M. de Jong, J. Kroon, and T. Reindl. The cooling effect of floating pv in two different climate zones: A comparison of field test data from the netherlands and singapore. *Solar Energy*, 219:15–23, 5 2021. ISSN 0038-092X. doi: 10.1016/J.SOLENER.2021.03.051.

[22] The Energy Blog. Aquabuoy 2.0 deployed off oregon coast, 2007. URL https://thefraserdomain.typepad.com/energy/2007/09/aquabuoy20-depl.html.

[23] L. Page The Register. Wave power prototype sinks after seven weeks, 2007. URL https://www.theregister.com/2007/11/09/aquabuoy_wave_power_renewable_sinks/.

[24] OEA. Country reports - china - research development, 2018. URL https://report2018.ocean-energy-systems.org/international-activities/china/research-and-development/.

[25] C. Ma, M. Wang, and D. Zhang. Representative technology development of marine renewable energy in china. volume 227. Institute of Physics Publishing, 3 2019. doi: 10.1088/1755-1315/227/2/022013.

[26] D. Zhang and C. Ma. Utilization of tidal current and wave energy help the implement of the carbon emissions peak and carbon neutrality strategy in china. volume 983. IOP Publishing Ltd, 2 2022. doi: 10.1088/1755-1315/983/1/012055.

[27] C. Ma, X. Wang, and B. Jiang. Ocean energy development under the background of carbon emissions peak and carbon neutrality in china. volume 966. IOP Publishing Ltd, 1 2022. doi: 10.1088/1755-1315/966/1/012003.

[28] D. Clemente, P. Rosa-Santos, T. Ferradosa, and F. Taveira-Pinto. Wave energy conversion energizing offshore aquaculture: Prospects along the portuguese coastline. *Renewable Energy*, 204:347–358, 3 2023. ISSN 18790682. doi: 10.1016/j.renene.2023.01.009.

[29] N. M. Kumar. Wavevoltaics: A new hybrid wave photon energy device. *Current Science*, 115:1251–1251, 5 2018.

[30] N. M. Kumar. Model to estimate the potential and performance of wavevoltaics. *Results in Physics*, 12:914–916, 3 2019. ISSN 22113797. doi: 10.1016/j.rinp.2018.12.057.

[31] K. A. Prasad, A. A. Chand, N. M. Kumar, S. Narayan, and K. A. Mamun. A critical review of power take-off wave energy technology leading to the conceptual design of a novel wave-plus-photon energy harvester for island/coastal communities' energy needs, 2 2022. ISSN 20711050.

[32] M. K. Deshmukh and S. S. Deshmukh. Modeling of hybrid renewable energy systems, 1 2008. ISSN 13640321.

[33] P. Rosa-Santos, F. Taveira-Pinto, M. López, and C. A. Rodríguez. Hybrid systems for marine energy harvesting, 5 2022. ISSN 20771312.

[34] N. H. Samrat, N. Bin Ahmad, I. A. Choudhury, and Z. Bin Taha. Modeling, control, and simulation of battery storage photovoltaic-wave energy hybrid renewable power generation systems for island electrification in malaysia. *Scientific World Journal*, 2014, 2014. ISSN 1537744X. doi: 10.1155/2014/436376.

[35] S. Ahmad, M. J. Uddin, I. H. Nisu, M. Ul Ahsan, I. Rahman, and N. H. Samrat. Modeling of grid connected battery storage wave energy and pv hybrid renewable power generation. pages 375–380. Institute of Electrical and Electronics Engineers Inc., 4 2017. ISBN 9781509056262. doi: 10.1109/ECACE.2017.7912933.

[36] M. A. Saheli, K. Lari, G. Salehi, and M. T. Azad. Feasibility study of a hybrid grid-tied photovoltaic-wave system on the shores of persian gulf. *Environmental Progress and Sustainable Energy*, 40, 11 2021. ISSN 19447450. doi: 10.1002/ep.13665.

[37] S. Oliveira-Pinto, P. Rosa-Santos, and F. Taveira-Pinto. Assessment of the potential of combining wave and solar energy resources to power supply worldwide offshore oil and gas platforms. *Energy Conversion and Management*, 223, 11 2020. ISSN 01968904. doi: 10.1016/j.enconman.2020.113299.

[38] M. H. Jahangir, A. Shahsavari, and M. A. V. Rad. Feasibility study of a zero emission pv/wind turbine/wave energy converter hybrid system for stand-alone power supply: A case study. *Journal of Cleaner Production*, 262, 7 2020. ISSN 09596526. doi: 10.1016/j.jclepro.2020.121250.

[39] M. H. Jahangir, S. Fakouriyan, M. A. V. Rad, and H. Dehghan. Feasibility study of on/off grid large-scale pv/wt/wec hybrid energy system in coastal cities: A case-based research. *Renewable Energy*, 162:2075–2095, 12 2020. ISSN 18790682. doi: 10.1016/j.renene.2020.09.131.

[40] C. Pérez-Collazo, D. Greaves, and G. Iglesias. A review of combined wave and offshore wind energy, 2015. ISSN 18790690.

[41] Ling Wan, Zhen Gao, Torgeir Moan, and Claudio Lugni. Comparative experimental study of the survivability of a combined wind and wave energy converter in two testing facilities. *Ocean Engineering*, 111:82–94, 1 2016. ISSN 00298018. doi: 10.1016/j.oceaneng.2015.10.045.

[42] WAVE ENERGY SCOTLAND. Floating offshore wind + wave, 2023. URL https://www.inspireoffshoreenergy.com/.

[43] S. Astariz, C. Perez-Collazo, J. Abanades, and G. Iglesias. Co-located wave-wind farms: Economic assessment as a function of layout. *Renewable Energy*, 83:837–849, 11 2015. ISSN 18790682. doi: 10.1016/j.renene.2015.05.028.

[44] S. Astariz and G. Iglesias. Output power smoothing and reduced downtime period by combined wind and wave energy farms. *Energy*, 97:69–81, 2 2016. ISSN 03605442. doi: 10.1016/j.energy.2015.12.108.

[45] WAVE ENERGY SCOTLAND. Shared floating wind and wave projects offer 12reduction to uk, 2023. URL https://www.waveenergyscotland.co.uk/news-events/shared-floating-wind-and-wave-projects-offer-12-combined-lcoe-reduction-to-uk/.

[46] Wes. Wave and floating wind energy opportunities for sharing infrastructure, services and supply chain first wes release, 2023. URL https://evolveenergy.eu/project-outputs/.

[47] NREL. Best research-cell efficiency chart, 2023. URL https://www.nrel.gov/pv/cell-efficiency.html.

[48] N. Martín-Chivelet. Photovoltaic potential and land-use estimation methodology. *Energy*, 94:233–242, 1 2016. ISSN 0360-5442. doi: 10.1016/J.ENERGY.2015.10.108.

[49] SolarSquare. All you need to know about bhadla solar power plant, 2022. URL https://www.solarsquare.in/blog/bhadla-solar-power-plant/.

[50] Management for professionals bbrajeshhkumar project finance structuring, valuation and risk management forrmajor projects. URL https://link.springer.com/bookseries/10101.

[51] M. Burke. Solar farms: Funding, planning and impacts. URL www.parliament.uk/commons-library|intranet.parliament.uk/commons-library|papers@parliament.uk|@commonslibrary.

[52] M. Godwin The Guardian F. Harvey. World's biggest floating solar farm powers up outside london, 2016. URL https://www.theguardian.com/environment/2016/feb/29/worlds-biggest-floating-solar-farm-power-up-outside-london.

[53] E. Solomin, E. Sirotkin, E. Cuce, S. P. Selvanathan, and S. Kumarasamy. Hybrid floating solar plant designs: A review, 2021. ISSN 19961073.

[54] M. Rosa-Clot, G. M. Tina, and S. Nizetic. Floating photovoltaic plants and wastewater basins: An australian project. volume 134, pages 664–674. Elsevier Ltd, 2017. doi: 10.1016/j.egypro.2017.09.585.

[55] A. Garanovic Offshore Energy. World's largest hydro-floating solar hybrid comes online in thailand, 2021. URL https://www.offshore-energy.biz/worlds-largest-hydro-floating-solar-hybrid-comes-online-in-thailand/.

[56] B. A. Horton AFP. Thailand creates world's biggest solar farm - but not everybody is happy about it., 2022. URL https://www.euronews.com/green/2022/03/11/huge-floating-solar-farm-sets-thailand-on-track-towards-carbon-neutrality.

[57] S. Oliveira-Pinto and J. Stokkermans. Assessment of the potential of different floating solar technologies – overview and analysis of different case studies. *Energy Conversion and Management*, 211, 5 2020. ISSN 01968904. doi: 10.1016/j.enconman.2020.112747.

[58] Z. A.A. Majid, M. H. Ruslan, K. Sopian, M. Y. Othman, and M. S.M. Azmi. Study on performance of 80 watt floating photovoltaic panel. *Journal of Mechanical Engineering and Sciences*, 7:1150–1156, 12 2014. ISSN 22318380. doi: 10.15282/jmes.7.2014.14.0112.

[59] A. El Hammoumi, A. Chalh, A. Allouhi, S. Motahhir, A. El Ghzizal, and A. Derouich. Design and construction of a test bench to investigate the potential of floating pv systems. *Journal of Cleaner Production*, 278, 1 2021. ISSN 09596526. doi: 10.1016/j.jclepro.2020.123917.

[60] R. Cazzaniga and M. Rosa-Clot. The booming of floating pv. *Solar Energy*, 219:3–10, 5 2021. ISSN 0038092X. doi: 10.1016/j.solener.2020.09.057.

[61] Grand View Research. Floating solar panels market size, share & trends analysis report by product (tracking, stationary), by region (asia pacific, north america, europe, middle east & africa) and segment forecasts, 2022 - 2030. https://www.grandviewresearch.com/industry-analysis/floating-solar-panels-market, 2021.

[62] H. M. Pouran. From collapsed coal mines to floating solar farms, why china's new power stations matter. *Energy Policy*, 123:414–420, 12 2018. ISSN 0301-4215. doi: 10.1016/J.ENPOL.2018.09.010.

[63] Power Technology. Power plant profile: Three gorges huainan floating solar pv park, china, 2023. URL https://www.power-technology.com/marketdata/power-plant-profile-three-gorges-huainan-floating-solar-pv-park-china/.

[64] N. Lewis Electrek. World's largest floating solar farm comes online with wind and storage, 2022. URL https://electrek.co/2022/01/07/worlds-largest-floating-solar-farm-comes-online-with-wind-and-storage/.

[65] C. Elton euronews.green. 'float-ovoltaics': How floating solar panels in reservoirs could revolutionise global power, 2023. URL https://www.euronews.com/green/2023/03/14/float-ovoltaics-how-floating-solar-panels-in-reservoirs-could-revolutionise-global-power#:~:text=The%20Dezhou%20Dingzhuang%20Floating%20Solar,and%20covers%20nearly%20600%20hectares.

[66] A. Habibic Offshore Energy. Amp energy partners with rumsl for india's 600mw floating solar project, 2022. URL https://www.offshore-energy.biz/amp-energy-partners-with-rumsl-for-indias-600mw-floating-solar-project/.

[67] M. Rosa-Clot and G. Marco Tina. Introduction, 2018.

[68] M. WILLUHN. The weekend read: Don't throw caution to the wind, 2020. URL https://www.pv-magazine.com/2020/02/22/the-weekend-read-dont-throw-caution-to-the-wind/.

[69] S.Oliveira-Pinto and J. Stokkermans. Marine floating solar plants: An overview of potential, challenges and feasibility, 12 2020. ISSN 17517737.

[70] S.Suzuki, N. Nishiyama, S. Yoshino, T. Ujiro, S. Watanabe, T. Doi, A. Masuda, and T. Tanahashi. Acceleration of potential-induced degradation by salt-mist preconditioning in crystalline silicon photovoltaic modules. volume 54. Japan Society of Applied Physics, 8 2015. doi: 10.7567/JJAP.54.08KG08.

[71] F. Setiawan, T. Dewi, and S. Yusi. Sea salt deposition effect on output and efficiency losses of the photovoltaic system; a case study in palembang, indonesia. volume 1167. Institute of Physics Publishing, 3 2019. doi: 10.1088/1742-6596/1167/1/012028.

[72] iec. Salt mist corrosion testing of photovoltaic (pv) modules, 1995. URL `www.iec.ch`.

[73] S. Z.Golroodbari and W. van Sark. Simulation of performance differences between offshore and land-based photovoltaic systems. *Progress in Photovoltaics: Research and Applications*, 28:873–886, 9 2020. ISSN 1099159X. doi: 10.1002/pip.3276.

[74] Oceans of Energy. Oceans of energy - homepage, 2023. URL `https://oceansofenergy.blue/`.

[75] Solar Duck. Solar duck - homepage, 2022. URL `https://solarduck.tech/#purpose`.

[76] Ocean Sun. Ocean sun - innovation, 2023. URL `https://oceansun.no/the-innovation/`.

[77] Profloating. Profloating - our solution, 2023. URL `https://www.profloating.nl/oplossing`.

[78] K.Trapani and D. L. Millar. The thin film flexible floating pv (t3f-pv) array: The concept and development of the prototype. *Renewable Energy*, 71:43–50, 2014. ISSN 09601481. doi: 10.1016/j.renene.2014.05.007.

[79] Nick Raymond SOFAR. What is biofouling and how can we stop it?, 2021. URL `https://www.sofarocean.com/posts/what-is-biofouling-and-how-can-we-stop-it`.

[80] S. Williams Clean Solar Solutions. The effects of bird droppings solar panels – the harsh reality, 2016. URL `https://cleansolar.solutions/effect-of-bird-droppings-on-solar-panels/`.

[81] S. Shaik, P. Vigneshwaran, A. Roy, K. J. Kontoleon, D. Mazzeo, E. Cuce, C A. Saleel, M. Alwetaishi, S. A. Khan, A. E. Gürel, and Ü. Ağbulut. Experimental analysis on the impacts of soil deposition and bird droppings on the thermal performance of photovoltaic panels. *Case Studies in Thermal Engineering*, 48:103128, 8 2023. ISSN 2214157X. doi: 10.1016/j.csite.2023.103128. URL https://linkinghub.elsevier.com/retrieve/pii/S2214157X23004343.

[82] Institute of Electrical, Electronics Engineers, IEEE Electron Devices Society, Wash. IEEE Photovoltaic Specialists Conference 37 2011.06.19-24 Seattle, and Wash. PVSC 37 2011.06.19-24 Seattle. *37th IEEE Photovoltaic Specialists Conference (PVSC), 2011 19 - 24 June 2011, Seattle, Washington ; conference proceedings*. IEEE, 2011. ISBN 9781424499656.

[83] M. M. Fouad, Lamia A. Shihata, and El Sayed I. Morgan. An integrated review of factors influencing the performance of photovoltaic panels, 2017. ISSN 18790690.

[84] A. K. Sisodia and R. k. Mathur. Impact of bird dropping deposition on solar photovoltaic module performance: a systematic study in western rajasthan. *Environmental Science and Pollution Research*, 26:31119–31132, 10 2019. ISSN 16147499. doi: 10.1007/s11356-019-06100-2.

[85] Bird Control Group. Solar farm solves bird problem with lasers, 2017. URL https://birdcontrolgroup.com/sheeplands-farm-finally-found-solution-bird-problem/.

[86] Scarecrow Bird Control. Gas bird control, 2017. URL https://www.scarecrow.eu/oil-gas-bird-control/.

[87] Jing Qin and Hao Lu. A review of self-cleaning coatings for solar photovoltaic systems: theory, materials, preparation, and applications, 8 2023. ISSN 16147499.

[88] Klemens Ilse, Leonardo Micheli, Benjamin W. Figgis, Katja Lange, David Daßler, Hamed Hanifi, Fabian Wolfertstetter, Volker Naumann, Christian Hagendorf, Ralph Gottschalg, and Jörg Bagdahn. Techno-economic assessment of soiling losses and mitigation strategies for solar power generation, 10 2019. ISSN 25424351.

[89] Nanoveu. Coatings, 2023. URL https://www.nanoveu.com/our-technology/coatings/.

[90] Benjamin Strauss; Fabiana Lisco; Farwah Bukhari; John M. Walls; Kurt L. Barth. Novel hydrophobic coatings for soiling mitigation in the pv industry: Durability and anti-soiling demonstrations.

[91] Michael L. Adekanbi, Ezekiel S. Alaba, Toluwalope J. John, Tomi D. Tundealao, and Titilope I. Banji. Soiling loss in solar systems: A review of its effect on solar energy efficiency and mitigation techniques. *Cleaner Energy Systems*, 7:100094, 2024. ISSN 2772-7831. doi: https://doi.org/10.1016/j.cles.2023.100094. URL https://www.sciencedirect.com/science/article/pii/S2772783123000444.

[92] Travis Sarver, Ali Al-Qaraghuli, and Lawrence L. Kazmerski. A comprehensive review of the impact of dust on the use of solar energy: History, investigations, results, literature, and mitigation approaches. *Renewable and Sustainable Energy Reviews*, 22:698–733, 2013. ISSN 1364-0321. doi: https://doi.org/10.1016/j.rser.2012.12.065. URL https://www.sciencedirect.com/science/article/pii/S136403211300021X.

[93] Hosna Titah-Benbouzid and Mohamed Benbouzid. Marine renewable energy converters biofouling: A critical review on impacts and prevention.

[94] Avinash Kumar, Vishal Mishra, Sushant Negi, and Simanchal Kar. A systematic review on polymer-based superhydrophobic coating for preventing biofouling menace, 9 2023. ISSN 19353804.

[95] Huichao Jin, Limei Tian, Wei Bing, Jie Zhao, and Luquan Ren. Bioinspired marine antifouling coatings: Status, prospects, and future. *Progress in Materials Science*, 124:100889, 2022. ISSN 0079-6425. doi: https://doi.org/10.1016/j.pmatsci.2021.100889. URL https://www.sciencedirect.com/science/article/pii/S0079642521001134.

[96] Leslie Diaz Jalaff, Eduardo Ortega Cancino, Manuela Altavilla, Karla Vargas Hurtado, Nicolas Nolan Mella, and Mirko Faccini. Eco-friendly solndash;gel coatings as microfouling barrier for marine applications. *Coatings*, 13(10), 2023. ISSN 2079-6412. doi: 10.3390/coatings13101755. URL https://www.mdpi.com/2079-6412/13/10/1755.

[97] IEC 61701:2020. Photovoltaic (pv) modules – salt mist corrosion testing. Standard, International Electrotechnical Commission, June 2020.

[98] Blackfish. Blackfish homepage, 2023. URL https://www.blackfishengineering.com/.

[99] EMEC. We provide the world's only multi-berth, purpose-built, open sea test facilities for wave and tidal energy converters., 2023. URL https://www.emec.org.uk/facilities/.

[100] S. Chander, A. Purohit, A. Sharma, S. P. Nehra, and M. S. Dhaka. Impact of temperature on performance of series and parallel connected mono-crystalline silicon solar cells. *Energy Reports*, 1:175–180, 11 2015. ISSN 2352-4847. doi: 10.1016/J.EGYR.2015.09.001.

[101] K. Hong Min, K. Hong Min, T. Kim, M. Gu Kang, H. Eun Song, Y. Kang, H. Seok Lee, D. Kim, S. Park, and S. Hee Lee. An analysis of fill factor loss depending on the temperature for the industrial silicon solar cells. *Energies*, 13, 6 2020. ISSN 19961073. doi: 10.3390/en13112931.

[102] S. Chander, A. Purohit, A. Sharma, Arvind, S. P. Nehra, and M. S. Dhaka. A study on photovoltaic parameters of mono-crystalline silicon solar cell with cell temperature. *Energy Reports*, 1:104–109, 11 2015. ISSN 2352-4847. doi: 10.1016/J.EGYR.2015.03.004.

[103] H. Qu and X. Li. Temperature dependency of the fill factor in pv modules between 6 and 40 °c. *Journal of Mechanical Science and Technology*, 33: 1981–1986, 4 2019. ISSN 1738494X. doi: 10.1007/s12206-019-0348-4.

[104] A. Garanovic. Partners get ready to demonstrate 'renewables for subsea power' solution, 2023. URL https://www.offshore-energy.biz/partners-get-ready-to-demonstrate-renewables-for-subsea-power-solution/.

[105] Renogy. 100 watt 12 volt flexible monocrystalline solar panel, 2023. URL https://uk.renogy.com/renogy-100-watt-12-volt-flexible-monocrystalline-solar-panel/.

[106] Solbian. Sr 186 l, 2022. URL https://www.solbian.eu/en/sr-series/63-sr-186-l.html.

[107] I. McConnell. Orkney: Scottish wave power test by mocean and verlume takes to seas, 2023. URL https://www.heraldscotland.com/business_hq/23367143.orkney-scottish-wave-power-test-mocean-verlume-takes-seas/.

[108] Victron Energy. Smartsolar mppt 75/10, 75/15, 100/15 100/20, 2023. URL https://www.victronenergy.com/solar-charge-controllers/smartsolar-mppt-75-10-75-15-100-15-100-20.

[109] Victron Energy. Lithium superpack 12,8v 25,6v, 2023. URL https://www.victronenergy.com/batteries/12,8v-lithium-superpack.

[110] Victron Energy. Cerbo gx, 2023. URL https://www.victronenergy.com/panel-systems-remote-monitoring/cerbo-gx.

[111] W. F. Holmgren, C. W. Hansen, and M. A. Mikofski. pvlib python: a python package for modeling solar energy systems. *Journal of Open Source Software*, 3:884, 9 2018. doi: 10.21105/joss.00884.

[112] R. Muhammad Hussnain, I. Hassan, A. Habeel, A. Muhammad Ashraful, and B. Nauman Zafar. Crop-specific optimization of bifacial pv arrays for agrivoltaic food-energy production: The light-productivity-factor approach. *IEEE Journal of Photovoltaics*, 12(2):572–580, 2022. doi: 10.1109/JPHOTOV.2021.3136158.

[113] W. M.Pabasara Upalakshi Wijeratne, Th. Samarasinghalage, R. Yang, and R. Wakefield. Multi-objective optimisation for building integrated photovoltaics (bipv) roof projects in early design phase. *Applied Energy*, 309:118476, 3 2022. ISSN 0306-2619. doi: 10.1016/J.APENERGY.2021.118476.

[114] D. E. Smith, M. D. Hughes, and D.A. Borca-Tasciuc. Towards a standard approach for annual energy production of concentrator-based building-integrated photovoltaics. *Renewable Energy*, 186:469–485, 3 2022. ISSN 0960-1481. doi: 10.1016/J.RENENE.2021.12.147.

[115] W. Hu, G. Cervone, A. Merzky, M. Turilli, and S. Jha. A new hourly dataset for photovoltaic energy production for the continental usa. *Data in Brief*, 40: 107824, 2 2022. ISSN 2352-3409. doi: 10.1016/J.DIB.2022.107824.

[116] CAMS. Cams solar radiation time-series, 2023. URL https://ads.atmosphere.copernicus.eu/cdsapp#!/dataset/cams-solar-radiation-timeseries?tab=overview.

[117] M. Schroedter-Homscheidt, F. Azam, J. Betcke, N. Hanrieder, M. Lefèvre, L. Saboret, and Y.-M. Saint-Drenan. Surface solar irradiation retrieval from msg/seviri based on apollo next generation and heliosat-4 methods. *Meteorologische Zeitschrift*, 12 2022. ISSN 16101227. doi: 10.1127/metz/2022/1132.

[118] Z. Qu, A. Oumbe, P. Blanc, B. Espinar, G. Gesell, B. Gschwind, L. Klüser, M. Lefèvre, L. Saboret, M. Schroedter-Homscheidt, and L. Wald. Fast radiative transfer parameterisation for assessing the surface solar irradiance: The heliosat-4 method energy meteorology fast radiative transfer parameterisation for assessing the surface solar irradiance: The heliosat-4 method. 26:33–57, 2017. doi: 10.1127/metz/2016/0781Ãŕ. URL https://hal.archives-ouvertes.fr/hal-01512589.

[119] A. B. Sproul. Derivation of the solar geometric relationships using vector analysis. *Renewable Energy*, 32:1187–1205, 2007. ISSN 09601481. doi: 10.1016/j.renene.2006.05.001.

[120] R. Perez, R. Stewart, R. Seals, and T. Guertin. The development and verification of the perez diffuse radiation model.

[121] R. Perez, R. Seals, P. Ineichen, R.Stewart, and D. Menicucci. A new simplified version of the perez diffuse irradiance model for tilted surfaces. *Solar Energy*, 39:221–231, 1987. ISSN 0038092X. doi: 10.1016/S0038-092X(87)80031-2.

[122] R. Perez, P. Ineichen, R. Seals, J. Michalsky, and R. Stewart. Modeling daylight availability and irradiance components from direct and global irradiance, 1990.

[123] Sandia National Laboratories. Perez sky diffuse model, 2023. URL https://pvpmc.sandia.gov/modeling-steps/1-weather-design-inputs/plane-of-array-poa-irradiance/calculating-poa-irradiance/poa-sky-diffuse/perez-sky-diffuse-model/.

[124] R. E. Payne. Albedo of the sea surface. *Atmospheric Sciences*, 29:959–970, 7 1972. doi: https://doi.org/10.1175/1520-0469(1972)029<0959:AOTSS>2.0.CO;2.

[125] S. Golroodbari and W. van Sark. On the effect of dynamic albedo on performance modelling of offshore floating photovoltaic systems. *Solar Energy Advances*, 2:100016, 2022. ISSN 26671131. doi: 10.1016/j.seja.2022.100016.

[126] S. Neven-Du Mont, M. Heinrich, A. Pfreundt, C. Kutter, A. Tummalieh, and H. Neuhaus. Energy yield modelling of 2d and 3d curved photovoltaic modules.

[127] X. Tian, J. Wang, J. Ji, and T. Xia. Comparative performance analysis of the flexible flat/curved pv modules with changing inclination angles. *Energy Conversion and Management*, 274, 12 2022. ISSN 01968904. doi: 10.1016/j.enconman.2022.116472.

[128] A. Karavadi and R. S. Balog. Novel non-flat photovoltaic module geometries and implications to power conversion. pages 7–13, 2011. ISBN 9781457705427. doi: 10.1109/ECCE.2011.6063742.

[129] D L King, W E Boyson, and J A Kratochvil. Photovoltaic array performance model, .

[130] D L King, W E Boyson, and J A Kratochvill. Sandia report photovoltaic array performance model, . URL `http://www.ntis.gov/help/ordermethods.asp?loc=7-4-0#online`.